

**KINETICS OF LEACHING OF CHALCOCITE IN ACID
FERRIC SULFATE MEDIA: CHEMICAL
AND BACTERIAL LEACHING**

by


SAMUEL ADEWALE BOLORUNDURO

B.Sc.(Hons.), Obafemi Awolowo University, Ile-Ife, 1990

A THESIS SUBMITTED IN PARTIAL FULFILLMENT OF THE
REQUIREMENTS FOR THE DEGREE OF
MASTER OF APPLIED SCIENCE

in

THE FACULTY OF GRADUATE STUDIES
Department of Metals and Materials Engineering

We accept this thesis as conforming
to the required standard 

THE UNIVERSITY OF BRITISH COLUMBIA

September, 1999

©Samuel Adewale Bolorunduro

In presenting this thesis in partial fulfilment of the requirements for an advanced degree at the University of British Columbia, I agree that the Library shall make it freely available for reference and study. I further agree that permission for extensive copying of this thesis for scholarly purposes may be granted by the head of my department or by his or her representatives. It is understood that copying or publication of this thesis for financial gain shall not be allowed without my written permission.

Department of METALS & MATERIALS ENGINEERING

The University of British Columbia
Vancouver, Canada

Date 27 | 09 | 99

ABSTRACT

The lack of a clear understanding of the rate of chalcocite (Cu_2S) and covellite (CuS) leaching in the presence and absence of bacteria has been a limitation on the optimization of hydrometallurgical processes for the recovery of copper from these minerals. In order to enhance the performance of heaps and other leaching processes for these minerals, there is a need to examine the conditions required to improve the rate of leaching. Such an investigation will produce a particle scale model (for the intrinsic rate of leaching), which can be combined with a heap scale model to form a comprehensive heap leaching model, or with a leaching macro-model to form a tank leaching model. The robustness of such a model will be its ability to determine the effects of changing parameters on the rate limiting steps.

Chalcocite oxidation was investigated by leaching high grade natural minerals in acidic ferric/ferrous sulfate solutions. The temperature was varied between 35° and 75° C. The ferric concentration varied between 0.015 and 0.232 mol/L, and the ferrous concentration varied between 0.001 and 0.233 mol/L. The redox potential of the solution (at 25°C) was varied between 450 and 651 mV (vs. Ag/AgCl) to determine the effect of this parameter on the leaching kinetics.

The two well known, significant stages of leaching were observed and characterized by mineralogical studies. The first stage leach was characterized by 50% copper extraction and the conversion of chalcocite, ultimately to second stage covellite (CuS). Some non-stoichiometric copper sulfides were formed prior to the formation of the second stage covellite. The first stage leaching reaction was rapid at all temperatures. The redox potential had no effect on the rate of this reaction.

The second stage leach was characterized by the conversion of the second stage covellite (which was the by-product of the first stage) to copper, elemental sulfur and sulfate. At higher temperatures, sulfur formation was predominant and the reaction was fast. At lower temperatures, sulfur formation was predominant up to about 70% copper extraction. Subsequently, sulfate formation occurred. The effect of the solution redox

potential on the kinetics of second stage leaching was significant. During bacterial leaching, it was observed that the principal role of the ferrous oxidizing bacteria (*Thiobacillus ferrooxidans*) was to maintain the required high redox potential at the surface of the minerals.

A mathematical model was formulated to explain the ferric leaching kinetics of chalcocite. The first stage kinetics can be explained in terms of a mixed diffusion/chemical reaction model, in which the rate of reaction is simultaneously limited by the diffusion of ferric ions to the mineral surface and by the chemical reaction. Though the partially oxidized particles disintegrate before the commencement of the second stage leach, each of the particles leaches as a discrete grain and the second stage kinetics are controlled by the chemical reaction, which is one-half order dependent on the ferric concentration. The leaching process can be described by an electrochemical mechanism in which the rate-limiting step of the first stage is electron transfer in the cathodic reaction, and the rate-limiting step of the second stage is electron transfer in the anodic reaction.

TABLE OF CONTENTS

ABSTRACT.....	ii
TABLE OF CONTENTS.....	iv
LIST OF TABLES.....	vi
LIST OF FIGURES	vii
LIST OF SYMBOLS	viii
CHAPTER 1: INTRODUCTION	1
CHAPTER 2: LITERATURE REVIEW	4
2.1 Properties of Chalcocite and Covellite.....	4
2.1.1 Crystal Structures	4
2.1.2 Leaching Implications of the Structures.....	7
2.1.3 Thermodynamics Considerations	7
2.1.4 Multiple Stage Dissolution of Chalcocite.....	11
2.2 Polarization Behaviour of Chalcocite and Covellite.....	13
2.2.1 Effect of Electrolytes on Polarization.....	17
2.2.2 Effect of Temperature on Polarization	21
2.3 Mixed Potential Theory of Leaching	22
2.3.1 Type I Leaching.....	26
2.3.2 Type II Leaching.....	27
2.3.3 Type III Leaching	29
2.4 Application of Mixed Potential Theory to Leaching	30
2.4.1 Leaching of Chalcocite.....	30
2.4.2 Leaching of Covellite	31
2.5 Chemical Leaching Kinetics	34
2.6 Effect of Parameters on the Kinetics in Sulfate Media.....	37
2.6.1 Effect of Stirring Speed	37
2.6.2 Effect of Temperature.....	38
2.6.3 Effect of Particle Size	38
2.6.4 Effect of Ferric Concentration.....	39
2.6.5 Effect of Acidity	39
2.7 Effect of Parameters on the Kinetics in Chloride Media.....	40
2.7.1 Effect of Temperature.....	40
2.7.2 Effect of Ferric Concentration.....	41
2.7.3 Effect of Particle Size	41
2.8 Proposed Mechanisms of Sulfate Leaching	41
2.8.1 Cathodically-Controlled Mixed Potential Mechanism.....	42
2.8.2 Iron Depassivation Mixed Potential Mechanism.....	44
2.9 Proposed Mechanisms of Chloride Leaching.....	47

2.10 Chalcocite Leaching in Other Media.....	53
2.11 Summary of Literature Review.....	53
CHAPTER 3: EXPERIMENTAL PROCEDURES	55
3.1 Chemical Leaching Experiments	55
3.1.1 Sample Preparation and Minerals.....	55
3.1.2 Chemical Analysis of the Sample.....	57
3.1.3 Mineralogical Characterization of the Sample	57
3.1.4 Selection of Monosize Particles	58
3.1.5 Chemical Leaching Apparatus and Procedures.....	59
3.1.6 Role of Potassium Permanganate	61
3.1.7 Slurry Filtration Method.....	65
3.1.8 Analytical Methods.....	65
3.1.9 Determination of Copper Extractions and Sulfide Oxidation.....	66
3.2 Mineralogical Characterization of Reaction Products	67
3.2.1 Qualitative Analysis	67
3.2.2 Phase Compositional Analysis	67
3.3 Bacteria leaching of Chalcocite	68
3.3.1 Bacterial Culture and Nutrient Media.....	68
3.3.2 Bacterial Leaching Experiment	69
CHAPTER 4: RESULTS AND DISCUSSION.....	71
4.1 Mineralogical Characterization	71
4.1.1 X-ray and Microscopic Analyses of Feeds.....	72
4.1.2 X-ray Analyses of Leached Residues.....	76
4.1.3 Qualitative Analyses of Leached Residues by SEM-EDX.....	78
4.1.4 Compositional Changes by Electron Microprobe Analysis	85
4.2 Results of Chemical Leaching Experiments: First Stage Leaching.....	88
4.2.1 Effect of Controlled Potential.....	88
4.2.2 Effect of Temperature.....	89
4.2.3 Effect of Initial Ferric Concentration	90
4.2.4 Effect of Particle size.....	92
4.2.5 Effect of Initial Ferrous Concentration.....	95
4.3 Results of Chemical Leaching Experiments: Second Stage Leaching	98
4.3.1 Effect of Controlled Potential.....	98
4.3.2 Effect of Temperature.....	99
4.3.3 Effect of initial Ferric Concentration.....	101
4.3.4 Effect of Initial Particle size	102
4.3.5 Effect of Initial Ferrous Concentration.....	103
4.3.6 Effect of Ferric/Ferrous Ratio.....	107
4.4 Effect of Leaching Parameters on Sulfur Distribution	110
4.5 Bacterial Leach Experiment	113
CHAPTER 5: THEORY AND MODELING	117
5.1 Physico-Chemical Model of First Stage Leaching	117

5.2 Physico-Chemical Model of Second Stage Leaching	120
5.3 Electrochemical Model of Second Stage Leaching	121
5.4 Rate Expression for First Stage Leaching.....	123
5.5 Rate Expression for Second Stage Leaching.....	126
CHAPTER 6: CONCLUSIONS	133
CHAPTER 7: RECOMMENDATIONS FOR FURTHER WORK	135
REFERENCES	136
APPENDIX 1: EH-PH DIAGRAM AT HIGH TEMPERATURE	143
APPENDIX 2: EXPERIMENTAL DATA.....	147
APPENDIX 3: POTASSIUM PERMANGANATE ADDITION	153
APPENDIX 4: TOPOCHEMICAL MECHANISM OF LEACHING	157

LIST OF TABLES

Table 2-1. Kinetics of first stage ferric leaching of Cu_2S	35
Table 2-2. Kinetics of second stage ferric leaching of Cu_2S and CuS	36
Table 3-1. Results of chemical analyses for the as-received and reground minerals ..	57
Table 3-2. Results of mineralogical composition of the chalcocite sample.....	58
Table 4-1. Summary of qualitative analyses of the leached residues by SEM.....	82
Table 4-2. Chemical compositions of the resulting phases by EPMA.....	86
Table 4-3. Chemical compositions of the minor phases by EPMA	87
Table 4-4. Geometric analysis of the different Particle size fractions.....	92
Table 4-5. Effect of redox potential on sulfur distribution in the leach residue.....	110
Table 4-6. Effect of temperature on sulfur distribution in the leach residue.....	112

LIST OF FIGURES

Figure 2-1. Crystal structure, bond lengths and bond angles of chalcocite.....	6
Figure 2-2. Crystal structure of covellite.....	6
Figure 2-3. Eh-pH diagram for the Cu-S-H ₂ O System at 25 °C, activity of copper ion at 0.01 mol/L and other ionic species at unit activity.....	8
Figure 2-4. Eh-pH diagram for the Cu-S-H ₂ O System at 75°C, activity of copper ion at 0.01 mol/L and other ionic species at unit activity	8
Figure 2-5. Anodic polarization curves for synthetic Cu ₂ S and CuS electrodes.....	14
Figure 2-6. Anodic polarization behavior of a pre-oxidized Cu ₂ S electrodes.....	15
Figure 2-7. Anodic polarization behavior of a CuS and pre-oxidized CuS electrodes	15
Figure 2-8. Passivation behaviour of massive and particulate Cu ₂ S anodes.....	16
Figure 2-9. Passivation behaviour of chalcocite anodes in cupric sulfate and cupric chloride electrolytes.....	18
Figure 2-10. Passivation behaviour of chalcocite anodes in H ₂ SO ₄ and NaCl electrolytes	19
Figure 2-11. Effect of chloride additions on the passivation behaviour of Cu ₂ S anodes in a sulfate electrolyte.....	20
Figure 2-12. Effect of temperature on the passivation behaviour of particulate Cu ₂ S anodes	22
Figure 2-13. Current density potential diagram showing curves for metal sulfide with rest potential E_{e1} and oxidant with rest potential E_{e2}	25
Figure 2-14. Polarization curve for Type I leaching.....	27
Figure 2-15. Polarization curve for Type II leaching	28
Figure 2-16. Polarization curve for Type III leaching.....	29

Figure 2-17. Polarization curves for anodic dissolution of Cu_2S (0.1 mol/L CuSO_4 , 0.5 mol/L MgSO_4 , 1 mol/L H_2SO_4) and cathodic reduction of ferric ions on graphite (0.1 mol/L Fe^{2+} , 1 mol/L H_2SO_4) at 25°C.....	31
Figure 2-18. Polarization curves for anodic dissolution of CuS (0.1 mol/L CuSO_4 and 0.1 mol/L H_2SO_4) and cathodic reduction of ferric ions on graphite at 55°C.....	33
Figure 2-19. Effect of temperature on the leaching of chalcocite (FeCl_3 , 0.5 mol/L, HCl 0.2 mol/L, $\text{Fe}^{3+}/\text{Fe}^{2+}$ ratio 10, 2.5 g of +150-300 μm Cu_2S).....	40
Figure 2-20. Illustration of half-cell and mixed potential variations during ferric leaching of chalcocite: 0.1 mol/L Cu_2S , 0.5 mol/L Fe^{3+} and 0.001mol/L Fe^{2+} and Cu^{2+}	44
Figure 2-21. Schematic Evans diagram of Cu_2S pressure leaching.....	46
Figure 2-22. Effect of chloride concentration on dissolution, at 303 K, 0.086 MPa oxygen pressure, 0.35 mol/L $[\text{H}^+]$ and 210 x 177 μm	48
Figure 2-23. Effect of temperature on the second stage leaching at 0.5 mol/L Cl^- 0.086 MPa pressure, 0.35 mol/L $[\text{H}^+]$ and 210 x 177 μm particles.....	49
Figure 2-24. Physico-chemical model for first stage chalcocite dissolution in the sulfate system	50
Figure 2-25. Physico-chemical model for first stage chalcocite dissolution in the chloride system	51
Figure 2-26. Physico-chemical model for second stage chalcocite dissolution in the sulfate system.....	52
Figure 2-27. Chalcocite dissolution in various media	54
Figure 3-1. Cumulative particle size distributions of the mineral samples as determined by screening with Tyler sieves.....	56
Figure 3-2. Schematic representation of the controlled potential Leaching set-up.....	61
Figure 4-1. X-ray diffraction pattern of chalcocite powder.....	72

Figure 4-2. X-ray display (elemental composition) analysis of a chalcocite rock section	73
Figure 4-3. Backscattered electron image of a rock section of covellite showing chalcocite zoning in covellite.....	74
Figure 4-4. X-ray display (elemental composition) analysis of a covellite rock section	74
Figure 4-5. X-ray diffraction pattern of natural covellite powder.....	75
Figure 4-6. Backscattered electron image of -250+212 μm grains of chalcocite showing chalcocite (1), pyrite (2) and bornite (3) at 0% extraction.....	76
Figure 4-7. X-ray diffraction pattern of the leached residue after 44% extraction from -250+212 μm grains of chalcocite at 35°C, 0.116 mol/L ferric and 0.020 mol/L ferrous concentration.....	77
Figure 4-8. Backscattered electron image of the leached grains (of chalcocite) after 30% extraction at 35°C, showing cracks, pores and breakage of particles. The identified grains are copper-bismuth-sulfide (1) and covellite (2)	79
Figure 4-9. Digital image of a leached grain showing cracks and pores after 44% extraction.....	79
Figure 4-10. Backscattered electron image of a leached grain of chalcocite showing puffy and fragile textures after 30% extraction.....	80
Figure 4-11. Backscattered electron image of selected leached grains for the microprobe (compositional) and elemental analysis of phases, after 44% extraction..	80
Figure 4-12. Backscattered electron image of selected leached grains after 10% extraction.....	81
Figure 4-13. Backscattered electron image of selected leached grains after 40% extraction.....	81
Figure 4-14. Backscattered electron image of a yarrowite grain showing cracks.....	83
Figure 4-15. X-ray analysis of a Cu-Bi-S phase, showing some paragenics effects.....	83

Figure 4-16. Backscattered electron image of an iron zone (1) in copper-sulfide phase (2).....	84
Figure 4-17. Backscattered electron image of adjacent grains of bornite and pyrite, showing the preferential leaching of the bornite grain.	85
Figure 4-18. Effect of potential on the first stage leaching of - 250+212 μm particles at 35°C 0.116 mol/L ferric and 0.0202 mol/L ferrous	88
Figure 4-19. Effect of temperature on the first stage leaching of -250+212 μm particles at 0.116 mol/L ferric and 0.0202 mol/L ferrous.....	89
Figure 4-20. Arrhenius plot for the first stage leaching.....	90
Figure 4-21. Effect of ferric on the first stage leaching of -250+212 μm particles at 35°C and 0.0101 mol/L ferrous.....	91
Figure 4-22. Log rate vs. log ferric concentration plot for the first stage leaching.....	92
Figure 4-23. Effect of particle size on the first stage leaching at 35°C, 0.116 mol/L ferric and 0.0202 mol/L ferrous.....	93
Figure 4-24. Rate vs. the reciprocal of radius squared plot for first stage leaching.....	94
Figure 4-25. Rate vs. the reciprocal of radius plot for first stage leaching.....	94
Figure 4-26. Effect of ferrous on the first stage leaching of -250+212 μm particles at 35°C and 0.116 mol/L ferric	95
Figure 4-27. Effect of ferrous on the first stage leaching of -250+212 μm particles at 35°C and 0.232 mol/L ferric	96
Figure 4-28. Log rate vs. log ferrous concentration plot for the first stage leaching of -250+212 μm particles at 35°C and 0.232 mol/L ferric.....	97
Figure 4-29. Reaction order vs. ferrous concentration plot for the first stage leaching.....	97
Figure 4-30. Effect of potential on the second stage leaching of -250+212 μm particles at 75°C, 0.116 mol/L ferric and 0.0202 mol/L ferrous.....	98
Figure 4-31. Effect of temperature on the second stage leaching of -250+212 μm particles at 75°C, 0.116 mol/L ferric and 0.0202 mol/L ferrous.....	99

Figure 4-32. Arrhenius plot for the second stage leaching.....	100
Figure 4-33. Effect of initial ferric on the second stage leaching of -250+212 μm particles at 75°C and 0.0101 mol/L ferrous.....	101
Figure 4-34. Log rate vs. log ferric concentration plot for the second stage leaching....	102
Figure 4-35. Effect of particle size on the second stage leaching at 75°C, 0.116 mol/L ferric and 0.0202 mol/L ferrous.....	103
Figure 4-36. Effect of ferrous on the second stage leaching of -250+212 μm particles at 75°C and 0.116 mol/L ferric.....	104
Figure 4-37. Log rate vs. log ferrous concentration plot for the second stage leaching of -250+212 μm particles at 75°C and 0.116 mol/L ferric.....	105
Figure 4-38. Reaction order vs. ferrous concentration plot for the second stage leaching at 75°C.....	106
Figure 4-39. Effect of ferrous on the second stage leaching of -250+212 μm particles at 35°C and 0.116 mol/L ferric.....	106
Figure 4-40. Log rate vs. log ferrous concentration plot for the second stage leaching of -250+212 μm particles at 75°C and 0.116 mol/L ferric.....	107
Figure 4-41. Effect of ferric/ferrous ratio on the second stage leaching of -250+212 μm particles at 75°C, 0.136 mol/L total iron and 0.287 mol/L sulfate.....	108
Figure 4-42. Log rate vs. log of ferric/ferrous ratio for the second stage leaching at 75°C.	109
Figure 4-43. Reaction order vs. ferric/ferrous ratio plot for the second stage leaching.....	109
Figure 4-44. Effect of bacteria on the leaching (first and second stage) of -250+212 μm particles at 35°C and 0.116 mol/L total-iron. The initial concentration of ferric was 0.0172 mol/L.....	115
Figure 4-45. Rate vs. extraction plot for the bacterial and chemical leaching (second stage) of -250+212 μm particles at 35°C and 0.116 mol/L total iron.....	116

Figure 4-46. Redox potential and pH profile of bacterial leaching and chemical leaching.....	116
Figure 5-1. Physico-Chemical model for the first step of first stage leaching.....	117
Figure 5-2. Physico-Chemical model for the second step of first stage leaching.....	118
Figure 5-3. Relationship between rate and cuprous concentration for the first stage leaching of -250+212 μm particles at 35°C, 0.116 mol/L ferric and 0.0101 mol/L ferrous	119
Figure 5-4. Physico-Chemical model for the second stage leaching.....	120
Figure 5-5. Evans diagram of theoretical polarization curves during ferric sulfate leaching of second stage covellite.....	122
Figure 5-6. Log rate vs. log of extraction for the second stage leaching of - 250+212 μm particles at 65 and 75°C, 0.116 mol/L ferric and 0.0202 mol/L ferrous	129
Figure 5-7. Predicted vs. actual extraction for the second stage leaching of - 250+212 μm particles at 75°C and different ferric / ferrous ratio.....	131
Figure 5-8. Log rate vs. log of extraction for the second stage leaching of - 250+212 μm particles at 55°C, 0.116 mol/L ferric and 0.0202 mol/L ferrous	132
Figure 5-9. Predicted vs. actual extraction for the second stage leaching of - 250+212 μm particles at 55°C, 0.116 mol/L ferric and 0.0202 mol/L ferrous	132

LIST OF SYMBOLS

G_T^o	Gibbs free energy at a temperature (T), kJ/mol
T	temperature, (K)
C	heat capacity, J/mol-K
a, b, c	heat capacity coefficients for the non-ionic species
α_T, β_T	Criss-Cobble heat capacity constants for the ionic species
S	entropy, J/mol-K
\bar{S}	absolute entropy, J/mol-K
E_e	reversible (or equilibrium) potential of the half cell, V
E or E_M	mixed-potential of the system, V
η	overpotential
i or j	current density
F	faraday, 96485 C/mol e^-
β	electron (or charge) transfer coefficient
\bar{k}	rate for the forward direction
\bar{k}	rate for the reverse direction
D	diffusivity, cm^2/min
δ	boundary layer thickness, cm
Cu_{calc}	calculated head assay of copper, g. %
$m_{\text{Cu}}^{\text{sol}}$	mass of copper solubilized, g,
$m_{\text{Cu}}^{\text{res}}$	mass of copper in the leach residue, g
m_t	mass of the head sample, g
$m_{\text{sulfide}}^{\text{head}}$	mass of sulfide sulfur in the head sample, g
$m_{\text{sulfide}}^{\text{res}}$	mass of sulfide in the leach residue, g
$m_{\text{sulfur}}^{\text{res}}$	mass of elemental sulfur in the leach residue, g
P_{90}	90% passing through

ACKNOWLEDGEMENTS

I would like to express my sincere gratitude to my supervisors, Dr. Ralph Hackl and Dr. David Dixon, for their constant guidance and support throughout the course of my study. It was the excellent initiative of Dr. Ralph Hackl which made it possible for me to pursue my masters degree in the University of British Columbia. Thanks are also extended to my wife (my pillar of inestimable strengths), whose understanding and encouragement during the trying times were appreciated.

I would like to extend my appreciation to my fellow graduate students and the research engineers in the Hydrometallurgy Group, especially to Dr. Berend Wassink for his assistance during the experimental setup.

The financial assistance from the Cy and Emerald Keyes Foundation and the University of British Columbia Graduate Award is gratefully acknowledged.

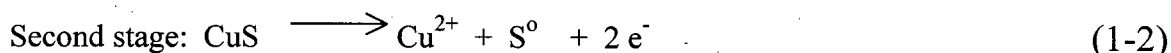
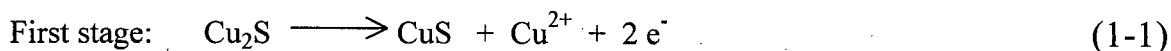
CHAPTER 1

INTRODUCTION

The mineral chalcocite is the most abundant copper sulfide after chalcopyrite, and the most amenable to hydrometallurgical treatment. Bacterial heap leaching, both with and without prior agglomeration and acid curing, is one of the most important emerging technologies for the treatment of low grade secondary copper sulfide, and mixed sulfide/oxide of copper ores. The process is popular especially in South America, because of its simplicity and low cost of operation. Regrettably, the process has been hindered by very low rates of extraction and lower ultimate copper extractions than expected. This poor performance is attributed to the slow kinetics of the second stage of chalcocite oxidation. The problem is compounded by the lack of clear understanding of the kinetics of chalcocite leaching. The various non-stoichiometric copper sulfide compounds, which are formed as a result of successive removal of copper atoms from the initial chalcocite matrix, have been blamed for the slow kinetics of this stage. It is also believed that the leach path (i.e., the transformation to different non-stoichiometric copper sulfides) changes with solution chemistry (such as ferric ion concentration).

The leaching of chalcocite has been investigated under different conditions in the laboratory for seventy years. The investigations began with Sullivan [1] in 1930 and several researchers [2-13] have since studied chalcocite leaching by using ferric ion as the oxidant in either a sulfate or chloride environment. Many of the laboratory studies have used electrochemical oxidation to shed light upon the phase transformations which occur when copper is removed from chalcocite and to explore the anodic dissolution of chalcocite as a recovery method for copper [14-17]. Also, some studies have investigated the oxidation of chalcocite by *Thiobacillus ferrooxidans* bacteria in oxygenated and non-oxygenated acid solutions [18-35].

It is widely known that chalcocite oxidation occurs roughly in two distinct stages.



The previous kinetic studies of chalcocite and covellite leaching by ferric [36] have revealed that the first stage leaching of chalcocite is very fast relative to the second stage leaching. It is generally accepted that the rate of first stage leaching is controlled by the diffusion of oxidant to the mineral surface. This view is supported by the low activation energies (between 1 and 3 kcal/mol [36]) and the first-order dependence on ferric concentration. On the other hand, second stage leaching of chalcocite (or the covellitic phase) is slow and is thought to be controlled by the rate of the chemical reaction. This view is supported by the high activation energies (between 15 and 25 kcal/mol [36]) and the small dependence of the rate on ferric concentration at low levels, and very little or no dependence at high levels. These studies were carried out in the absence of bacteria, and it is worth noting that no attempts were made to control the redox potential, which would be expected to fall from time zero in every case as oxidant is consumed. This may explain some of the discrepancies previously reported with regard to the dependence of rates on ferric concentration and other parameters. Hence the primary objective of the present work was to control the redox potential in each experiment, and thereby to establish a clear understanding of the leaching kinetics of chalcocite. In addition to quantifying the effects of ferric ion, temperature, ferrous ion, and particle size, the work also focused on confirming or disproving the hypotheses that the rate of second stage leaching is governed by the redox potential (as established by the ferric / ferrous ratio).

The reasons for the resistance of the second stage to ferric leaching at low temperatures has never been clearly established. The initial rate of reaction always declines at about forty percent copper extraction, which has led to the conclusion that a reaction product (blue remaining covellite $\text{Cu}_{1.2}\text{S}$) is formed prior to the formation of covellite (CuS) and that a long period of time is required for this transition. Therefore, one of the objectives of the present work was to undertake mineralogical characterization of the reaction products formed prior to second stage.

Some investigators believe that a passivating layer of sulfur or some other oxidation products are formed on the mineral surface during the second stage leaching, and this is corroborated by some electrochemical studies. In the present study, although the focus was not the mineral surface, chemical analyses of the entire solid product by

using an electron-probe microanalyzer (EPMA) were helpful in the investigation of the passivation phenomenon. The morphological analyses of the intermediate phases by using a scanning electron microscope (SEM) were helpful in interpreting the leaching curves obtained.

The mechanisms by which bacteria such as *Thiobacillus ferrooxidans* promote the leaching of chalcocite (Cu_2S) and covellite (CuS) have been the subject of considerable controversy. The two mechanisms which have been proposed are the "direct" mechanism (sulfides oxidized directly by oxygen) and the "indirect" mechanism (sulfides oxidized by bacterially-generated ferric). In any case, the presence of an active bacterial population is absolutely essential to the success of copper sulfide heap leaching as currently practised. In this work, a preliminary attempt was made to confirm or disprove the hypothesis that the role of bacteria is simply to maintain a high redox potential in the vicinity of the mineral surface.

The approach taken was twofold. First, the entire time history of the leaching kinetics in the presence and absence of bacteria was studied. The kinetics were defined and quantified independently by varying one variable at a time while keeping other rate-determining parameters constant. The minerals were leached in batch-wise mode while the solution redox potential was controlled. This concept is termed "controlled potential leaching". The redox potential, feed types, retention time, temperature, pH, ferric and total iron concentrations were monitored independently. Second, the oxidation products were characterized qualitatively by scanning electron microscope and quantitatively by electron-probe microanalysis.

Finally, mathematical models were formulated to describe the first and second stage leaching kinetics of chalcocite.

CHAPTER 2

LITERATURE REVIEW

2.1 Properties of Chalcocite and Covellite

The crystal structures of chalcocite and natural covellite have been inconsistently reported in the literature. This can be attributed to the similarity between the phases, which are formed during leaching or geological transformation of the minerals.

2.1.1 Crystal Structures

The crystal structure of chalcocite, which is illustrated in Figure 2-1 [37] has been widely disputed. This is partly attributed to the closeness of its structure to that of djurleite ($\text{Cu}_{1.97}\text{S}$), which occurs naturally and as an intermediate product during the leaching of chalcocite. It can be considered as several minerals and solid solutions whose relations are not well understood [38]. These relations are complicated by high temperature transformations, although the low temperature form occurs more frequently than the high temperature form. The three phases that can be identified are the linear copper co-ordination, triangular copper co-ordination and tetrahedral copper co-ordination [39]. The copper atoms are mainly in triangular, three-fold co-ordination with a Cu-S bond length of 2.3 Å and S-Cu-S angles ranging from 111.8° to 131.6°. The linear and tetrahedral co-ordinations could result from crystal distortions. The position of a copper atom could be imposed by another copper atom. The distance between the copper atoms was reported to be about 2.52 Å [39], which compared favourably with the Cu-Cu distance of 2.556 Å in metallic copper (with a resistivity of $1.7 \times 10^{-8} \Omega\text{m}$). Based on this, a metal-metal interaction or stability by metal-metal bonds is suggested [38], though it had been previously concluded that chalcocite is a *p*-type semi-conductor with resistivity varying from 2×10^{-4} to $1.0 \Omega\text{m}$ [38]. The structure of low-temperature chalcocite is

considered as interstitial compounds of copper in an approximate hexagonal-closest-packed framework of sulfur. The reported Cu-S bond length is less than the sum of the Cu^+ and S^{2-} ionic radii of 2.80 Å, but corresponds to the sum of the covalent radii. If covalency were ignored, the copper-deficient chalcocite minerals could be represented as $\text{Cu}^{+}_{2-2x}\text{Cu}^{2+}_x\text{S}^{2-}$ and each missing Cu^+ can be considered as an acceptor defect.

In the covellite crystal structure, which is illustrated in Figure 2-2 [40], copper occurs in both triangular and roughly tetrahedral co-ordination and four of the sulfur atoms are combined in S_2^{2-} dianion units. The formula which has been proposed for covellite is $(^{\text{IV}}\text{Cu}^+)_4(^{\text{III}}\text{Cu}^{2+})_2(\text{S}_2)^{2-}_2(\text{S}^{2-})_2$ in which Cu^{2+} occupies triangular and Cu^+ occupies tetrahedral sites [41]. The S_2 group has a bond length of 2.071 Å indicating a strong covalent bond and the strong bond in the S_2 group requires an average valence of copper to be less than 2. The average bond length in the $\text{Cu}(2+)\text{-S}$ tetrahedron is 2.312 Å, which is slightly greater than that of chalcopyrite and for $\text{Cu}(1+)\text{-S}$, it is 2.190 Å (Figure 2-2). The thermal motion is markedly varied and anisotropic for the different atoms in the covellite. Natural covellite is a *p*-type semiconductor, with a resistivity of $7 \times 10^{-7} \Omega\text{m}$.

The valence of copper in covellite is still a subject of dispute, however an X-ray photoelectron spectroscopic study has shown that copper is monovalent in most sulfides, including covellite [42]. In another study, the same instrument was used (by Folmer and Jellinek) to conclude that copper is monovalent in covellite and chalcocite [43]. The valence state of one is a shift from the previous position of divalent-copper in chalcocite, which was previously reported by Jellinek [44].

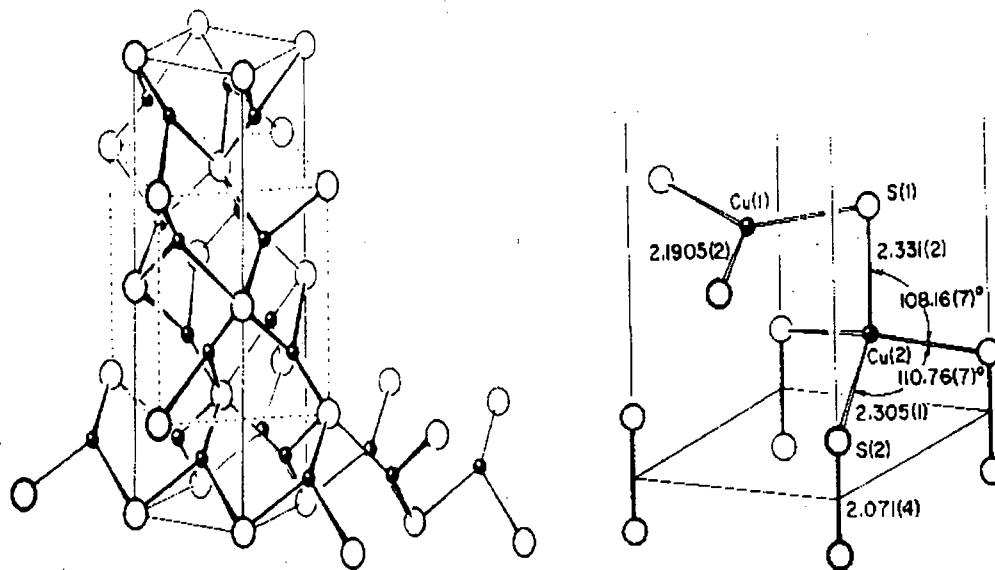


Figure 2-1. Crystal structures, inter-atomic bond lengths and angles of chalcocite [37].

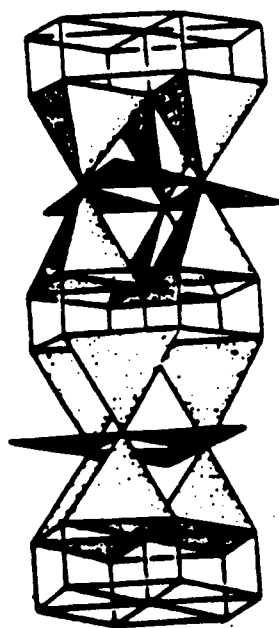


Figure 2 -2. Crystal structure of covellite [40].

2.1.2 Leaching Implications of the Structures

In the structures of chalcocite and covellite, the top of the valence band is formed by a band (sometimes partly filled) of largely copper $3d$ orbital character which is able to accommodate variations in metal concentration [45,46]. The leaching of chalcocite by ferric ion media requires successive removal of metal atoms from the structure, to form sequences of non-stoichiometric copper sulfides before second stage covellite (CuS) is formed.

Also, the sulfur sublattice behaves rather as a framework within which the metal atoms are quite mobile even at ambient temperature. The triangular co-ordination of copper atoms has been found only in a few species of sulfides which are rich in copper, others are bornite, anilite and stromeyerite (AgCuS).

2.1.3 Thermodynamic Considerations

The stability domains of sulfide minerals in aqueous media are commonly shown in Eh-pH diagrams [47]. Figure 2-3 shows the Eh-pH diagram for the $\text{Cu-S-H}_2\text{O}$ system at 25°C . It indicates that both chalcocite and covellite are stable in the water stability-zone (acidic and basic solutions). At low pH values (acidic media), low oxidizing-potentials between 0.2 and 0.4 volts are required (according to the diagram) to convert these copper sulfides into sulfur species and soluble copper. In neutral or basic solutions, insoluble oxides are formed and low oxidizing potentials are required to decompose these minerals. The stability of the species depends on the equilibrium constant (K) of the reactions involved and this constant is a function of the temperature of reactions. Therefore, a specie which is not stable at 25°C may be stable at higher temperatures, while others may decrease or vanish. In order to construct an Eh-pH diagram (at a particular temperature) relative to standard hydrogen electrode (SHE) at 298K, there is need to calculate the free energy for all the species involved at this temperature.

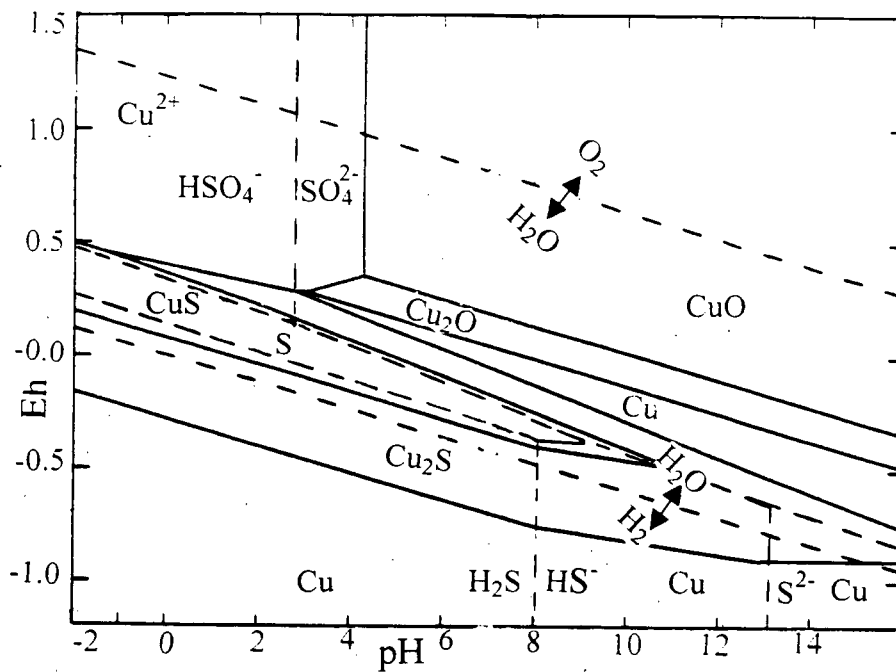


Figure 2-3. Eh-pH diagram for the Cu-S-H₂O system at 25°C, activity of copper ion at 0.01 mol/L and other ionic species at unit activity.

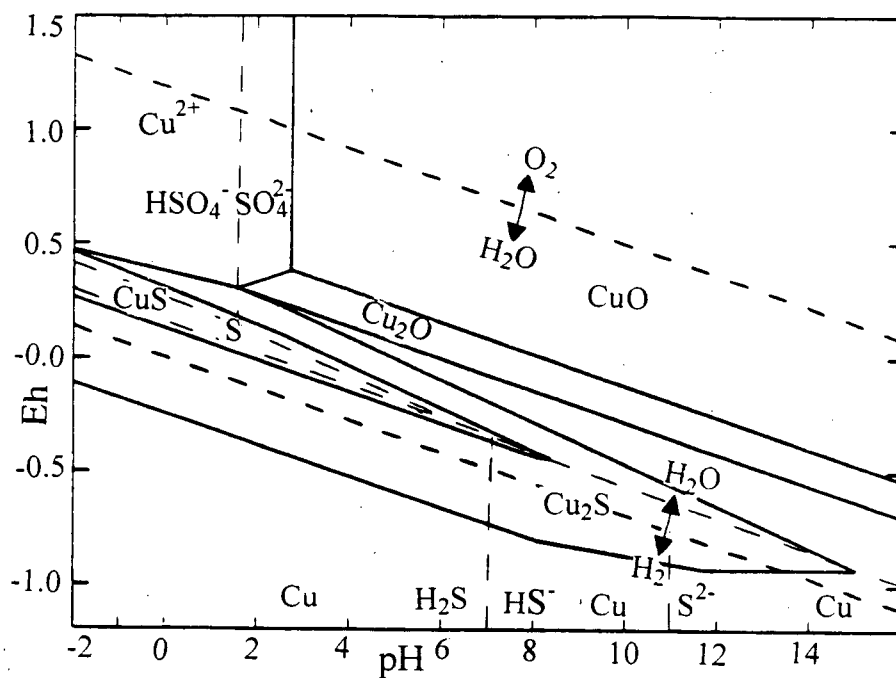


Figure 2-4. Eh-pH diagram for the Cu-S-H₂O system at 75°C, activity of copper ion at 0.01 mol/L and other ionic species at unit activity.

The free energy at any temperature can be calculated from the following equation;

$$G_T^o = G_{298}^o + C_p^o \Big|_{298}^T \theta - (T - 298) S_{298}^o \quad (2-1)$$

Where; $\theta = T - 298 - T \ln \left(\frac{T}{298} \right) \quad (2-2)$

The detailed derivations of equation 2-1 and equation 2-2 by Dixon [48] are included in Appendix 1.

For the non-ionic species, the heat capacity can be obtained from the following equation;

$$C_p^o \Big|_{298}^T = a + b \left(\frac{T + 298}{2} \right) + \frac{c}{298T} \quad (2-3)$$

where a, b and c are the heat capacity functions, which can be obtained from the literature [49].

For the ionic species, the method of Criss and Cobble [50 and 51] can be used to determine the heat capacity by the following equations;

$$C_p^o \Big|_{298}^T = \alpha_T + \beta_T \bar{S}_{298}^o \quad (2-4)$$

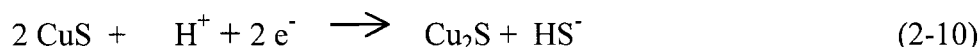
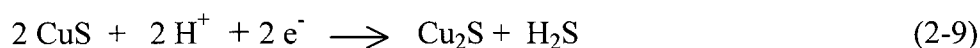
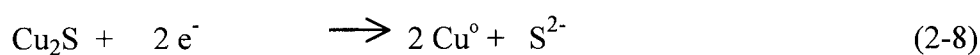
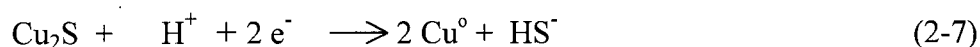
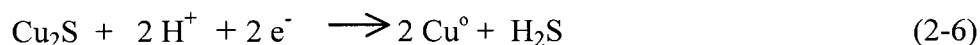
$$\bar{S}_{298}^o = S_{298}^o + z \bar{S}_{abs}(H^+) \quad (2-5)$$

where α and β are the Criss-Cobble heat capacity constants, which are available for 60, 100, 150, 200, 250 and 300°C. The values at 75°C can be obtained by interpolation.

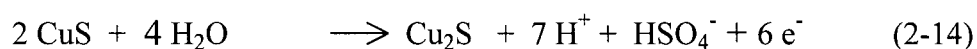
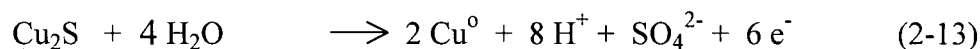
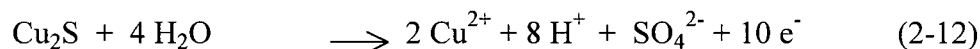
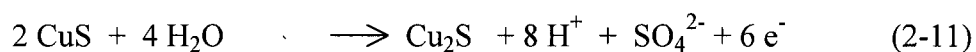
The values of free energy (G_{298}^o) are available in the literature [52] for equation 2-1. Based on the above techniques, a high temperature (75°C) stability diagram for the Cu-S-H₂O was developed and this is shown in Figure 2-4. In comparison to Figure 2-3, the Cu²⁺ and HSO₄⁻ stability-zone decreased while that of SO₄²⁻ decreased. The stability-zone of covellite (pH range) also decreased. The direct oxidation of the minerals to Cu₂O

at pH of about 2.7 is possible at high temperature and there are slight decreases (by about 20 mV) in the oxidation potentials required to dissolve the minerals at pH of about 1.0. The examination of these Eh-pH diagrams (Figure 2-3 and 2-4) reveals that chalcocite and covellite decomposition could occur by about nine reactions.

Reduction:



Oxidation:



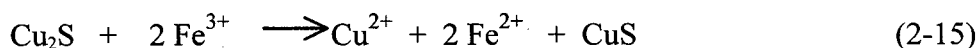
The reduction routes of leaching chalcocite and covellite have not been reported in the literature.

When chalcocite and covellite are oxidatively leached, none of the reactions depicted by equations 2-11 to 2-14 is observed. The diagrams also predict that covellite will oxidize to chalcocite by equation 2-11 and 2-14, these reactions occur over geologic time [53].

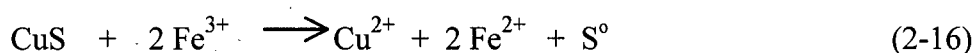
2.1.4 Multiple Stage Dissolution of Chalcocite

The dissolution of chalcocite in ferric sulfate solutions is usually reported as occurring in two distinct stages;

First stage:



Second stage:



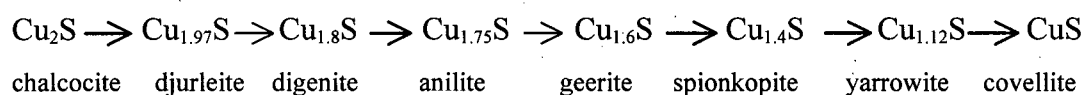
The second stage is much slower and much more temperature sensitive than the first. These two equations are convenient, but they are over-simplified representations of what actually takes place. In reality, the first stage consists of a series of steps in which the reaction products may or may not be observed experimentally depending on the rate of transformation of the successive phase. Previous electrochemical studies have revealed with accuracy some phase transformations which can take place under different oxidizing conditions. It was proposed by Cavallotti and Salvago [54] that Cu_2S first transforms to djurleite ($\text{Cu}_{1.97}\text{S}$), then to digenite ($\text{Cu}_{1.8}\text{S}$), and anilite ($\text{Cu}_{1.75}\text{S}$), before transforming to blue-remaining covellite ($\text{Cu}_{1.2}\text{S}$). The transition from blue-remaining covellite to normal covellite is believed [14] to be possible only under conditions of high potential or current density (1400 mV/SHE or 9 A/dm²).

From the leaching experiments of chalcocite (Cu_2S) and digenite ($\text{Cu}_{1.8}\text{S}$) in ferric sulfate $\text{Fe}_2(\text{SO}_4)_3$ and ferric chloride FeCl_3 , Moh [55] reported that the non-stoichiometric covellite ($\text{Cu}_{1.2}\text{S}$) is formed only as an intermediate product prior to the appearance of normal covellite. The long period of time required for this reaction is believed to be responsible for the slow kinetics of second stage leaching. Ignoring the transformation to digenite, Moh proposed the following equation for the overall reaction of the solid phase transformation.



In this proposition, x varies from 0.1 to 0.4. The idea that the blue remaining covellite is formed and is responsible for the slow dissolution of second stage covellite became acceptable because little knowledge was available then, on the mineralogy of the blue-remaining (*blaubleibender*) covellite.

Whiteside and Goble [56] later classified the reaction products into a series of non-stoichiometric copper sulfides by using X-ray diffraction-patterns (for the structural changes) and electron-microprobe analyzer (for the chemical changes) to analyze the grains. The following sequence of transformations was postulated;



At ten percent copper extraction, the major phase is supposed to be digenite (theoretically based on the stoichiometry of the solid), while covellite is the major phase formed at fifty percent copper extraction based on the copper to sulfur atomic ratio of each phase. It was shown that two or more phases could be present at a particular copper extraction level. At 33% copper extraction, geerite, spionkopite and yarrowite (with a small percentage of covellite) were present. The experiments shed light on the composition of the previously classified "blue-remaining" covellite mineral, which are geerite, spionkopite and yarrowite. The yarrowite phase, and to a lesser extent, spionkopite are natural occurring minerals and observed copper sulfide components of leached heaps or dumps, while geerite occurs very rarely as a natural mineral. The experiment, though without solution control and with a limitation based on the fact that compositions determined for selected individual grains do not give the gross representative of the reaction-product, revealed non-homogenous leaching of the grains and the high rate of leaching up to the formation of second stage covellite. In this work, first stage is referred to as the end of 50% copper extraction and the formation of second stage covellite. In addition to the above phases, which are formed prior to second stage covellite, another phase was identified by Whiteside and Goble as copper disulfide

(CuS₂). This was identified from covellite dissolution product diffraction patterns, which resembled that of the high pressure compound CuS₂. This has been synthesized only under high pressures and temperatures in excess of 10 kbars and 300°C respectively from covellite and sulfur [57], and has a cubic (NiS₂) pyrite structure. At 25°C, it is completely stable only above 8 kbars and it is metastable at 130°C and 1 atmospheric pressure [58]. However, thermodynamic data on this compound are not available in the literature and little or nothing has been reported about its chemical properties. The natural occurring copper disulfide mineral (villamaninite) has been identified and reported in the literature [59].

2.2 Polarization Behaviour of Chalcocite and Covellite

The anodic dissolution reaction of a covellite electrode was also observed to be slower than that of chalcocite by Cavalotti and Salvago [54]; this was attributed to the greater energy required to break the sulfur sub-lattice formed on the covellite. In a similar electrochemical study by Wright [60], potential sweeps for chalcocite produced a smooth potential-current behaviour, while that of covellite resulted in a series of passivation events as shown in Figure 2-5. The curves revealed that the polarization characteristics of synthetic Cu₂S and CuS are markedly different. Whereas the polarization curve for Cu₂S was relatively simple and no passivation effects were apparent, the curve for CuS produced a series of current peaks indicating that some type of passivation was taking place. It was probable that the current peak is due to a process of film formation and subsequent breakdown, or the successive oxidation of the intermediate reaction products.

In order to investigate the influence of existing reaction layers on the polarization behaviour of Cu₂S and CuS, a series of anodic polarization curves were produced for electrodes which had been previously oxidized at specified potential for 24 hours. These are shown in Figure 2-6 and Figure 2-7 [60]. The polarization curves for chalcocite were similar regardless of the extent or the potential of the previous oxidation. This suggests that oxidation products have little effect on the rate of dissolution of Cu₂S. The slime,

that oxidation products have little effect on the rate of dissolution of Cu_2S . The slime, which formed on the surface of the electrode was highly porous or non-adherent. In fact, during the pre-oxidation process, the agitated solution became progressively more cloudy as electrolysis proceeded and this could be the reaction products, which were breaking away from the electrode surface.

On the other hand, the pre-oxidized covellite electrode was strongly passivated from the outset, suggesting that the oxidation products formed during pre-oxidation formed a protective layer on the covellite. Notably, the solution remained clear throughout the pre-oxidation process, which revealed that the reaction products did not break away from the electrode surface. However, the oxidation products which could be causing the passivation were not identified and nothing was mentioned about their properties.

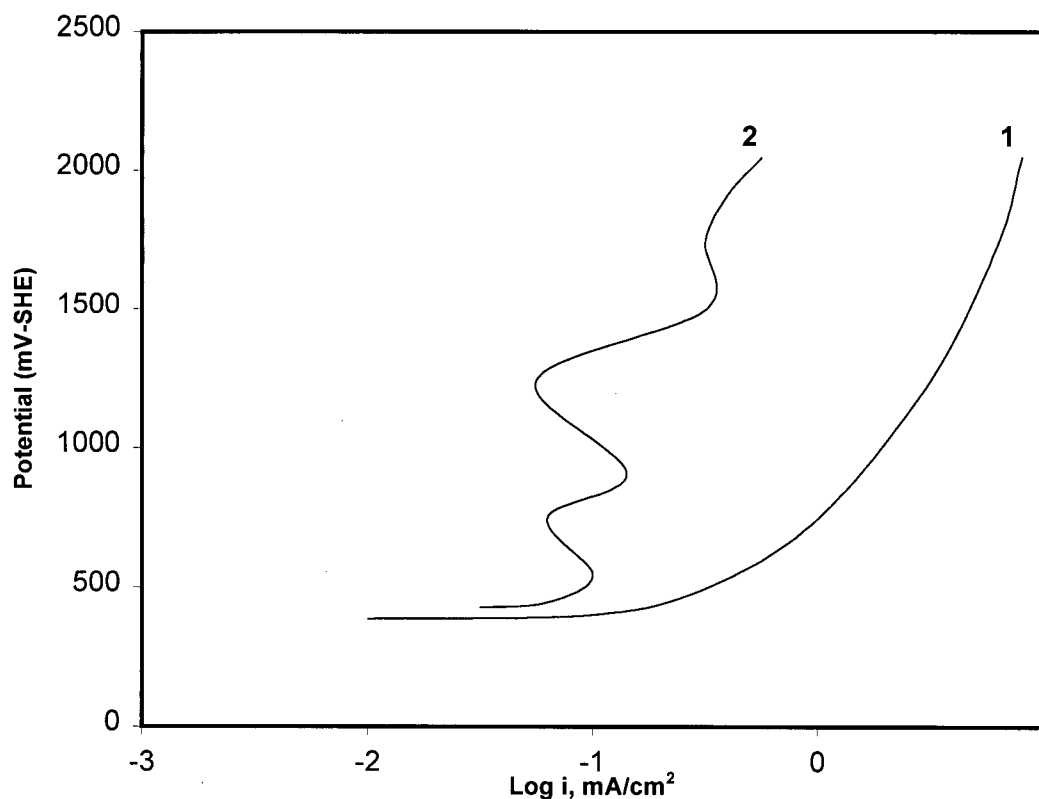


Figure 2-5. Anodic polarization curves for synthetic Cu_2S (1) and CuS (2) electrodes, Scan rate, 1000 mV/min (0.01 M CuSO_4 , pH 3) after Wright [60].

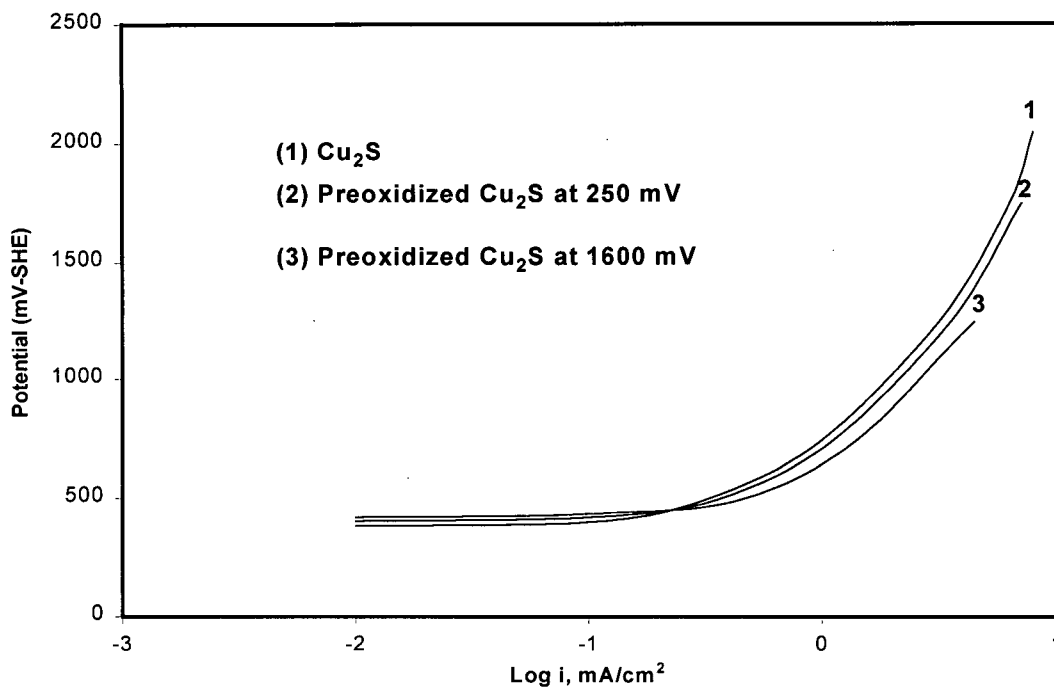


Figure 2-6. Anodic polarization behaviour of a pre-oxidized Cu_2S electrode (2) and (3) (0.01 M CuSO_4 , pH 3) [60].

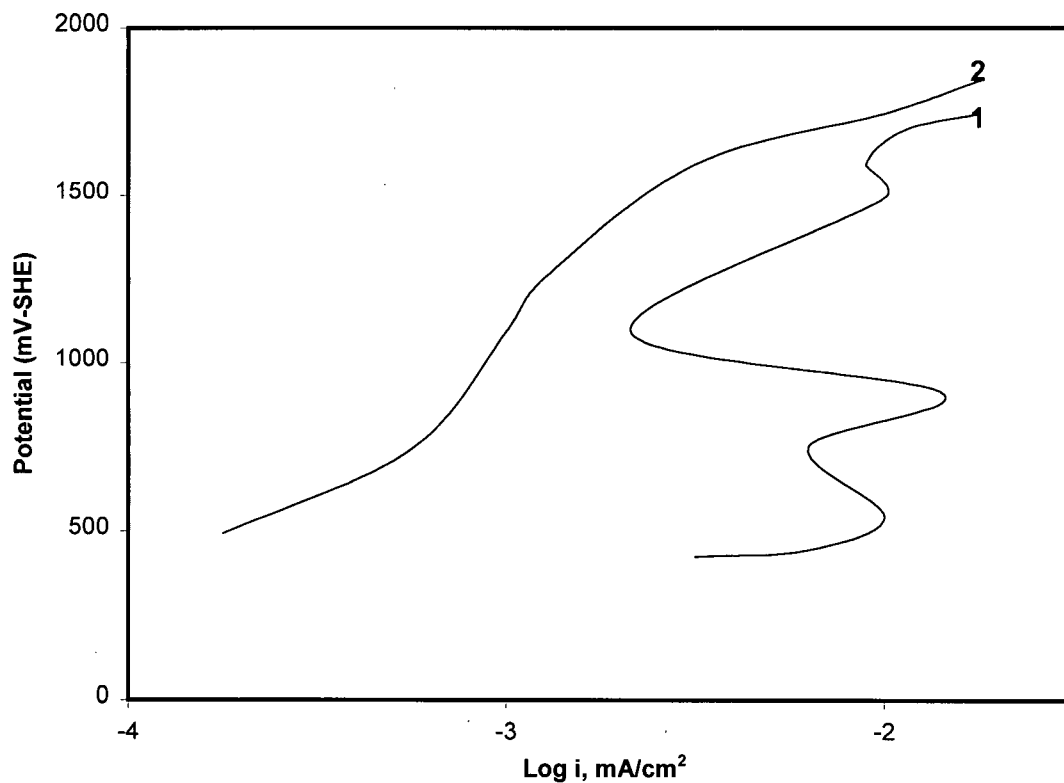


Figure 2-7. Anodic polarization behaviour of a CuS (1) and pre-oxidized CuS (2) (0.01 M CuSO_4 , pH 3) [60].

Mao and Peters [17] studied the direct electrorefining of chalcocite (Cu_2S) anodes. They found that a volume decrease accompanied the electrolysis, during which pores and cracks formed within the CuS-S^0 reaction product layer, which were then filled with electrolyte. The copper ions enter the electrolyte at the bottom of these pores and cracks, and must be transported to the surface by diffusion. Thus, at high currents, the concentration gradient of Cu^{2+} increased continuously until, finally, the solubility of $\text{CuSO}_4 \cdot 5\text{H}_2\text{O}$ was reached and the salt crystallizes within the pores. At this point, a massive anode would be passivated as shown in curves I and II of Figure 2-8 [17].

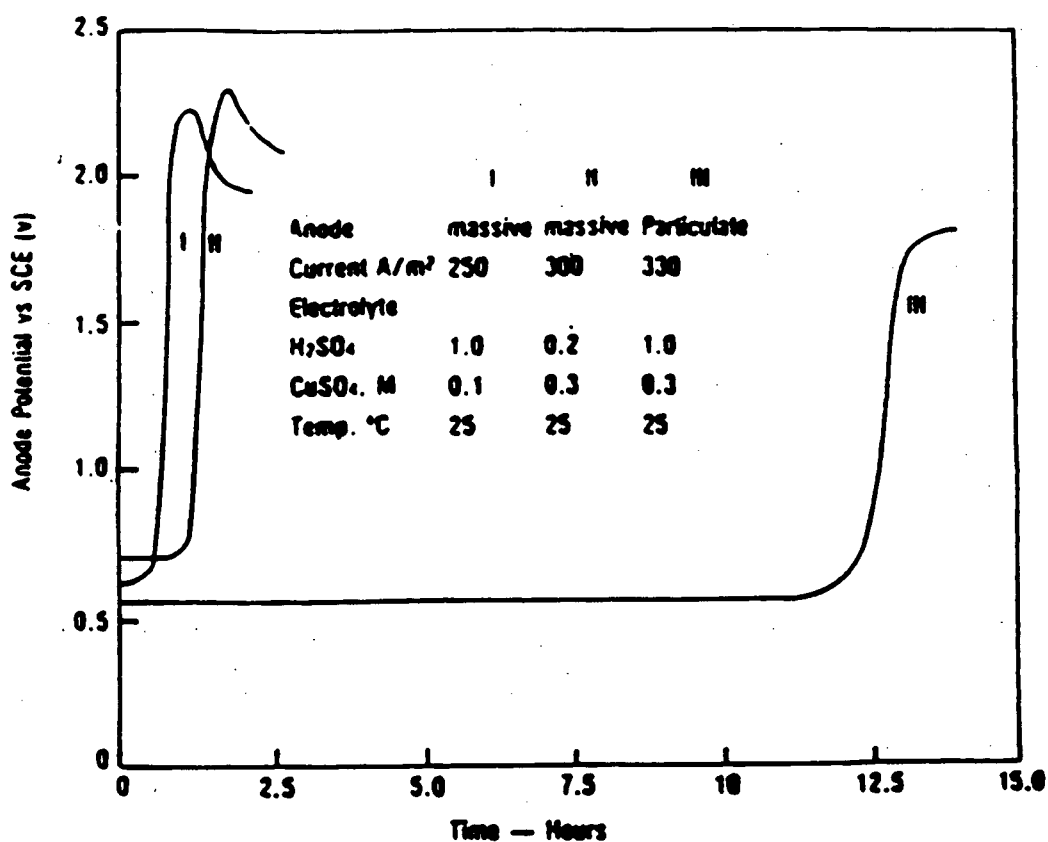


Figure 2-8. Passivation behaviour of massive and particulate Cu_2S anodes, after Mao and Peters [17].

However, a particulate anode took much longer to achieve passivation as shown in curve III, because the steep concentration gradients could not be established at the higher porosity. In fact, at the time of passivation, Mao and Peters calculated that sufficient coulombs had already been passed to convert the anode completely to a mixture of covellite and sulfur. Hence, they postulated that the passivation in this case was probably due to the formation of protective sulfur layer on the remaining covellite particles. It is not obvious if crystallization of copper sulfate salt could cause passivation of grains of chalcocite or second stage covellite in acidic ferric leaching of the minerals.

2.2.1 Effect of Electrolytes on Polarization

Venkatachalam and Mallikarjunan [15] carried out polarization tests on anodes of chalcocite, synthetic copper-iron mattes and commercial 40% grade copper matte in sulfate, chloride and mixed sulfate-chloride electrolytes (Figures 2-9 to 2-11). As shown in Figure 2-9, anode passivation occurred much more readily in the sulfate electrolytes than in the chloride electrolytes.

Also, the addition of chloride salt to a sulfate bath delayed passivation significantly, even when low concentration of chloride was added. It was concluded that the addition of sodium chloride to sulfate solutions reduced the passivity developed at the sulfide electrodes. However, the process through which Cl^- depassivates the electrode was not provided.

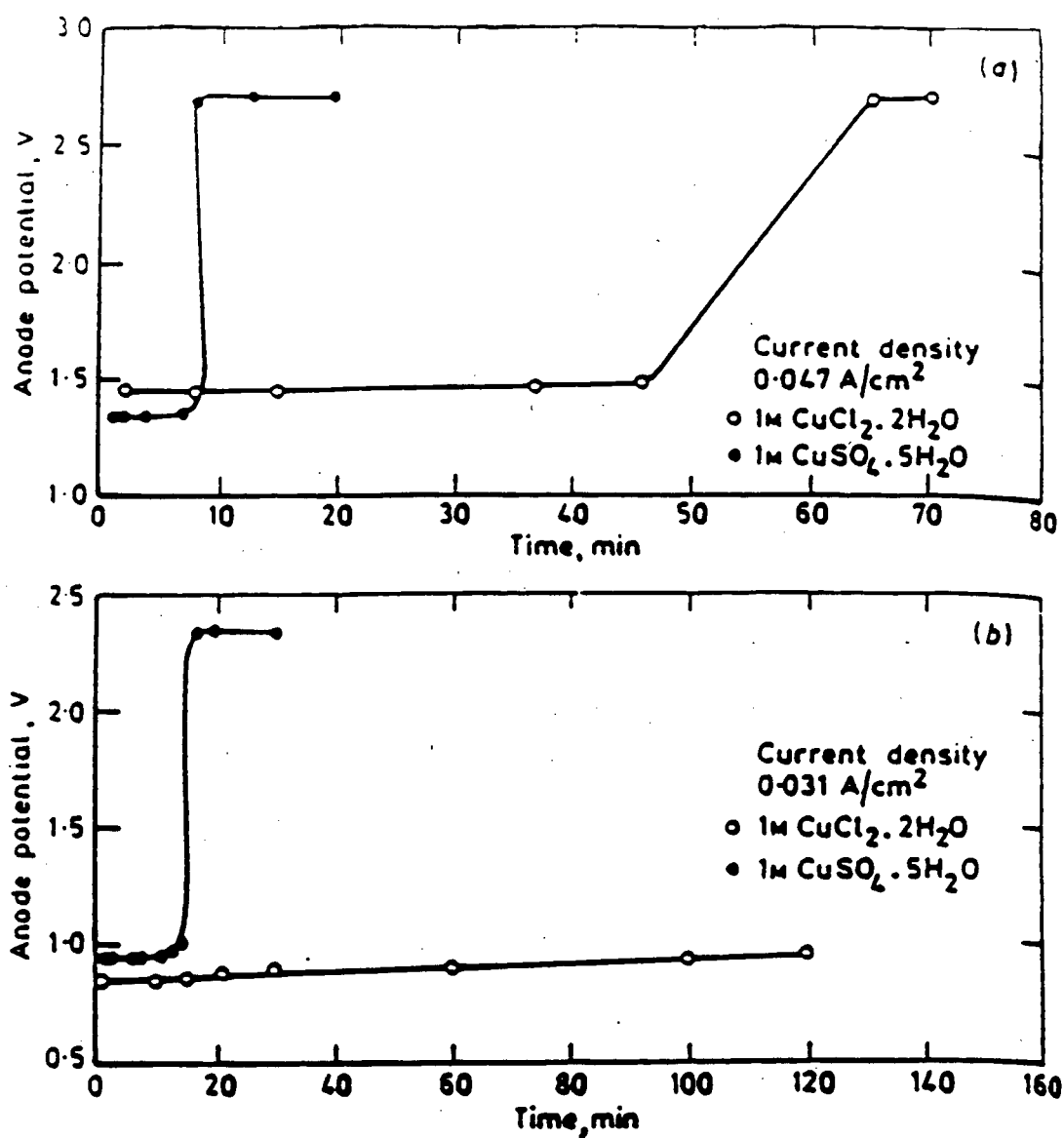


Figure 2-9. Passivation behaviour of chalcocite anodes in cupric sulfate and cupric chloride electrolytes, after Venkatachalam and Mallikarjuna [15].

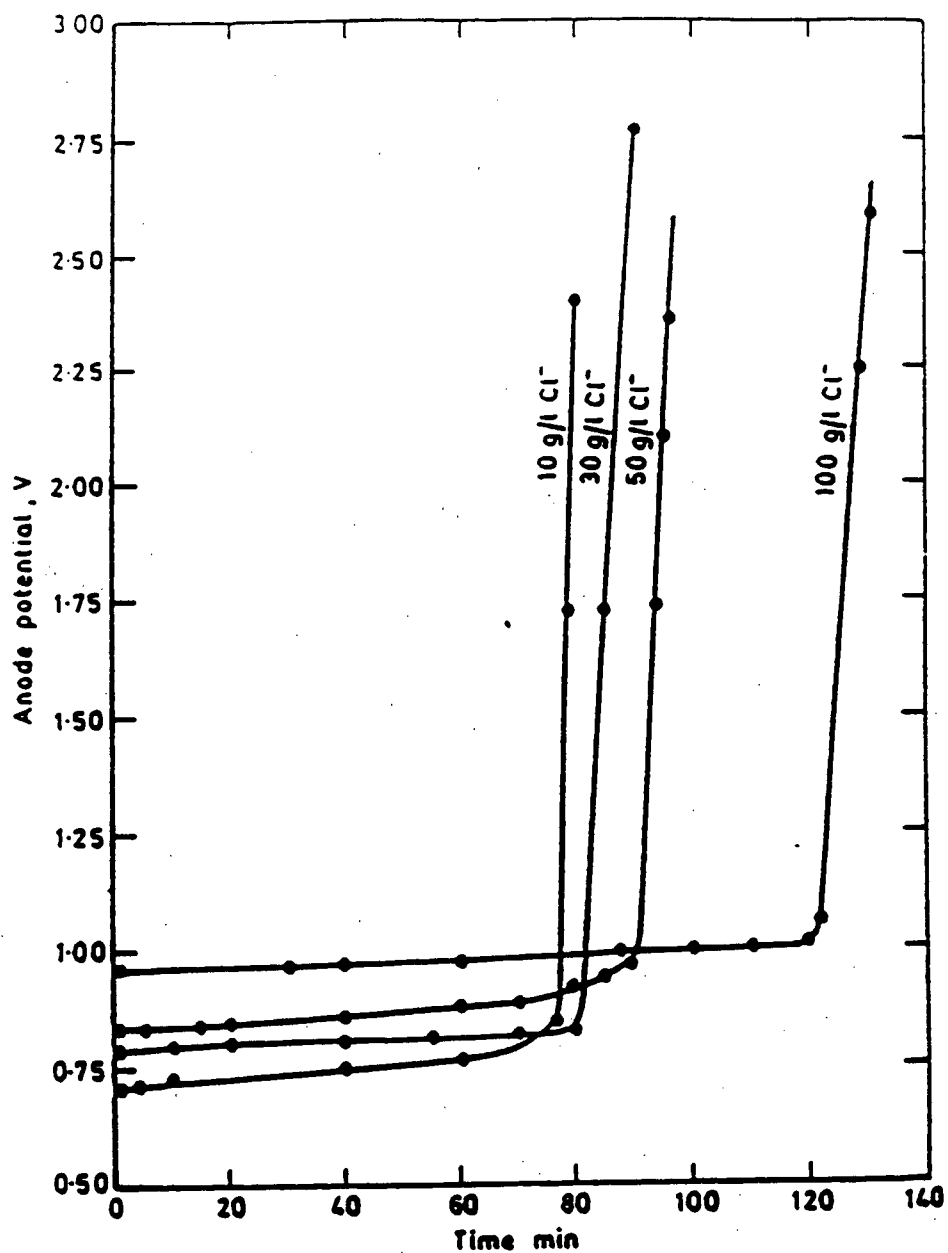


Figure 2-10. Passivation behaviour of Cu₂S anodes in H₂SO₄ and NaCl electrolytes, after Venkatachalam and Mallikarjunan 15].

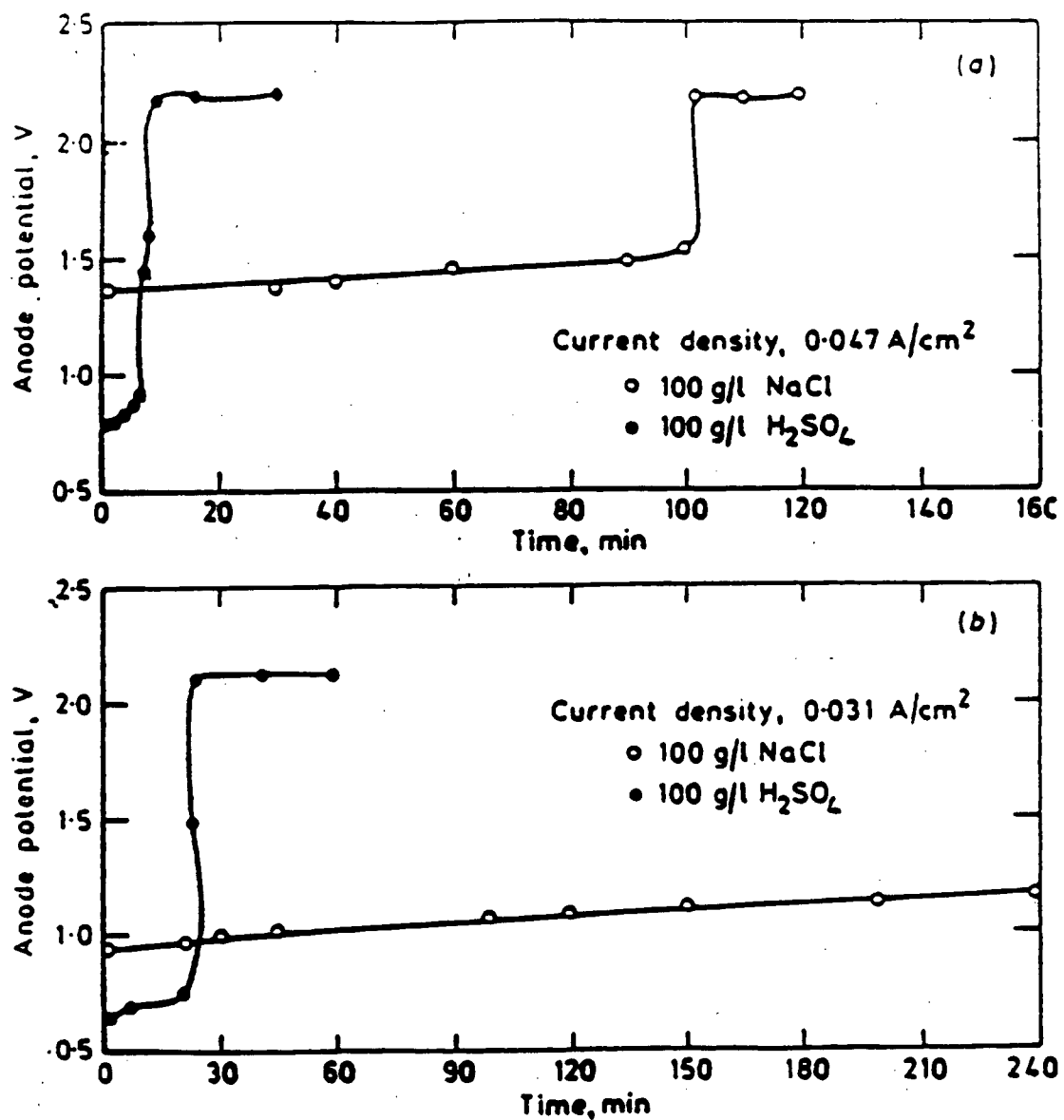
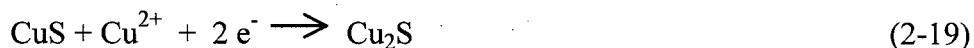


Figure 2-11. Effect of chloride additions on the passivation behaviour of Cu_2S anodes in a Sulfate electrolyte, after Venkatachalam and Mallikarjuna [15].

Cavalotti and Salvago [54] investigated the cathodic behaviour of covellite electrodes in solutions containing large amounts of cupric ions and small amounts cuprous ions in acid solutions of sulfate, perchlorates, perchloric acid and sulfuric acid which were saturated with H₂S. When elemental sulfur was present in the starting electrode, the cathodic process observed was as follows;



When no elemental sulfur was present initially, the potential was found to be near the theoretical value for the following reaction;



The Cu₂S (in equation 2-19) was identified by using X-ray diffraction patterns. However, in a cupric chloride CuCl₂ electrolyte, no Cu₂S was obtained, but the following reaction occurred instead;



It was postulated that chloride de-passivates covellite through this reaction by removing cupric ions from solution and preventing reaction represented by equation (2-18). From this investigation, (cathodic) reaction products were postulated to be responsible for passivation.

2.2.2 The Effect of Temperature on Polarization

The passivation behaviour of particulate Cu₂S anodes at various temperatures is shown in Figure 2-12, after Mao and Peters [17]. At 22°C, they postulated that the solubility of CuSO₄·5H₂O was low enough to passivate the highly porous particulate

anode by copper sulfate salt formation. However, at higher temperatures, passivation was attributed to the formation of a protective sulfur layer.

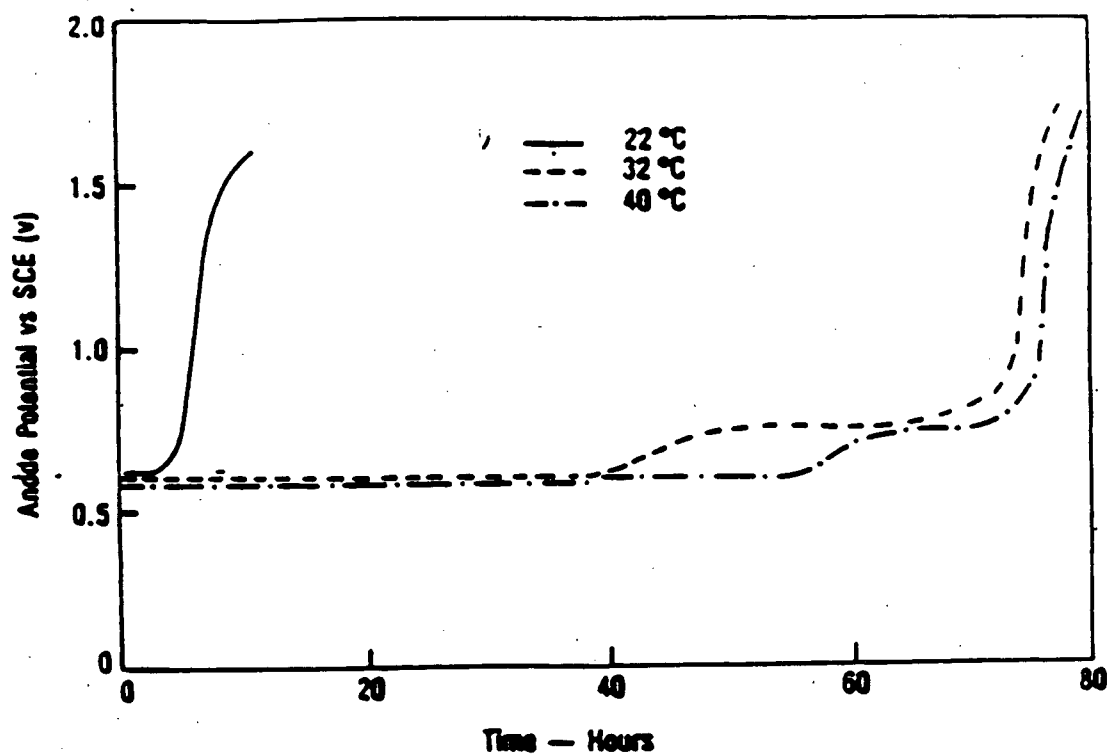


Figure 2-12. Effect of temperature on the passivation behaviour of particulate Cu_2S anodes, after Mao and Peters [17].

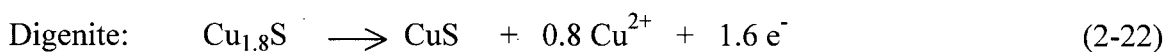
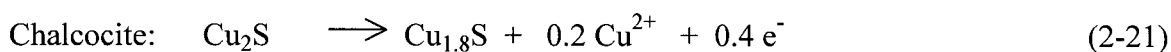
2.3 Mixed Potential Theory of Leaching

An electrochemical process which involves two simultaneous reactions has often been proposed to account for the aqueous oxidation of sulfides. The reduction of the oxidant and oxidation of the mineral take place at the mineral surface, while electrons are transferred through the sulfide lattice. This process is similar to the corrosion of metals and the electronic conductivity of copper sulfides makes it possible. The rates of these

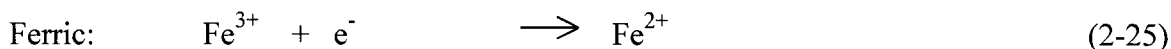
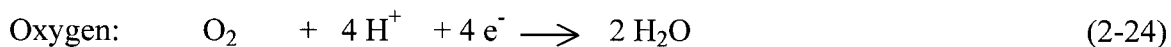
electrochemical reactions are functions of the electrochemical potential in addition to the concentrations of the species taking part in the rate-determining process. This theory was originally presented by Nicol *et al.* [61] and later refined by Wadsworth [62] and Dixon [63].

The oxidative dissolution of chalcocite, and many other sulfide minerals, is a short-circuited electrochemical process, or corrosion couple, involving both anodic and cathodic steps.

Anodic decomposition of the mineral phases;



Cathodic reduction of oxidant:



The sulfide mineral, which is a semi-conductor, acts as a conduit for electron transfer between cathodic and anodic sites on the mineral surface. Also, because the cell is short-circuited, it develops a mixed potential somewhere between the reversible potentials of the two half-cells.

In general for electrochemical reactions, the difference between the actual cell potential and the reversible potential of the half-cell, E_e , is called the overpotential, η . This provides the driving force for reaction. Hence, each half-cell reaction bears a certain fixed relationship between rate and potential (typically described by the Butler-Volmer equation). In electrochemical reactions, this rate is manifested as current density, i (or j in some literature), which has units of current per unit electrode surface area.

In any electrochemical cell, electrons must be conserved. Hence, assuming equal surface areas for the anodic and cathodic processes, then the mixed potential will be that

at which the rates of both half cells are equal and opposite, according to the rate-potential relationships of each cell.

This concept is illustrated by the polarization curves in Figure 2-13 [62], for the dissolution of a metal sulfide (MS) in the presence of a cationic oxidant N^{n+} (such as Fe^{3+} in acid solution), which has a more positive equilibrium potential. In any electrochemical reaction, the two half-cell reactions are short-circuited and the solid phase acquires a mixed potential (E). It worth noting that E is not equidistant between the reversible (or equilibrium) potentials E_{e1} and E_{e2} , but is instead located such that the partial currents, I_1 and I_2 (expressed here as current densities, i_a and i_c), are equal and opposite. The anodic overvoltage η_a is defined as $(E - E_{e1})$ and is positive. The cathodic overpotential η_c is defined as $(E - E_{e2})$ and is negative. The electrochemical basis for electron transfer in simple reversible reactions may be expressed quantitatively by the Butler-Volmer equation, which relates the current density at a solid-solution interface to the established overpotential (for a single electron transfer process).

$$i = z F \vec{k} \exp\left[\frac{\beta FE}{RT}\right] - z F \overleftarrow{k} [Cu^{2+}] \exp\left[\frac{-(1-\beta)FE}{RT}\right] \quad (2-26)$$

The first term in the above equation is the partial current density for the anodic (forward) direction of equation 2-23 and the second term is the partial current density for the cathodic (reverse) direction. F is the Faraday, k represents the rates for the forward and reverse directions, respectively, in the absence of potential. β is the transfer coefficient. The activity coefficient is assumed to be unity in this equation.

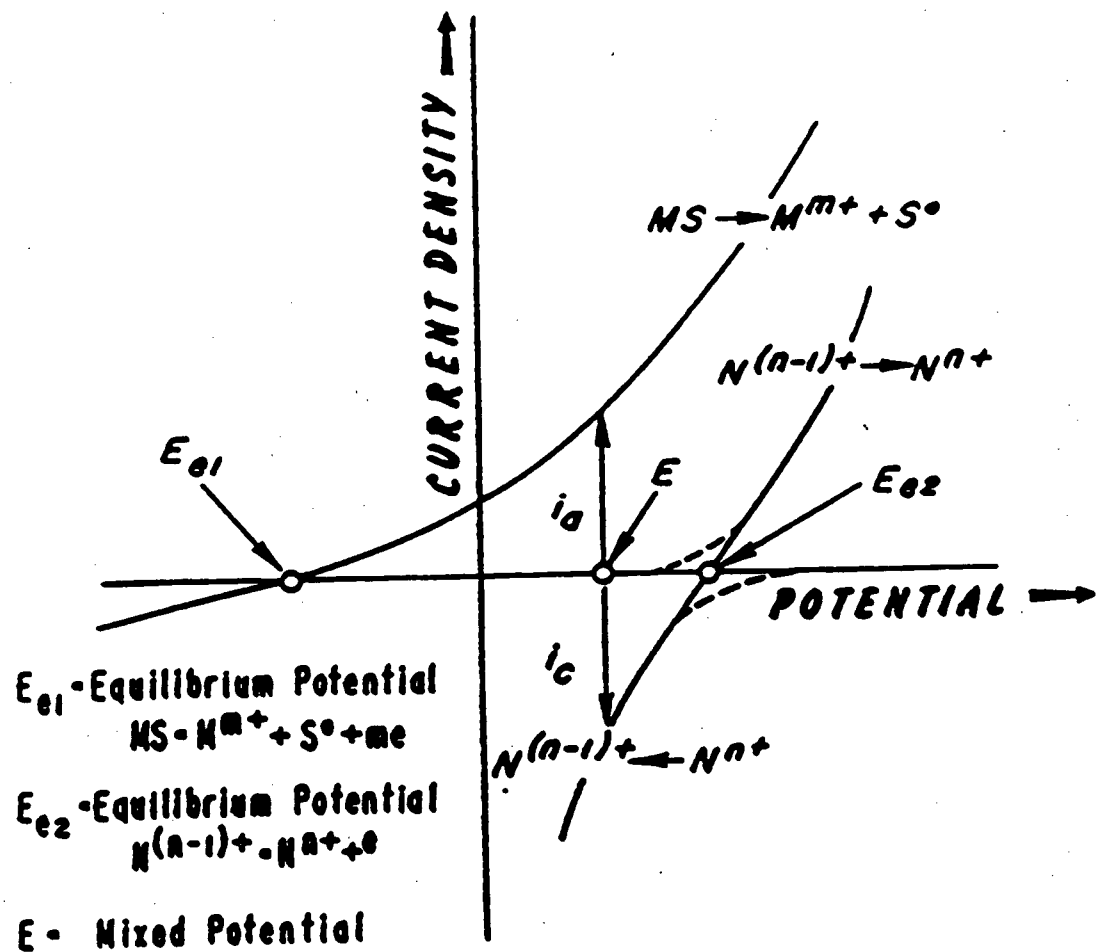


Figure 2-13. Current density potential diagram showing curves for metal sulfide with rest potential E_{e1} and redox-ions with rest potential E_{e2} , which formed mixed potential E [62].

Also, the relationship between the rate (current density) and the concentration of reactants can be quantified by using the simpler forms of the Butler-Volmer equation. This depends on the type of leaching. Generally, there are three major types, according to Dixon [63] and these are presented as follows;

2.3.1 Type I Leaching

This type is observed when the exchange current densities of the two half cells (ferric/ferrous and the mineral) are similar in magnitude, but the reversible potentials of the half-cells are far apart. The situation is shown schematically in Figure 2-14 below. The current density of either half-cell reaction is j_d , the subscript d represents dissolution. This particular diagram represents the simplest situation to analyze, since both the ferric and the dissolving mineral are in their so-called "high-field regions" and the mixed potential intersects their Tafel slopes. The anodic and cathodic overvoltage are equal. In some cases, the cathodic overvoltage will be much more than that of the anodic or vice versa. The anodic dissolution rate of many sulfide minerals is found to be limited by a single electron transfer step. Hence, the anodic (dissolution) current density, which is similar to the first term in equation 2-26 may be taken here as:

$$j_d = 2 F k_a \exp \left(\frac{\alpha_a F E_M}{RT} \right) \quad (2-27)$$

The cathodic (ferric reduction) current density is:

$$j_c = F k_c a_{\text{Fe}^{3+}} \exp \left(\frac{-(1 - \alpha_c) F E_M}{RT} \right) \quad (2-28)$$

If we set these equal and solving for the mixed potential:

$$E_M = \left(\frac{RT}{\alpha_a + 1 - \alpha_c} \right) \frac{1}{F} \ln \frac{k_c a_{\text{Fe}^{3+}}}{2 k_a} \quad (2-29)$$

Hence, the leaching current density is:

$$j_d = j_a = -j_c = 2Fk_a \left(\frac{k_c a_{\text{Fe}^{3+}}}{2k_a} \right)^{\frac{\alpha_a}{\alpha_a + 1 - \alpha_c}} = Fk_c a_{\text{Fe}^{3+}} \left(\frac{2k_a}{k_c a_{\text{Fe}^{3+}}} \right)^{\frac{1 - \alpha_c}{\alpha_a + 1 - \alpha_c}} \quad (2-30)$$

In most cases, $\alpha_a \approx \alpha_c \approx 0.5$. Hence:

$$j_d = F(2k_a k_c a_{\text{Fe}^{3+}})^{0.5} \approx Fk_d [\text{Fe}^{3+}]^{0.5} \quad (2-31)$$

The rate of leaching is proportional to the square root of the ferric ion concentration.

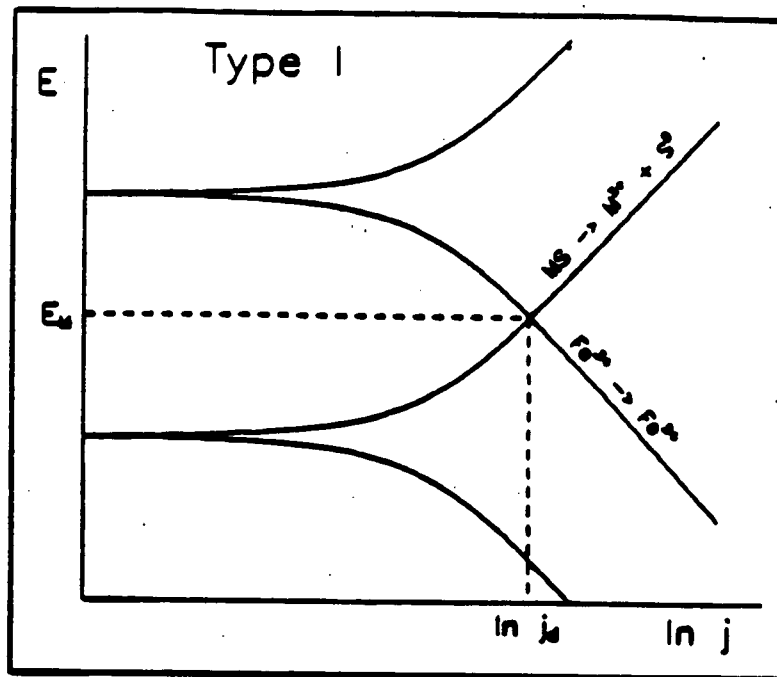


Figure 2-14. Polarization curve for Type I Leaching.

2.3.2 Type II Leaching

This type is observed when the exchange current density of the oxidizing couple is higher than that of the dissolution reaction by several orders of magnitude, and the mixed potential thus corresponds to the reversible potential of the oxidizing couple as

shown in Figure 2-15. For this to occur, the reduction of dissolved oxidants takes place more or less reversibly on the surface of the minerals. This is always true for the $\text{Cu}^{2+}/\text{Cu}^+$ couple and often true for the $\text{Fe}^{3+}/\text{Fe}^{2+}$ couple. The mixed potential can be represented as follows;

$$E_M = E^0 - \frac{RT}{F} \ln \frac{a_{\text{Fe}^{2+}}}{a_{\text{Fe}^{3+}}} \quad (2-32)$$

By inserting equation 2-32, into equation 2-27 then;

$$j_d = 2Fk_a \left(\frac{a_{\text{Fe}^{3+}}}{a_{\text{Fe}^{2+}}} \right) \exp \left(\frac{\alpha_a F E^0}{RT} \right) \approx Fk_d \left(\frac{[\text{Fe}^{3+}]}{[\text{Fe}^{2+}]} \right)^{0.5} \quad (2-33)$$

In this type, the leaching rate is proportional to the square root of the ratio of concentrations of the oxidized and reduced forms of the oxidant.

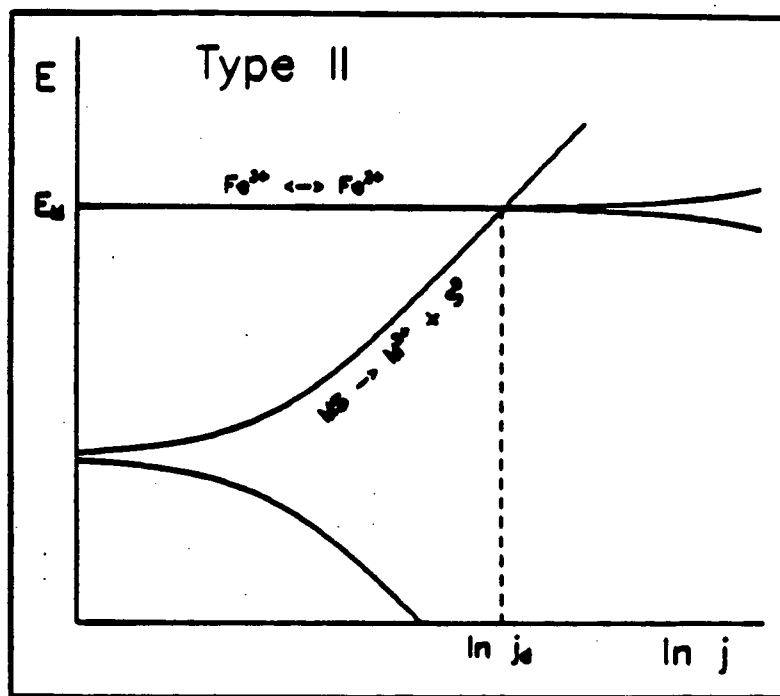


Figure 2-15. Polarization curve for Type II Leaching.

2.3.3 Type III Leaching

In some systems, the leaching reaction is particularly fast and the leaching rate is limited by mass transfer of the oxidant to the mineral surface. This is shown in Figure 2-16 and in this case, the leaching reaction will proceed at the limiting current density of the ferric/ferrous couple (cathodic limiting current density). Hence, the leaching current density is given by:

$$j_d = \frac{FD_{\text{Fe}^{3+}}a_{\text{Fe}^{3+}}}{\delta} \approx Fk_d[\text{Fe}^{3+}] \quad (2-34)$$

In this type, the leaching rate is proportional to the oxidant concentration and this will be the case when the reversible potentials of the half-cell reactions involved in the leaching are relatively far apart. It is expected that Type III will revert to Type II leaching above a certain critical oxidant concentration.

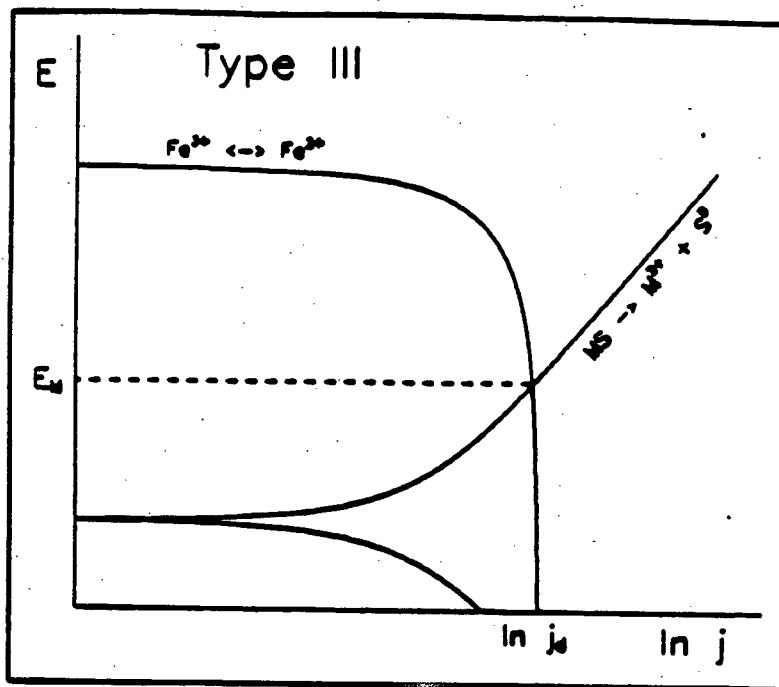


Figure 2-16. Polarization curve for Type III Leaching.

2.4 Application of Mixed Potential Theory to Leaching

The qualitative application of mixed potential theory to the kinetics of chalcocite and covellite leaching is useful in providing an explanation for the observed sudden change from one kinetic regime to another and could provide a fundamental explanation for the sequential phase transformations associated with some sulfide leaching reactions. In order to apply the mixed potential theory (which has been presented in section 2.3), the first step is to obtain experimentally the polarization curve of the mineral. Then, calculate the cathodic curve for the ferric/ferrous couple (based on the electrode kinetics of this couple) which has been previously investigated on platinum electrodes [64]) and finally, combine the polarization curve of the mineral with that of the ferric/ferrous couple.

2.4.1 Application of Mixed Potential Theory to the Leaching of Chalcocite

The approach enumerated in section 2.4 was used by Li *et al.* [65] to construct the steady-state polarization curves for anodic dissolution of chalcocite and (theoretical) cathodic reduction of ferric ions on graphite. This is shown in Figure 2-17; the data used for the anodic polarization of the chalcocite were obtained from the previous work of Wadsworth and Zhong [66]. From this figure, the mixed potential of the half-cell is close to the anodic rest potential (of the mineral) at low concentrations of ferric ions. At low ferric ion concentration range of 0.005 and 0.05 mol/L, Type III leaching is envisioned, the dissolution of chalcocite will occur at small anodic over-potentials and large cathodic over-potential. Hence, the kinetics are determined principally by the diffusion rate of ferric ions. At the cathode, the back reactions which involve ferrous ion may be neglected. At high concentrations, the anodic over-potential increases and a change of mechanism to Type I or II may be expected. Though Figure 2-17 does not indicate the possibility of having the mixed potential very close to the reversible potential of the ferric/ferrous couple, this has been observed in some leaching experiments, in which the rate depends on the ferric/ferrous ratio.

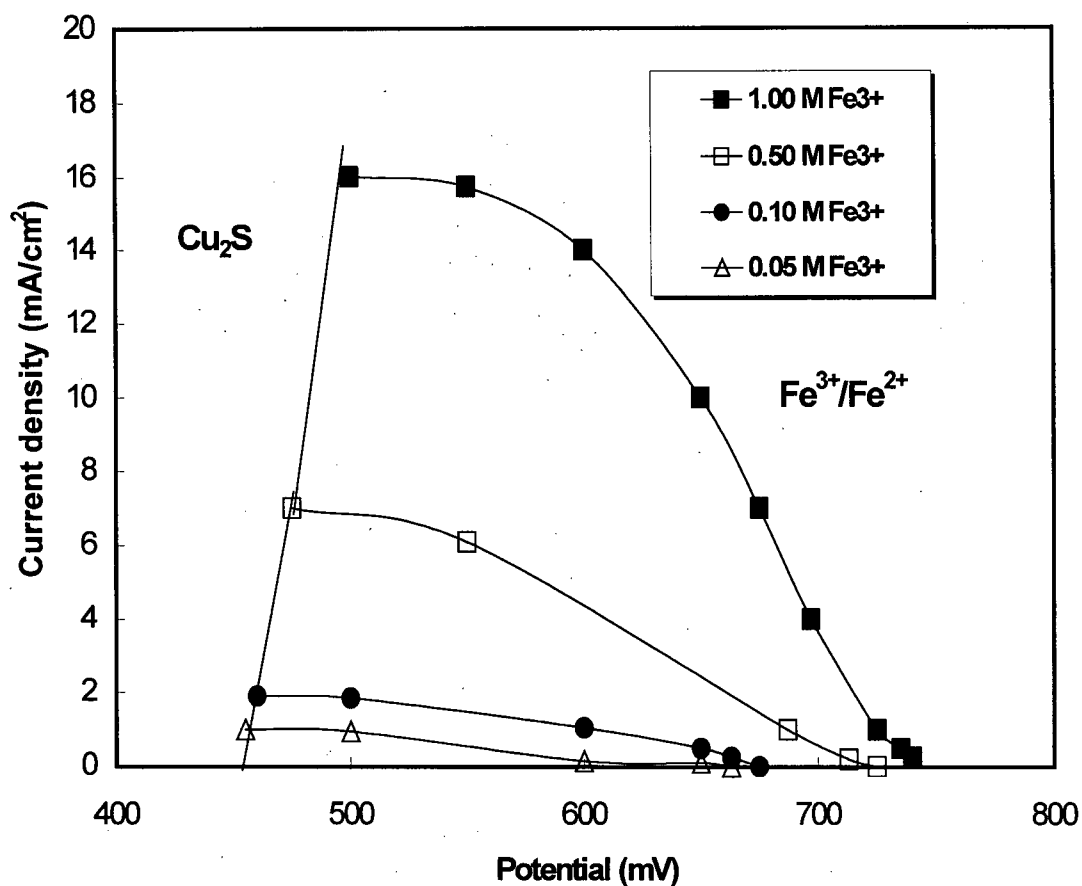
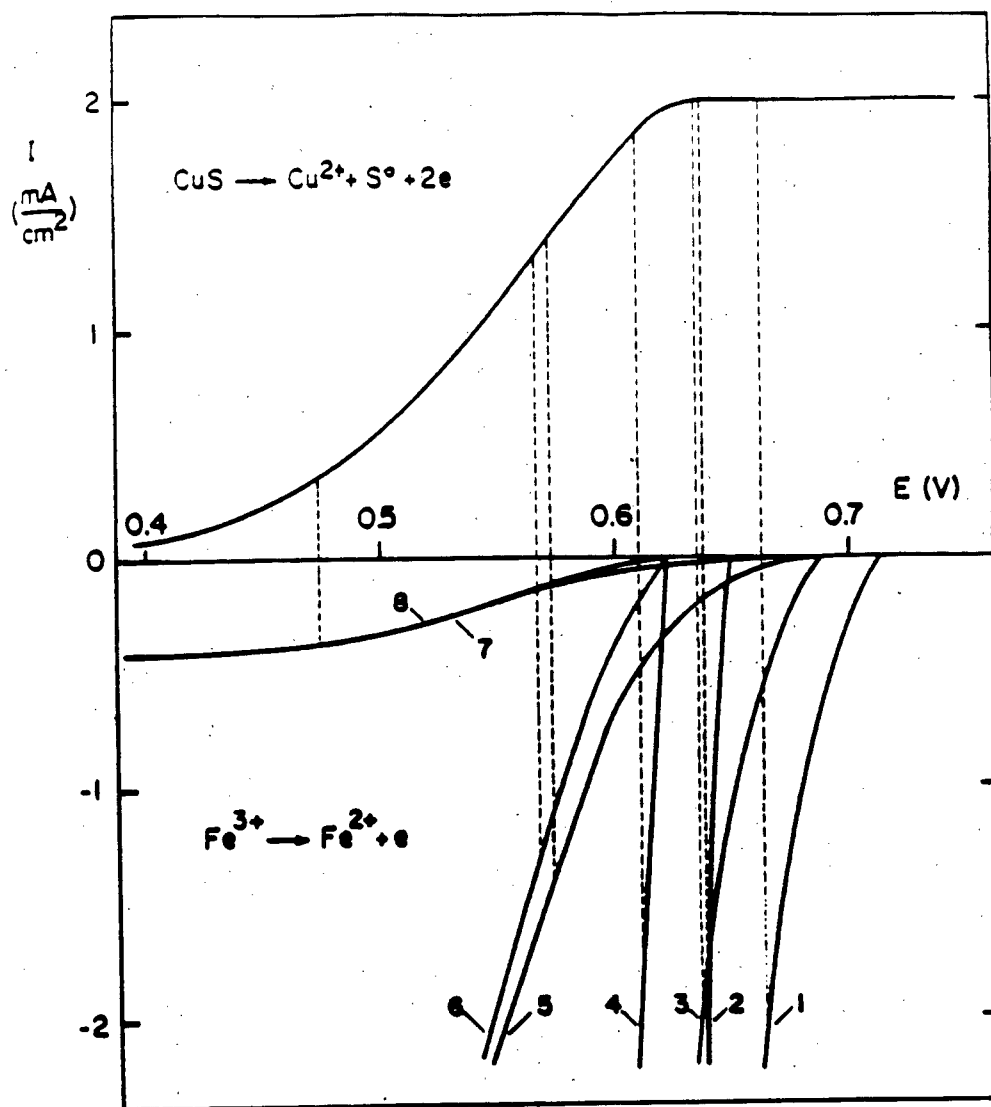


Figure 2-17. Polarization curves for anodic dissolution of Cu_2S (0.1 mol/L CuSO_4 , 0.5 mol/L MgSO_4 , 1 mol/L H_2SO_4) and cathodic reduction of ferric ions on graphite (0.1 mol/L Fe^{2+} , 1 mol/L H_2SO_4) at 25°C [65].

2.4.2 Application of Mixed Potential Theory to the Leaching of Covellite

The polarization curves for anodic dissolution of covellite and (theoretical) cathodic reduction of ferric ions on graphite is shown in Figure 2-18 [67]. The data used for the anodic polarization of the mineral were obtained from the experimental polarization of a covellite anode in 0.1 mol/L CuSO_4 solution. This figure is similar to

that of Figure 2-17, except that the polarization of the ferric/ferrous couple is shown in the cathodic direction. The mixed potential of the half-cells (which is the potential where $i = i_a = -i_c$) is represented by the voltage of the dotted lines at different ferric/ferrous concentrations. At high concentrations of ferric (ferric/ferrous curves 1 and 2), the leaching rate is independent of the ferric concentration as a result of the limiting dissolution rate of covellite. The plateau current corresponds to the voltage region where the limiting current density was observed during the polarization of covellite anode. The electrode reaction did not proceed until the applied current was increased, leading to a very high electrode potential. The limited diffusion rate of copper was speculated at this plateau, although this was inconclusive. For qualitative application, it is obvious from Figure 2-18 that at high concentrations of ferric ion (0.1 and 0.25 mol/L), the anodic overvoltage is very large, which indicates type II leaching. The back reactions at the cathode, which involves ferrous ions can not be ignored, though the kinetics are expected to be controlled mainly by the oxidation of the covellite. At very low concentration of ferric (0.001 mol/L), there is large cathodic over-potential and the leaching rate is expected to be controlled by the limited rate of diffusion of the ferric ions to the covellite. Type III leaching is envisioned. In the middle range of ferric concentration (0.01 mol/L), there are cathodic and anodic over-potentials and the rate of leaching is expected to be controlled by both the oxidation kinetics of covellite and the reduction kinetics of the ferric. This tends towards Type I leaching. Although, the qualitative information provided by Figure 2-18 on the effect of ferrous ion concentration is limited, it shows that at 0.1 and 0.01 mol/L ferric concentration, an increase in ferrous concentration will affect the rate of leaching inversely.



1 $\left\{ \begin{array}{l} \text{Fe}^{3+} (0.25 \text{ M}) \\ \text{Fe}^{2+} (10^{-1} \text{ M}) \end{array} \right\}$
 2 $\left\{ \begin{array}{l} \text{Fe}^{3+} (0.25 \text{ M}) \\ \text{Fe}^{2+} (10^{-2} \text{ M}) \end{array} \right\}$
 3 $\left\{ \begin{array}{l} \text{Fe}^{3+} (0.1 \text{ M}) \\ \text{Fe}^{2+} (10^{-3} \text{ M}) \end{array} \right\}$
 4 $\left\{ \begin{array}{l} \text{Fe}^{3+} (0.1 \text{ M}) \\ \text{Fe}^{2+} (10^{-2} \text{ M}) \end{array} \right\}$

5 $\left\{ \begin{array}{l} \text{Fe}^{3+} (10^{-2} \text{ M}) \\ \text{Fe}^{2+} (10^{-4} \text{ M}) \end{array} \right\}$
 6 $\left\{ \begin{array}{l} \text{Fe}^{3+} (10^{-2} \text{ M}) \\ \text{Fe}^{2+} (10^{-3} \text{ M}) \end{array} \right\}$
 7 $\left\{ \begin{array}{l} \text{Fe}^{3+} (10^{-3} \text{ M}) \\ \text{Fe}^{2+} (10^{-5} \text{ M}) \end{array} \right\}$
 8 $\left\{ \begin{array}{l} \text{Fe}^{3+} (10^{-3} \text{ M}) \\ \text{Fe}^{2+} (10^{-4} \text{ M}) \end{array} \right\}$

Figure 2-18. Polarization curves for anodic dissolution of CuS at 55°C, 0.1 mol/L CuSO₄, 0.1 mol/L H₂SO₄ and cathodic reduction of ferric ions on graphite.

2.5 Chemical Leaching Kinetics

Dutrizac and Macdonald [36], in a review paper on ferric leaching of sulfides, tabulated the findings of all previous kinetic studies on chalcocite and covellite. These, along with the results of more recent studies, are tabulated below in Table 2-1 and Table 2-1. The first stage leaching of chalcocite is very fast relative to second stage leaching, or the leaching of natural covellite. The concurrence is that the rate of the first stage is controlled by the diffusion of oxidant to the mineral surface. This view is supported the observed low activation energies (which are between 1.0 and 7 kcal/mole). In most of the experiments, the rate was found to be first-order dependence on ferric ion concentration, which implied that the rate of diffusion of cuprous ion through the lattice is so fast that it never becomes a rate-controlling step. This assumption is corroborated by Jost [68], that copper ion in minerals like chalcocite has high diffusivity, which is as great as that of aqueous diffusivities, so the cuprous ion diffuses to the reaction site very fast and then react with ferric ions. None of the previous work considered the depleting effect of copper ion concentration (which is available for the first stage) on the rate of reaction. This may explain a change of rate observed in all the cases especially, when the copper extraction is greater than 25%.

The second stage leaching of chalcocite (or leaching of covellite) is typically very slow, and the rate is thought to be controlled by the anodic dissolution reaction. This view is supported by high activation energies (between 15 and 25 kcal/mole) in the ferric sulfate system, an indication of chemical reaction control kinetics. The rate dependence on ferric ion concentration decreases at low levels and there is little or no dependence at high levels.

This results presented in Table 2-1 and Table 2-2 were obtained in the absence of bacteria. Also, it bears noting that no attempt was made to control the potential in any of these experiments. Therefore, since pure ferric solutions were used in every case, one would have expected the oxidizing potential to fall markedly from time zero in every case, which may explain some of the discrepancies with regard to dependence of the rates on ferric ion concentration.

Table 2-1. Kinetics of first stage ferric leaching of Cu_2S .

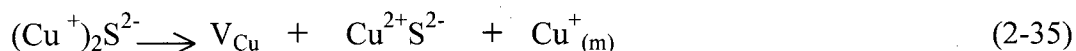
Material	Medium	Rate dependence on $[\text{Fe}^{3+}]$	Activation Energy (kcal/mol)	Temp. ($^{\circ}\text{C}$)	Rate-controlling process	Ref.
Natural minerals	Ferric Sulfate	Independent	Low	23-95	Mass transfer	1
Cu_2S Ores and Tailings	Ferric Sulfate	Independent	-	25	-	10
Pure natural Cu_2S	Ferric Chloride	-	Low	60-105	Mass transfer	5
Synthetic Cu_2S ; Rotating disk	Ferric Sulfate	First order between 0.005 and 0.05 mol/L	1.5 5.3	30-60 60-90	Mass transfer Mixed kinetics	6
Natural Cu_2S	Ferric Sulfate	Slight dependence	Low	20-70	Mass transfer	7
Pure synthetic Cu_2S	Ferric Chloride	Independent	0.8	20-80	Solid state diffusion of Cu^+	8
Synthetic Cu_2S and $\text{Cu}_{1.8}\text{S}$; Rotating disk	Ferric Sulfate	First order	5-6	5-80	Mass transfer	9
Mounted natural crystals	Ferric Sulfate	First order	6.7	28-70	Mass transfer	4
Natural Cu_2S	Ferric Sulfate	First order at low $[\text{Fe}^{3+}]$, decreasing at higher $[\text{Fe}^{3+}]$	2.79	30-90	Mixed kinetics	2

Table 2-2. Kinetics of second stage ferric leaching of Cu_2S and ferric leaching of CuS .

Material	Medium	Rate dependence on $[\text{Fe}^{3+}]$	Activation Energy (kcal/mol)	Temp. ($^{\circ}\text{C}$)	Rate-controlling process	Ref
Natural minerals	Ferric Sulfate	Independent up to $\text{Fe}^{3+} > 1 \text{ g/l}$	High	35-95	-	11
Synthetic Cu_2S ; Rotating disk	Ferric Sulfate	First order at $\text{Fe}^{3+} < 0.005 \text{ mol/L}$ and independent at $[\text{Fe}^{3+}] > 0.005 \text{ mol/L}$	22	$T < 60$	Chemical	12
			8	60-80	Mixed kinetics	12
Synthetic Cu_2S ; dispersed particles	Ferric chloride	Increased with increasing Fe^{3+} conc. in the range 0.25-1.0 mol/L	25	20-80	Chemical	8
Mounted natural crystals	Ferric Sulfate	Increased with conc. in the range of 0.0128 - 0.424 mol/L Fe^{3+}	14	40-70	Chemisorption / Chemical	4
Synthetic powders; Dispersed particles	Ferric Sulfate	Independent at $[\text{Fe}^{3+}] > 0.005 \text{ mol/L}$, first order $[\text{Fe}^{3+}] < 0.005 \text{ mol/L}$	20	30-90	Chemical	3
Pure synthetic and natural crystals; Rotating disk	Ferric Sulfate	Independent at $[\text{Fe}^{3+}] > 0.005 \text{ mol/L}$, first order at $[\text{Fe}^{3+}] < 0.005 \text{ mol/L}$	18	15-95	Chemical	13
Natural Cu_2S	Ferric Sulfate	\sim one-half order	18	30-90	Electrochemical	2

Initially, all the cuprous ions within the chalcocite matrix are extremely mobile. As reaction proceeds, approximately half the copper becomes fixed into the second stage

covellite phase and is immobile. The following reaction occurs at the digenite/blue-remaining covellite interface [2];



where V_{Cu} is a cuprous ion vacancy and (m) denotes a mobile ion. The structure of covellite, which is given by equation 2-35, is unstable and changes according to the following reaction;



The mobile cuprous ion in equation (2-35) is then free to diffuse to the particle surface, where it is oxidized by ferric ion thus;



The second stage kinetics are controlled by an electrochemical reaction, which occurs all over the porous surfaces of the particle. Marcantonio [2] found the ferric ion dependence to be about 0.3 order, but assumed one-half order. This confirms the shift from a diffusion controlled mechanism during the first stage of leaching to an electrochemical controlled mechanism during the second stage.

2.6 Effect of Parameters on the Kinetics in Sulfate Media

2.6.1 Effect of Stirring Speed

As long as off-bottom conditions and the limiting thickness of the laminar layer around the particles are achieved in the reactor, stirring speed has virtually no effect on the leaching kinetics of chalcocite and covellite [2].

2.6.2 Effect of Temperature

The effect of temperature on the first stage dissolution rate has been reported consistently to be little on the first stage leaching and that reaction proceeds rapidly at room temperature [1]. The various activation energies reported in the literature are included in Table 2-1.

The kinetics of the second stage dissolution rate are much slower and more temperature sensitive than that of the first stage. The reaction rate is extremely slow at room temperature and increases with increase in temperature. The various activation energies obtained for the second stage leaching are provided in Table 2-2. Linear rates were reported for the second stage by the previous investigators, however, a dual-mechanism over the temperature range of 25 and 80°C was reported by Thomas and Ingraham [12]. In their work, the observed rate was controlled by a chemical reaction at temperature below 60°C and above this temperature, the rate was reported to be controlled by solution transport. Also, there were initial induction periods at all temperatures, but these deviations from other investigations were not explained clearly in their work and the ion, which was responsible for the mass transfer at high temperature was not mentioned.

2.6.3 Effect of Particle Size

The effect of particle size on the leaching of chalcocite has been inconsistent. A direct relationship was obtained by Marcantonio [2] when the rates were plotted against reciprocal radius, which did not support his conclusion that rate was controlled by diffusion through the product layer. If diffusion through the product layer was the rate controlling step, the rate would have been proportional to the reciprocal radius squared.

The second stage has been reported to be independent of the particle size [12]. A direct relationship was observed between the rates and the outer surface area of the disk in the leaching of covellite disks [12].

2.6.4 Effect of Ferric Concentration

The effects of ferric ion concentration on the rate of leaching have been summarized in Table 2-1 and Table 2-2 respectively. An independent relationship has been reported between rate and ferric ion concentration [1] in some previous experiments. Also in some investigations, the rate was said to be directly proportional to ferric ion concentration (first order), but at higher concentrations, the dependence decreased [4,6,9].

The second stage response to ferric ion concentration is much less than that of the first stage. In dilute solution of ferric ions (which varies between 0.0005 and 0.005 mol/L), a direct relationship was observed by Thomas and Ingraham [12] and at concentration higher than 0.005 mol/L, the rate was almost independent of the ferric ion concentration. Dutrizac and MacDonald [13] in a different investigation observed the same relationship, though the ferric ion concentration increased up to 0.3 mol/L, the rate remained the same. However, Lowe [4] observed an increase in rate up to 0.42 mol/L, while Marcantonio [2] obtained a dependence on ferric concentration up to 0.61 mol/L and a rate order of 0.3 (which was approximated to 0.5 in his work). One of the reasons for this inconsistency could be the deviation of the redox potential in all the previous experiments.

2.6.5 Effect of Acidity

At constant ferric strength, the rate of leaching is independent of the sulfuric acid concentration over the range of 0.03 mol/L and 0.3 mol/L [12]. At a concentration less than 0.03 mol/L, the rate reduction observed has been attributed to ferric hydrolysis and precipitation. The main purpose of the acid may be limited to keeping the trivalent iron in solution. Other investigators [1,2] have found the rate to be relatively independent of the acid concentration. Nevertheless, it will be important to control acidity especially when other side reactions (which are acid consuming or generating) can occur such as gangue reactions and oxidation of ferrous to ferric ion.

2.7 Effect of Parameters on the Kinetics in Chloride Media

In this section, the kinetics of chalcocite leaching in ferric chloride is presented. A summary has been included in Table 2-1 and Table 2-2.

2.7.1 Effect of Temperature

As shown in Figure 2-19, the kinetics of second stage leaching of chalcocite are much more temperature sensitive in chloride media than in sulfate media. Also, the activation energy increases as leaching proceeds, due perhaps to the progressive formation of a protective sulfur coating.

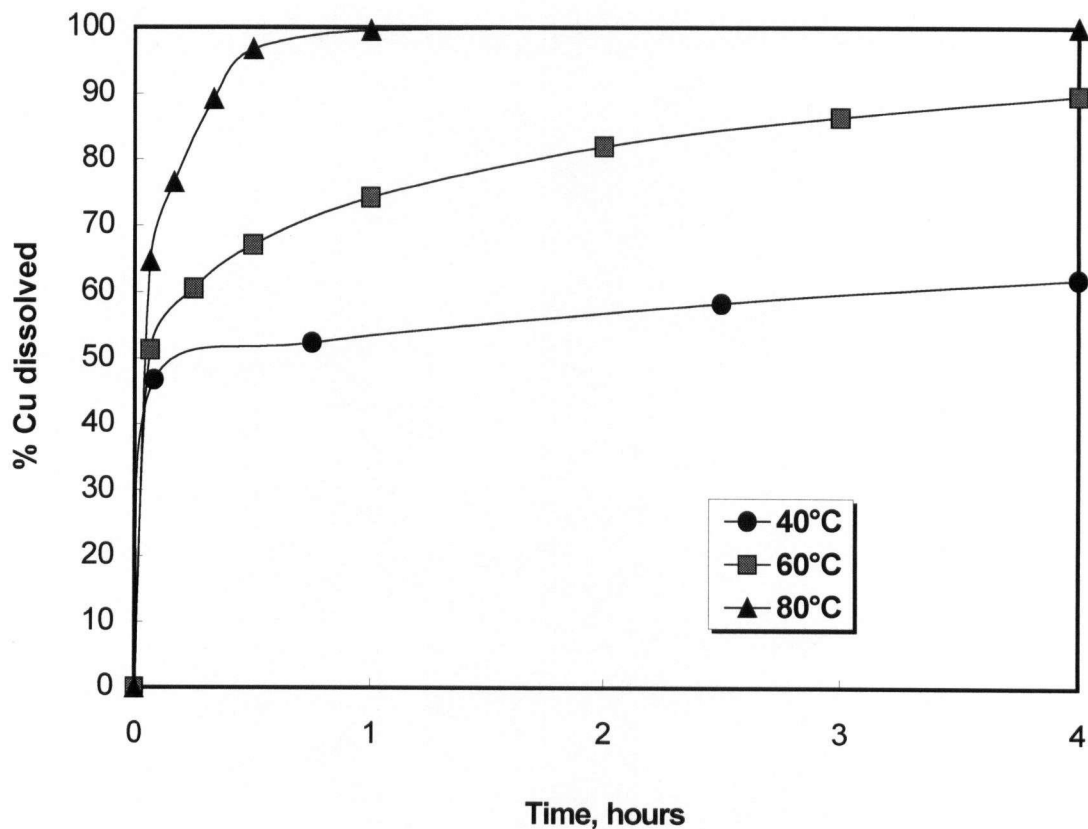


Figure 2-19. Effect of temperature on the leaching of chalcocite in chloride (FeCl_3 0.5 mol/L, HCl 0.2 mol/L, $\text{Fe}^{3+}/\text{Fe}^{2+}$ 10, 2.5 g +150-300 μm Cu_2S) [8].

2.7.2 Effect of Ferric Concentration

The rate of the first stage leaching is first order with respect to ferric ion concentration when the concentration is between 1.25×10^{-4} and 1.56×10^{-2} mol/L. However, the rate has no dependence on the concentration if the level is between 0.25 and 1.0 mol/L [8]. This suggests that, at a level above a certain ferric ion concentration, rate control shifts from mass transfer of ferric ions through the stagnant boundary layer to another mechanism. This could be solid state diffusion of cuprous ions through the chalcocite crystal matrix or desorption (or mass transfer) of the dissolved products, which are Fe^{2+} or Cu^{2+} away from the mineral surface. However, the solid state process has been shown by Price [69] to give significantly higher activation energies than are typically reported for the first stage dissolution of chalcocite. The rate of the second stage leaching depends on ferric iron concentration with an estimated order of reaction of about 0.2 or 0.3.

2.7.3 Effect of Particle Size

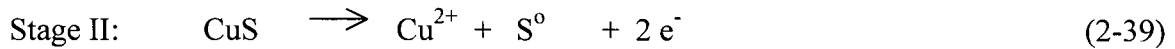
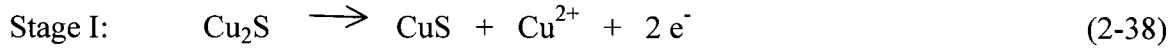
The particle size only affects the rate of the first stage of dissolution, as expected for diffusion controlled kinetics.

2.8 Proposed Mechanisms of Sulfate Leaching

A complete review of the previously proposed mechanisms of chalcocite leaching in sulfate media is important, since most of the reaction steps are similar whether the oxidant is ferric or dissolved oxygen.

2.8.1 Cathodically-Controlled Mixed Potential Mechanism

Marcantonio [2] expressed the two stages of chalcocite dissolution with the following anodic half cells:



Brennet *et al.* [14] measured the reversible half-cell reduction potentials of these reactions as $E_1^0 = 440$ to 505 mV (SHE) and $E_2 = 520$ to 570 mV (SHE) respectively, while Sato [70] reported them as $E_1^0 = 530$ mV (SHE) and $E_2^0 = 591$ mV (SHE) respectively. The standard half-cell potential for ferric reduction is 771 mV and is represented as follows;



Assuming an ideal solution, the Eh of the $\text{Fe}^{3+}/\text{Fe}^{2+}$ couple could vary (theoretically) from 917 mV at the beginning of the first stage (I) to 781 mV at the end of the first stage and the beginning of the second stage (I, II) according to the above stoichiometry, then to 735 mV at the end of the second stage (II). In this mechanism, the half-cell potential for *blaubleibender* is taken as that for normal covellite.

Consequently, if the mixed potential initially falls below the range of half-cell potential for stage II (according to Brennet), then elemental sulfur will be unstable in the presence of cupric ion. This is expected from the diagram in Figure 2-20, since the slow discharge of ferric ion (cathodic reaction) is said to be the slower electrochemical process, the mixed potential is shifted towards the reversible potential of the anode (mineral). This means a large cathodic overpotential η_c and small anodic overpotential, η_a . If the mixed potential is close to that of the mineral (as proposed), one would expect a drastic fall of the redox potential from time zero, which is not the case when covellite is

leached. The Eh profile or the profile for the rate of ferric discharge was not presented by the author.

At low temperatures, the half-cell potential ranges for stage I and II are distinct, and the processes do not overlap. At higher temperatures, the ranges overlap to a certain extent, denoted “a” on the diagram. It is doubtful if the overlap will take place at a mixed potential, which is close to the reversible potential of the chalcocite as shown by Marcantonio [2]. Once second stage covellite is formed, two mixed potentials are established and one is closed to the reversible potential of the chalcocite while the other which is lower in magnitude is closed to that of the covellite. It is envisioned that some particles leach at higher potential and others leach at lower mixed potential but faster rate. The two stages leach at these potentials until the first stage leaching finishes and the mixed potential is predominantly determined by the kinetics of the second stage leaching. The leaching of second stage covellite continues at this newly established mixed potential.

When chalcocite is leached, the redox potential does not fall drastically from time zero because the mixed potential is very close to the reversible potential of the ferric/ferrous couple. This is what is observed in practice during the leaching of second stage covellite and natural covellite. One would have expected a small cathodic overvoltage and a large anodic overvoltage in which the rate controlling step is the electron transfer in the anodic reaction.

The electrochemical model proposed by Marcantonio for the second stage leaching is therefore faulty because it was based on the cathodically-controlled mechanism.

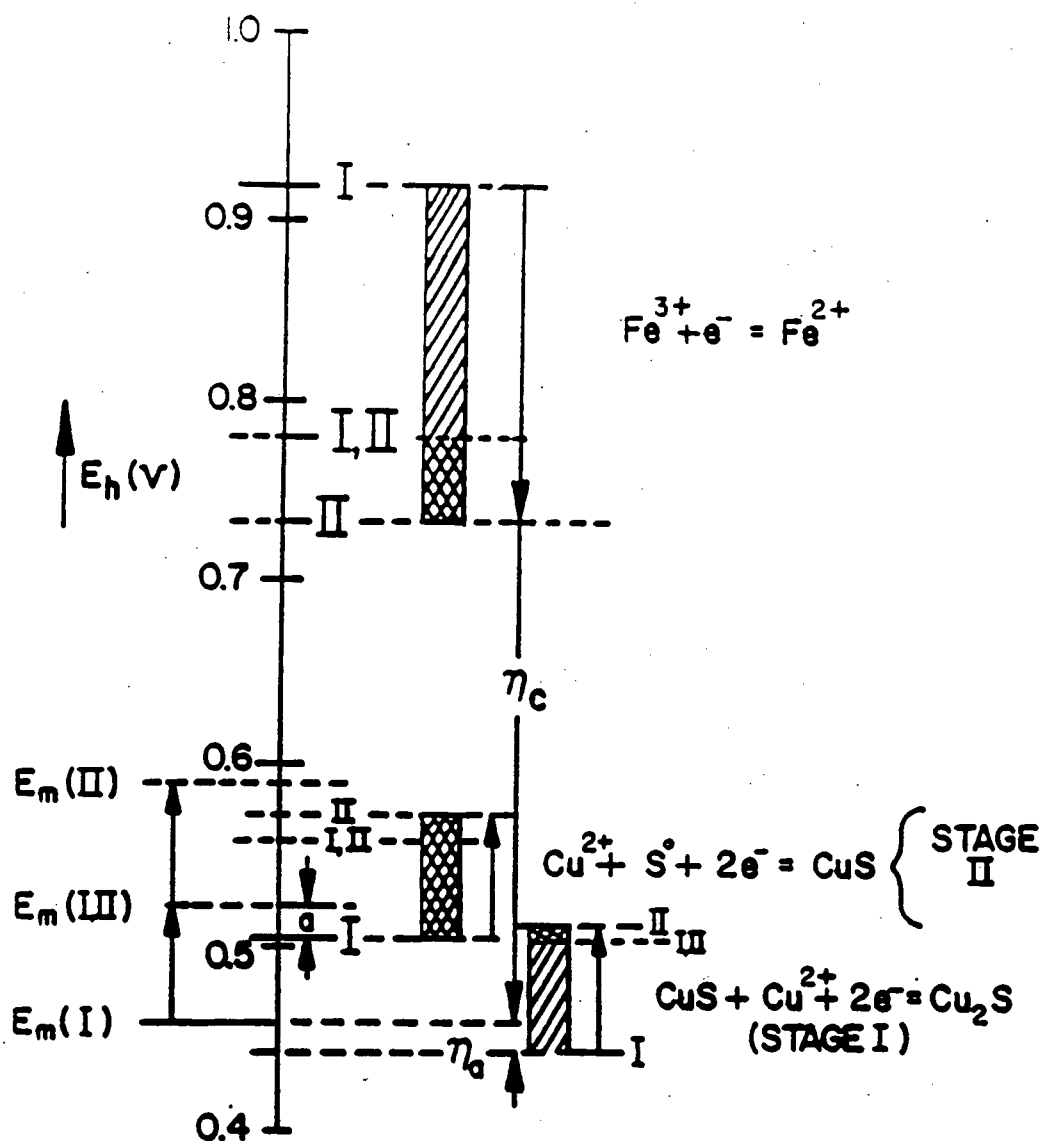


Figure 2-20. Illustration of half-cell and mixed potential variations during ferric leaching of chalcocite: 0.1mol/L Cu_2S , 0.5mol/L Fe^{3+} , 0.001mol/L Fe^{2+} and Cu^{2+} [2].

2.8.2 Iron Depassivation Mixed Potential Mechanism

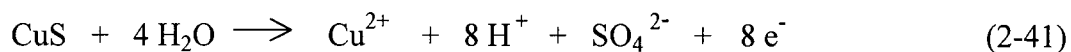
An alternative mixed potential model was derived by Mao and Peters [71] as part of their study of the acid pressure leaching in sulfate medium. In their model of oxygen

pressure leaching, the first stage of leaching is controlled predominantly by the cathodic half-cell (either oxygen reduction or ferric ion reduction), which is similar to Marcantonio's model of leaching. During the second stage, however, covellite is passivated by oxygen, leading to a high mixed potential. However, the anode is de-passivated in the presence of ferric ions, which leads to higher leaching rates and lower sulfate yield.

The observed progress of the reaction is portrayed on the Evans diagram, which is shown in Figure 2-21. When leaching commences, oxygen is reduced on a fresh chalcocite surface (curve 1), which is steadily transformed to digenite, thus undergoing about 7 % shrinkage. The outer particle surface is rapidly transformed to digenite, which changes the cathodic process to a combination of oxygen reduction on digenite (curve 2) and pore-diffusion-limited reduction of oxygen on unreacted chalcocite at the base of pores (the dotted vertical section of curve 1).

The first step of the first stage is concluded, when covellite (CuS) is formed on the outer particle surface. The leaching reaction, which had migrated from point A to point B during the first step, now jumps to point C as oxygen is reduced on the covellite surface. Point C represents an increase in both the exchange current (leaching rate) and the mixed potential. As the digenite covellite interface area decreases, the sloping part of the anodic curve rises and point C traces curve 3 to higher mixed potentials and lower rates.

The second stage begins when point C migrates to D, at which the covellite is passivated by oxygen in the absence of ferric ions. The mixed potential rises quickly to the transpassive point E. At this point, the potential is well above that of $\text{Fe}^{2+}/\text{Fe}^{3+}$ couple and this potential is also probably sufficient to form sulfate according to the following reaction;



The observed role of iron as a catalyst in this system was explained on the basis that it acts as a surrogate oxidant for oxygen at the mineral surface, whereby the anodic

dissolution of covellite may be carried out at the lower mixed potential. This is represented by Point D, where the rate is significantly higher and the potential is low enough to give a low yield of sulfate. Therefore, stage II leaching is envisioned as some particles leaching at point E and others leaching at Point D, with the proportion of the latter increasing with increasing iron concentration.

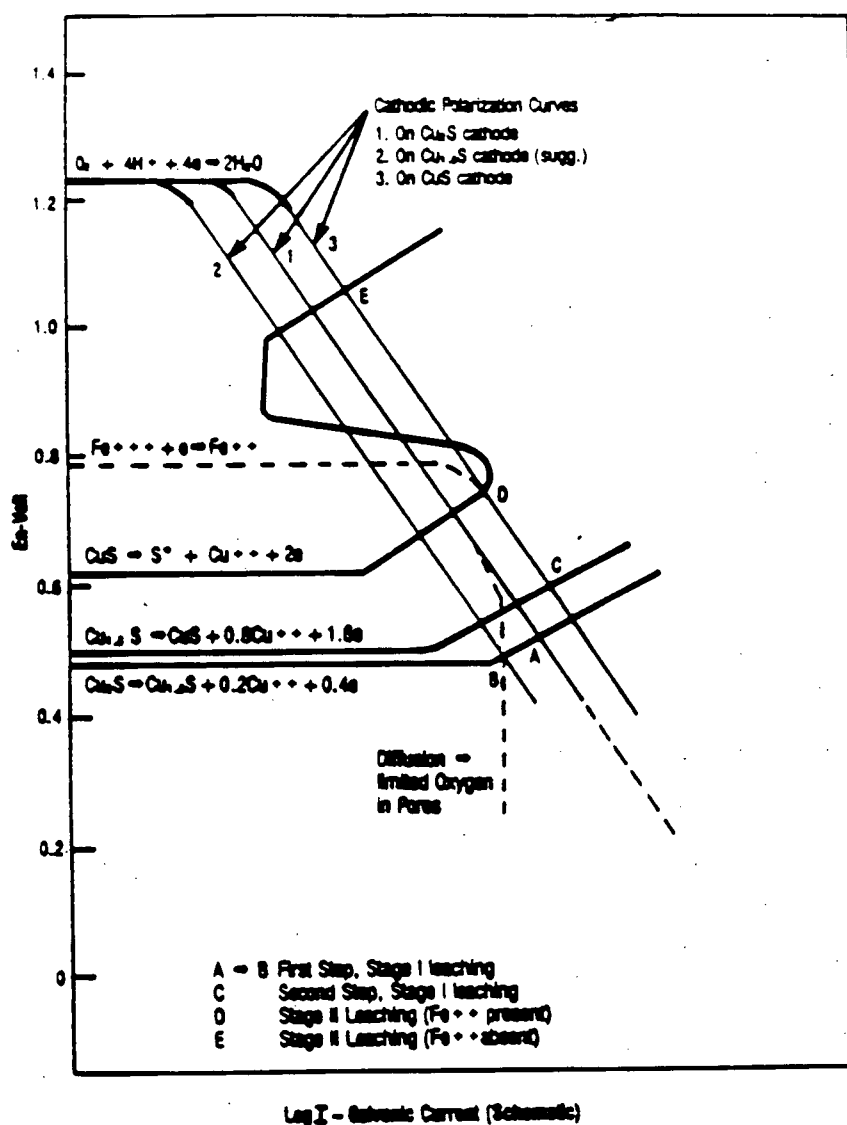
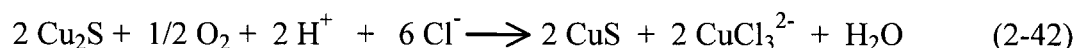


Figure 2-21. Schematic Evans diagram of Cu_2S pressure leaching, after Mao and Peters [71].

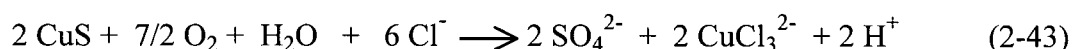
2.9 Proposed Mechanism of Chloride Leaching

The mechanisms proposed by Fisher et al.[72] for the oxygen pressure leaching of chalcocite in chloride and sulfate media are presented for comparison purposes. No iron was present in the experiments, the pressure varied between 0.039 and 0.165 MPa, while the temperature varied between 303 and 347 K.

The first stage leaching was about seventy times faster in chloride media than the rate in sulfate solution. This large difference was attributed to the formation of the stable chlorocuprate (I) complex CuCl_3^{2-} (according to equation 2-42), which allows cuprous ions to be extracted from chalcocite without oxidation to cupric at the particle surface. The rate of leaching in sulfate media is proportional to the pressure during the first stage, with an activation energy which is 31.5 kJ/mol and presumably associated with oxygen adsorption. The rate in the chloride system is directly proportional to the chloride concentration, with an activation energy which is 22.6 kJ/mol and presumably associated with chloride ion (Cl^-) mass transfer.



The second stage (in chloride) is independent of all the leaching variables except temperature, with an activation energy of 34.6 kJ/mol. This was attributed to the electron transfer in the anodic (dissolution) reaction. The second stage leaching in chloride solution is given by the following equation;



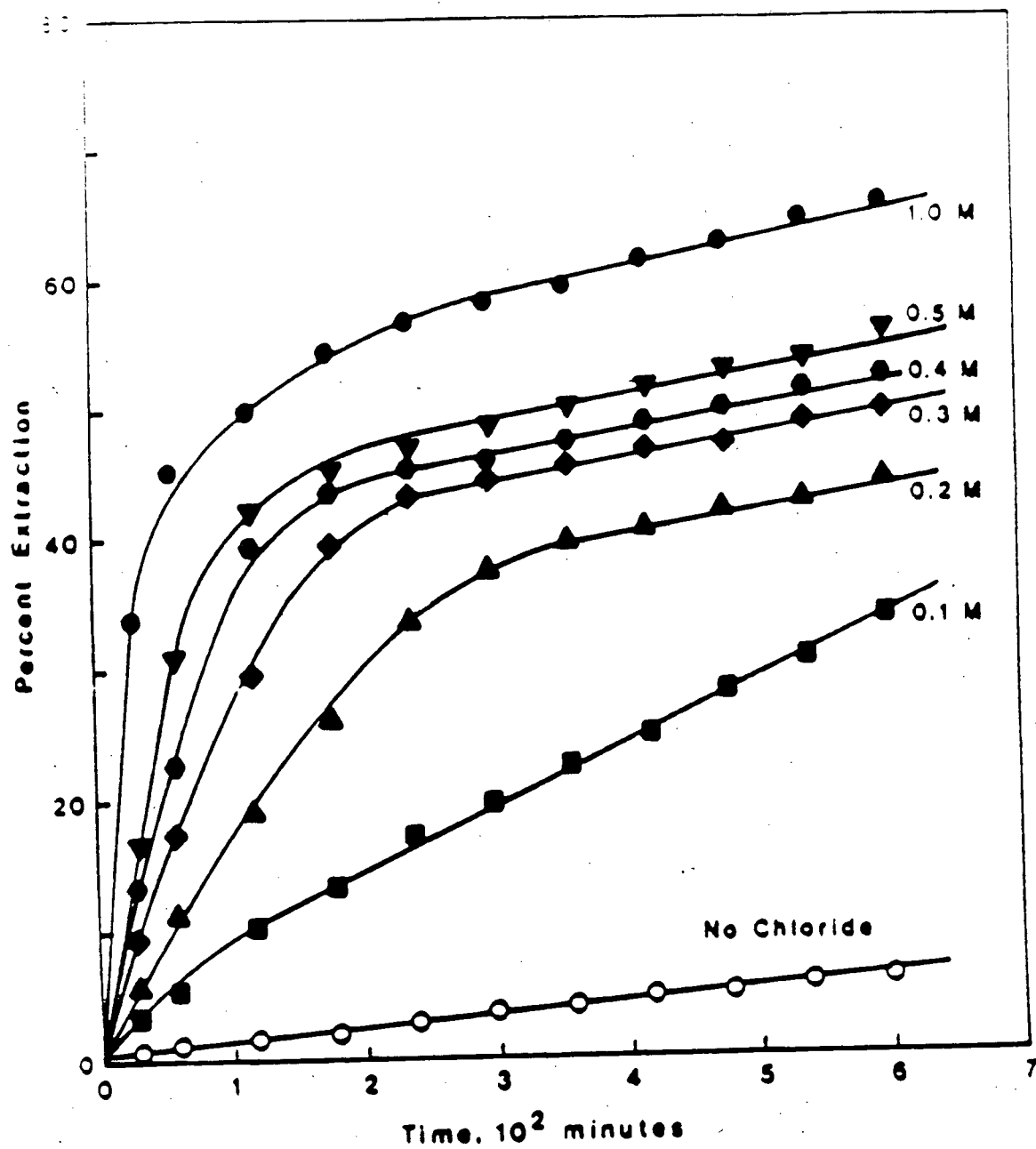


Figure 2-22. Effect of chloride concentration on dissolution, at 303 K, 0.086 MPa oxygen pressure, 0.35 mol/L $[H^+]$ and 210 x 177 μm particles [72].

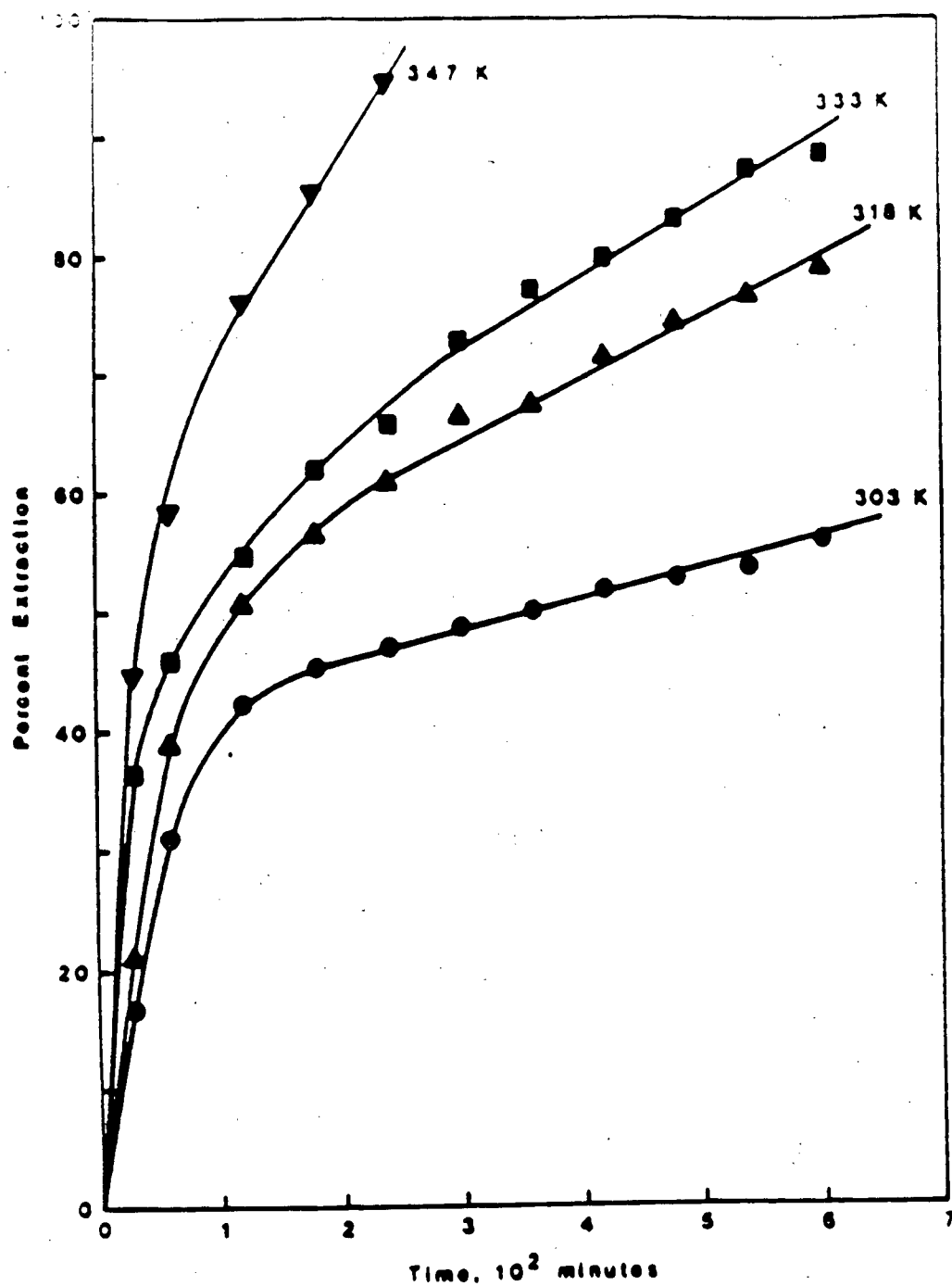


Figure 2-23. Effect of temperature on the second stage leaching at 0.5 mol/L Cl^- , 0.086 MPa pressure, 0.35 mol/L H^+ and $210 \times 177 \mu\text{m}$ particles [72].

Figure 2-24 [72] illustrates the first stage leaching process in the sulfate system. The adsorbed oxygen on the surface is reduced by one electron transfer mechanism to water as shown by:

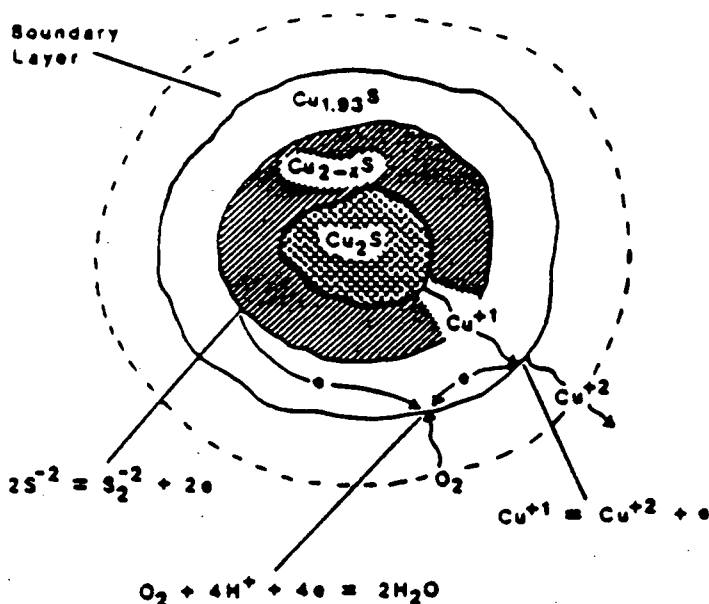


Figure 2-24. Physico-chemical model for first stage chalcocite dissolution in the sulfate system [72].

The electrons for oxygen reduction are supplied by the oxidation of Cu^+ to Cu^{2+} at the particle surface and S^{2-} to S_2^{2-} in the particle interior. Cuprous ion diffuses from the particle interior to the surface where it is oxidized to cupric ion which is released into the solution.

Figure 2-25 [72] shows the first stage dissolution process in the chloride system. The rate controlling step is believed to be the diffusion of chloride ion through the solution boundary layer to the particle surface. Cuprous ions diffuse from the particle interior to the surface where they react with chloride ions to form CuCl_3^{2-} , which is then released into solution. Oxygen adsorbed on the particle surface is reduced as shown in equation (2-44) to (2-47) by the electrons, which are liberated in the oxidation of S^{2-} to S_2^{2-} .

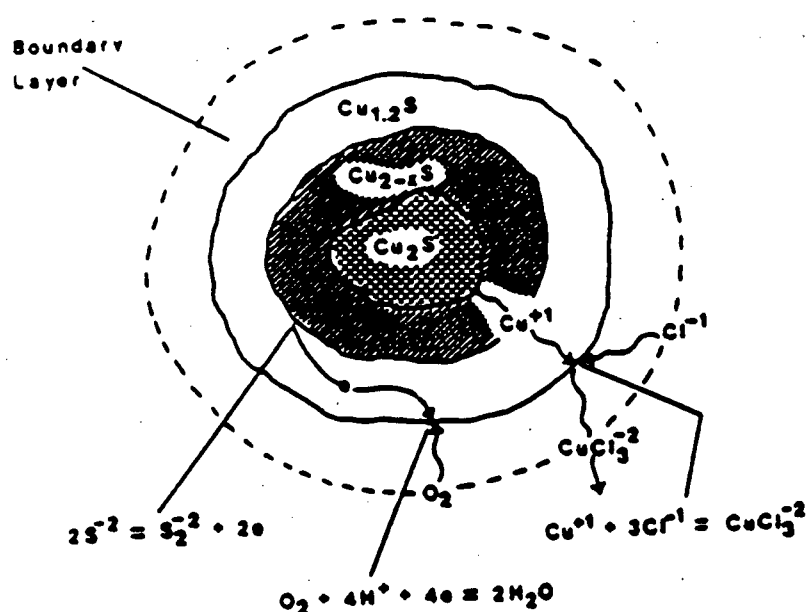


Figure 2-25. Physico-chemical model for first stage chalcocite dissolution in the chloride system [72].

Figure 2-26 [72] illustrates the second stage dissolution process in the chloride system. Oxygen adsorbed on the particle surface is reduced to water as shown in equation (2-44) to (2-47). The electrons are supplied by the oxidation of blue-remaining covellite as shown in Figure 2-26. This reaction occurs as a sequence of simple electrochemical steps involving one electron transfer. Since the rate does not vary with oxygen pressure, it is postulated that the rate-controlling step is the electron transfer in the anodic reaction.

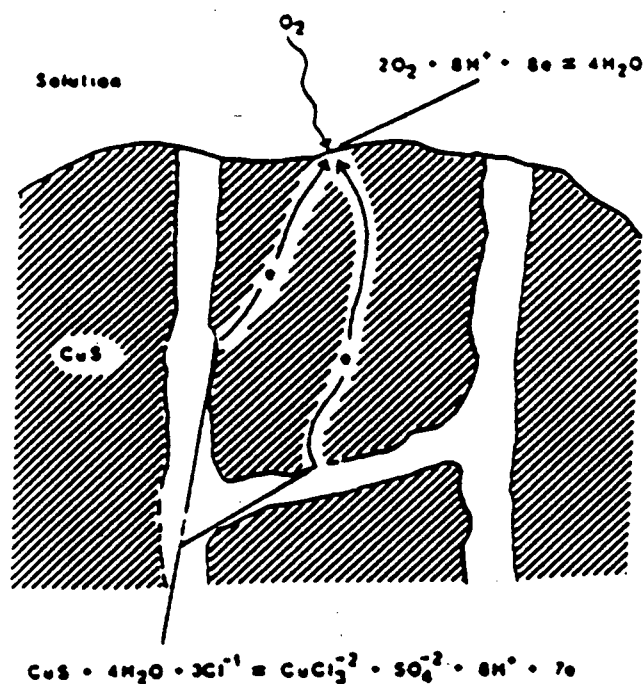
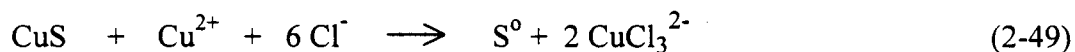
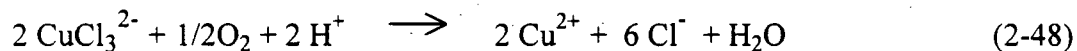


Figure 2-26. Physico-chemical model for first stage chalcocite dissolution in the sulfate system [72].

One thing that Fisher *et al.* failed to point out is that, in light of the work of Mao and Peters, the anodic dissolution of covellite in second stage must be de-polarized automatically in chloride media by the presence of an active $\text{Cu}^{2+}/\text{Cu}^+$ couple at the mineral surface. This couple is absent in sulfate media, though this may be stable at very high temperature (about 200°C or higher). In the presence of sufficient Cl^- , the actual leaching reactions would be as follows;



In any case, the rate of the second stage leaching is still significantly faster than that of ferric (or iron catalyzed oxygen pressure) leaching under similar circumstances.

2.10 Chalcocite Leaching in Other Media

Fisher [73] has compared the rates of chalcocite leaching in oxygenated solutions. In non-complexing systems (such as SO_4^{2-} , NO_3^- , ClO_4^-), the rate of first stage leaching is very slow (second stage leaching was not observed within the duration of the experiment) at low temperature.

In complexing systems which require chalcocite oxidation (such as Cl^- and NH_3), the rate of first stage leaching is very fast and the rate of second stage leaching is slow.

In complexing systems which do not require chalcocite oxidation (such as CN^-) there is only one stage of leaching, and it is extremely fast (probably mass transfer controlled), like the dissolution of a soluble salt.

2.11 Summary of Literature Review

It is widely known that chalcocite oxidation occurs roughly in two distinct stages, the first stage leaching of chalcocite is very fast relative to the second stage leaching. The rate of first stage leaching is controlled by the diffusion of oxidant to the mineral surface. This is supported by the low activation energies (between 1 and 3 kcal/mol) and the first-order dependence on ferric concentration. On the other hand, second stage leaching of chalcocite (or the covellitic phase) is slow and is controlled by the rate of the chemical reaction. This is supported by the high activation energies (between 15 and 25 kcal/mol) and the small dependence of the rate on ferric concentration at low levels, and very little or no dependence at high levels. It is worth noting that no attempts were made to control the redox potential, which would be expected to fall from time zero in every case as oxidant is consumed. This may be responsible for the discrepancies previously reported with regard to the dependence of rates on ferric concentration and other parameters. Hence the objective of the present work was to control the redox potential in each experiment in order to quantify the variables independently. The experimental procedures required to achieve this objective are presented in the following Chapter.

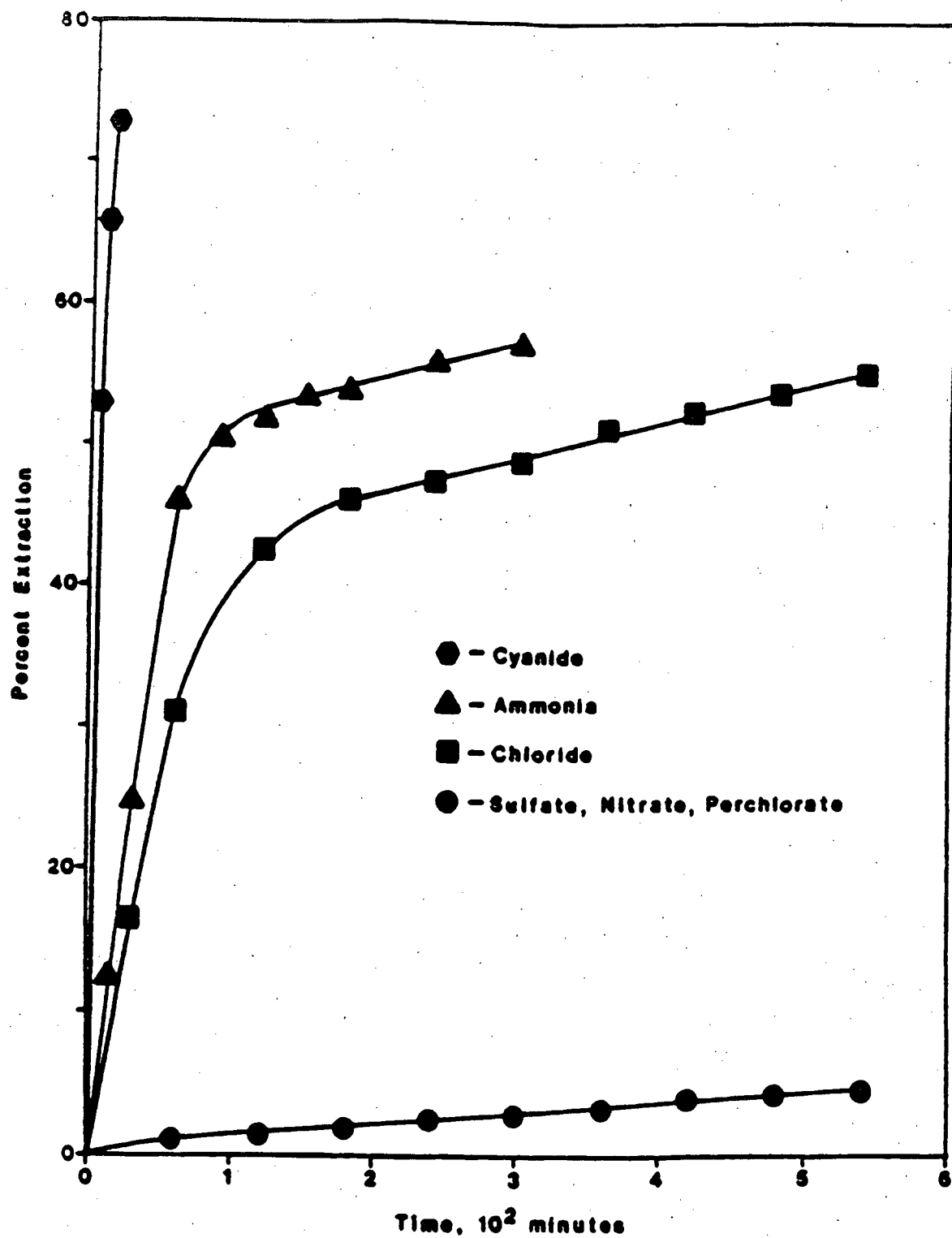


Figure 2-27. Chalcocite dissolution in various media [73].

CHAPTER 3

EXPERIMENTAL PROCEDURES

The experimental program developed for this study can be divided into three phases;

1. Controlled potential chemical leaching of chalcocite and second stage covellite;
2. Bacterial leaching of chalcocite and second stage covellite;
3. Mineralogical characterization of the reaction products to examine the compositional changes which occur during leaching.

3.1. Chemical Leaching Experiments

The chemical leaching of chalcocite by ferric/ferrous ions under controlled potential was achieved by using potassium permanganate solution. The resulting phase from the leaching of chalcocite (second stage covellite) was also investigated

3.1.1 Sample Preparation and Minerals

The samples of chalcocite and covellite ores were obtained from the Mineralogical Research Center Inc., San Jose, U.S.A. These were in the form of rocks with average size of 2 cm. A mechanical splitter was used to select a fraction with a good representation of the as-received ore samples. This fraction was used in the mineralogical studies and the leaching tests. Qualitative analyses of a rock section (from the selected fraction) and a powder were made for comparisons of the particle size to ensure good liberation of all the phases. Smaller fractions (about 500 g each), which were good representatives of the selected fraction of the ore were crushed and ground to achieve 90% coarser than 150 μm . The choice of using coarser particles for the dissolution tests was to obtain results which could be upgraded easily to plant scale. Prior to screening, about 500 g of portions were first screened for 3 hours through the # 115 mesh sieve to remove most of the fines.

The plus 115 mesh fraction was screened for 1 hour on a Rotap shaker by using the Tyler sieves # 35 (425 μm aperture size), # 42 (355 μm), # 48 (300 μm), # 60 (250 μm), # 65 (212 μm), # 80 (180 μm), # 100 (150 μm) and # 115 (125 μm). The major portions (about 90%) of these particles were in the narrow sized range of -425+355, -355+300, -300+250, -250+212, -212+180 and -180+150 μm . These particle fractions were stored in sealed polyethylene bags until they were required, to minimize oxidation of the mineral surface. A mono-sized fraction (-250+212 μm) was selected (based on section 3.1.4) for all the dissolution tests and other fractions were used to investigate the effect of particle size. The cumulative particle size distribution determined by sieving is plotted in Figure 3-1.

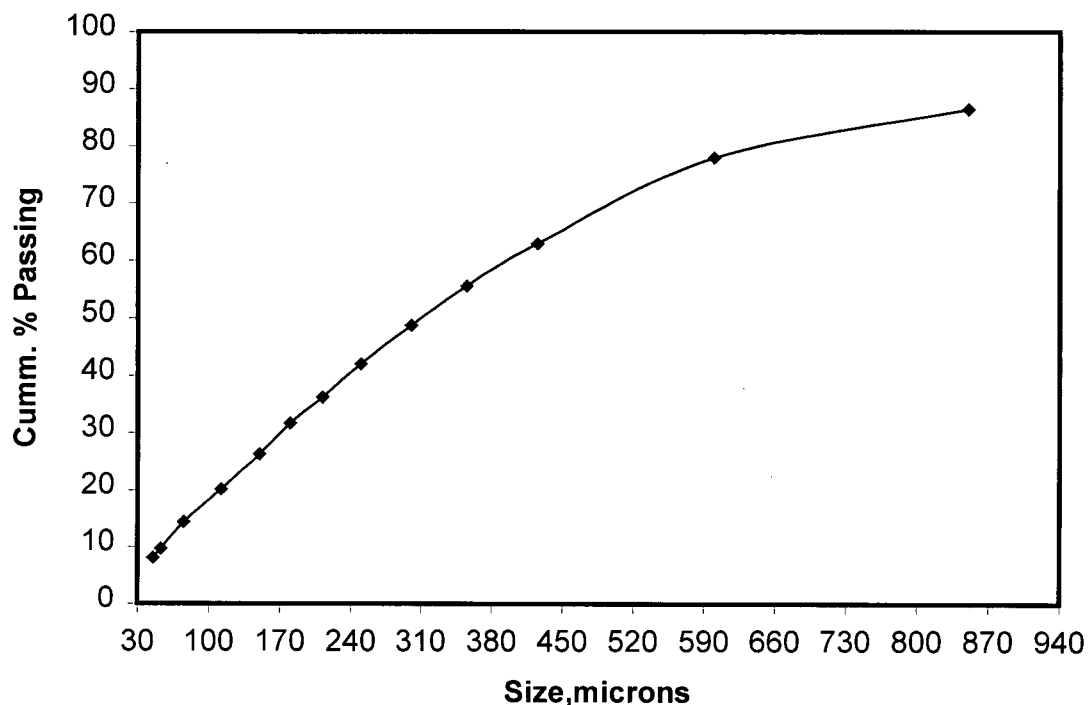


Figure 3-1. Cumulative particle size distribution of the mineral samples as determined by screening with Tyler sieves.

3.1.2 Chemical Analysis of the Sample

A sample (from the selected fraction) was sent to Chem. Met Consultants Inc. (CMC) and International Plasma Laboratory (IPL) for chemical analysis. A comparison was made between the two results from the laboratories. The results of the chemical analysis provided guides on the minerals, which were present in the sample before the commencement of leaching. Analytical results from the two laboratories have little variation (less than 0.2%) except for copper compositions, which shows about 0.5% and 0.7% difference between the two laboratories for chalcocite and covellite respectively. The average gravimetric composition of each element is summarized in Table 3-1.

Table 3-1. Results of chemical analyses for the as-received and reground minerals.

Sample	Cu (%)	Fe (%)	S _T (%)	S ²⁻ (%)	Insol. ² (%)	Others ³ (%)
Chalcocite ¹	70.48	3.25	21.80	21.70	2.96	1.51
Cu ₂ S (theoretical)	79.87	0.00	20.13	20.13	0.00	0.00
Covellite ¹	65.32	3.25	27.80	27.80	2.26	1.37
CuS (theoretical)	66.49	0.00	33.51	33.51	0.00	0.00

¹ Assay results are average values obtained from duplicate analyses.

² Acid insoluble constituent, indicative of siliceous gangue.

³ Other elements such as bismuth, arsenic and antimony.

3.1.3 Mineralogical Characterization of the Sample

In order to corroborate the chemical analyses and to obtain the phase abundance, qualitative analyses by X-ray powder diffractometry were carried out. The X-ray diffraction pattern of the chalcocite feed was helpful in determining the initial phases (minerals) present before leaching. The transformation of these phases could then be monitored by a similar method. The instrument used for this purpose was a Siemens D5000 powder diffractometer, which uses monochromatized CuK α radiation. This was

operated at 40 mA and 40 kV. The spectra were collected from 3 to 70° (2θ) in 0.01° steps at a count-rate of 0.4 s per step. The small samples (grains) from the ground and screened fractions were ground further in a mortar to obtain fine powder. The fine powder was mixed with ethanol to form a paste, which was spread on a glass slide to form thin layers and allowed to dry before inserting into the instrument for analysis. Based on the phases that were identified (by using X-ray diffractometry) and the chemical analyses (Table 3-1), the phase abundance was determined and summarized in Table 3-2.

Table 3-2. Results of mineralogical composition of the chalcocite sample

Sample	Covellite (%)	Chalcocite (%)	Bornite (%)	Pyrite (%)	Quartz (%)	Others ¹
Chalcocite	<0.01	80.56	11.48	3.49	2.96	1.51
Covellite	89.34	N/E ²	0.00	7.03	2.26	1.37

¹This may be enargite as revealed in section 4.1.

²Not estimated.

3.1.4 Selection of Monosize Particles

This qualitative identification of the phases was used as a litmus test to select the mono-sized fraction used in the leaching tests. In order to select this fraction, a small quantity of grains from each fraction was spread on different stubs and then carbon-coated. These grains were analyzed by scanning electron microscope, which is equipped with an energy-dispersive detector. The elemental composition analysis of all the phases were made. The size fraction (-250+212 μm) in which all the previously identified-phases (section 3.1.3) were present and well liberated was selected for dissolution tests.

3.1.5 Chemical Leaching Apparatus and Procedures

A schematic diagram of the controlled potential leaching set-up (and the monitoring equipment) is shown in Figure 3-2. At the heart of the apparatus was a stirred tank reactor (STR), which enabled the redox potential in mV, and other variables such as temperature and pH to be carefully measured and controlled. The STR had the following features;

1. Air-sealed, baffled (by three plexiglass baffles) glass reactor with a working volume of 1 L;
2. Overhead variable-speed stirrer;
3. Gas sparge line through which nitrogen gas was added;
4. Reflux condenser to control evaporative solution losses;
5. A pH controller, which delivered acid or base as required;
6. Redox-potential controller coupled to a peristaltic pump, which added potassium permanganate at rate set to regenerate ferric from ferrous ions and thereby maintained a constant redox potential. The interface circuit between the controller and the pump was developed in house. This was used to ensure proportional control (redox potential only varied by 1 mV) and data logging of the redox potentials into a desktop computer;
7. Air-tight plexiglass cover with eight ports, which contained a condenser, sampling frit, nitrogen sparge tube, stainless-steel stirrer shaft, potassium permanganate tube, sulfuric acid replenishment tube, redox potential probe and pH probe;
8. A pitched-blade axial flow impeller was inserted at the end of the shaft to provide proper mixing and to ensure effective particle suspension at 900 rpm;
9. The entire reaction assembly was clamped into place in a water bath, which has a temperature controller to maintain constant high temperature operations.

To start an experiment, the water bath was first heated up to the desired temperature. A 1-liter solution (which contains known concentrations of ferric sulfate $\text{Fe}_2(\text{SO}_4)_3 \cdot 5 \text{H}_2\text{O}$ and ferrous sulfate $\text{FeSO}_4 \cdot 7 \text{H}_2\text{O}$ in distilled water) was added to the

reactor and brought to the operating temperature in the bath. Five grams of chalcocite from the mono-sized particles of $-250+212\ \mu\text{m}$ were charged into the reactor (in all the tests) and the redox potential and pH controllers were initiated. The leach solution redox potential was kept constant by oxidizing the ferrous ions (which were formed as a result of the leaching reaction) back to ferric ions. This was done with potassium permanganate solution, which was added by a peristaltic pump. The peristaltic pump was controlled proportionally by a redox potential controller, which used inputs from the solution submerged redox potential probe. A platinum redox electrode combined with a silver/silver chloride reference electrode was used. In order to maintain the initial acidity of the solution, a pH controller system, which uses inputs from the pH-probe to initiate mechanically (on/off), a peristaltic pump to add 6 M sulfuric acid into the solution was used. A gel-filled combination pH probe with a silver/silver chloride reference electrode was used in all the experiments.

The standard test for the first stage leaching was at 35°C , ferric ion concentration of 0.116 mol/L, ferrous ion concentration of 0.0202 mol/L and 0.095 mol/L of sulfuric acid. The redox potential of this solution was 501 mV at 25°C (vs. Ag/AgCl). The same conditions were used as a standard test for the second stage leaching, but at a temperature of 75°C . The higher temperature (for the second stage leaching) was chosen based on the experimental observations described in section 4.3.1. Solution samples of about 2 mL were taken from the reactor through a glass frit to keep all solids in the reactor (during leaching) and these were analyzed for copper by atomic absorption spectrometry. The sampling time varied from 1 to 30 minutes from the beginning to the end of the test and the residence time varied (from 30 minutes to 72 hrs) depending on the leaching parameters. After leaching for the desired residence time, the reactor contents were suction filtered and the residue was washed thoroughly with deionized water as described in Section 3.1.6.

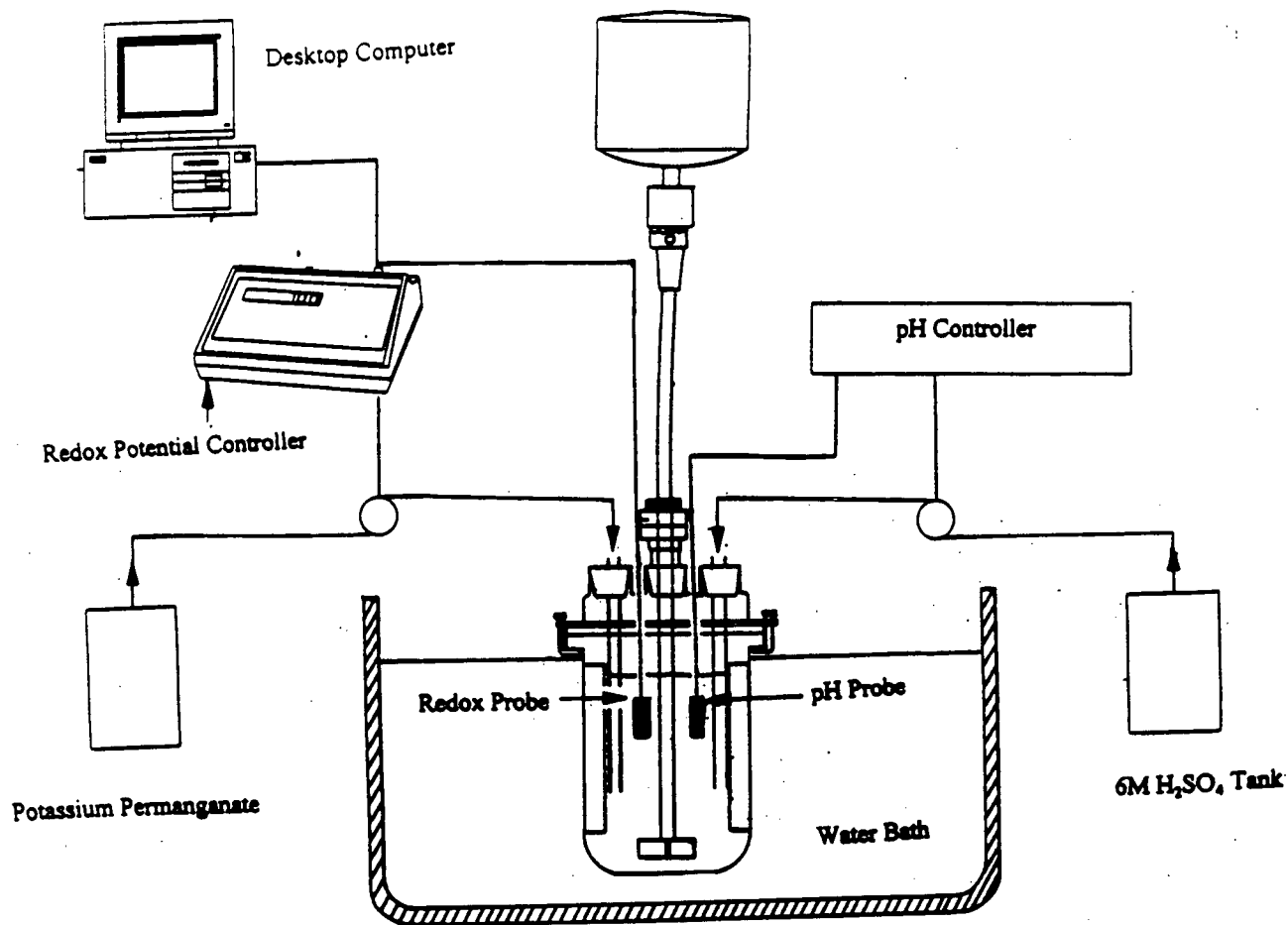
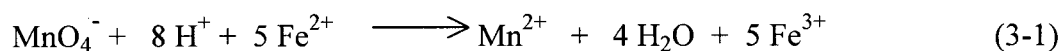


Figure 3-2. Schematic representation of the controlled potential leaching set-up.

3.1.6 Role of Potassium Permanganate

The role of potassium permanganate in the chemical leaching experiments was to control the solution potential without it itself taking part in the leaching. The leaching of the minerals was by the ferric/ferrous sulfate solution, which was introduced at the beginning of each test. Since ferrous ion formation from the leaching reaction would reduce the redox potential of the solution, there was a need to oxidize this back to ferric

ion and maintain the initial redox potential throughout the duration of each test. The (acidic) oxidation of ferrous ion by potassium permanganate is represented by the following reaction:

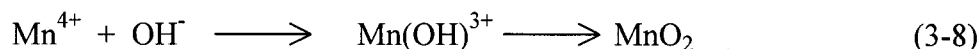
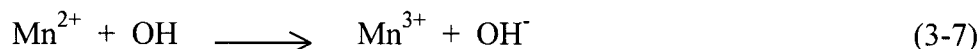
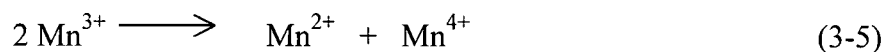
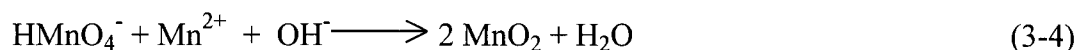
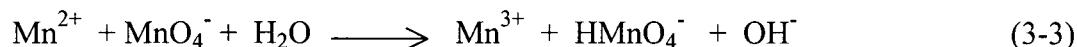


The standard potential (with reference to hydrogen electrode) of potassium permanganate in acid solution, E^θ is 1.51 volts, therefore permanganate in acid solution is a strong oxidizing agent.

In the presence of manganese(II) ions, the following side reaction with permanganate, which is called the Guyard reaction [74] could occur;

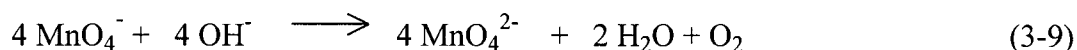


The free energy change for reaction 3-2 was calculated by Turney [74] as -61.1 kcal/mol. The precipitation of the manganese dioxide depends on this free energy change, the solubility of manganese dioxide and the hydrogen ion concentration. Highly acidic conditions (about $0.1 \text{ mol/L H}_2\text{SO}_4$) were used in the volumetric oxidation by permanganate to prevent the formation of manganese dioxide. The mechanism involved in this side reaction has been thoroughly investigated by Tompkins [75] and the following reaction steps are involved.

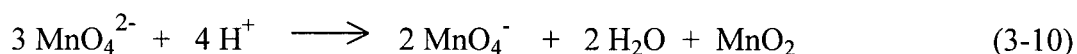


The manganese dioxide is formed primarily by reaction (3-8) because reaction (3-4) is slow. The addition of the first hydroxyl ion in equation (3-8) is the rate-controlling step in the hydrolysis of the tetravalent manganese ion. The reaction in equation (3-5) is inhibited by the presence of complexes in solution.

The decomposition of permanganate in alkaline solution is represented as follows;



Turney [74] calculated the free energy change of the reaction as -25.0 kcal. At the saturation solubility of oxygen in water, the reaction gives the green manganate ion in sodium hydroxide solution (which is above 1 N concentration). When the concentration of the sodium hydroxide is less than 1 N, the manganate disproportionate according to the following equation;



Other side reactions of permanganate (dis-proportioning) in strong alkaline solutions could be through the following two consecutive partial reactions;



Reaction (3-11) is relatively rapid, while reaction (3-12) is slow [76]. The standard potential E^θ of reaction (3-11) is 0.56 volt and of reaction (3-12) is 0.60 volt.

In order to avoid the side reactions represented by equations 3-2 to 3-12 in the use of potassium permanganate to maintain the ferric/ferrous ratio, it was necessary to use a highly acidic medium, pure distilled water and almost perfectly pure potassium permanganate (reagent grade standardized solution). These conditions were strictly

employed in this work. If ferric ions were to be absent initially, the calculated amount of potassium permanganate (based on stoichiometric) required to leach 0.056 moles/L of copper would be 0.0224 moles/L. In this work, ferric/ferrous solutions were used (and present at the commencement) in the leaching experiment to reduce the volume of potassium permanganate solution required to maintain the redox potential and to ensure that the kinetics were that of ferric leaching. The volume (or quantity) of potassium permanganate used in the experiments varied with the initial ferric concentration, kinetics of the reaction and the residence time. The maximum volume of potassium permanganate used in the experiments was 100 mL (of 0.1 mol/L standard solution). This was equivalent to about 0.012 mol/L at the end of the experiment.

In acidic medium, ferrous oxidation by equation (3-1) can be considered as titration of ferrous ions by permanganate because it takes place (almost) stoichiometrically and rapidly. The potential during the titration corresponds to the redox potential for $\text{Fe}^{3+}/\text{Fe}^{2+}$ and rises rapidly. The potential of the half-cell involved is given by the following;

$$E_{\text{Ag}/\text{AgCl}} = 1.3110 - 0.0946 \text{ pH} + 0.0118 \log \frac{[\text{MnO}_4^-]}{[\text{Mn}^{2+}]} \quad (3-13)$$

By using solution redox potential of $E_{\text{Ag}/\text{AgCl}} = 0.501\text{V}$ and $\text{pH} = 1.1$ (which is the standard experimental condition in this work), the calculated ratio of MnO_4^- to Mn^{2+} is 3.22×10^{-27} . This low value demonstrates the absence of free MnO_4^- (which is needed for the initiation of the side reaction in equation 3-3). This calculation was confirmed by a leaching experiment (controlled chemical leaching), in which ferric/ferrous ions were absent and leaching of the solid minerals was carried out by potassium permanganate solution.

3.1.7 Slurry Filtration Method

The slurries were filtered using the re-pulp wash method. This method involved filtering the solids twice. After the first filtration, the filtrate volume was recorded and the filtrate solution sampled. Then the solids were washed in a volume of deionized water which was approximately four times the filtrate volume. The essence of this repulping step was to wash dissolved copper containing solution out of the first filter cake. The solids were suspended in this solution by stirring for about 10 minutes before being filtered again. After the second filtration, the wash volume was recorded and the wash solution sampled. The filtrate and wash solutions were analyzed for copper and iron concentrations. The final filtration residues were dried for two or three days, at ambient temperature to minimize the tendency for oxidation of sulfide sulfur or elemental sulfur.

3.1.8 Analytical Methods

The soluble iron (ferric plus ferrous) and the dissolved copper in the solution were analyzed in-house by atomic absorption spectrophotometry (AAS), while the solid samples were sent to local Vancouver analytical laboratories for analysis. The dissolved ferrous iron was determined by titration with ceric sulfate. The filtration residues were divided into several parts for various analyses. Parts of the residues were analyzed for copper and iron by AAS after digesting in aqua regia/bromine. The sulfur species were determined by a sequential leach/digestion procedure. The total sulfur was determined gravimetrically as BaSO_4 after digesting in a $\text{KBr-Br}_2/\text{HNO}_3$ solution. The other sulfur species were determined gravimetrically after carrying out the following procedure. Initially, elemental sulfur was dissolved in boiling perchloroethylene (the boiling point is 121°C), then the perchloroethylene leach residue was boiled with 10% Na_2CO_3 solution to selectively dissolve sulfate. Finally, the Na_2CO_3 leach residue was digested in a $\text{KBr-Br}_2/\text{HNO}_3$ solution to dissolve the remaining sulfur, which was assumed to be sulfide.

3.1.9 Determination of Copper Extraction and Sulfide Oxidation

Copper balances were conducted for some tests to understand the reaction mechanisms and to ensure the calculated copper extractions were reasonably accurate. If the metal out / metal in mass ratio did not fall within the target variation of 0.98 to 1.02, the solution and / or residue analyses were repeated to check for any analytical error, and in some cases the tests were repeated. The mass balance yielded a calculated head assay, Cu_{calc} , defined by:

$$Cu_{cal} = \left(\frac{m_{Cu}^{sol} + m_{Cu}^{res}}{m_t} \right) \cdot 100\% \quad (3-14)$$

Where m_{Cu}^{sol} is the mass of copper solubilized, m_{Cu}^{res} is the mass of copper in the leach residue and m_t is the total starting mass of the head sample. The percent copper extraction was based on the calculated head assay:

$$\text{Percent copper extraction} = \frac{m_{Cu}^{sol}}{(Cu_{calc}/100)(m_t)} \cdot 100\% \quad (3-15)$$

The sulfur species analyses of the head and leach residue were used to calculate percent sulfide oxidation levels by using the following formulas:

$$\text{Total } S^{2-} \text{ oxidation (to } S^o + SO_4^{2-}) = \left(\frac{m_{sulfide}^{head} - m_{sulfide}^{res}}{m_{sulfide}^{head}} \right) \cdot 100\% \quad (3-16)$$

$$S^{2-} \text{ oxidation to } S^o = \left(\frac{m_{sulfur}^{res}}{m_{sulfide}^{head}} \right) \cdot 100\% \quad (3-17)$$

$$S^{2-} \text{ oxidation to } SO_4^{2-} = (\text{total sulfide oxidation}) - (S^{2-} \text{ oxidation to } S^o) \quad (3-18)$$

Where $m_{sulfide}^{head}$ is the mass of sulfide sulfur in the head sample, $m_{sulfide}^{res}$ is the mass of sulfide in the leach residue and m_{sulfur}^{res} is the mass of elemental sulfur in the leach residue.

3.2 Mineralogical Characterization of Reaction Products

The following techniques were used for the qualitative and quantitative analyses of the reaction products.

3.2.1 Qualitative Analysis

The same techniques used for the feed materials in Section 3.1 were utilised for the X-ray powder analysis of the leached residues. The leached grains were also analyzed by using a scanning electron microscope, which was attached to an energy-dispersive detector for spot analysis. The leached grains (which were washed and dried) were cold-pressed into plugs made of epoxy-resin and polished using alumina slurries down to 1 μm . These were carbon-coated for use in scanning electron microscopy (SEM). The SEM-EDX provided qualitative analysis vis-à-vis the elemental composition analysis of each grain by using spot analysis. These polished sections of the particles were used to reveal the phase changes, which occurred during leaching and where the phases were initiated. Subsequent to elemental analysis, different spots and grains were mapped for compositional analysis.

Also, the scanning electron microscope (SEM) was used to observe the dissolution features on the surface of the particles.

3.2.2 Phase Compositional Analysis

The same grains, which were leached under similar conditions and washed in distilled water were analyzed for chemical composition by using an automated CAMECA SX-50 electron-probe microanalyzer (EPMA). The operating conditions were 12 kV and 1.2 nanoamperes for the accelerating voltage and beam current respectively. The standards used were synthetic covellite for Cu, S and pyrite for Fe. Apparent concentrations were corrected for absorption, secondary fluorescence and atomic number effects by using the ZAF program to determine the analytical compositions of the grains (or spots), previously mapped in Section 3.2.

3.3 Bacterial Leaching of Chalcocite

The bacterial experiments were similar to the standard chemical leaching experiments except that oxygen and bacterial inoculum were introduced.

3.3.1 Bacterial Culture and Nutrient Media

The bacterial culture used was a mixed culture containing *Thiobacillus ferrooxidans*. The culture was initially obtained from the Gibraltar Mine and was used in previous studies at the University of British Columbia. It had been grown on the Gibraltar concentrate (chalcopyrite) in shake flasks and serially transferred at the exponential growth stage. The shake flask culture contained 16 g of solid and 100 mL of “modified 9K” solution. This is similar to the nutrient solution developed by Silverman and Lundgren [77], but differed in the concentration of ferrous iron. The modified 9K had no ferrous ions (equivalent to 0K).

In order to ensure that a bacterial culture with optimal activity level was used for the bacterial leaching experiments, the culture from the shake flask was grown on the chalcocite feeds in a 2-L nutrient solution (which differed from that of the shake flask). This was necessary to adapt the culture to the chalcocite minerals and to have a leach solution with total iron concentration similar to that of the chemical leaching experiment. The batch culture nutrient solution was the Silverman and Lundgren solution containing 0.116 mol/L ferrous iron (equivalent to 6K) and without potassium chloride (KCl) to avoid chloride dissolution of the mineral. The batch culture was initiated by transferring the contents of a flask (at exponential-growth stage) into a 1.5 L nutrient solution, which contained 24 g of chalcocite (with particle size of P_{90} 75 μm). The 2 L volume was then achieved by adding nutrient solution. The tank and the tank lid for the batch culture were made from acrylic material. A tank diameter to tank height ratio of approximately 0.6 was used. The tank was baffled and the slurry stirred by a four blade, forty-five degree pitch down type impeller with a diameter, which is 0.4 times the tank. The stirring speed was the same as that used for the chemical leaching experiments. Air was sparged into the

tank below the bottom impeller. The air supply came from a compressor and was CO₂-enriched to 1% v/v CO₂ using a CO₂ gas cylinder and a gas proportioner. A gas flow-meter was positioned at the inlet of the tank; this was used to regulate the CO₂-enriched air flow-rate at about 0.25 L air/L pulp/minute. The temperature of the batch culture was controlled at 35°C by using an immersion heater connected to a temperature controller. The pH of the culture was maintained at about pH 1.5 by addition of 6M H₂SO₄ as required.

3.3.2 Bacterial Leaching Experiment

This was similar to the batch-culturing, but the experiment was done in the glass reactor used for the chemical leaching tests. The particle size was -250+212 µm and the working volume was 1 L. The pulp density was 0.5% (w/w). The experiment was initiated by adding 750 mL of 6K nutrient (with pH of 1.74) into the reactor. This was the Silverman and Lundgren solution containing 0.116 mol/L ferrous iron (equivalent to 6K) and without potassium chloride to avoid chloride effect. The solution was brought to 35°C by the water bath. The reactor was inoculated approximately 2 hrs after starting the experiment, but this was not done until the solid minerals were added. The time interval between the addition of solid and inoculum was 5 minutes. A sample of the inoculum was taken before inoculating the reactor and the leach solution was also sampled immediately after inoculation. Time zero was considered to be the time of inoculation. The inoculum consisted of 160 mL of a stock batch-culture in the late exponential growth phase. This was a solid free solution taken after allowing the batch-culture slurry to settle for 3 hours. The initial 1 L working-volume was achieved by adding nutrient and the solution was then sampled. The acidity was maintained at about pH 1.8 by adding some 6M H₂SO₄ and when the acidity started falling below pH 1.74, a lime slurry was added.

The solution pH and redox potential (vs. Ag/AgCl) were measured. The dissolved copper and iron concentrations were analyzed by using AAS. The initial concentration of

copper (inoculum-Cu) was subtracted from the subsequent concentrations to calculate copper extraction.

A sterile control experiment was conducted in the same reactor with the same conditions, except that 10 mL of bactericide (2g/L thymol in methanol) was substituted for the bacterial inoculum.

CHAPTER 4

RESULTS AND DISCUSSION

4.1 Mineralogical Characterization

4.1.1 X-ray and Microscopic Analyses of Feeds

Analysis of the powder by X-ray diffraction showed that the chalcocite sample consisted mainly of chalcocite, with traces of bornite, quartz and pyrite. This was used to determine the phase abundance, which was presented in Table 2-2.

The complex X-ray patterns of the natural chalcocite samples are shown in Figure 4-1. These patterns were collected after purification of the material and this was used to establish the phases that were present before the commencement of leaching. These major phases as shown in Figure 4-1 are chalcocite, pyrite, bornite and quartz (the djurleite phase could be considered an alteration phase of chalcocite). The SEM-EDX analysis of a rock section of chalcocite (~ 2.5 mm diameter) revealed only a chalcocite phase. The spot analysis of this phase is shown in Figure 4-2. The K_{α} peak intensity of copper is twice that of the sulfur in this phase, in accordance with the atomic ratio (which is 2:1). A compositional image analysis of a rock section of covellite revealed principally two phases as shown in Figure 4-3. There were some chalcocite phases zoned in the covellite. X-ray display analysis (obtained by using SEM-EDX spot analysis) of the covellite phase is shown in Figure 4-4. This revealed a copper to sulfur atomic ratio of about 1.0. The K_{α} peak of copper is slightly lower than that of sulfur because copper has a higher atomic number than sulfur. However, the X-ray powder diffraction analysis of the covellite powder revealed the presence of pyrite and quartz in addition to covellite and chalcocite phases as shown in Figure 4-5.

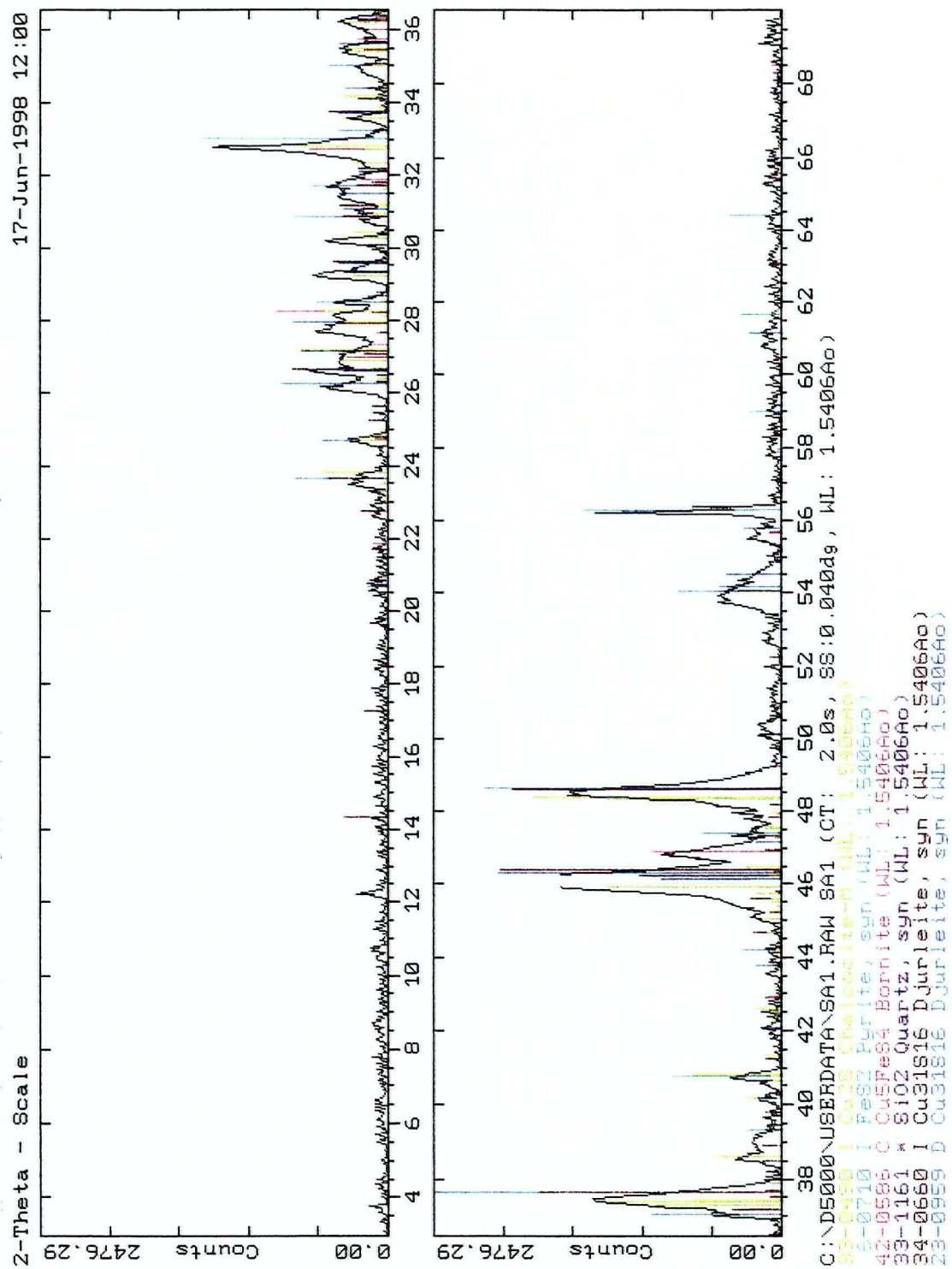


Figure 4-1. X-ray diffraction pattern of chalcocite powder.

In Figure 4-6, the grains from mono-sized particles of $-250+212\ \mu\text{m}$ chalcocite feed showed all the phases, which were previously established by the X-ray diffraction analysis of Figure 4-1. It was intriguing that all the phases were liberated in grains in a rock section (with 2.5 mm diameter), which indicated only one phase. Based on the X-ray (powder) diffraction analysis and the qualitative analysis by SEM-EDX, the mono-sized fraction of $-250+212\ \mu\text{m}$ chalcocite was selected for the leaching experiments. Also, the phases of interest which were selected for analysis were chalcocite, covellite, bornite, pyrite and other non-stoichiometric copper sulfide phases which could have formed during the dissolution reactions.

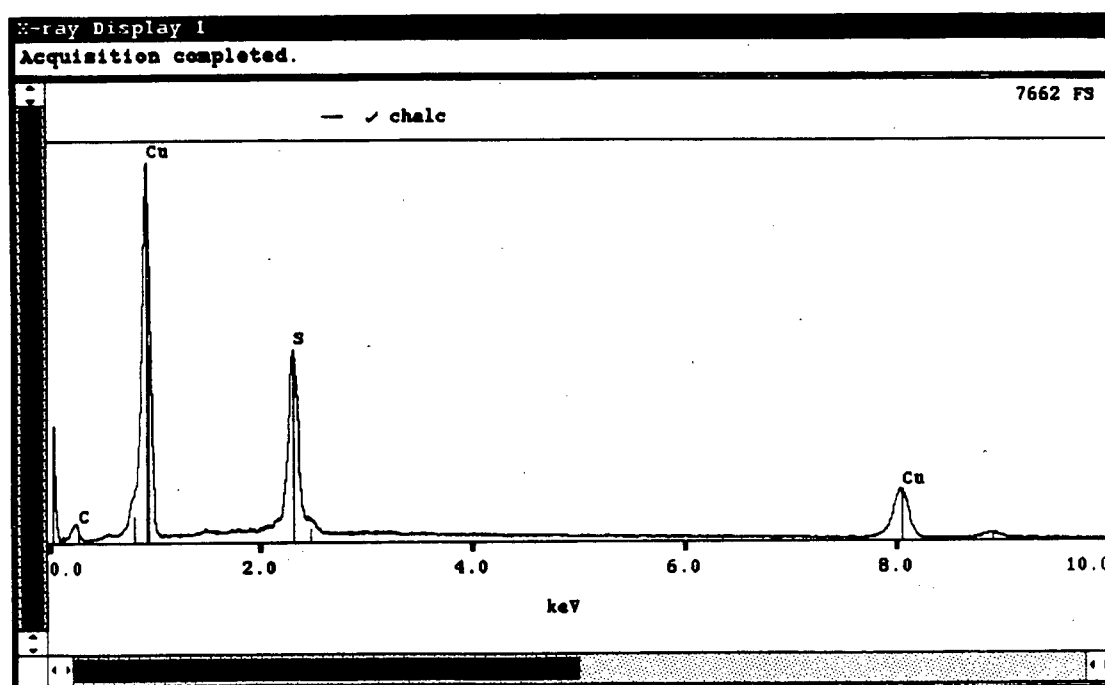


Figure 4-2. X-ray display (elemental composition) analysis of a chalcocite rock section.

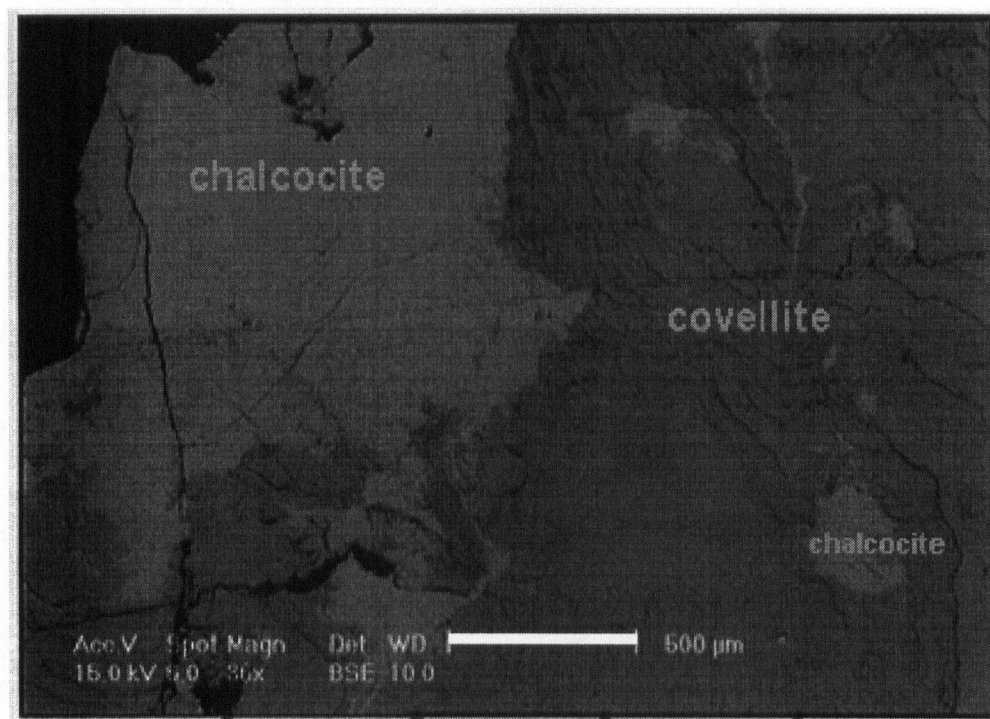


Figure 4-3. Backscattered electron image of a rock section of covellite showing chalcocite zoning in covellite.

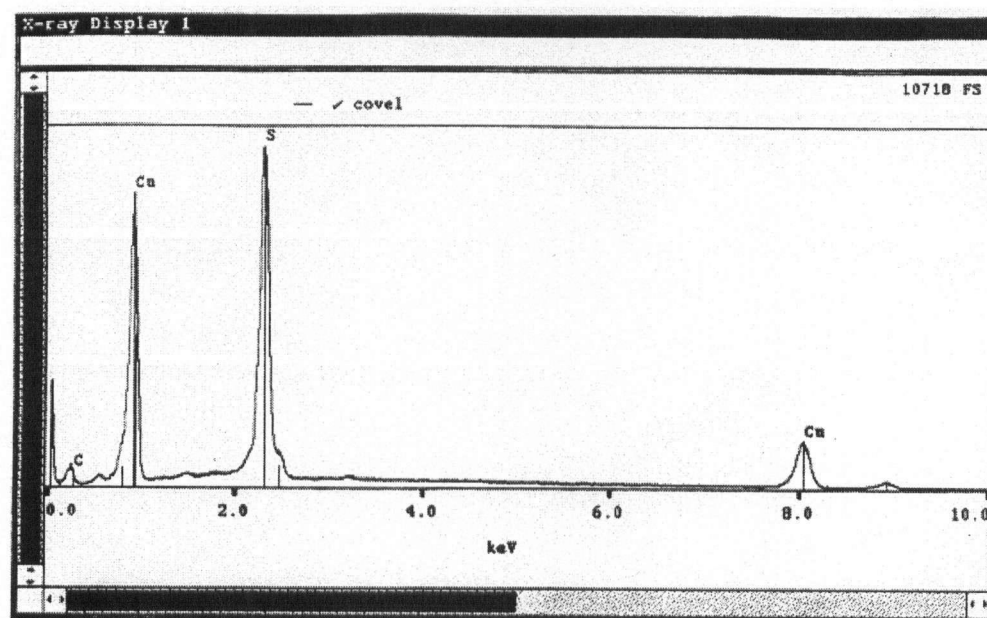


Figure 4-4. X-ray display (elemental composition) analysis of a covellite rock section.

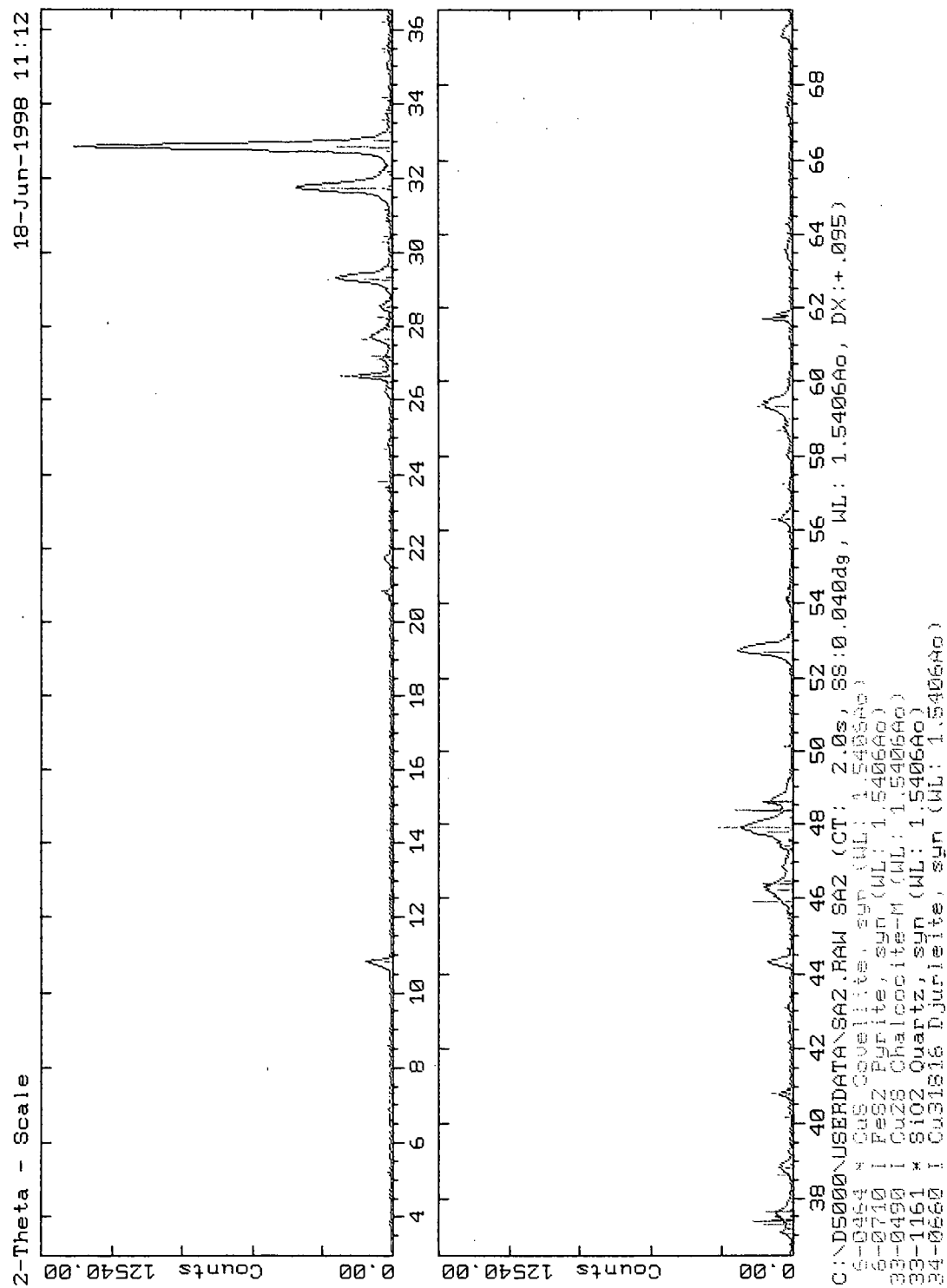


Figure 4-5. X-ray diffraction pattern of natural covellite powder.

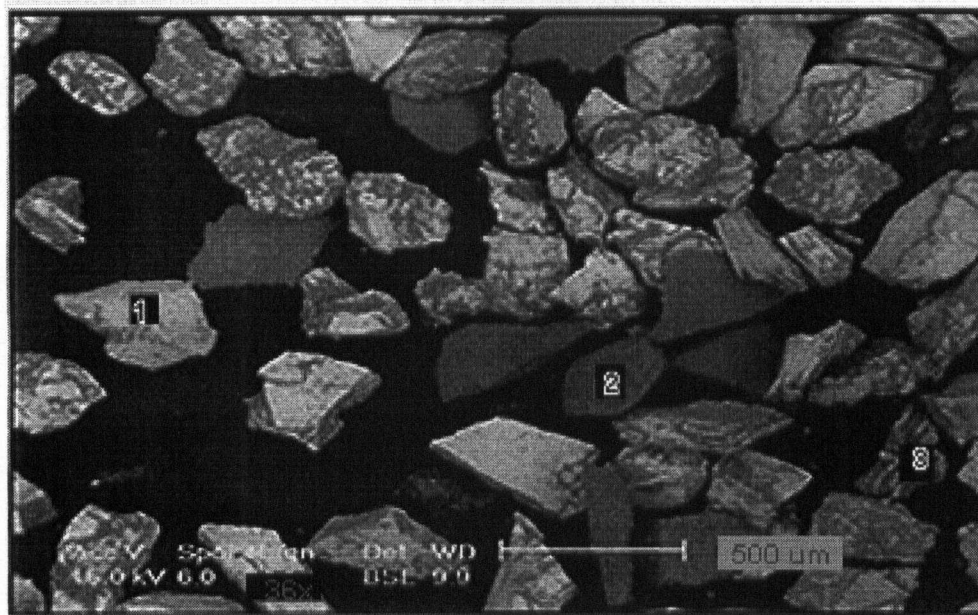


Figure 4-6. Backscattered electron image of -250+212 μm grains of chalcocite showing chalcocite (1), pyrite (2) and bornite (3) at 0% extraction.

4.1.2 X-ray Analyses of Leached Residues

The mineralogical characteristics of the leached residue were compared with that of the natural covellite mineral. The X-ray (powder) diffraction pattern of the leached residue, obtained after 44% copper extraction at 35°C by using standard conditions is shown in Figure 4-7. The major phases in the leached residue were second stage covellite, quartz and pyrite. The skewing of the peaks in the first stage chalcocite leach residue (Figure 4-7) is apparent and the intensities of the major peaks in natural covellite (Figure 4-5) are twice that of the leached residue (especially at $2\theta = 33^\circ$).

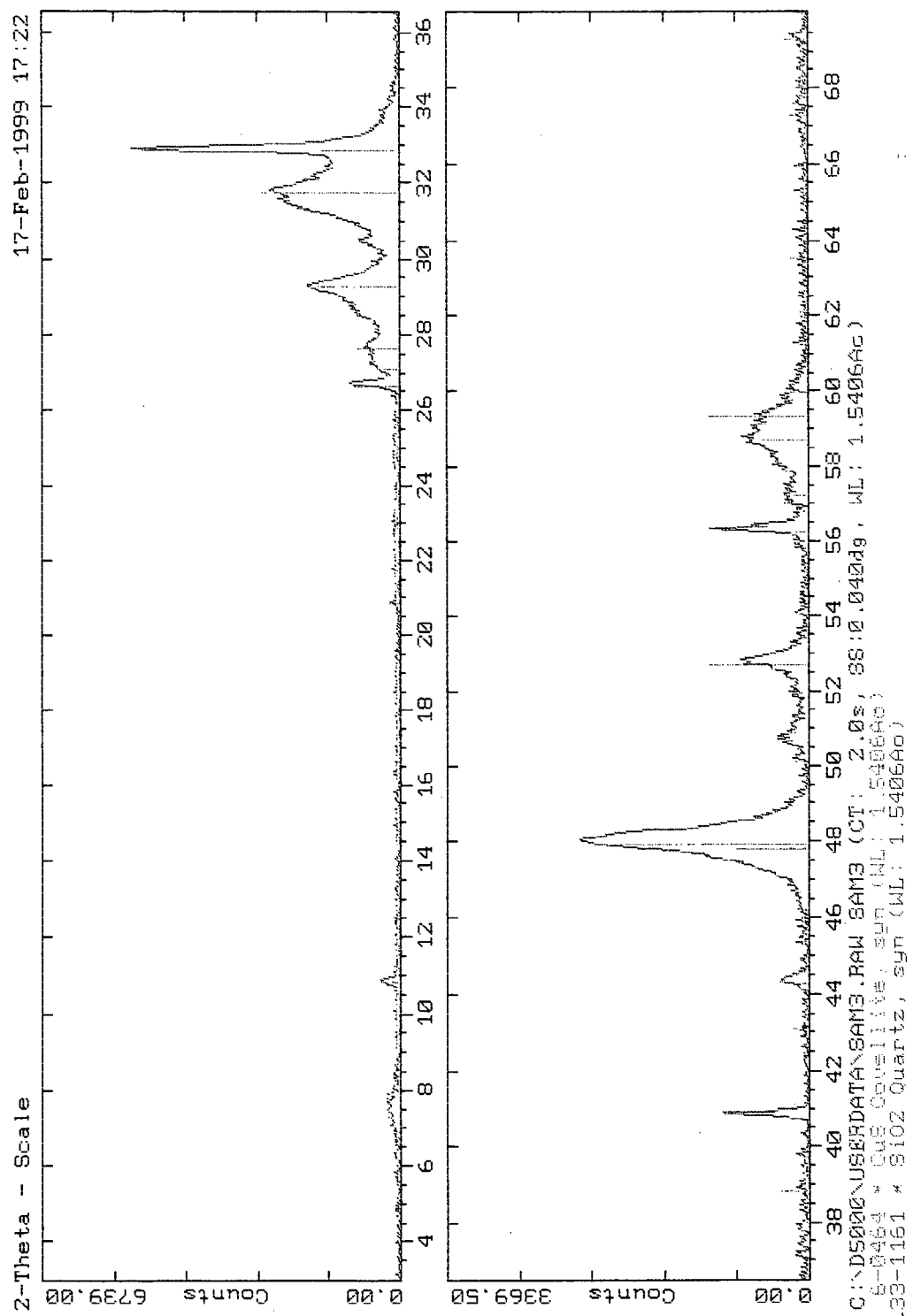


Figure 4-7. X-ray diffraction pattern of the leached residue after 44% extraction, from $-250+212\ \mu\text{m}$ grains of chalcocite at 35°C , $0.116\ \text{mol/L}$ ferric and $0.0202\ \text{mol/L}$ ferrous concentration.

It is possible that the presence of other phases in the leach-residue was responsible for the skewing of the peaks, however, covellite was the principal phase. The diffraction properties and the (indigo-blue) color were the same. Several attempts to match the peaks with copper disulfide (CuS_2), yarrowite ($\text{Cu}_{1.12}\text{S}$), spionkopite ($\text{Cu}_{1.4}\text{S}$) and geerite ($\text{Cu}_{1.6}\text{S}$) failed. It is probable that further grinding of the residue to form powder (which is required by the instrument) altered these phases.

4.1.3 Qualitative Analyses of Leached Residues by SEM-EDX

The leached grains were analyzed for elemental composition of the major phases and local variations in composition. The morphology of the leached particles, which could affect dissolution, is shown in Figure 4-8. Some of the particles retained their initial sizes ($\sim 212 \mu\text{m}$), while some were broken into smaller particles (subsequent to cracks and pore formation). A digital image of a leached grain in Figure 4-9 reveals the formation of cracks at the sub-surface and surface. A sponge-like structure enhanced the reaction throughout the porous particle as well as on the surface. During leaching the grains became puffy (like pop corn) and fragile as shown in Figure 4-10. The cracks and pores were present at both low and high temperature, the mechanism by which high temperature produces a higher rate of leaching (of second stage covellite) must be more than just the physiological changes which are observed on the particle surface. The elemental compositions of the selected phases in Figure 4-11 are summarized in Table 4-1. The grey level intensity shows variations in the composition of grains and local variation within the grains.

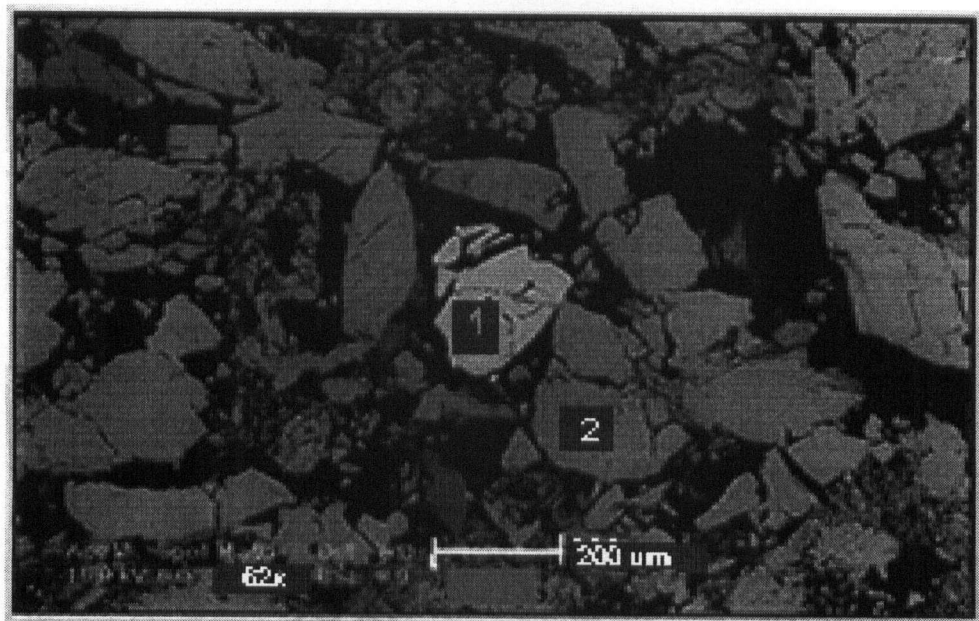


Figure 4-8. Backscattered electron image of the leached grains of chalcocite after 30% extraction at 35°C, 0.116 mol/L ferric, 0.020 mol/L ferrous and 525 mV redox potential (at 35°C). Identified grains in this field are copper-bismuth-sulfide (1) and covellite (2).



Figure 4-9. Digital image of a leached grain showing cracks and pores after 44% extraction at 35°C, 0.116 mol/L ferric, 0.020 mol/L ferrous and 525 mV redox potential (at 35°C).

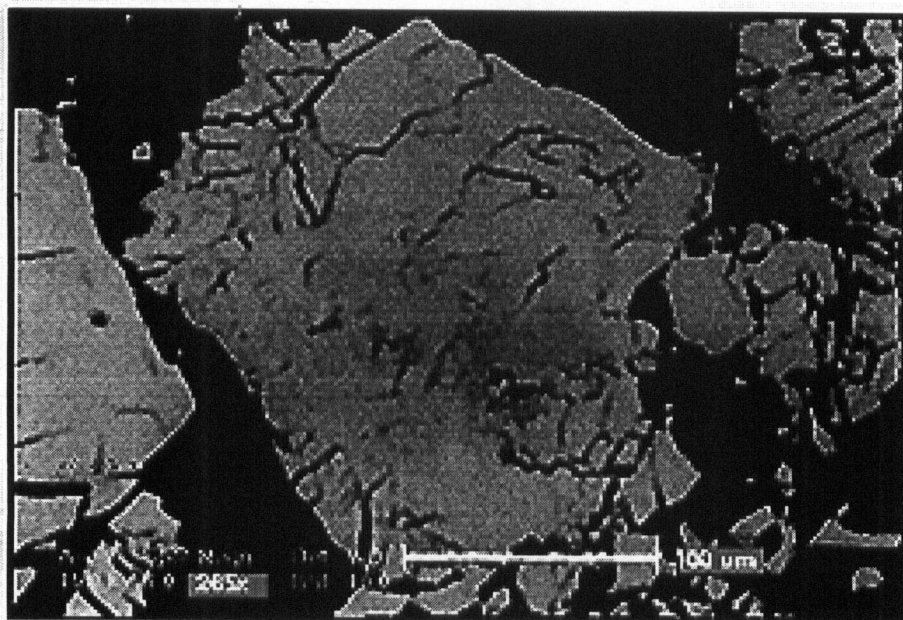


Figure 4-10. Backscattered electron image of a leached grain of chalcocite, showing puffy and fragile textures after 30% extraction at 35°C, 0.116 mol/L ferric, 0.020 mol/L ferrous and 525 mV.

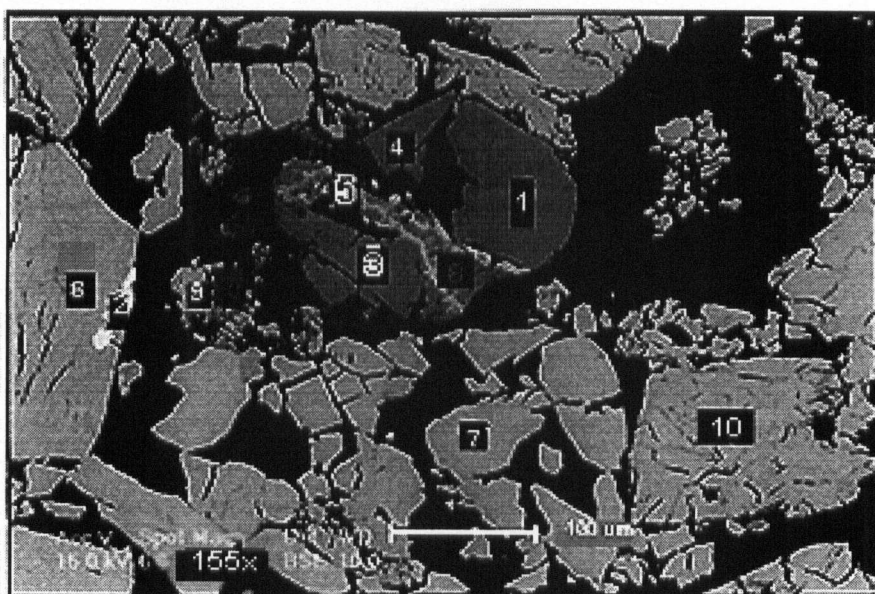


Figure 4-11. Backscattered electron image of selected leached grains for the microprobe (compositional) and elemental analysis of phases, after 44% extraction at 35°C, 0.116 mol/L ferric, 0.0202 mol/L ferrous and 525 mV.

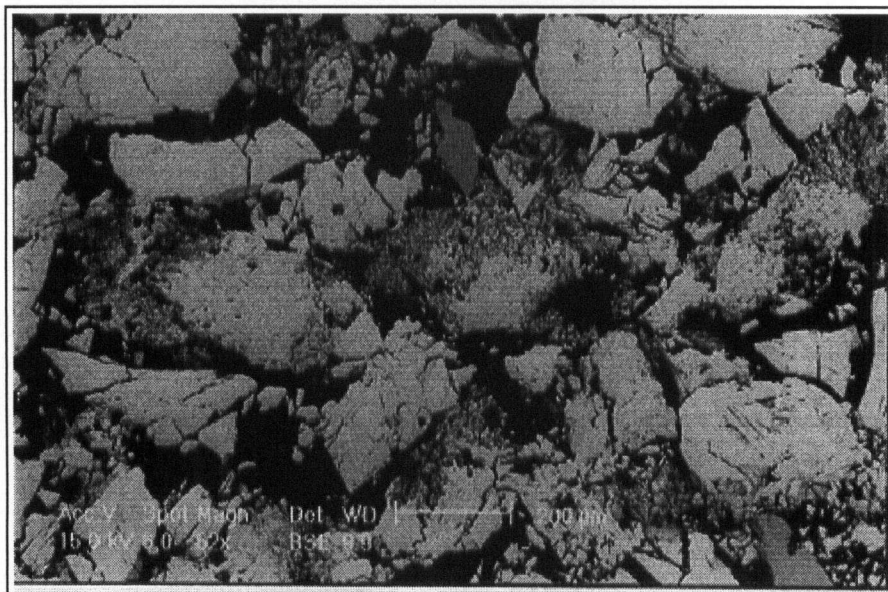


Figure 4-12. Backscattered electron image of selected leached grains after 10% extraction at 35°C, 0.116 mol/L ferric, 0.0202 mol/L ferrous and 525 mV.

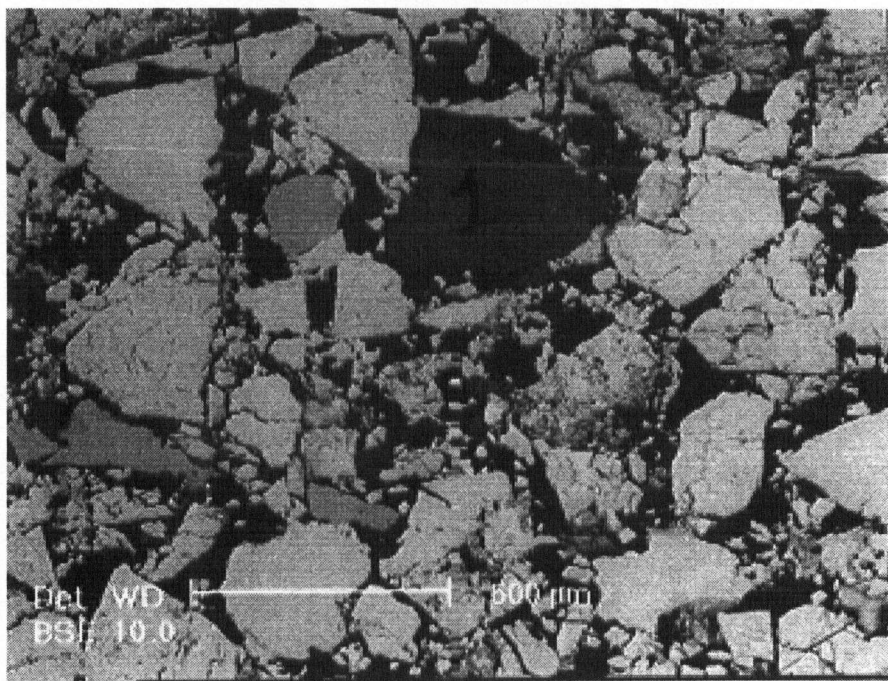


Figure 4-13. Backscattered electron image of selected leached grains after 40% extraction at 75°C, 0.116 mol/L ferric, 0.0202 mol/L ferrous and 567 mV.

Table 4-1. Summary of qualitative analyses of the leached residues by SEM

Spot Number	Elemental Composition	Remarks
1	Fe, S	Pyrite (Figure 4-11)
2	Cu, Bi, S	Bismuth, associated previously with chalcocite as a replacement atom for copper (Figure 4-11)
3	Fe, S	Pyrite associated with two other phases within a grain
4	Fe, S	Pyrite
5	Cu, S, As, Fe	Unleached enargite (Cu_3AsS_4) initially present in the (hydrothermal) veins of the feed as a result of paragenesis effects (Figure 4-11).
6	Cu, S	Covellite; equal intensity of K_α peaks
7	Cu, S	Covellite
8	Cu, S	Non-stoichiometric copper sulfide phase; yarrowite
9	Cu, S	Covellite phase forming from yarrowite; this is shown by the grey level difference (between spot 8 and 9 in Figure 4-11) within the same grain.
10	Cu, S	Non-stoichiometric copper sulfide (yarowite) single phase. (Figure 4-14 below)

The dissolution features on the yarrowite grains are shown in Figure 4-14. The Cu-Bi-S phase was observed as a single phase in one of the grains and its X-ray (display) analysis which differed from that of covellite phase (Figure 4-4) is shown in Figure 4-15. The dissolution features (cracks and pores) which were present on the surface of this grain revealed the prior leaching of the Cu-S portion leaving the bismuth and where the Cu-Bi-S occurred with other phases in a grain, less cracks were formed on this phase unlike the other phases. The origin of the bismuth is unclear although, substitution of copper atoms in the altered chalcocite phase is possible because the chalcocite lattice

behaves as a solid solution which can accommodate other atoms. However, naturally occurring copper-bismuth sulfide minerals have not been reported in the literature.

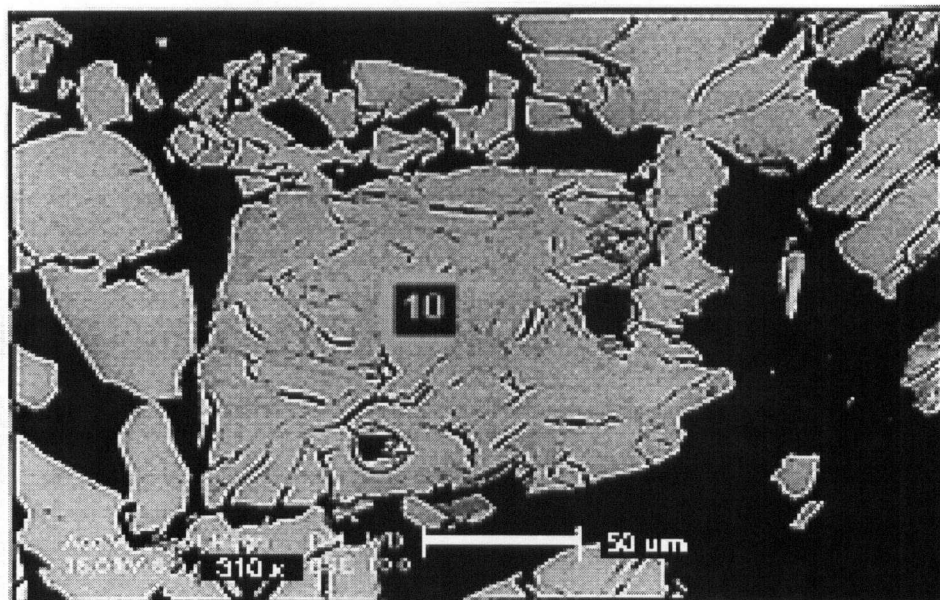


Figure 4-14. Backscattered electron image of a yarrowite grain showing cracks.

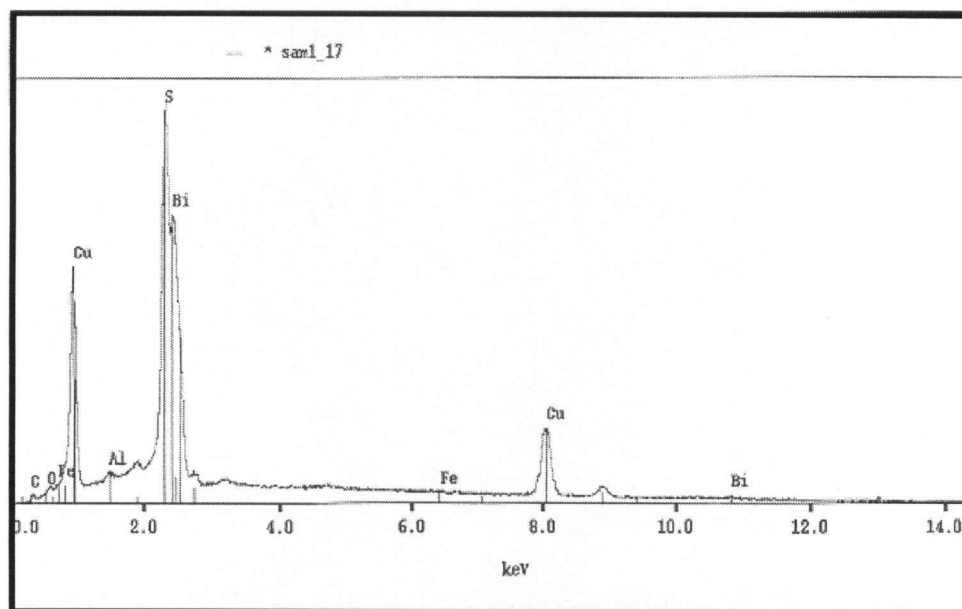


Figure 4-15. X-ray analysis of a Cu-Bi-S phase, showing the reduction of K_{α} peak intensity for copper as a result of some paragenesis effects. This differed from that of Figure 4-4.

As shown in Figure 4-16, some elemental zoning was observed on the leached particles, such as iron zoning (spot 1) in the copper sulfide grains. This is one of the paragenesis effects, which could have occurred over a geological time as a result of chemical changes or crystallographic changes to the initial ores. It was apparent that zoning affects leaching because fewer cracks were formed on these zones compared with the iron-free copper sulfide matrix. The preferential leaching of the iron-free matrix (spot 2) may be due to a galvanic effect making this phase more susceptible to ferric oxidation than the iron zone.

The leaching of each grain is influenced by the adjacent grains, especially when the grains are joined together as shown in Figure 4-17. The pyrite grain (spot 1) which is adjacent to a non-stoichiometric bornite grain (spot 2). The bornite leached preferentially to the adjacent pyrite phase.

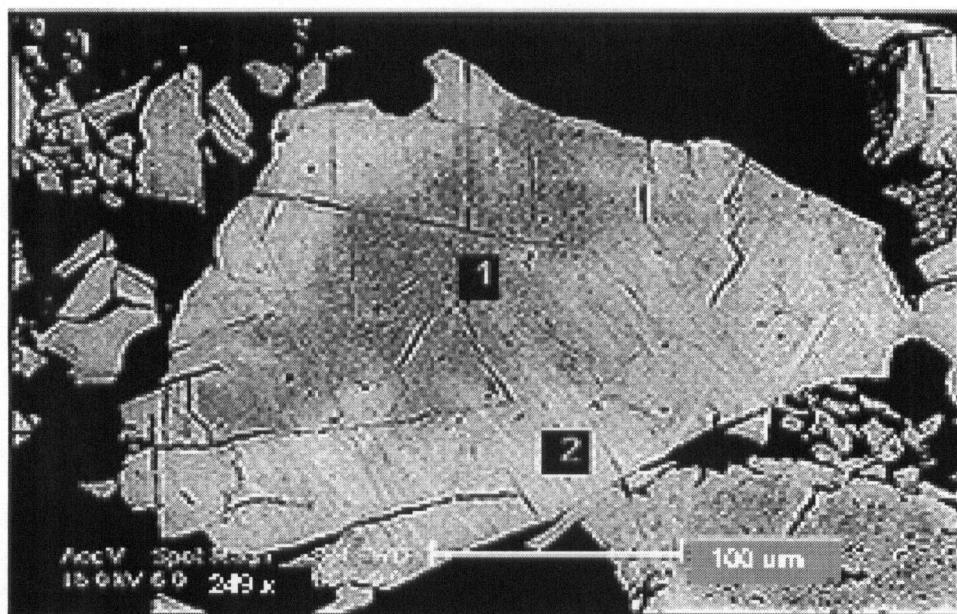


Figure 4-16. Backscattered electron image of an iron zone (1) in copper sulfide phase (2). The grey level intensity shows differences in composition within the grain. Leach conditions: 35°C, 0.116 mol/L ferric, 0.0202 mol/L ferrous and 525 mV redox potential (at 35°C).

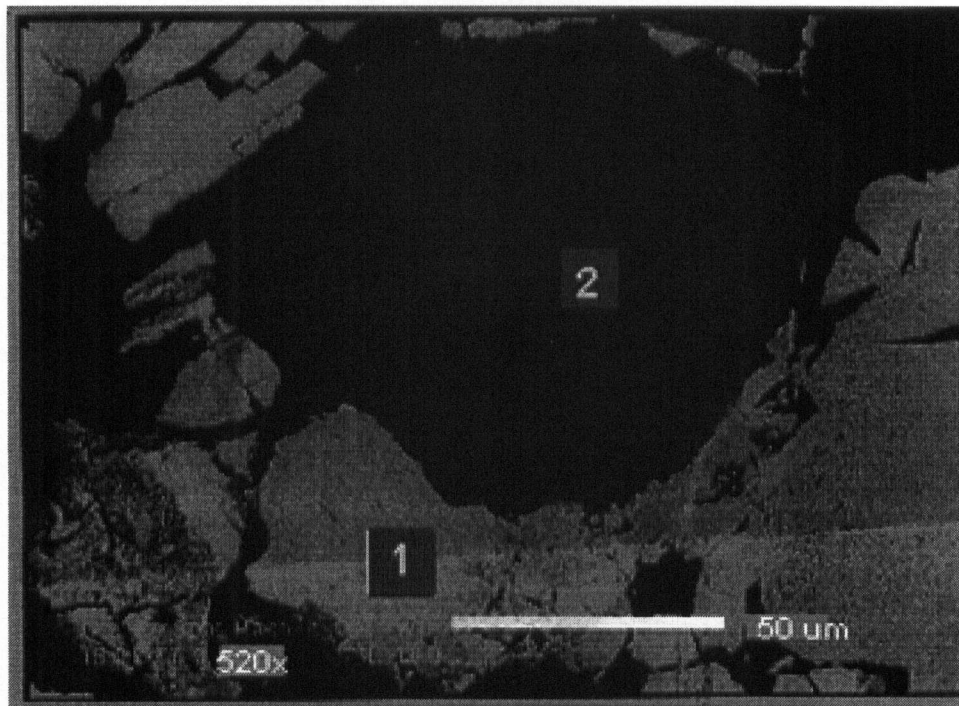


Figure 4-17. Backscattered electron image of adjacent grains of bornite (1) and pyrite (2), showing the preferential leaching of the bornite grain. Leach conditions: 35°C, 0.116 mol/L ferric, 0.0202 mol/L ferrous ferrous and 525 mV redox potential (at 35°C).

4.1.4 Compositional Changes by Electron Microprobe Analysis

The analyzed grains were from the standard leaching experiment carried out at 35°C by using a leach solution of 0.116 mol/L ferric, 0.0202 mol/L ferrous and with a redox potential maintained at 525 mV. The initial ferric to copper (in the solid minerals) mole ratio was 2.0. The experiment was terminated after 90 minutes. The chemical analysis of the leach solution revealed 44% copper extraction at this stage. The chemical compositions of the phases, which were found in the leached grains are presented in Table 4-2. The electron microprobe analyses of the phases, which were previously identified by SEM-EDX analysis, revealed that the pyrite phase remained unchanged with the Fe: S atomic ratio remaining at 0.50.

Some chalcocite phase (at this copper extraction stage) had changed to yarrowite and covellite with Cu : S atomic ratios of 1.12 and 1.00 respectively. Though the copper extraction was less than 50%, some covellite phases were formed, which means once a phase is formed the transformation to the next phase commences. The bornite phase was transformed to a non stoichiometric phase ($\text{Cu}_{3.6}\text{FeS}_{4.2}$), while the Fe : S atomic ratio remained approximately at 0.25. This is equal to that of the initial (stoichiometric) bornite (Cu_5FeS_4), while the Cu : S and Cu : Fe atomic ratios decreased. This non-stoichiometric bornite is approximately idaite (Cu_3FeS_4), which has been identified previously (by the same technique) in the leached residue of bornite at about 40% copper extraction [78].

Table 4-2. Chemical compositions of the resulting phases by EPMA

Phase	W%(S)	W%(Fe)	W%(Cu)	Total	A%(S)	A%(Fe)	A%(Cu)	Fe/S	Cu/S
Pyrite	53.90	46.33	0.10	100.33	66.86	33.00	0.06	0.49	0.00
Pyrite	53.75	46.17	0.09	100.00	66.89	32.99	0.05	0.49	0.00
Covellite	31.90	1.25	66.33	99.48	48.22	1.09	50.60	0.02	1.05
Yarrowite	30.66	1.20	67.84	99.70	46.72	1.05	52.16	0.02	1.12
Yarrowite	30.56	0.10	67.58	98.24	47.16	0.09	52.62	0.00	1.12
Covellite	32.58	0.07	66.60	99.25	49.15	0.06	50.70	0.00	1.03
Idaite	31.75	13.06	54.26	99.07	47.57	11.23	41.02	0.24	0.86
Idaite	31.21	12.92	53.19	97.32	47.60	11.31	40.94	0.24	0.86

W= weight percent; A= atomic percent

The enargite phase (Cu_3AsS_4) which was present initially in association with pyrite either as a replacement deposit or in the hydrothermal veins of pyrite (Figure 4-10, spot 5), remained unreacted. The Cu : S, Cu : As and As : S atomic ratio remained at

~0.80, 3.00 and 0.25 respectively (Table 4-3). This is significant because a hydrometallurgical process, which will leach copper from copper sulfide minerals without dissolving arsenic (from the trace mineral) is highly desirable because of the stringent environmental requirements on arsenic disposal.

The composition of the copper bismuth sulfide after leaching revealed that the chalcocite transformed to covellite, without the dissolution of the substituted bismuth.

Table 4-3. Chemical compositions of the minor phases by EPMA

Phase	W%(S)	W%(Cu)	W%(Bi)	W%(As)	A%(S)	A%(Cu)	A%(As)	A%(Bi)	Total, A%
Enargite	27.72	45.46	0.46	16.07	45.08	37.31	11.18	0.11	93.68
Enargite	28.34	47.03	0.27	18.39	45.50	38.10	12.64	0.07	96.31
Cu(Bi)S	19.50	38.72	42.21	0.00	42.69	42.77	0.00	14.18	99.64
Cu(Bi)S	19.66	37.61	41.38	0.00	43.58	42.08	0.00	14.08	99.74

W= weight percent; A= atomic percent

4.2 Results of Chemical Leaching Experiments: First Stage Leaching

The effects of the leaching parameters on the first stage kinetics are presented in the following sections.

4.2.1 Effect of Controlled Potential

The effect of controlled potential on the kinetics of first stage is shown in Figure 4-18. By allowing the redox-potential to drift from 525 mV (at the beginning of the experiment) to 460 mV (at the end), the rate of leaching was strongly altered when compared with the profile which was obtained at constant potential of 525 mV.

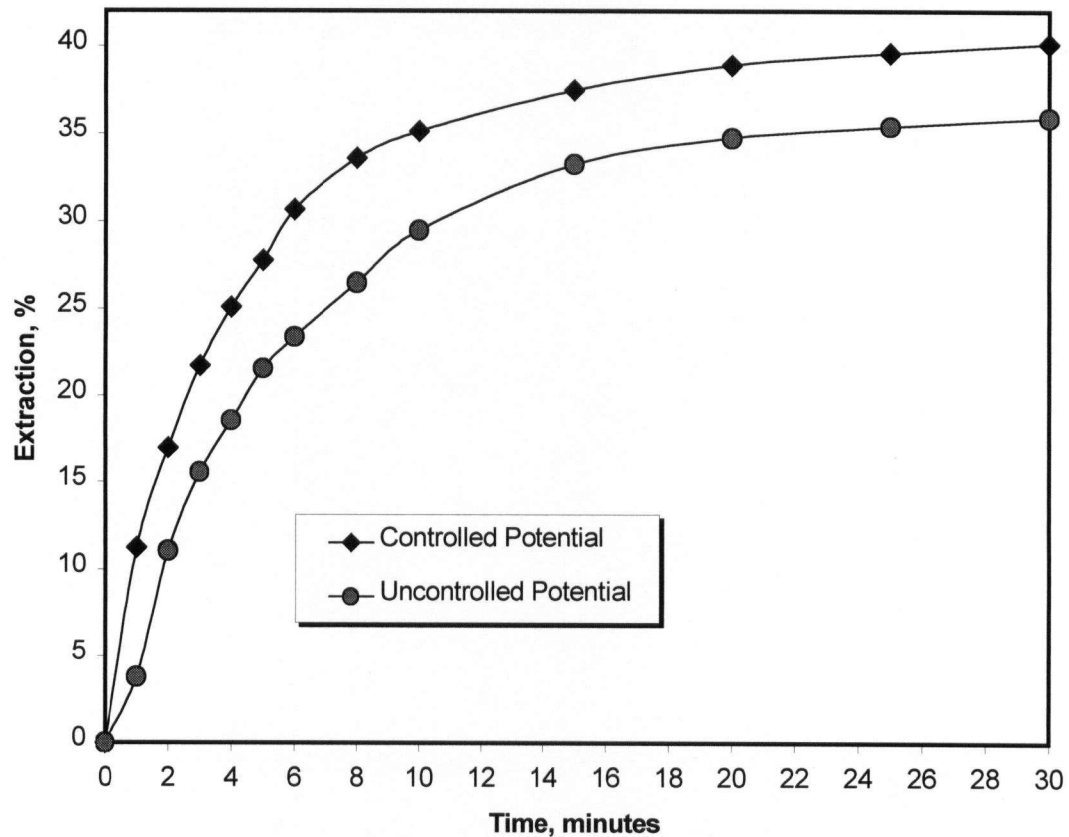


Figure 4-18. Effect of potential (525 mV) on the first stage leaching of -250+212 μ m particles at 35°C, 0.116 mol/L ferric and 0.0202 mol/L ferrous.

4.2.2 Effect of Temperature

The effect of temperature on first stage leaching is shown in Figure 4-19. The results were obtained by using the same leach solution (standard conditions) at different temperatures. The ferric/ferrous ratio was kept constant in each test. The rate of leaching was very fast at all temperatures and at 75°C, the first stage was completed within 15 minutes. An Arrhenius plot based on the reaction rate is shown in Figure 4-20. The method of initial rates [79] was used by drawing tangents to the extraction versus time curves. The slope of the tangent between 0% and 40% extraction was taken as the rate of leaching in each experiment. An activation energy of 34.0 kJ/mol indicates mixed kinetics, in which the rate is controlled simultaneously by diffusion and chemical reaction. This is higher than most of the values (section 2.5) which have been reported previously by about 50%.

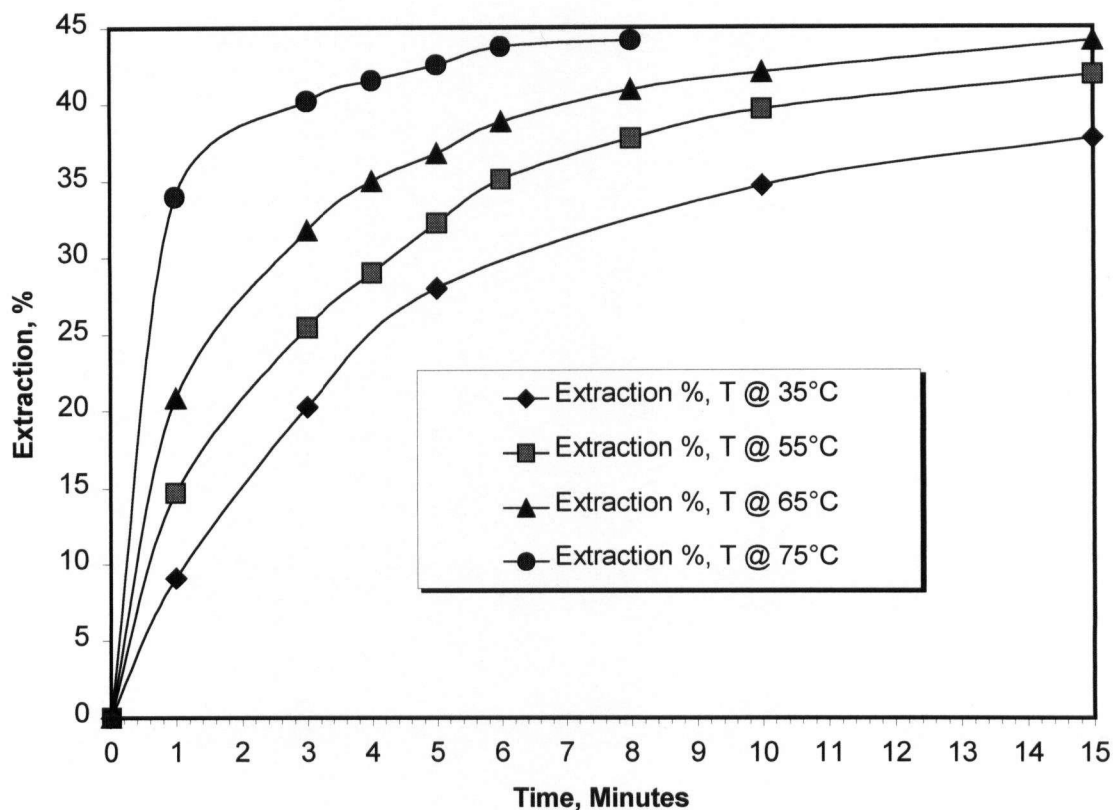


Figure 4-19. Effect of temperature on the first stage leaching of $-250+212\ \mu\text{m}$ particles at 0.116 mol/L ferric and 0.0202 mol/L ferrous.

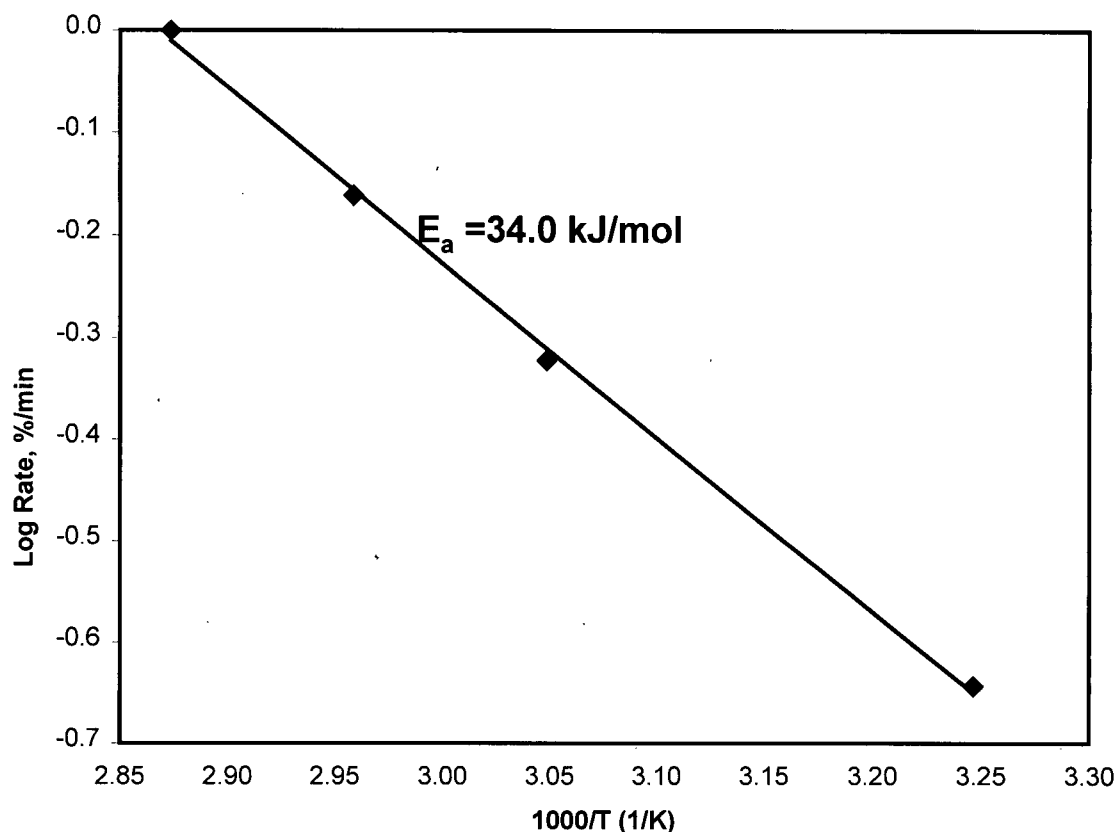


Figure 4-20. Arrhenius plot for the first stage leaching.

4.2.3 Effect of Initial Ferric Concentration

The effect of ferric concentration on the first stage is shown in Figure 4-21. The standard condition was used in all the experiments except that ferrous concentration was changed to 0.0101 mol/L. The ferric concentrations of 0.007, 0.0145, 0.029, 0.058, 0.116, 0.174 and 0.232 mol/L correspond to initial ferric : copper (in solid mineral) mole ratios of 0.125, 0.25, 0.50, 1.00, 2.00, 3.00 and 4.00 respectively. The kinetics were similar at very low concentrations (at 0.0145 and 0.029 mol/L) up to 20% copper extraction (which corresponds to geerite) and linear (up to 30% copper extraction) at high concentrations. At concentration of 0.058 mol/L, the reaction was markedly more rapid and there may have been a change of mechanism at this level. At low concentrations (below 0.058 mol/L), the rate was directly proportional to the ferric concentration (first order with respect to ferric concentration) as shown in Figure 4-22. In this range, the rate was most

likely limited by mass transfer of ferric to the mineral surface (which is similar to Type III leaching in section 2.2.3) and the reaction rate corresponded to the limiting current density of the ferric/ferrous couple. At high concentrations (above 0.058 mol/L), the order of reaction decreased to 0.5 (as shown in Figure 4-22) with respect to ferric concentration. The change in the order of reaction at high concentration (as a result of a change of mechanism) has not been quantified previously in the literature.

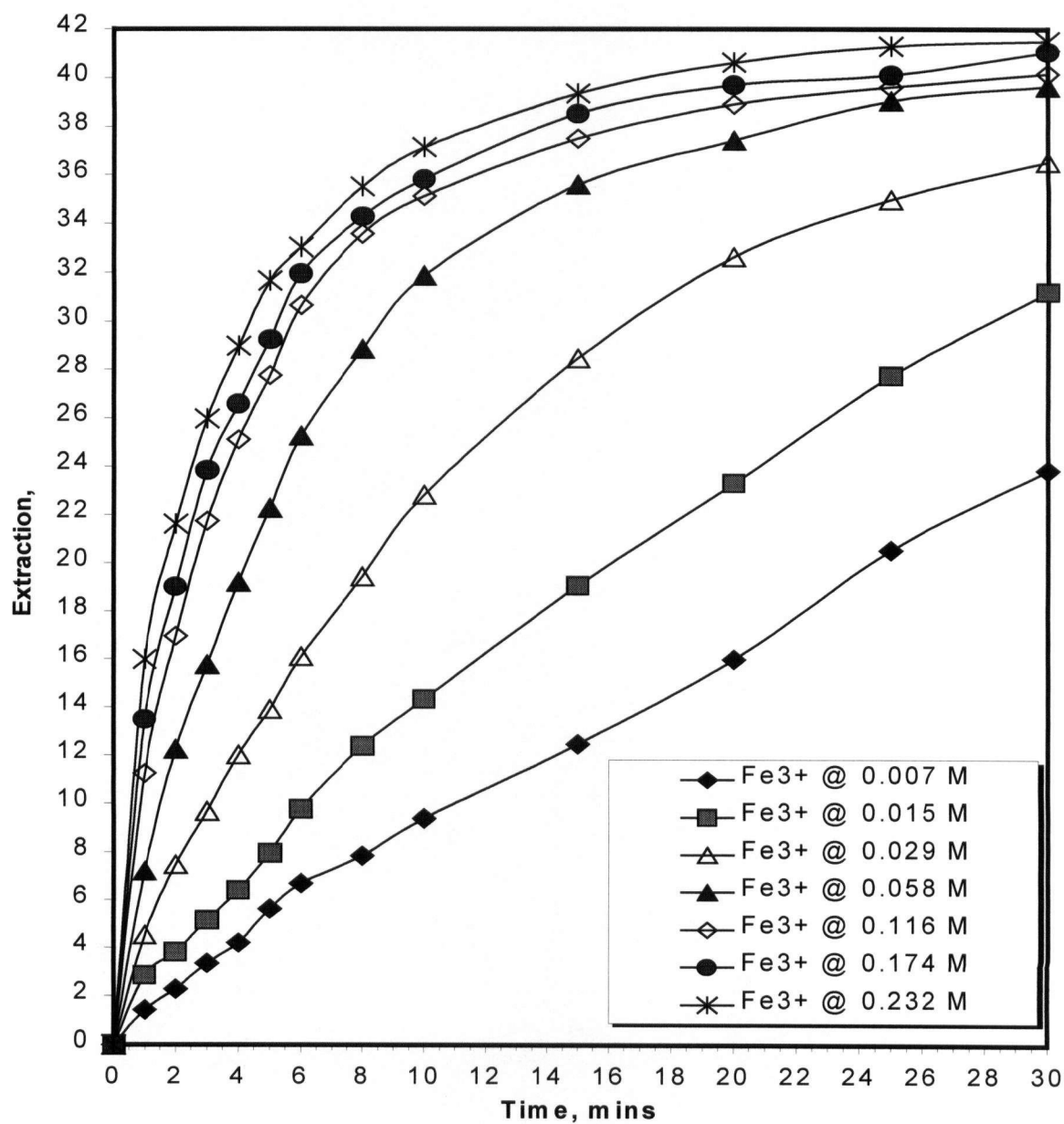


Figure 4-21. Effect of ferric on the first stage leaching of $-250+212 \mu\text{m}$ particles at 35°C and 0.0101 mol/L ferrous.

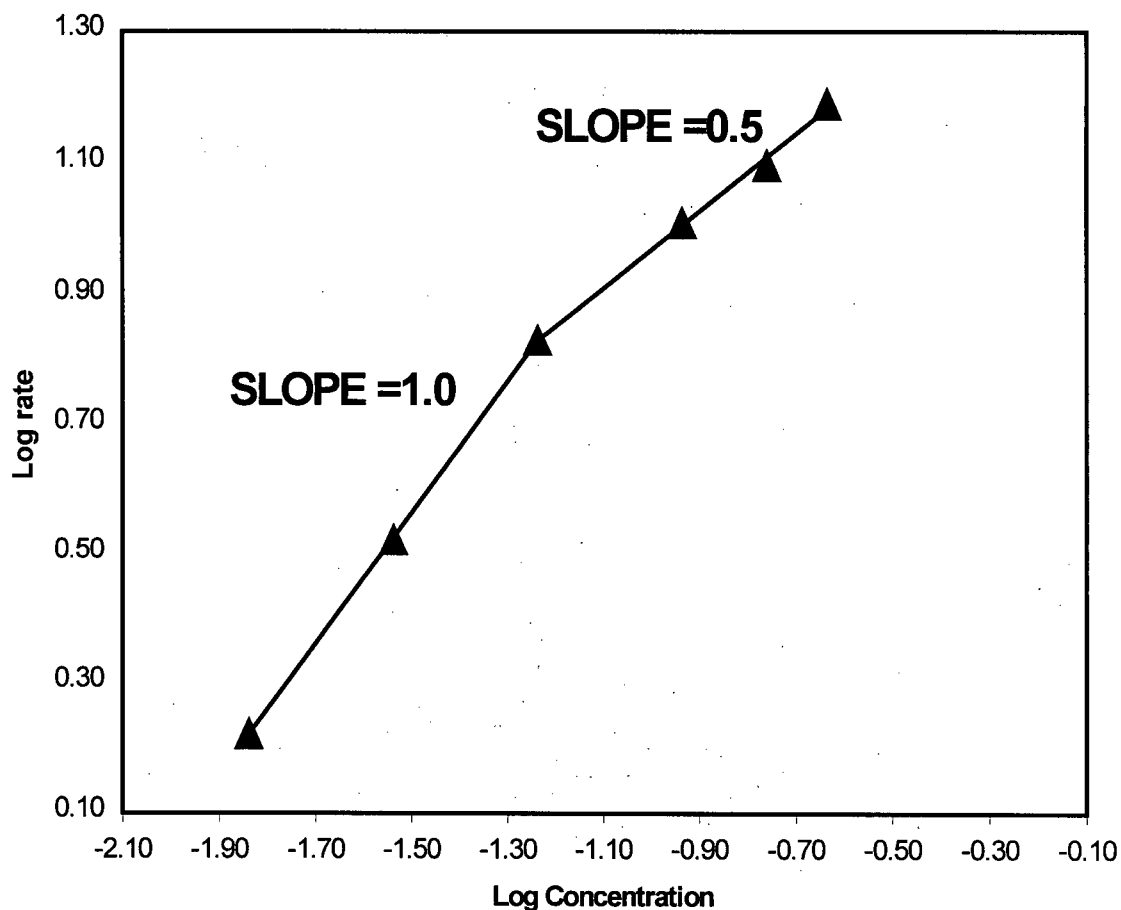


Figure 4-22. Log rate vs. log ferric concentration plot for the first stage leaching.

4.2.4 Effect of Initial Particle size

The geometric mean radius and the area of the different particle size fractions (based on spherical geometry) are summarized in Table 4-4.

Table 4-4. Geometric analysis of the different particle size fractions.

Size Fraction (X), μm	Mean Radius, cm	Area, cm^2
-355+300	0.01632	0.00335
-300+250	0.01369	0.00236
-250+212	0.01151	0.00167
-180+150	0.00822	0.00085

The standard conditions were used to obtain the results shown in Figure 4-23. The instantaneous rates of reaction were obtained by differentiating the extraction-time data and these were plotted against the reciprocal of radius squared in Figure 4-24, and against the reciprocal of radius in Figure 4-25. At less than 20% copper extraction, the rate of reaction was inversely proportional (a straight line through the origin) to the radius squared. This implies that the rate is controlled initially by diffusion of ferric ions through the product layer to the interface, which is formed by the transformation of chalcocite, djurleite, digenite and anilite. At 20% copper extraction (which corresponds to geerite), the rate of reaction was inversely proportional to the radius. Subsequent to 30% extraction, the rates were equal for the different size fractions as shown in Figure 4-23. The mineralogical studies showed that cracks, breakage and pores were formed before the end of the first stage, and became much more pronounced at about 25% extraction. The (newly) exposed area reacted at the same rate and the kinetics shifted to chemical reaction control.

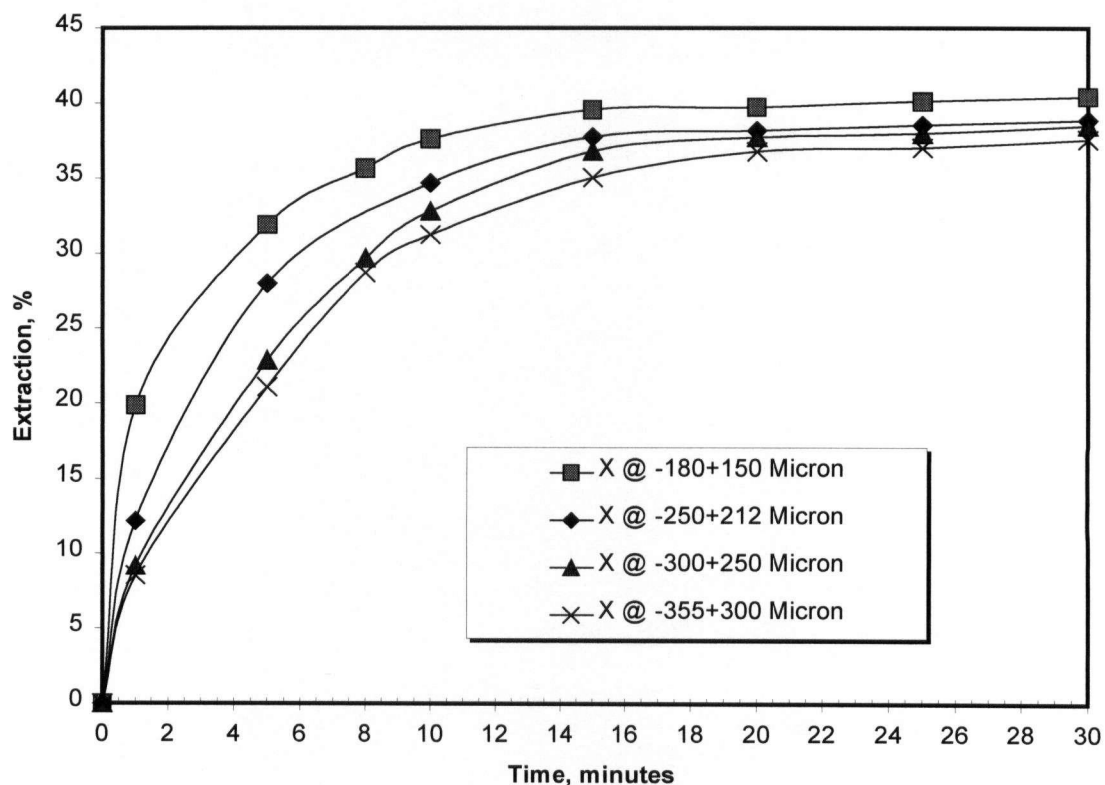


Figure 4-23. Effect of particle size on the first stage leaching at 35°C, 0.116 mol/L ferric and 0.0202 mol/L ferrous.

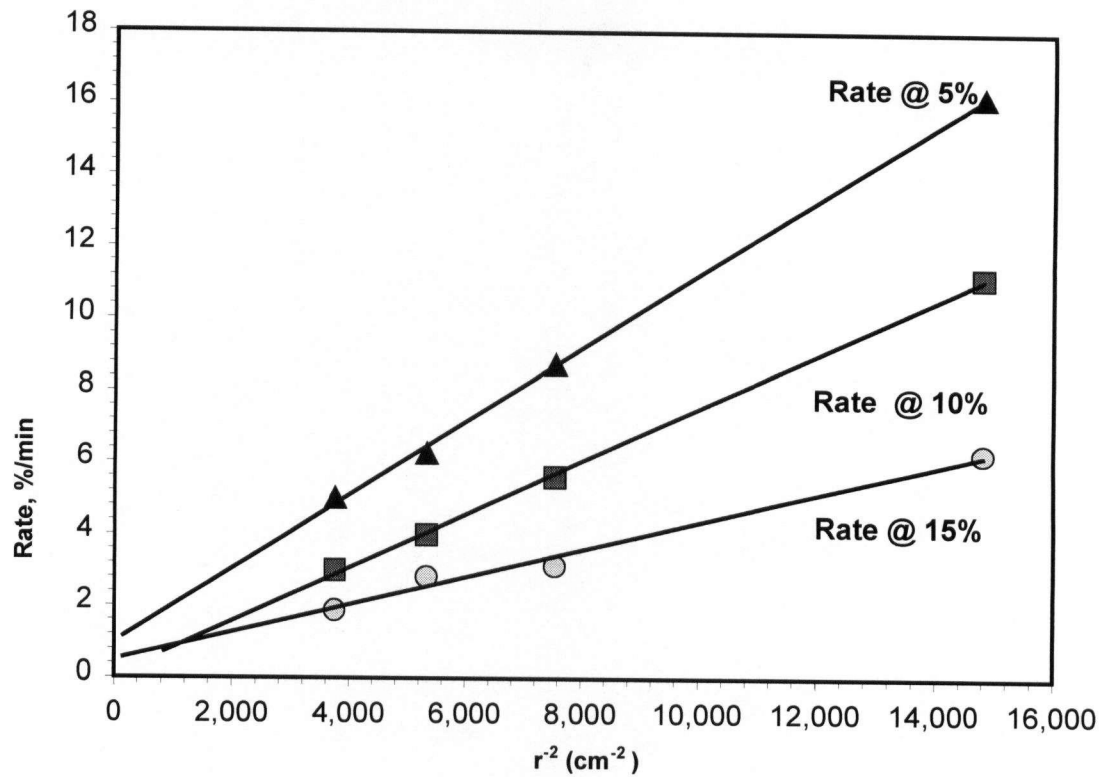


Figure 4-24. Rate vs. the reciprocal of radius squared plot for first stage leaching.

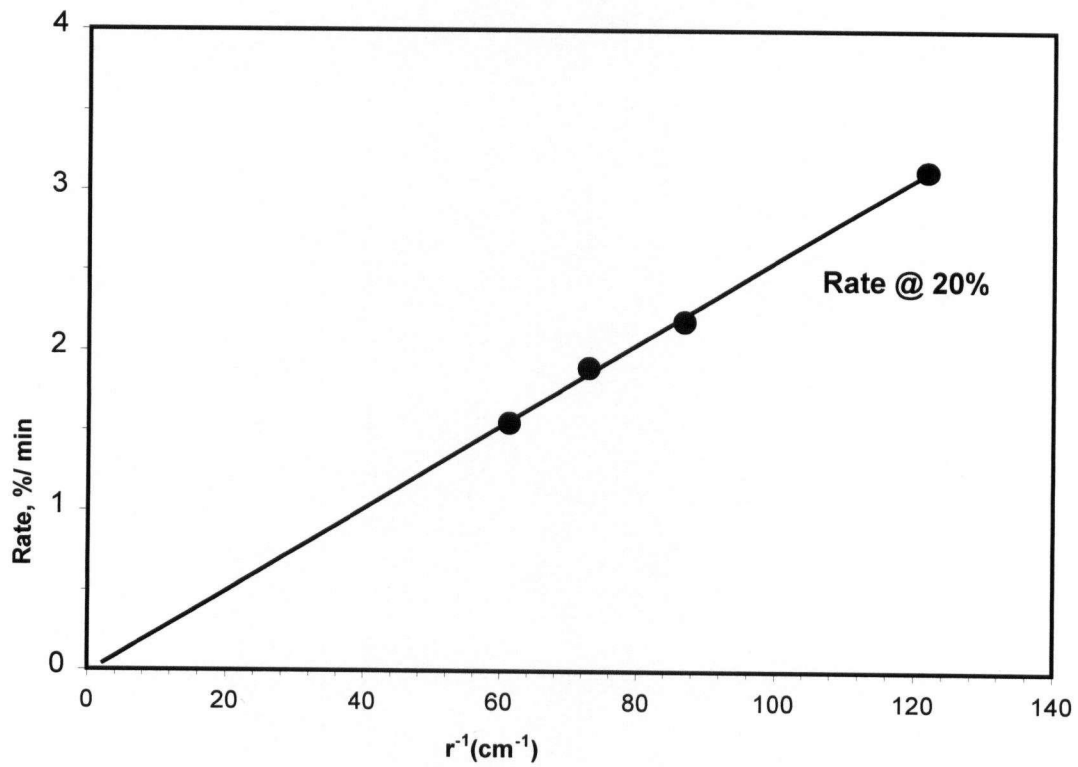


Figure 4-25. Rate vs. the reciprocal radius plot for first stage leaching.

4.2.5 Effect of Initial Ferrous Concentration

The effect of ferrous concentration on the kinetics of first stage leaching is shown in Figure 4-26 and Figure 4-27. The two sets of results were obtained at low and high concentration of ferric (0.116 and 0.232 mol/L respectively) to corroborate the previous observations in section 4.2.2. Other operating conditions were the same in each set. At the low concentration of ferric (0.116 mol/L), an increase in ferrous concentration up to 0.108 mol/L had no effect on the kinetics of first stage leaching (Figure 4-26). This confirmed that the rate of the first stage is controlled by the mass transfer of ferric ions to the mineral surface and that the reaction is occurring at the cathodic limiting current density. The back reaction involving ferrous ions at the cathode has no effect on the rate.

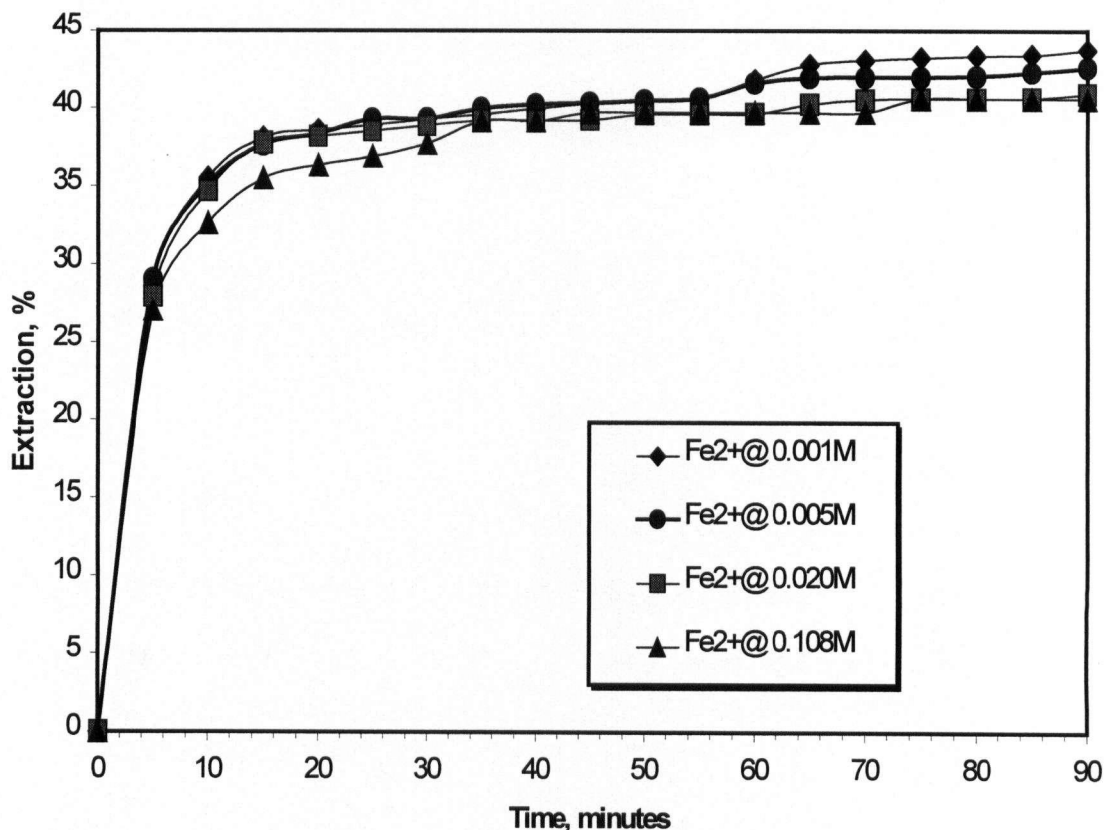


Figure 4-26. Effect of ferrous on the first stage leaching of -250+212 μ m particles at 35°C and 0.116 mol/L ferric.

However, at the higher concentration of ferric (0.232 mol/L), in which the mixed-potential becomes more positive and corresponds to the reversible potential of the ferric/ferrous couple, an inverse relationship between rate and ferrous concentration was observed (Figure 4-27).

The fractional order of reaction was obtained by plotting log rate vs. log ferrous concentration as shown in Figure 4-28. The rates were obtained by the same method used in Section 4.2.2, but the slopes of the tangents were evaluated between 20% and 50% extraction. The fractional order decreased from -0.15 to -0.4 (approximately) as the ferrous concentration increased as shown Figure 4-29. This is similar to type II leaching, in which an electron transfer mechanism in the anodic (dissolution) reaction is the rate-controlling step.

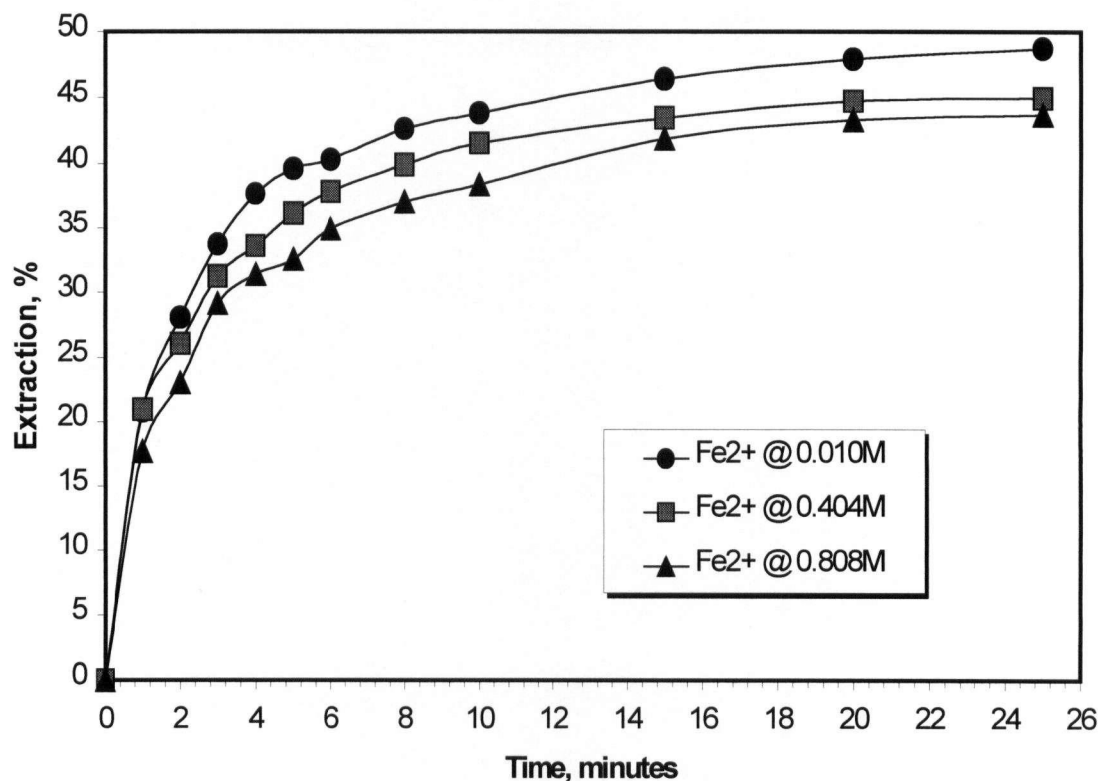


Figure 4-27. Effect of ferrous on the first stage leaching of -250+212 μ m particles at 35°C and 0.232 mol/L ferric.

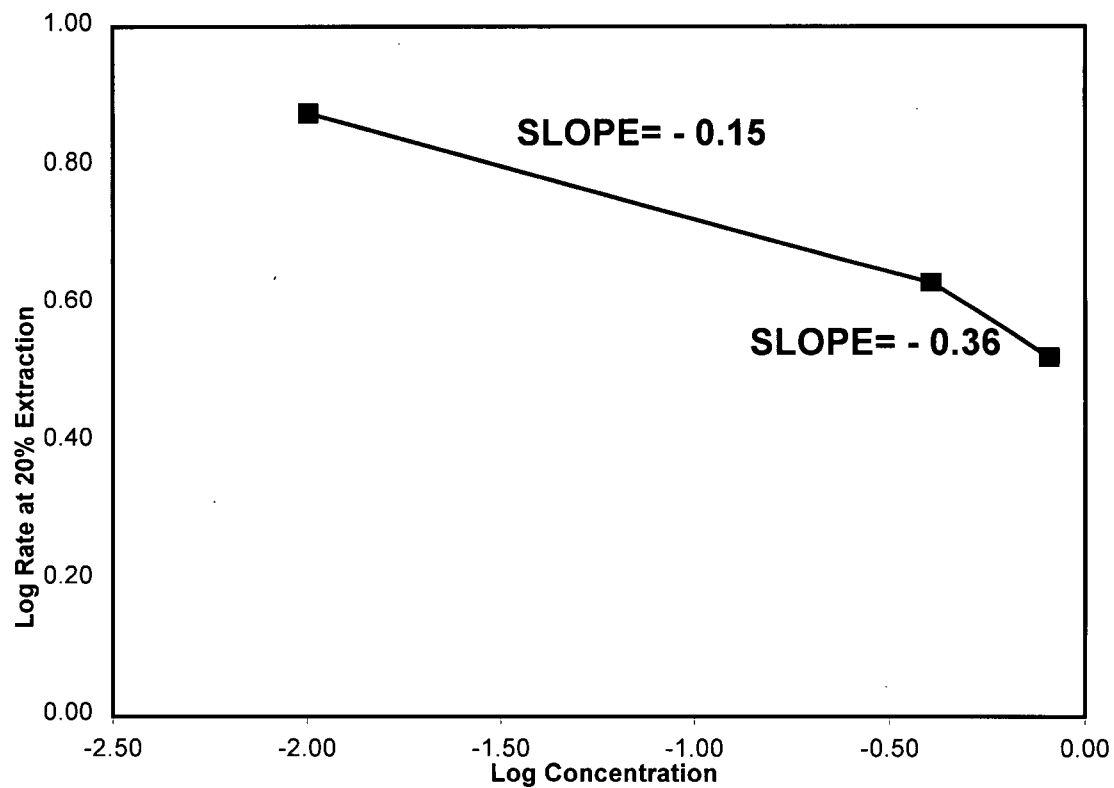


Figure 4-28. Log rate vs. log ferrous concentration plot for the first stage leaching of -250+212 μm particles at 35°C and 0.232 mol/L ferric.

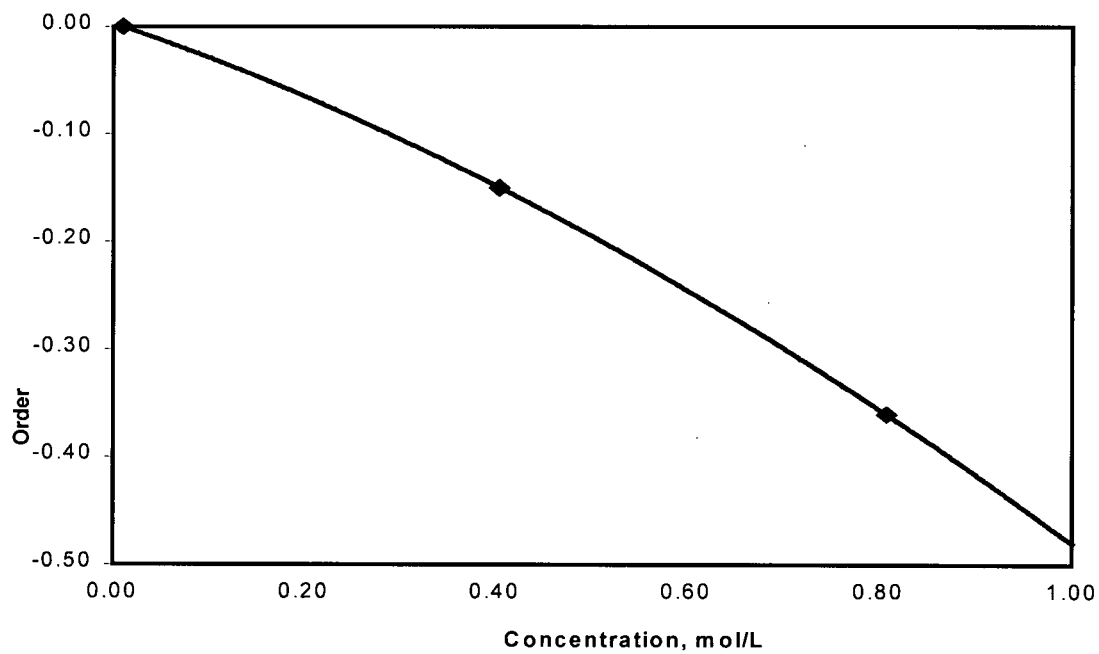


Figure 4-29. Reaction order vs. ferrous concentration plot for the first stage leaching.

4.3 Results of Chemical Leaching Experiments: Second Stage Leaching

The product of first stage leaching is covellite, with a structure and chemical composition identical to natural covellite. The effects of leaching parameters on the kinetics of second stage leaching are presented in the following sections.

4.3.1 Effect of Controlled Potential

The effect of controlled potential on the kinetics of second stage leaching is shown in Figure 4-30. The ferric/ferrous solutions were the same in the experiments. By allowing the redox-potential to drift from 567 mV to 500 mV (at 75°C) for 15 minutes before engaging the controller to maintain the potential at this level for the subsequent period of time, the leaching profile was strongly altered.

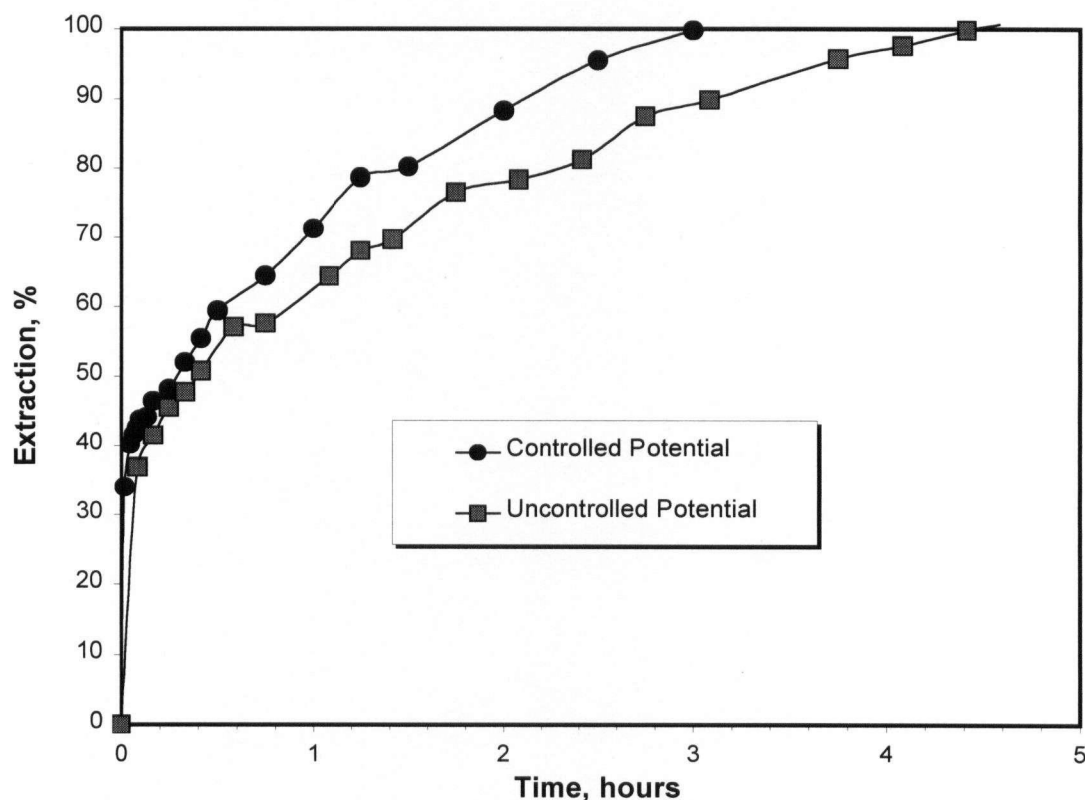


Figure 4-30. Effect of potentials (500 and 567 mV) on the second stage leaching of the -250+212 μ m particles at 75°C, 0.116 mol/L ferric and 0.020 mol/L ferrous.

4.3.2 Effect of Temperature

The effect of temperature on second stage leaching is shown in Figure 4-31. The standard conditions were used at different temperatures and at a constant ferric/ferrous ratio. The redox potential of the leach solution at 35°C, 55°C, 65°C and 75°C are 525, 545, 556 and 567mV. The second stage was much more temperature sensitive than the first stage. At high temperature (75°C), the first stage leaching was complete within 15 minutes. The rate of leaching at 75°C compared favourably with that of oxygen pressure leaching experiments [71] some of which were done at higher temperatures.

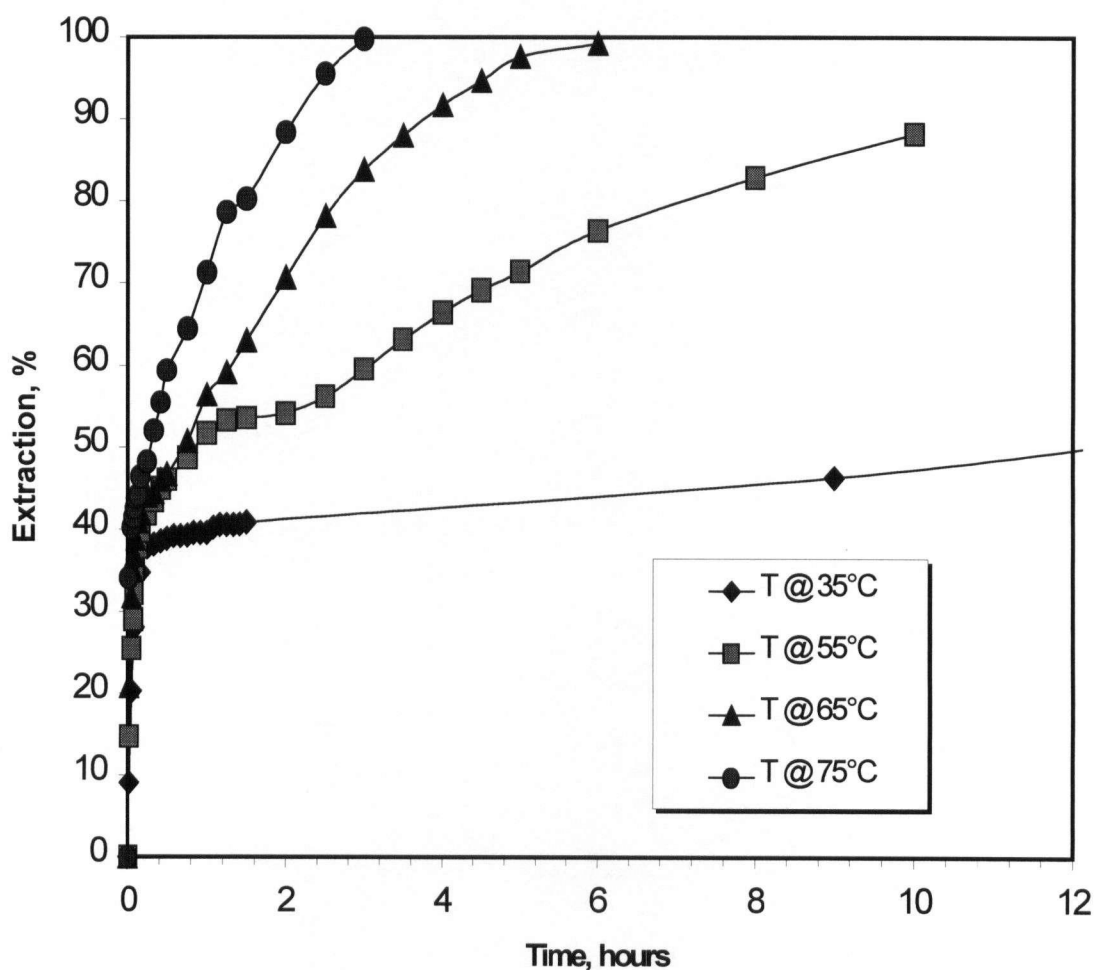


Figure 4-31. Effect of temperature on the second stage leaching of -250+212 μm particles at 75°C, 0.116 mol/L ferric and 0.0202 mol/L ferrous.

At 35°C, leaching was very slow and substantial copper extraction was not obtained after 12 hours. At 55°C, a point of inflection was observed between 50 and 60% copper extraction, which may indicate (probably) a change of mechanism or the formation of an intermediate product (with a corresponding change of rate). This observation was confirmed by repeating the tests with exactly the same results. At temperatures higher than 55°C, the point of inflection was absent, which may indicate rapid decomposition of the probable intermediate product.

An Arrhenius plot for second stage leaching is shown in Figure 4-32. The method of initial rates was used by drawing tangents to the extraction versus time curves. The slope of the tangent between 50% and 100% extraction was taken as the rate of leaching in each experiment. An activation energy of 97.0 kJ/mol was obtained, indicating that the rate is controlled by chemical reaction.

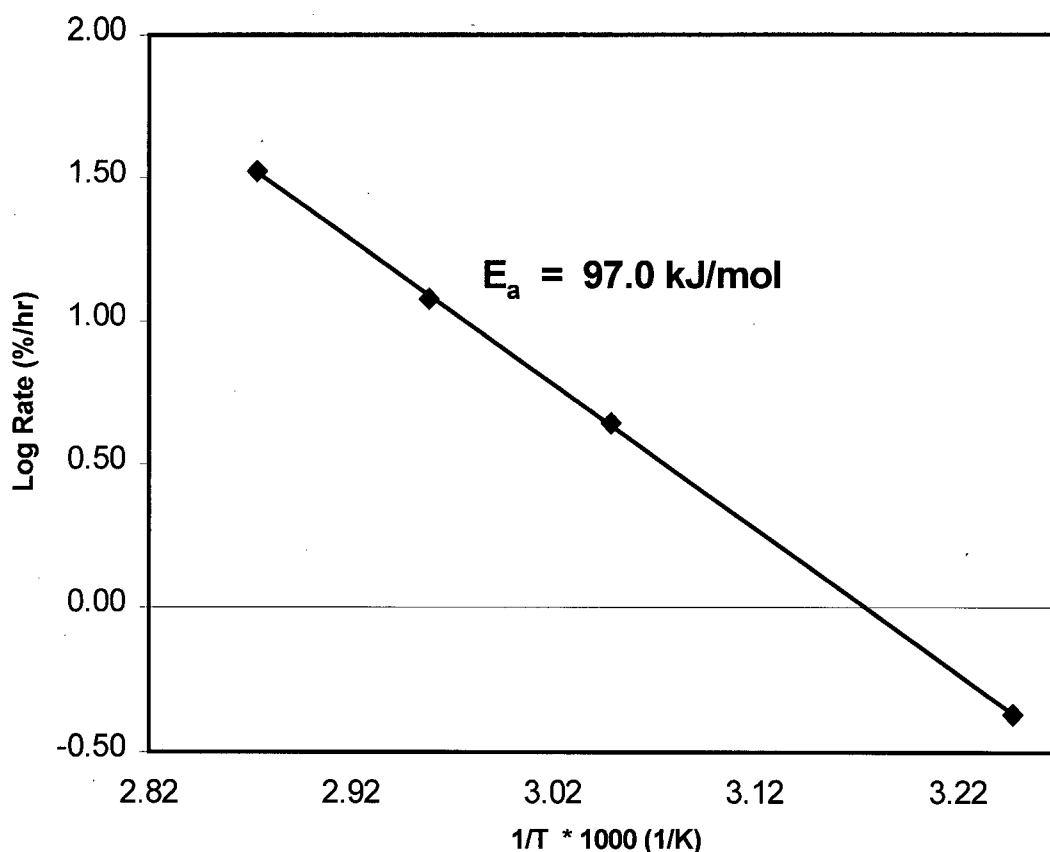


Figure 4-32. Arrhenius plot for the second stage leaching.

4.3.3 Effect of Initial Ferric Concentration

The effect of ferric concentration on second stage leaching is shown in Figure 4-33. The standard conditions were used in all of the experiments, except that ferrous concentration was changed to 0.0101 mol/L. Ferric concentrations of 0.058, 0.116, 0.232 and 0.348 mol/L correspond to initial ferric : copper (in solid mineral) mole ratios of 1.00, 2.00, 4.00 and 6.00, respectively. Generally, the change of rate with ferric concentration was less significant when compared to the first stage. A reaction order of 0.5 with respect to ferric concentration was obtained over the whole ferric concentration range studied as shown in Figure 4-34.

This indicates an electrochemical mechanism which could be either Type I or Type II depending on the effect of ferrous concentration.

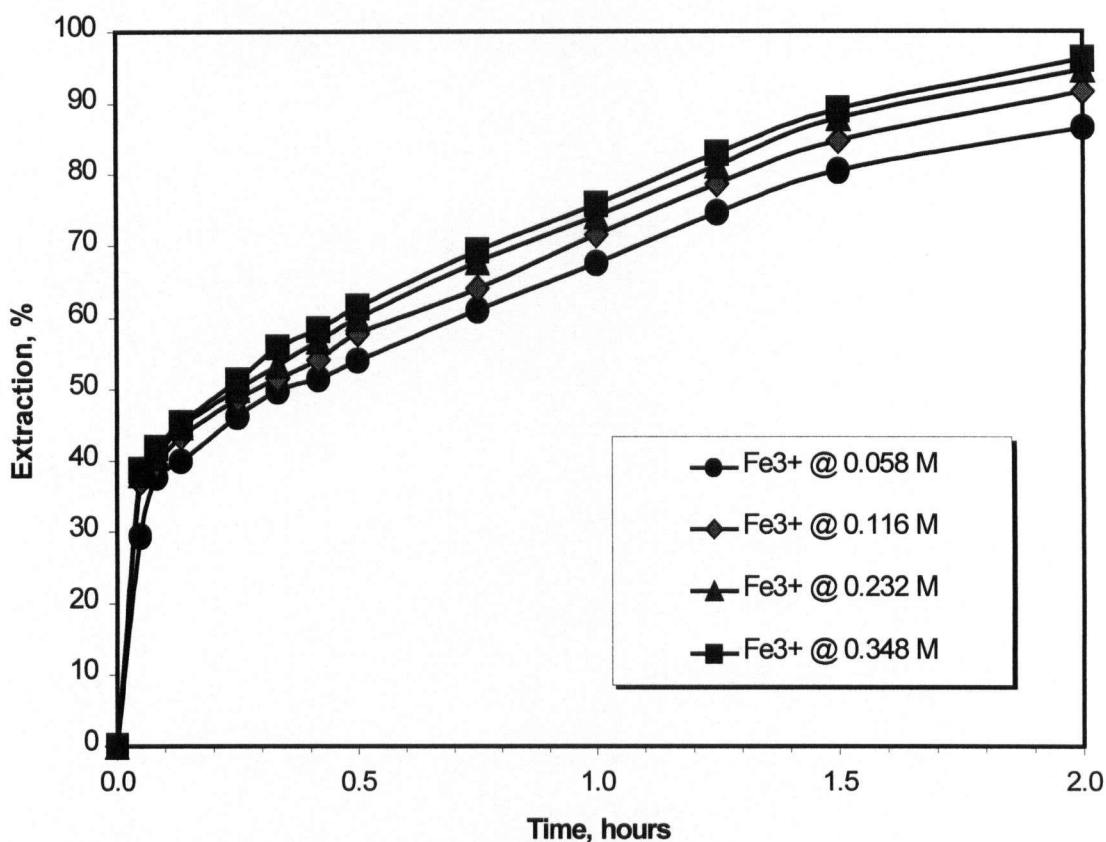


Figure 4-33. Effect of initial ferric on the second stage leaching of -250+212 μm particles at 75°C and 0.0101 mol/L ferrous.

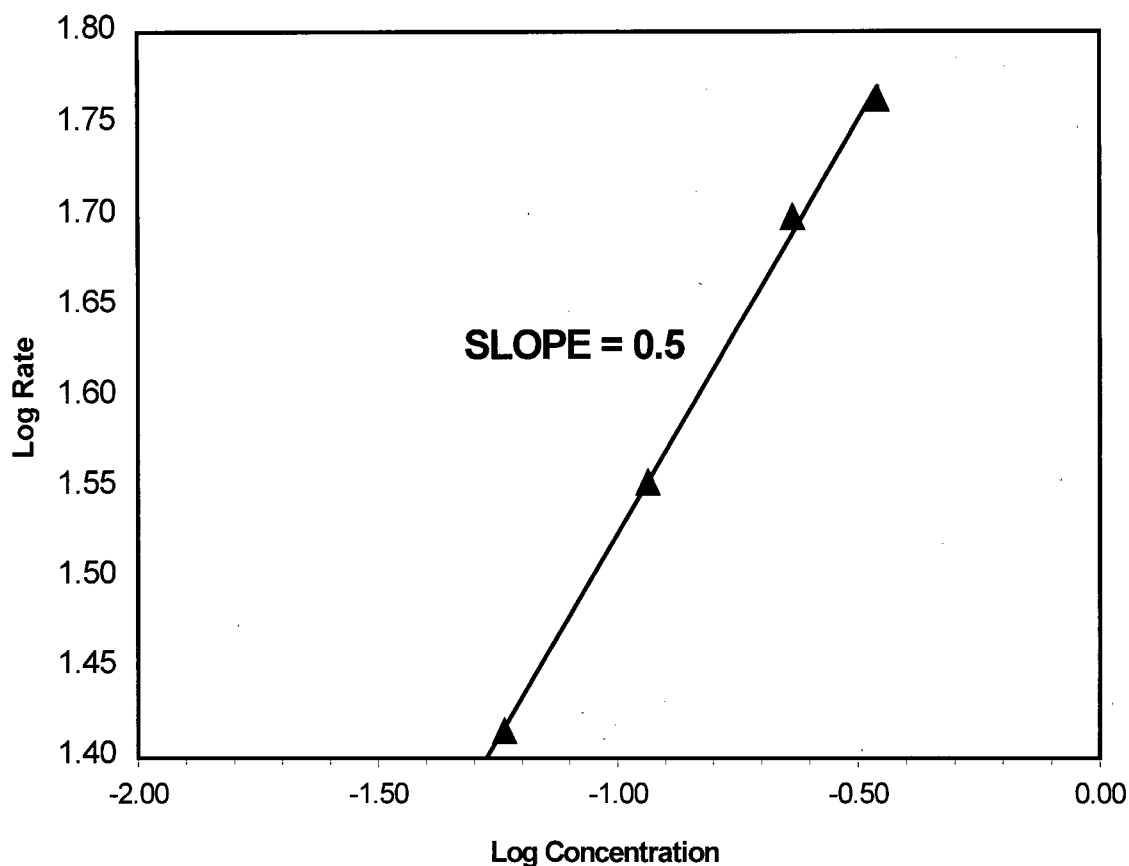


Figure 4-34. Log rate vs. log ferric concentration plot for the second stage leaching.

4.3.4 Effect of Initial Particle size

The effect of the particle size on second stage leaching is shown in Figure 4-35. These tests were run at the standard conditions. There was no relationship between particle size and the rate of extraction, although one would have expected an inverse relationship between rate and particle size because of the chemical controlled kinetics obtained in section 4.3.2. From the mineralogical analysis (in section 4.1), dissolution features (such as cracks and pores) and particle breakage were observed. This resulted in an enlarged surface area such that the initial surface area of the particles became insignificant when compared with the new surface area formed.

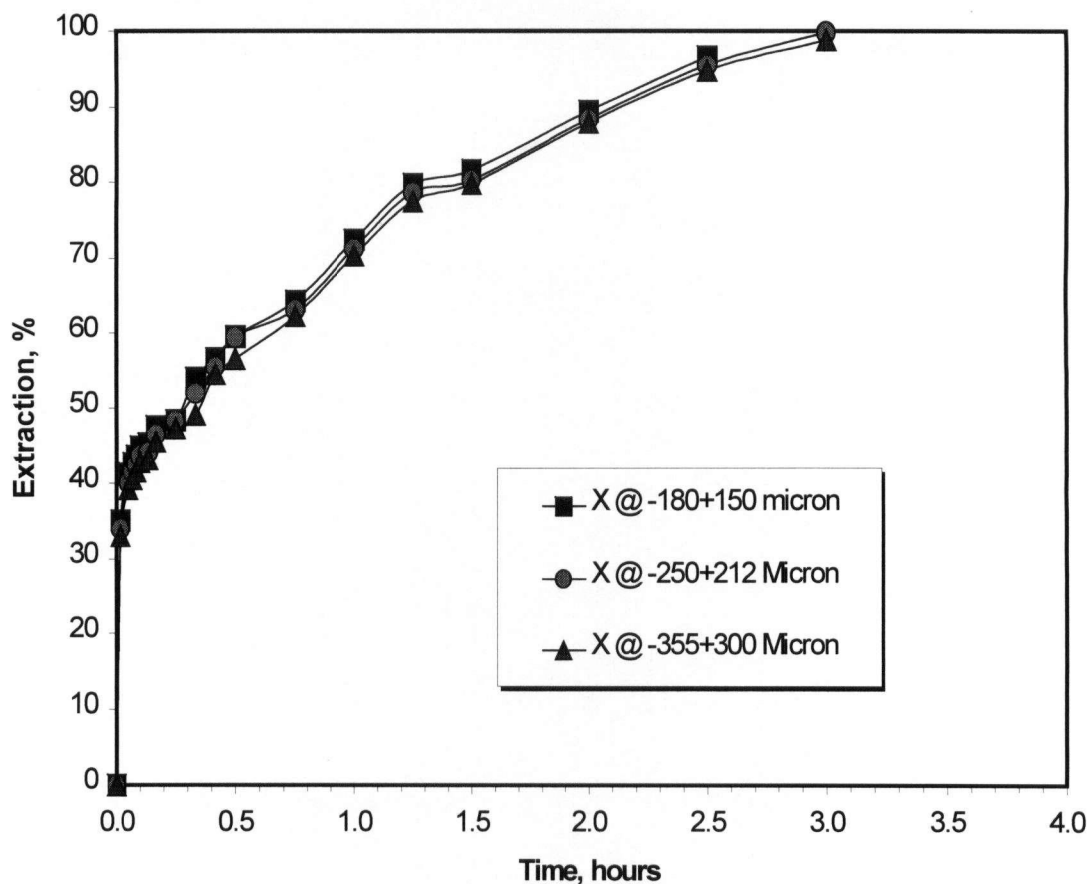


Figure 4-35. Effect of particle size on the second stage leaching at 75°C, 0.116 mol/L ferric and 0.0202 mol/L ferrous.

4.3.5 Effect of Initial Ferrous Concentration

The effect of initial ferrous concentration on second stage leaching is shown in Figure 4-36. The ferric concentration (0.116 mol/L) and temperature (75°C) were held constant in all of the experiments. The fractional order of reaction was obtained by plotting the logarithm of rate against that of ferrous concentration as shown in Figure 4-37. This is a case of type II leaching (section 2.3.2), in which the rate is controlled by an electron transfer mechanism in the anodic (dissolution) reaction. It is expected that the kinetics will depend on the ferric/ferrous ratio.

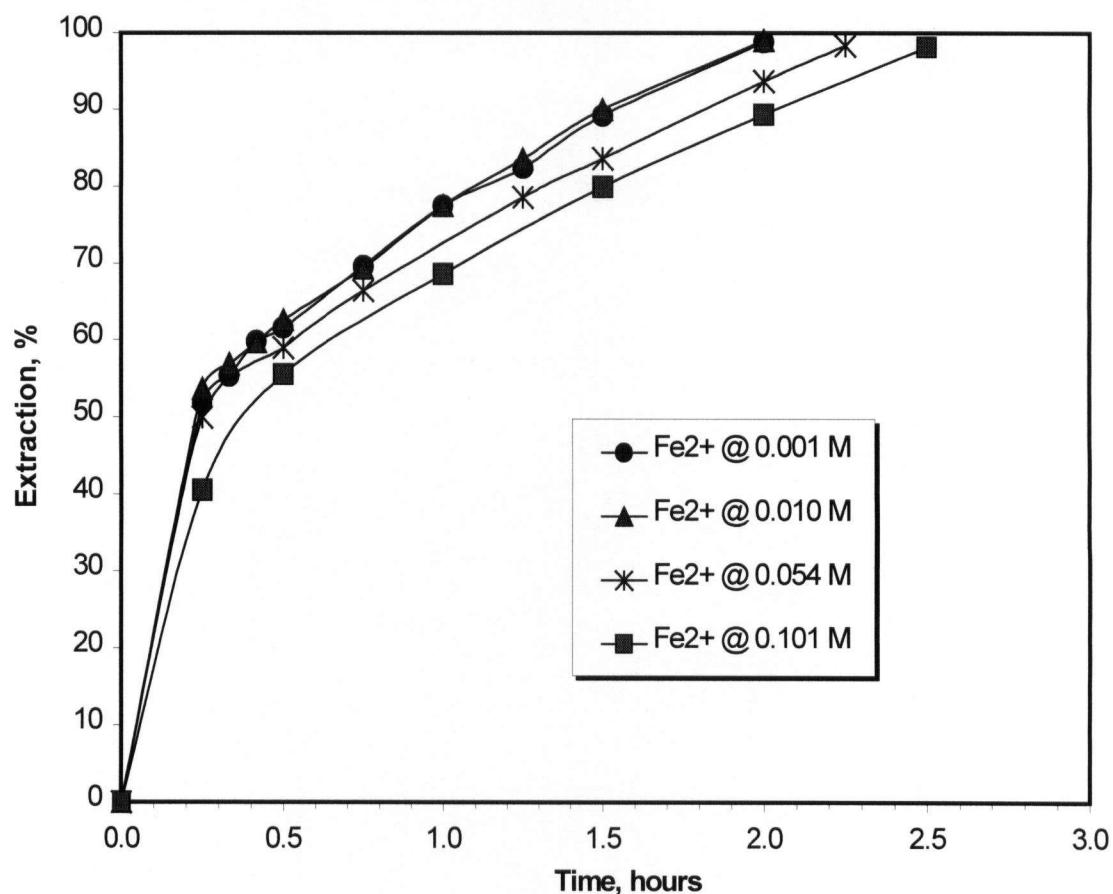


Figure 4-36. Effect of ferrous on the second stage leaching of -250+212 μm particles at 75°C and 0.116 mol/L ferric.

The effect of ferrous concentration on second stage leaching at low temperature is shown in Figure 4-38. The ferric concentration (0.116 mol/L) and temperature (35°C) were held constant. The redox potential of the solutions at 25°C, were 601, 551, 501 and 451mV. These were in the same range (0.001 to 0.101 mol/L) as the high temperature experiments (75°C). The effect of ferrous at low temperature was significant up to 70% extraction and subsequently the rates were almost the same at different levels of ferrous. At high concentration of ferrous (0.101 mol/L and 451 mV), the reaction did not proceed beyond 70% within 70 hours. At 75°C, the change of rate was not observed in any of the experiments and reaction proceeded beyond 70% extraction at 0.101 mol/L ferrous.

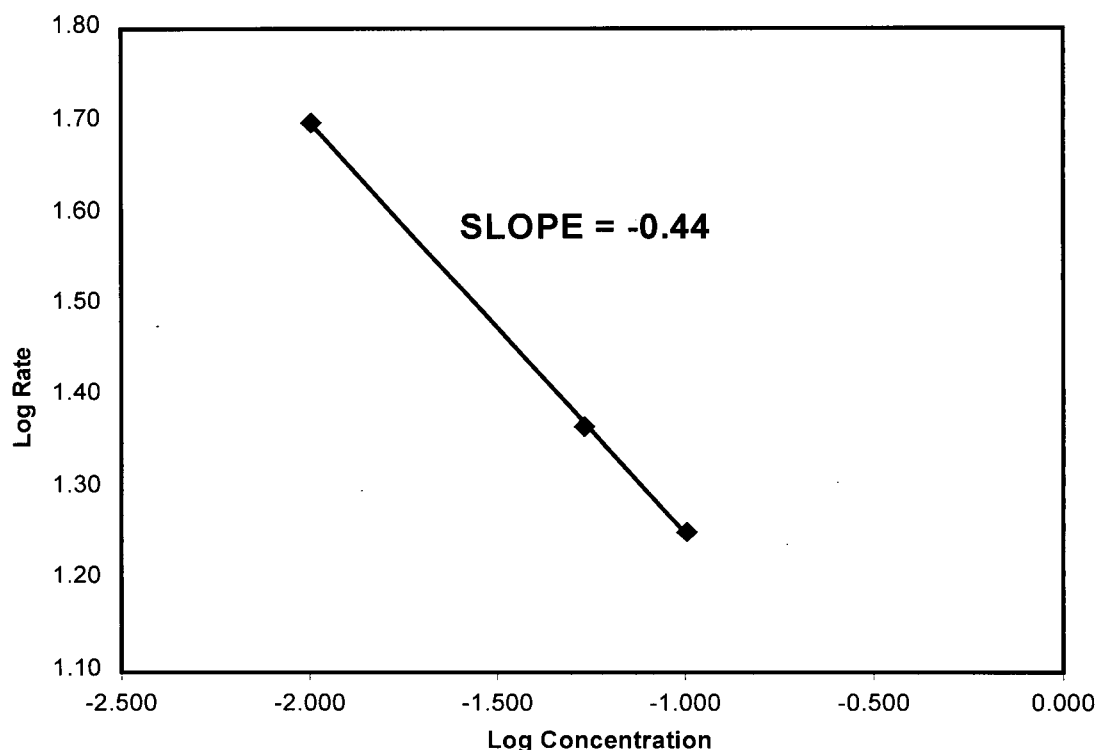


Figure 4-37. Log rate vs. log ferrous concentration plot for the second stage leaching of +250-212 μm particles at 75°C and 0.116 mol/L ferric.

The fractional order of reaction was obtained by plotting the logarithm of rate against that of ferrous concentration as shown in Figure 4-39. The rates were determined by drawing tangents to the extraction versus time curves. The slope of the tangent between 50% and 70% extraction was taken as the rate of leaching in each experiment. Although, the rate is controlled by an electron transfer mechanism in the anodic reaction at both high and low temperatures, it is apparent that the leaching system of second stage covellite is closer to type II leaching (section 2.3.2) at high temperatures than at low temperatures. At low temperature, the Tafel slope of the anodic reaction (mineral dissolution) changes rapidly as reaction proceeds such that the limiting current density of the mineral is reached at about 70% extraction and the subsequent leaching occurs at the limiting current density of the mineral. The driving force for the leaching reaction is the anodic overvoltage and this must be sufficiently large to force the reaction to proceed

beyond 70% extraction. The increase in ferric/ferrous ratio may not translate to a significant change in rate because the dissolution is occurring at the limiting current density of the mineral. The high ferric/ferrous ratio is still required to force the leaching beyond 70% extraction. At high temperature, the initial exchange current density of the second stage covellite is larger than that of the low temperature and as leaching progresses the dissolution current density is always higher than the exchange current change of the covellite. Though the Tafel slope of the anodic reaction (mineral dissolution) changes as reaction proceeds, the limiting current density of the mineral is not reached at about 70% extraction and leaching occurs throughout at the dissolution current density which is larger than the limiting current density of the mineral.

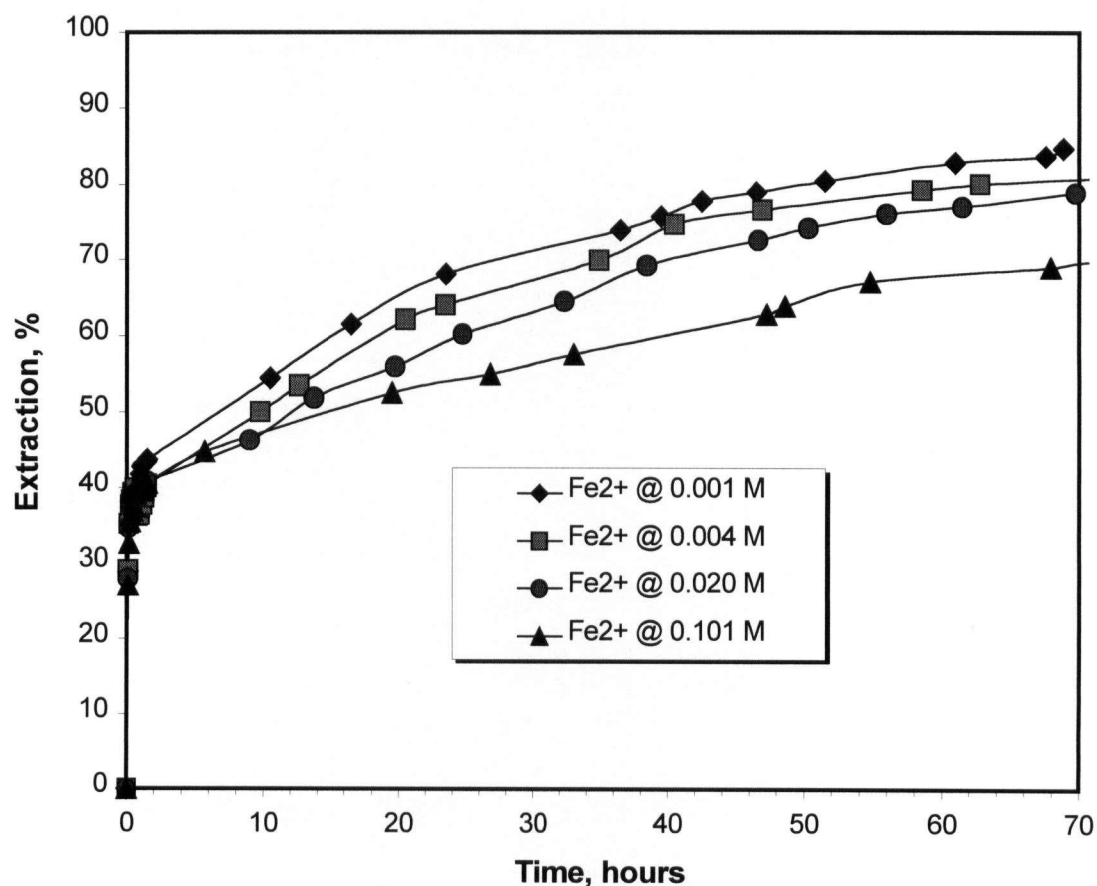


Figure 4-38. Effect of ferrous on the second stage leaching of -250+212 μm particles at 35°C and 0.116 mol/L ferric.

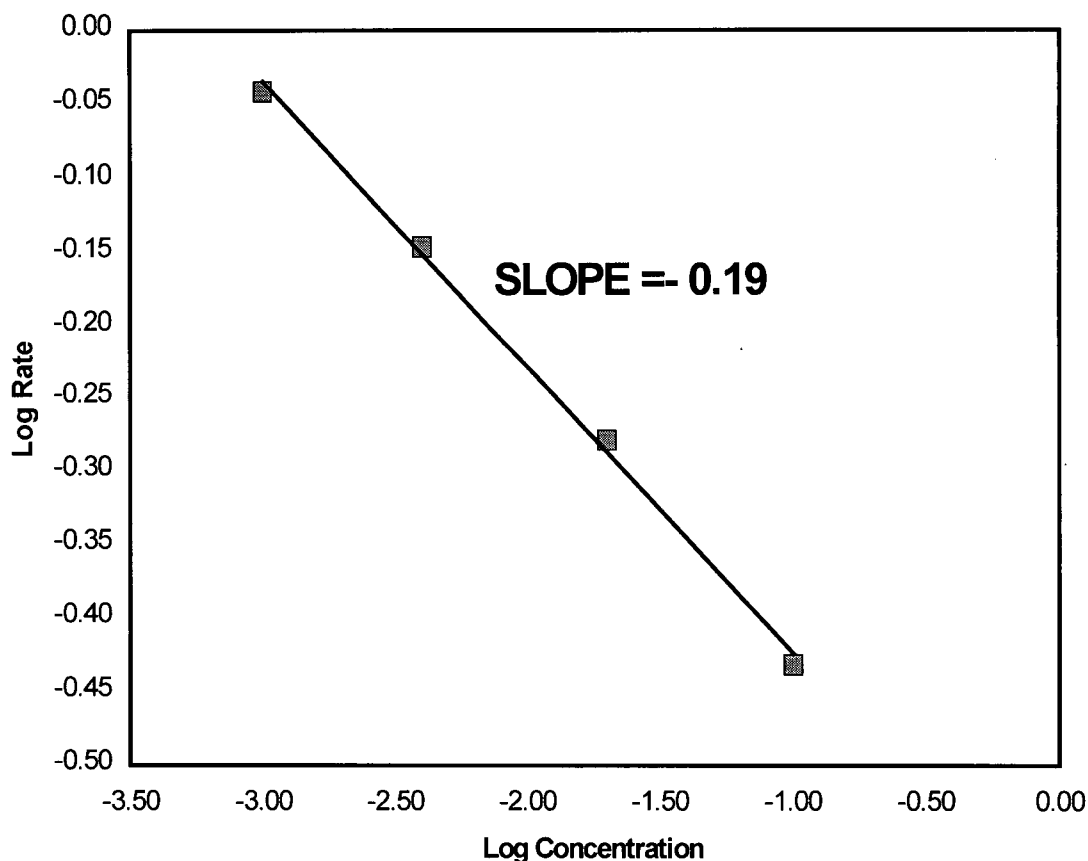


Figure 4-39. Log rate vs. log ferrous concentration plot for the second stage leaching of -250+212 μm particles at 35°C and 0.116 mol/L ferric.

4.3.6 Effect of Ferric/Ferrous Ratio

The effect of ferric/ferrous ratio on second stage leaching is shown in Figure 4-40. The total iron concentration (0.136 mol/L), total sulfate concentration (0.287) and temperature (75°C) were held constant in all of the experiments. Three different ferric/ferrous ratios were investigated: 0.116/0.020, 0.10/0.036 and 0.082/0.054 mol/L corresponding to ferric / ferrous ratios of 5.80, 2.78 and 1.52 respectively. The redox potentials (vs. Ag/AgCl) of the solutions were 567, 546 and 531 mV at 75°C respectively. The fractional order of reaction was obtained by plotting the logarithm of rate against that of ferric/ferrous ratio as shown in Figure 4-41. The rates were determined by drawing

tangents to the extraction versus time curves. The slope of the tangent between 50% and 100% extraction was taken as the rate of leaching in each experiment. The second stage leaching is sensitive to the ferric / ferrous ratio at high temperature. In this range of ferric /ferrous ratio, the ferric/ferrous couple is near equilibrium, with large exchange current density and the mixed potential is within the anodic (second stage covellite) Tafel region. This is a case of type II leaching (section 2.3.2), in which the rate is controlled by an electron transfer mechanism in the anodic (dissolution) reaction.

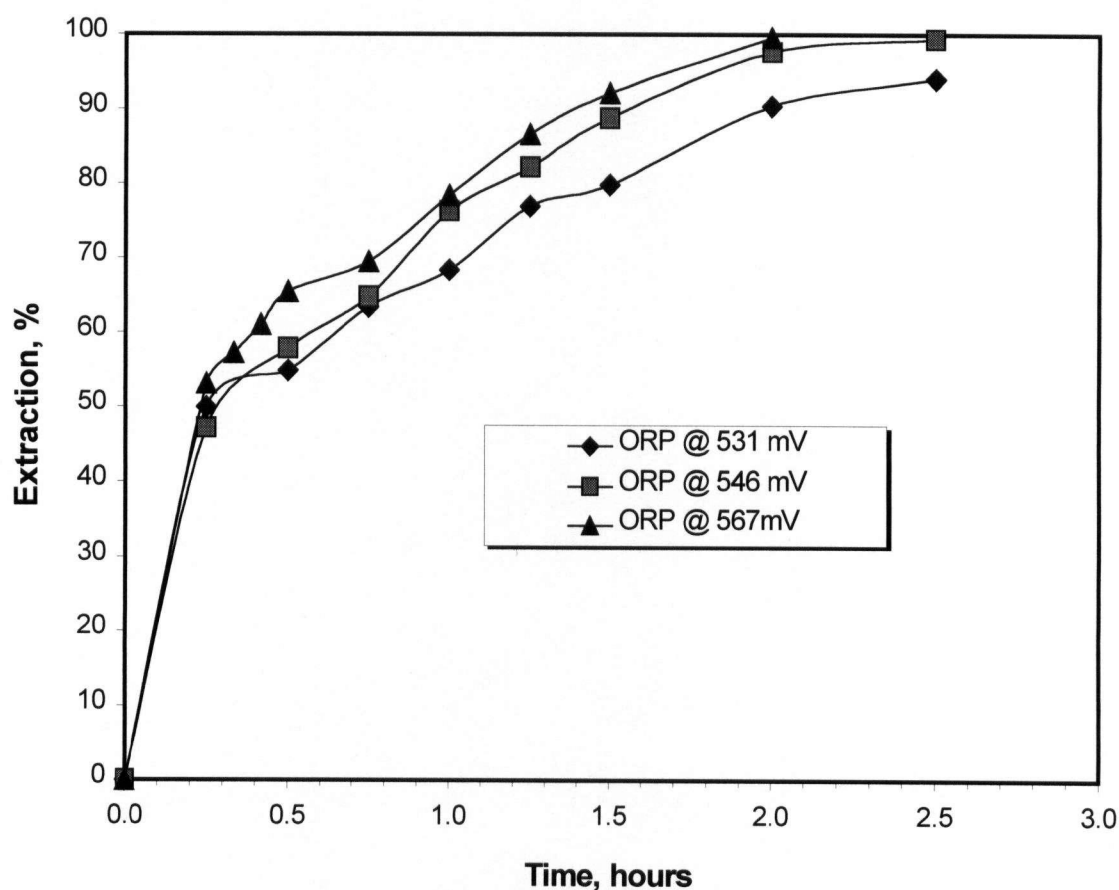


Figure 4-40. Effect of ferric/ferrous ratio on the second stage leaching of $-250+212 \mu\text{m}$ particles at 75°C , 0.136 mol/L total iron and 0.287 mol/L sulfate.

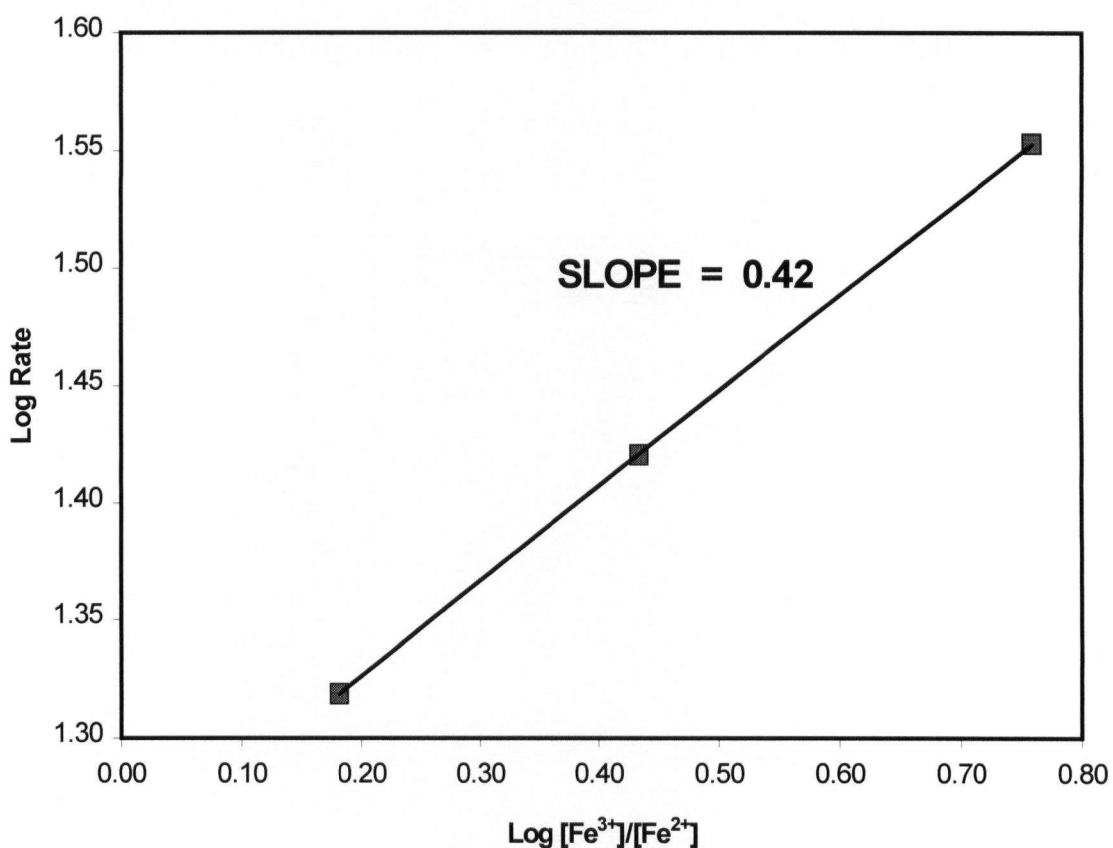


Figure 4-41. Log rate vs. log of ferric/ferrous ratio for the second stage leaching at 75°C.

4.4 Effect of Leaching Parameters on Sulfur Distribution

The effect of the redox potential on the reaction product distribution is presented in Table 4-5. The ferric concentration (0.116 mol/L) and temperature (35°C) were held constant in all the experiments. At low temperature (35°C) and at the standard conditions ($E_{Ag/AgCl} = 501$ mV at 25°C), first-stage leaching (up 40% copper-extraction) occurred with negligible sulfur formation (2% total sulfide oxidation).

At 35°C, the initial oxidation of second stage covellite (which corresponds to 50-70% copper extraction) was much more favourable at higher potential (601 mV) than at lower potential (501 mV), resulting in a higher rate of extraction at 601 mV.

Table 4-5. Effect of redox potential on sulfur distribution in the leach residue. Test conditions: 35°C, 0.055 mol/L initial copper, 1.085 g of sulfur (in the solid mineral) and 0.116 mol/L ferric (leach solution).

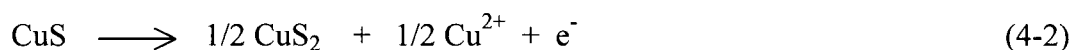
Redox Potential (mV at 25°C)	Copper Extraction %	S _S ⁰ %	S _{SO4} %	S _{CuS} %	Cu/S Molar Ratio ¹	Cu/SO ₄ Molar Ratio ¹	Time Hrs	Cu/S Moles Ratio ³
501	40	2.00	0.00	98.00	N/A ²	N/A ²	1.5	1.00
501	60	16.24	5.60	78.16	1.00	8.69	22	0.83
601	60	19.92	8.04	72.04	0.81	6.06	20	0.90
451	71	23.02	15.27	61.71	1.48	6.69	79	0.76
501	77	23.40	25.73	50.87	1.87	5.11	72	0.73
601	80	25.38	30.12	44.50	1.92	4.85	69	0.73

¹Obtained by using the moles of copper which dissolved during the second stage.

²Not applicable because there was no leaching of copper from second stage covellite at this stage.

³Obtained from the moles of copper remaining in the solid residue.

Two possible competing reaction paths which may be responsible for the different rates and reaction products (up to 70% extraction) are:

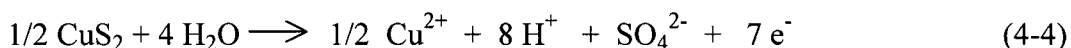
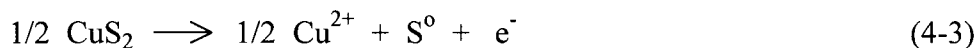


The free energy change of the reaction 4-1 at 25°C is 118.9 kJ/mol. The free energy of formation of CuS₂ was estimated by adding the difference between the free energy of formation of pyrite (FeS₂) and pyrrhotite (FeS) to that of CuS. Based on the

estimated free energy of formation of CuS_2 and that of CuS , the free energy change of reaction (4-2) was estimated to be 26.2 kJ/mol at 25°C.

The first path would be more favourable than the second at higher potentials. Any leaching situation in which reaction 4-1 occurs more rapidly than equation 4-2 would show a higher initial rate of extraction and a higher content of elemental sulfur. At 60% extraction (which corresponds to 10% extraction from second stage covellite) the elemental sulfur formed at 601 mV was more than that at 501 mV. The corresponding dissolved copper to sulfur mole ratio were 0.81 and 1.00 at 601 and 501 mV, respectively. The elemental sulfur formed at this level of copper extraction (60% extraction) was 78% and 69% of the entire sulfur formed when leaching was prolonged (to obtain copper extraction greater than 70%) at 601 mV and 501 mV respectively. This shows that a substantial part of the entire sulfur was formed at this stage via reaction (4-1).

The sulfate formed at 60% copper extraction was 27% and 22% of the entire sulfate formed when leaching was prolonged (to obtain copper extraction greater than 70%) at 601 mV and 501 mV, respectively. Also, additional sulfur was formed subsequent to 60% copper extraction, but its increase was less than that of sulfate. It is possible that the following reactions may be responsible for the formation of additional sulfur and sulfate:



The free energy changes of reactions (4-3) and (4-4) were estimated to be 92.7 kJ/mol and 296.9 kJ/mol at 25°C. At about 80% copper extraction (which corresponds to 30% extraction from second stage covellite), the sulfate formed at 601 mV was more than that at 501 mV. The corresponding dissolved copper to sulfate mole ratios were 4.85 and 5.11 at 601 and 501 mV, respectively.

The effect of temperature on the product distribution is presented in Table 4-6. The operating conditions were the same in all the experiments except temperature and time. The quantity of elemental sulfur formed increased with temperature possibly because the dissolution of the CuS_2 through reaction 4-3 is more favourable than reaction 4-4 at high temperature.

Table 4-6. Effect of temperature on the sulfur distribution in the leach residue. Test conditions: 0.055 mol/L initial Cu, 1.085 g of sulfur (in the solid mineral), 0.116 mol/L ferric and 0.020 mol/L ferrous.

Leach Temp. °C	Copper Extraction %	S_s° %	S_{SO_4} %	S_{CuS} %	Cu/ S° Molar Ratio ¹	Cu/ SO_4 Molar Ratio ¹	Time Hrs	Cu/ S_{CuS} Moles Ratio ²
35	60	16.24	5.60	78.16	1.00	8.69	22	0.83
55	63	22.82	2.94	74.24	0.92	21.51	5	0.81
75	87	56.55	5.91	37.54	1.07	30.73	4.5	0.56

¹Obtained from the moles of copper formed during the second stage.

²Obtained from the moles of copper remaining in the solid residue.

At the highest temperature (75°C), the oxidation of copper disulfide through equation 4-3 was very fast such that the copper disulfide from reaction 4-2 was almost instantaneously oxidized. This occurred as if equation (4-2) and (4-3) were combined into one reaction. The net free energy change of reactions (4-2) and (4-3) is 118.9 kJ/mol, however the activation energy observed in section 4.3.2 is 97 kJ/mol. The elemental sulfur was 90% of the total sulfide oxidized. It is possible that the sulfur formed at high temperatures is porous and non-adherent to the mineral surface. Otherwise, one would have expected sulfur to insulate the mineral surface, having an adverse effect on the kinetics.

4.5 Bacterial Leach Experiment

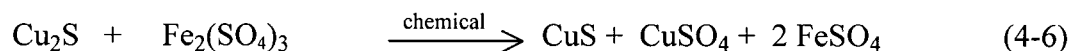
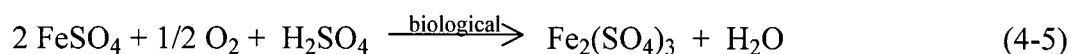
The effect of the bacteria is shown in Figure 4-42. The bacterial leaching rates compared favourably with the chemical leaching rates (at 35°C), for which the same total iron concentration (0.116 mol/L) was used. The initial concentration of copper and ferric ion (from the inoculum) was 0.0155 and 0.0172 mol/L respectively in the bacterial leaching experiment. The initial redox potential was 366 mV (vs. Ag/AgCl). At high population and activity of the bacteria, the lag period before the exponential growth phase was greatly reduced as shown in Figure 4-44. Acid addition was only required during the first stage leaching, while lime slurry was added after 45 hrs (during the second stage).

The instantaneous rate of reaction at different level of extraction was plotted for bacterial and chemical leaching in Figure 4-43. The significant rates of extraction were obtained from the bacterial leaching when the redox potential was in the range of 450 and 650 mV. The chemical leaching was carried out at constant redox potential of 601 mV. The rates of extraction for the chemical leaching were higher than that of bacterial, but subsequent to 65% extraction, the difference in rates tapered off and became equal at 80% extraction.

There was no substantial copper extraction (beyond the acid soluble copper) in the sterile experiment (without bacteria).

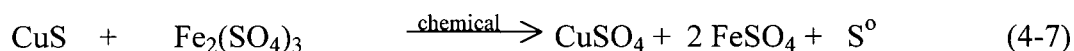
Though conclusions cannot be drawn on the mechanisms involved in this bacterial leaching experiment, the results do reveal how efficient the bacteria are in maintaining the solution potential and sustaining the rate of reaction. The rate of second stage leaching depends on the redox potential (Section 4.3.), which appears to be the primary role of the bacteria.

The substantial addition of the acid occurred during the first stage, when the redox potential was in the range of 366 and 512 mV. When compared with the results of the chemical leaching in section 4.2, the probable reaction path can be represented as follows.

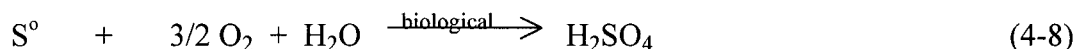


In this mechanism, there is ferrous oxidation by the bacteria, which increases the ferric concentration. The redox potential was low during the first stage leaching because of the high consumption requirement of ferric ions by the rapid dissolution reaction of chalcocite. Under active bacterial leaching conditions, during which ferrous is oxidized to ferric faster than ferric is reduced by the mineral, high ferric / ferrous ratios and redox potentials (exceeding 650 mV) are obtained. This was observed during the second stage leaching and the rate-determining step in this (indirect) mechanism is the anodic (dissolution) reaction at the mineral surface.

In second stage leaching, the probable path is represented as follows:



Another reaction which occurred during the second stage was sulfur oxidation (catalyzed by bacteria) to produce sulfuric acid. This was responsible for the decrease in pH after the previous upward trend.



There was a change of rate at about 70% copper extraction in bacterial and chemical leaching but this was more pronounced in chemical leaching. At this stage, the pH of the bacterial leaching was low as a result of reaction (4-8). This could mean that sulfur oxidation by the bacteria is desirable for achieving a high rate of oxidation during the second stage leaching.

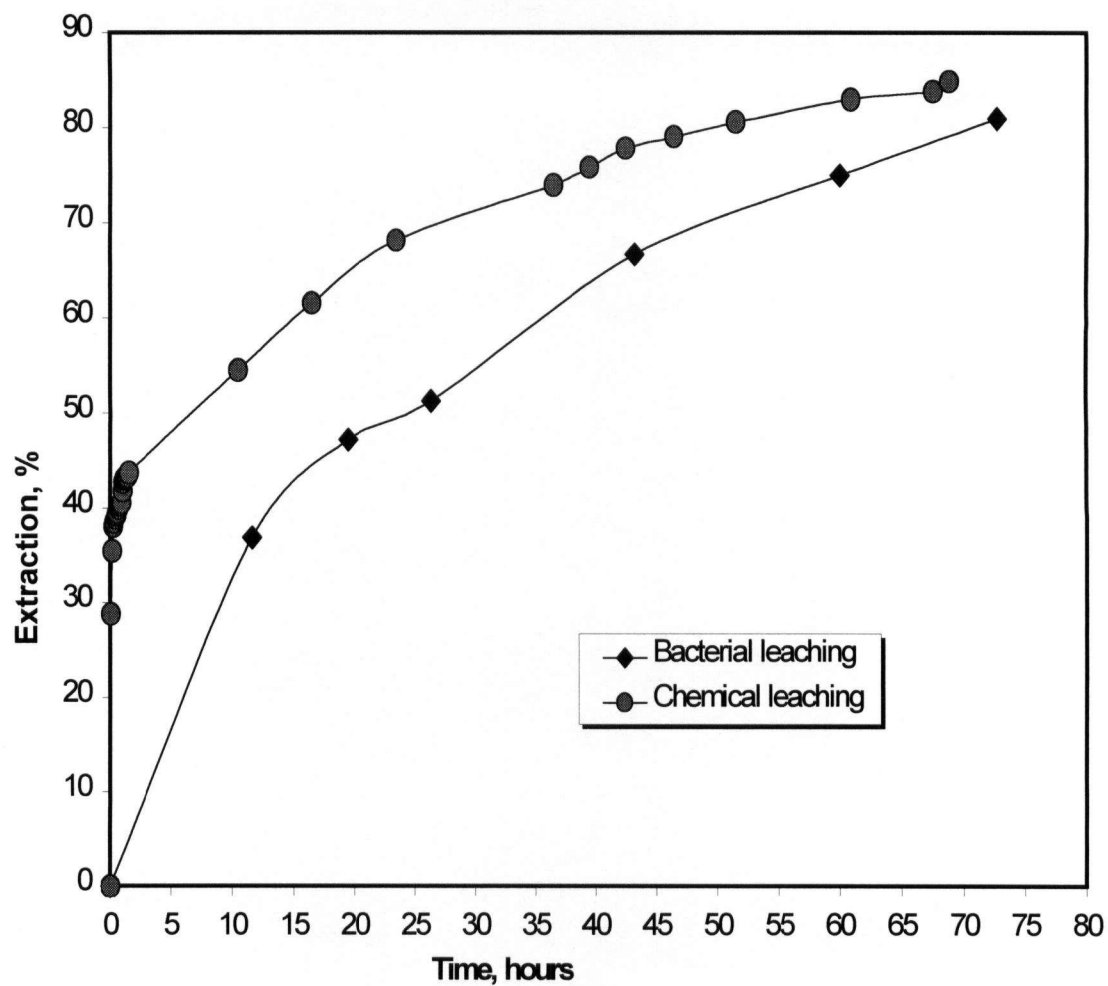


Figure 4-42. Effect of bacteria on the leaching (first and second stage) of $-250+212\ \mu\text{m}$ particles at 35°C and $0.116\ \text{mol/L}$ total iron. The initial concentration of ferric was $0.0172\ \text{mol/L}$. The redox potential for the chemical leaching experiment was controlled at $601\ \text{mV}$.

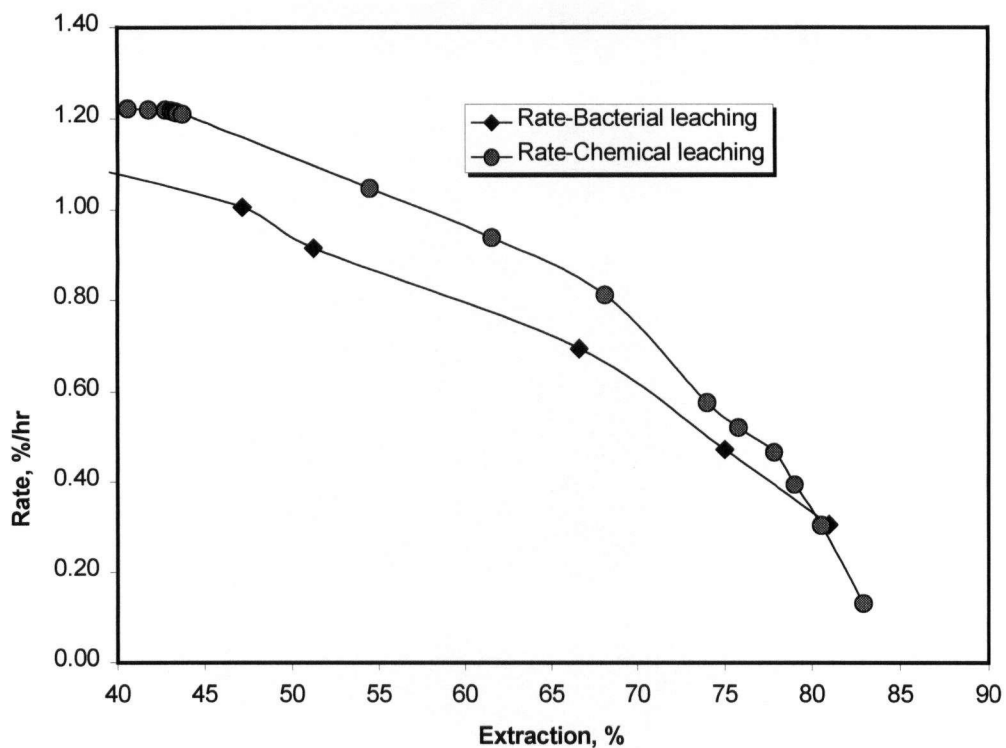


Figure 4-43. Rate vs. extraction plots for the bacterial and chemical leaching (second stage) of $-250+212\ \mu\text{m}$ particles at 35°C and $0.116\ \text{mol/L}$ total iron.

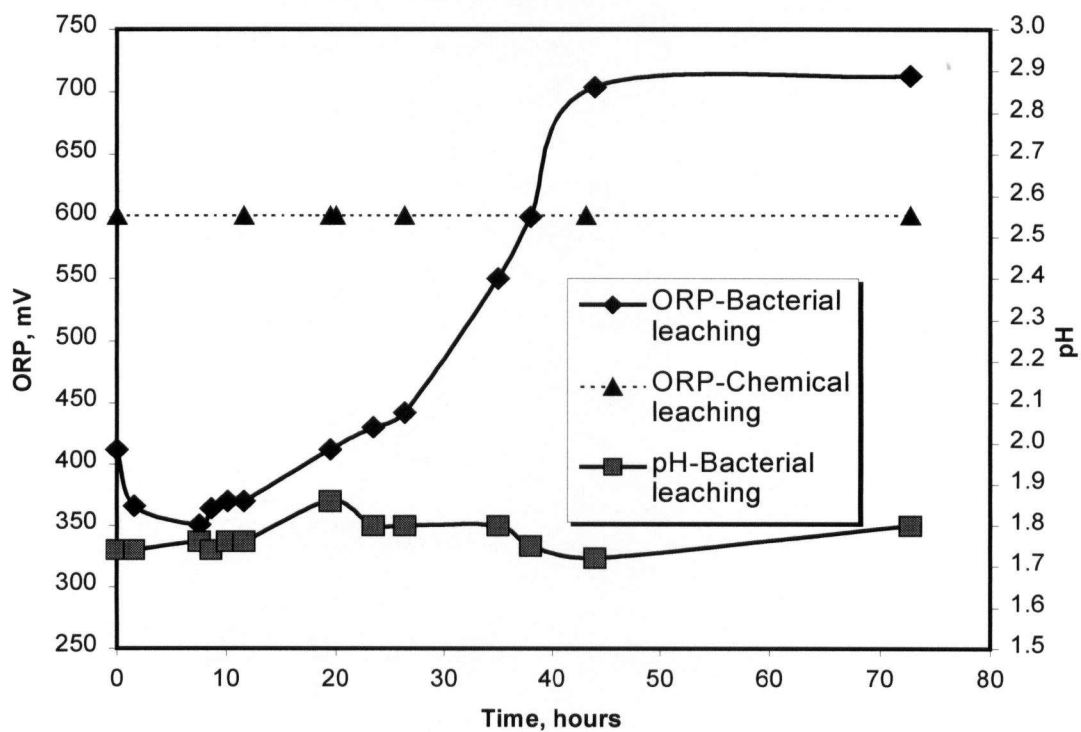


Figure 4-44. Redox potential and pH profiles of bacterial and chemical leaching.

CHAPTER 5

THEORY AND MODELING

5.1 Physico-Chemical Model of First Stage Leaching

The leaching rate of chalcocite shifted twice during the experiments (section 4.2.4), first at about 20% copper extraction and second at about 38% copper extraction. Subsequent to 38% copper extraction, the rate decreases drastically. Two steps are obvious and these are described as the first-step which produces up to 20% copper extraction and the second-step, which produces the remaining 30% extraction.

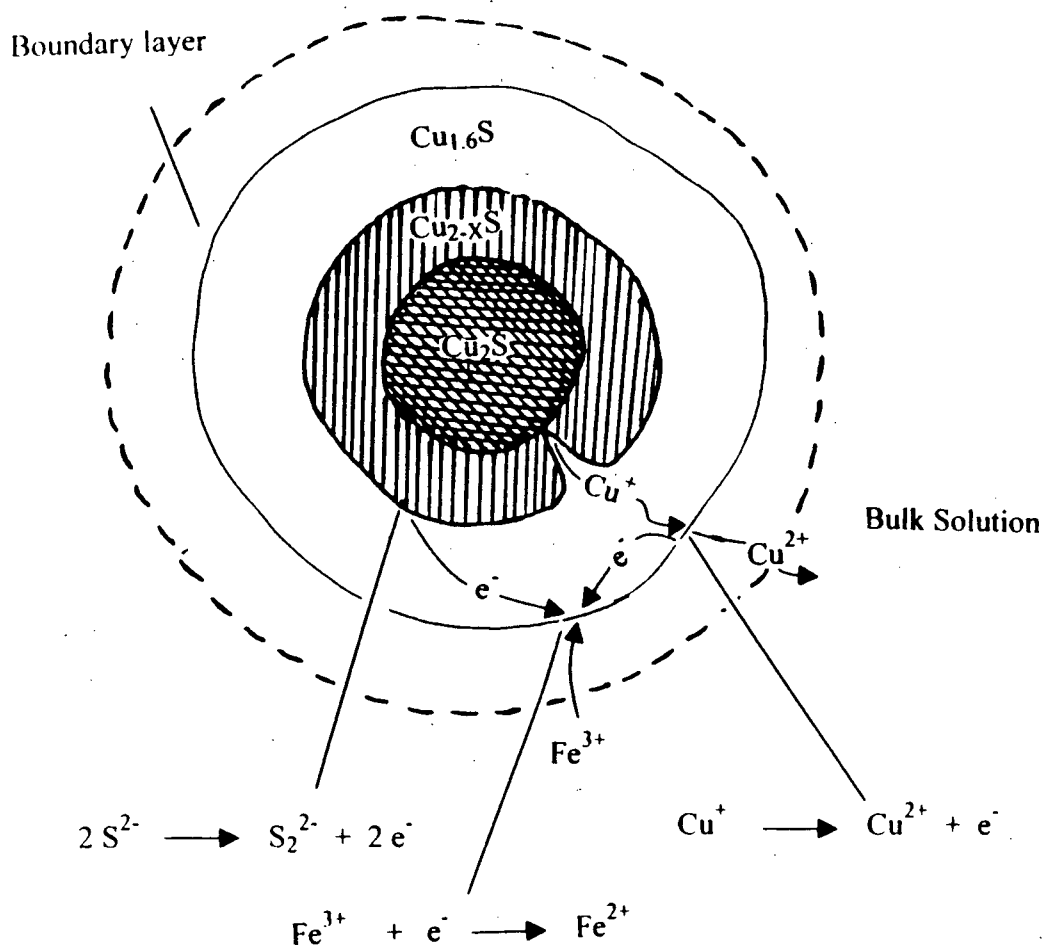


Figure 5-1. Physico-Chemical model for the first step of first stage leaching.

The first step is illustrated in Figure 5-1. In this, x increases sequentially from 0 to 0.4 and the kinetics of leaching are controlled simultaneously by the following:

1. Diffusion of the Fe^{3+} ions through the product layer to the interface,
2. Diffusion of mobile Cu^+ from the chalcocite (interior) to the interface,
3. The oxidation of the Cu^+ to Cu^{2+} , which releases electrons for the ferric reduction,
4. The reduction of the Fe^{3+} ions,
5. The diffusion of Cu^{2+} and Fe^{2+} through the product layer to the bulk solution.

The particle is transformed sequentially from chalcocite to djurleite, digenite, anilite and geerite ($\text{Cu}_{1.6}\text{S}$). The oxidation of S^{2-} to S_2^{2-} also supplies electrons for the reduction of ferric ions and this can take place in the interior of the chalcocite particle, or at the interface. Subsequent to 20% extraction, the cracks become enhanced and the second step commences.

The leaching of the second step is illustrated below in Figure 5-2.

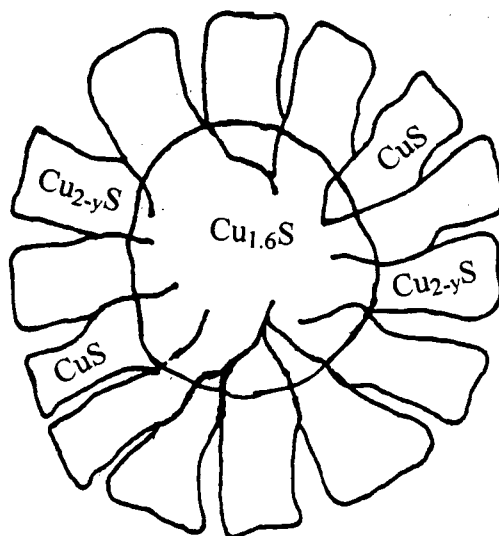


Figure 5-2. Physico-Chemical model for the second step of first stage leaching.

Based on microscopic examination (section 4.1), cracks and pores formed on the surface and subsurface as shown in Figure 5-2. In this model, y increases sequentially from 0.4 to 1.0. The pronounced dissolution features (cracks and breakage) minimized the mass transfer limitation of ferric ions to the interface and that of cupric ions to the bulk solution. One would have expected an increase in the rate up to 50% extraction as a result of increase in surface area associated with cracks and particle breakage, but this was not the case. This is because the rate of the first stage (generally) is proportional to the concentration of cuprous ions which are available (and mobile) for oxidation during the first stage. Though, the dissolution features became pronounced as the leaching proceeded the concentration of the mobile cuprous ions was already at low level. The relationship between the rate and the concentration of cuprous ions is shown in Figure 5-3. X is the fraction of copper extracted. The trendline intercepted the concentration at 0.034 mol/L, which corresponds to about 39% copper extraction.

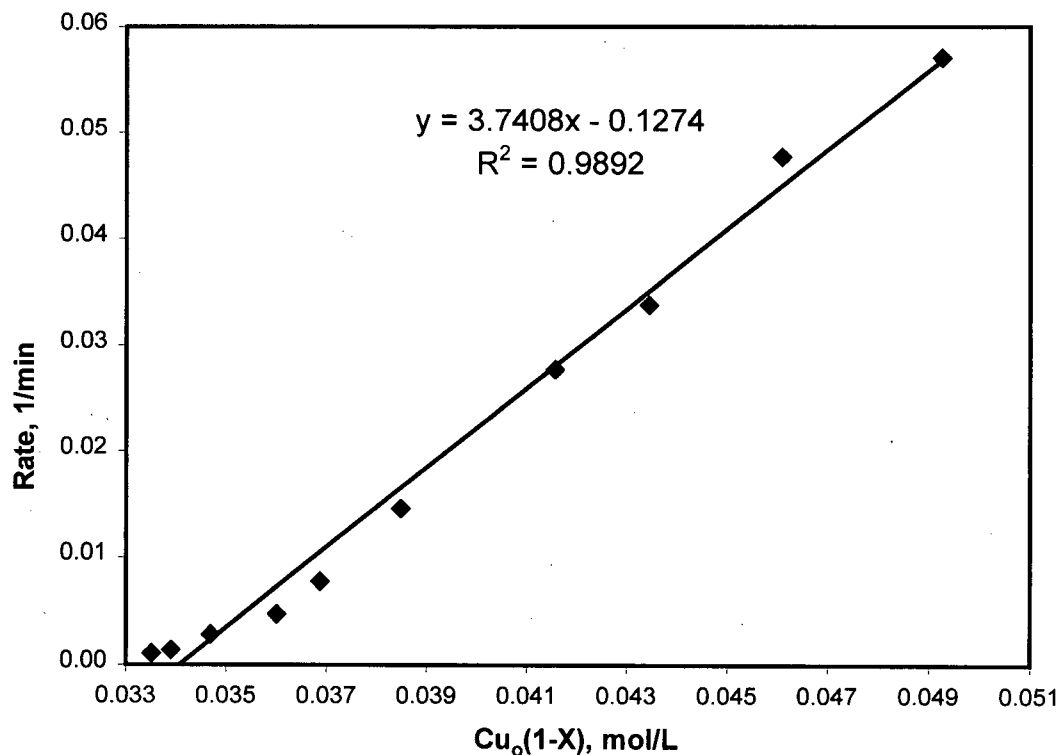


Figure 5-3. Relationship between rate and cuprous ion concentration for the first stage leaching of $-250+212\ \mu\text{m}$ particles at 35°C , 0.116 mol/L ferric ion and 0.0101 mol/L ferrous ion concentration.

5.2 Physico-Chemical Model of Second Stage Leaching

The particles break up at the end of first stage leaching, while the second stage covellite phase (and negligible elemental sulfur) is formed. Each particle then leaches discretely. The reduction of ferric ions takes place on the surface of covellite and the electrons are produced by the oxidation of covellite as shown in Figure 5-4. This is similar to that of Peters and Mao [71]. Since a high activation energy is involved in the electron transfers, simple sequential electrochemical reactions involving one electron transfer (in each reaction) are proposed, and the rate controlling step is one of the electron transfer steps in the anodic reaction. This is clearly illustrated by an electrochemical model.

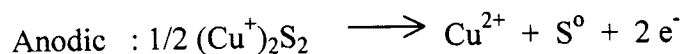
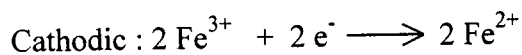
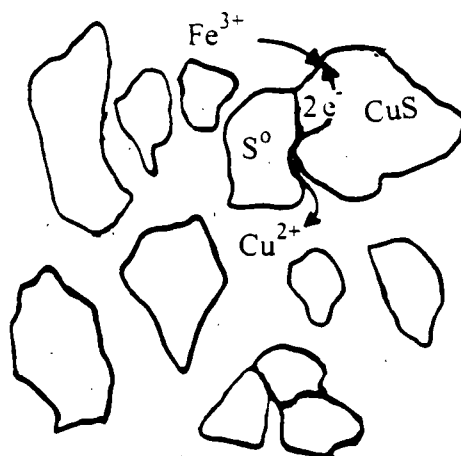


Figure 5-4. Physico-Chemical model for second stage leaching.

5.3 Electrochemical Model of Second Stage Leaching

At high temperature (75°C), the second stage leaching commences before the end of first stage once second stage covellite is formed. The first stage leaching is completed within 15 minutes. Then the mixed potential is determined principally by the reversible potentials of the second stage covellite and the ferric / ferrous couple. The position of the mixed potential relative to that of the ferric/ferrous couple can be determined (qualitatively) by using the volume of potassium permanganate required to keep the potential of the solution constant at the initial stage of reaction (Appendix 3). The volume required for the first stage was much more than that required during second stage leaching. The electrochemical model illustrated in Figure 5-5 explains the half order dependence on ferric concentration which was observed in this work (4.3.3). This can be Type I or Type II leaching (section 2.3) and the exact kinetics can be quantified by electrochemical oxidation experiments. Over the range of ferric concentration used in this work (0.058 to 0.348 mol/L), the leaching rate may be controlled by both the oxidation kinetics of second stage covellite and the reduction rate of ferric ions.

If the mechanism is Type I leaching, there would be cathodic and anodic overvoltages and the half order dependence would be on ferric concentration alone, and not on ferric / ferrous ratio. The (calculated) exchange current density of the ferric/ferrous couple on a graphite electrode (for 0.1mol/L ferric and 0.01 mol/L ferrous) is about 9.486 mA/cm² [67], which is significantly higher than the experimental value for covellite, which is about 1.4 mA/cm² [67]. However, high temperature could increase the exchange current density of the mineral [17] so that it becomes similar in magnitude to that of the ferric / ferrous couple and the mixed potential [$E_{M(I)}$] then intersects the Tafel slopes of the two half-cells as anticipated in Figure 5-5. Though the mixed potential is lower than that of Type II, the rate of reaction which corresponds to $\text{Log } j$ is higher in this case. The cathodic overpotential is large, the back reaction involving ferrous ions at the cathode is not significant and the rate depends only on the ferric concentration. The rate of reaction is controlled by charge transfer steps in both the cathodic and anodic reactions.

If the mechanism is type II leaching, there would be a large anodic overpotential (with negligible cathodic overpotential) and the dissolution current density would be less than the exchange current density of the ferric/ferrous couple. Since the mixed potential $[E_{M(II)}]$ corresponds to the reversible potential of the ferric / ferrous couple, the rate of leaching depends inversely on the ferrous concentration.

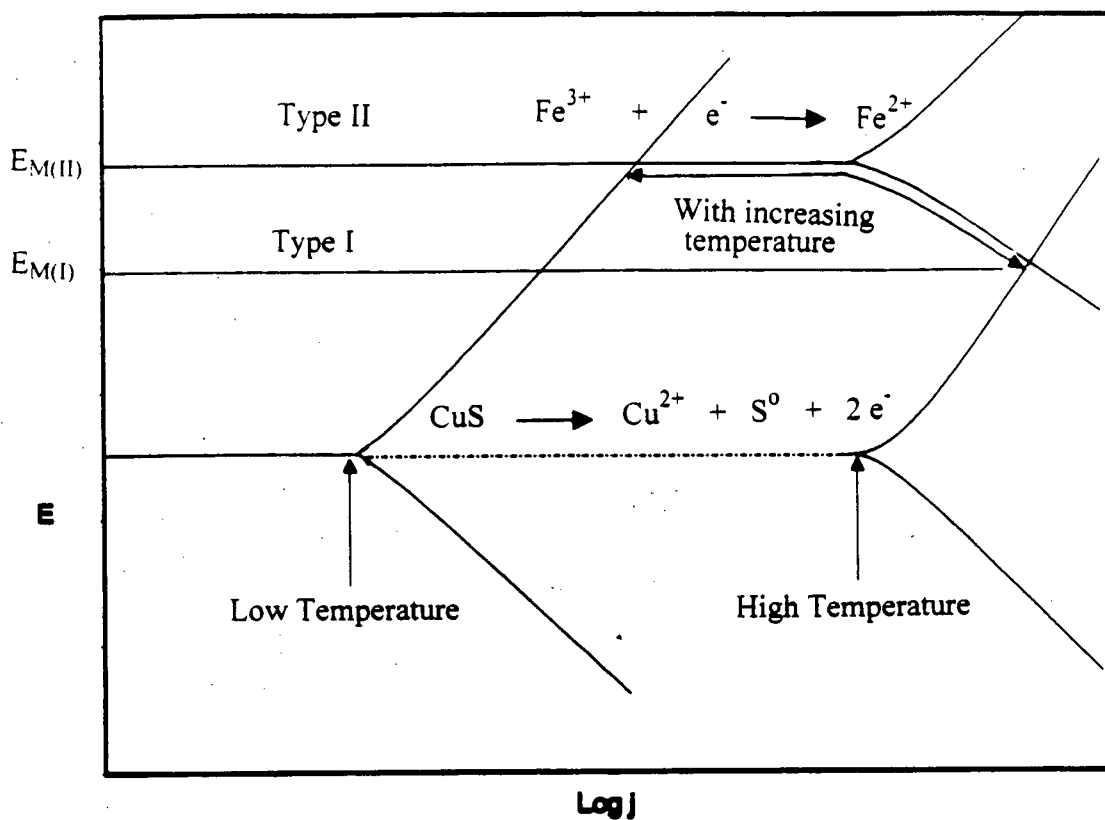


Figure 5-5. Evans diagram of theoretical polarization curves during ferric sulfate leaching of second stage covellite.

In this work, fractional order dependence on both ferric and ferrous concentrations was observed at low temperature (35°C) and at high temperature (75°C) which indicates that the increase in temperature does not change the leaching to type I leaching as envisaged in Figure 5-5. Also, the mixed potential which is a kinetic measurement does not change significantly. The rate of leaching is controlled principally by charge transfer in the anodic reactions and, hence, Type II leaching in which the rate depends on ferric and ferrous is inferred.

5.4 Rate Expression for First Stage Leaching

The rate of first stage leaching was fast at low ferric concentration (0.007-0.116 mol/L) and this can be predicted by a mixed kinetics model in which the rate is controlled simultaneously by the diffusion of ferric ions and subsequent chemical reaction with cuprous ions. The mechanism changes to chemical reaction control at about 20% copper extraction, when the particles break and the cracks become much more pronounced.

The rate also follows the concentration of cuprous ion, which is available and mobile for chemical reaction (Figure 2-3). Initially, all of the cuprous ions in the chalcocite are very mobile, but as reaction continues, some of these become fixed into the resulting phases (solid products) and immobile for further first stage reaction. Hence, a shrinking sphere model, which incorporates the effect of the cuprous ion concentration profile (section 5.1) is derived to describe the rate of first stage leaching at low ferric concentrations. This is based on the particle leaching theory presented by Fogler [79] and Levenspiel [80].

The rate of first stage leaching can be entirely chemical reaction controlled, in which case the rate of reaction is described by the following expression;

$$\frac{d\alpha_1}{dt} = \frac{k_r[Fe^{3+}]_s}{\alpha_a} \quad (5-1)$$

Also, the rate can be entirely diffusion controlled, in which case the rate of reaction would be expressed:

$$\frac{d\alpha_1}{dt} = \frac{k_c([Fe^{3+}]_b - [Fe^{3+}]_s)}{\alpha_a} \quad (5-2)$$

Since $[Fe^{3+}]_s$ is not easily measured (as is the bulk concentration $[Fe^{3+}]_b$), it must be defined in terms of $[Fe^{3+}]_b$.

In order to develop a mixed kinetics model, equations (5-1) and (5-2) were equated and solved for the surface concentration of ferric ions:

$$[Fe^{3+}]_s = \frac{k_c [Fe^{3+}]_b}{k_r + k_c} \quad (5-3)$$

Also, there is a relationship between rate and the concentration of copper in the solid mineral as explained in section 5.1. This can be represented as follows:

$$\frac{d\alpha_1}{dt} = k[Cu]_o(1 - \alpha_1) \quad (5-4)$$

By substituting equation (5-3) into equation (5-1) and combining with equation (5-4);

$$\text{Then } \frac{d\alpha_1}{dt} = \frac{k_r k_c k [Cu^+]_o (1 - \alpha_1) [Fe^{3+}]_b}{2n_o \alpha_a (k_r + k_c)} \quad (5-5)$$

Where

α_1 = fraction of copper extracted which can be leached in the first stage and

this is $\alpha_1 = \frac{\alpha}{\alpha_a}$;

α = fraction of total copper extracted

α_a = upper limit of first stage, which is 0.44

t = the leach time (minutes).

k_c = mass-transfer coefficient (cm/min)

k_r = chemical reaction rate constant (in units which will give the rate expression units of min^{-1}).

k = rate constant with respect to cuprous concentration, L/(mol-min)

n_o = initial total moles of copper in chalcocite sample, mol/L.

$[Cu^+]_o(1 - \alpha_1)$ = concentration of mobile cuprous ions at different fractions of copper extraction.

For small particles with negligible shear stress at the fluid boundary, the mass transfer correlation (Frossling equation [79]) for flow around a spherical particle is reduced to the following equation:

$$Sh = \frac{k_c d_p}{D} = 2 \quad (5-6)$$

Then, $k_c = \frac{2D}{d_p} \quad (5-7)$

Where

Sh = Sherwood number

D = diffusivity (cm²/min)

d_p = diameter of particle in cm

The substitution of equation (5-7) into equation (5-5) produces:

$$\frac{d\alpha_1}{dt} = \frac{k_r k [Cu^+]_o (1 - \alpha_1) [Fe^{3+}]_b}{2n_o \alpha_a (1 + \frac{k_r d_p}{2D})} \quad (5-8)$$

This can be simplified further as:

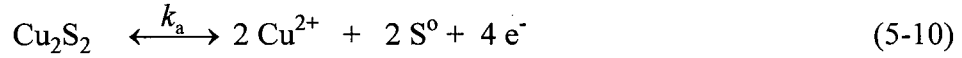
$$\frac{d\alpha_1}{dt} = \frac{k_r k [Cu^+]_o (1 - \alpha_1) [Fe^{3+}]_b}{2n_o \alpha_a (1 + \frac{d_p}{D^*})} \quad (5-9)$$

Where D* = diameter at which the resistances to mass transfer and reaction rate are equal,

that is $D^* = \frac{2D}{k_r}$

5.5 Rate Expression for Second Stage Leaching

The rate of second stage leaching can be predicted by an electrochemical reaction model with fractional dependence on both ferric and ferrous concentrations. At high temperature, the predominant anodic reaction is the oxidation of covellite to copper and sulfur as discussed in section 4.4 by the following overall reaction:



And the cathodic half-cell reaction is:



Though two electrons are involved per mole of copper ion produced from equation (5-10), an assumption of a series of steps involving the transfer of only one electron is considered. If only one of these is rate-controlling, the Butler-Volmer expression may be invoked to describe the net anodic and cathodic current densities, i_a and i_c , respectively:

$$i_a = z_a F \vec{k}_a \exp\left[\frac{\beta_a FE}{RT}\right] - z_a F \overleftarrow{k}_a [\text{Cu}^{2+}] \exp\left[\frac{-(1-\beta_a)FE}{RT}\right] \quad (5-12)$$

$$i_c = z_c F \vec{k}_c [\text{Fe}^{2+}] \exp\left[\frac{\beta_c FE}{RT}\right] - z_c F \overleftarrow{k}_c [\text{Fe}^{3+}] \exp\left[\frac{-(1-\beta_c)FE}{RT}\right] \quad (5-13)$$

At mixed potential, $i_a = -i_c$, and by assuming $\beta_a \cong \beta_c \approx \beta$; the two equations (5-12 and 5-13) can be combined to give the following expression:

$$\exp[FE/RT] = \frac{A_a z_a \overleftarrow{k}_a [\text{Cu}^{2+}] + A_c z_c \overleftarrow{k}_c [\text{Fe}^{3+}]}{A_a z_a \vec{k}_a + A_c z_c \vec{k}_c [\text{Fe}^{2+}]} \quad (5-14)$$

Where E is the mixed potential. In the second stage, there is a large anodic overpotential; hence the anodic back reaction can be ignored in equation (5-14) and, since the rate is controlled by charge transfer in the anodic reaction, the rate of oxidation can be written thus:

$$\begin{aligned} -\frac{dn_{\text{CuS}}}{dt} &= \frac{A_a i_a}{z_a F} = A_a \bar{k}_a \left(\exp \frac{FE}{RT} \right)^\beta \\ &= \frac{[A_c z_c \bar{k}_c]^\beta [Fe^{3+}]^\beta A_a \bar{k}_a}{[A_a z_a \bar{k}_a + A_c z_c \bar{k}_c [Fe^{2+}]]^\beta} \end{aligned} \quad (5-15)$$

The ferric/ferrous couple is near equilibrium, with large exchange current density, and the mixed potential is within the anodic (covellite) Tafel region. Thus equation (5-15) becomes:

$$-\frac{dn_{\text{CuS}}}{dt} = A_a \bar{k}_a \left(\frac{\bar{k}_c}{\bar{k}_c} \right)^\beta \frac{[Fe^{3+}]^\beta}{[Fe^{2+}]^\beta} \quad (5-16)$$

In terms of the rate of copper extraction, we obtain the following:

$$\frac{d\alpha}{dt} = -\frac{1}{2n_o} \frac{dn_{\text{CuS}}}{dt} \quad (5-17)$$

$$\frac{d\alpha_2}{dt} = -\frac{1}{\alpha_b - \alpha_a} \frac{d\alpha}{dt} \quad (5-18)$$

Substituting equation (5-16) and (5-17) into equation (5-18)

$$\frac{d\alpha_2}{dt} = \frac{1}{2(\alpha_b - \alpha_a)n_o} A_a \bar{k}_a \left(\frac{\bar{k}_c}{\bar{k}_c} \right)^\beta \frac{[Fe^{3+}]^\beta}{[Fe^{2+}]^\beta} \quad (5-19)$$

The fractional order of reaction obtained in this work with respect to ferric / ferrous ratio was 0.42. This fraction can be substituted in equation (5-19) to obtain the following expression.

$$\frac{d\alpha_2}{dt} = \frac{1}{2(\alpha_b - \alpha_a)n_o} A_a \bar{k}_a \left[\frac{\bar{k}_c}{\bar{k}_a} \right]^{0.42} \left[\frac{[Fe^{3+}]}{[Fe^{2+}]} \right]^{0.42} \quad (5-20)$$

Where

α_2 = fraction of copper extracted which can be leached in the second stage and

this is $\alpha_2 = \frac{\alpha - \alpha_a}{\alpha_b - \alpha_a}$

α = fraction of total copper extracted

α_b = upper limit of the second stage, which is 1.00

t = time in hrs.

k_c = cathodic rate constant

\bar{k}_a = anodic rate constant in the forward direction

n_o = initial total moles of copper in the chalcocite mineral

The surface area changes with the reaction time as leaching progresses and more pores are formed. The net result of physical changes to the ore particle which occur as leaching progresses is called the topochemical effect (Appendix 4). This can be correlated by some common mechanisms [80] such as linear leaching with chemical reaction at the particle surface rate-controlling, and parabolic leaching with the diffusion of a reactant solute through a porous product layer rate-controlling. In Figure 5-6, the logarithm of the instantaneous rate of extraction (of copper available for leaching in the second stage) is plotted against the fraction unreacted ($1 - \alpha_2$). The best power law fit obtained in this work leads (approximately) to a chemical controlled mechanism with shrinking cylinder geometry.

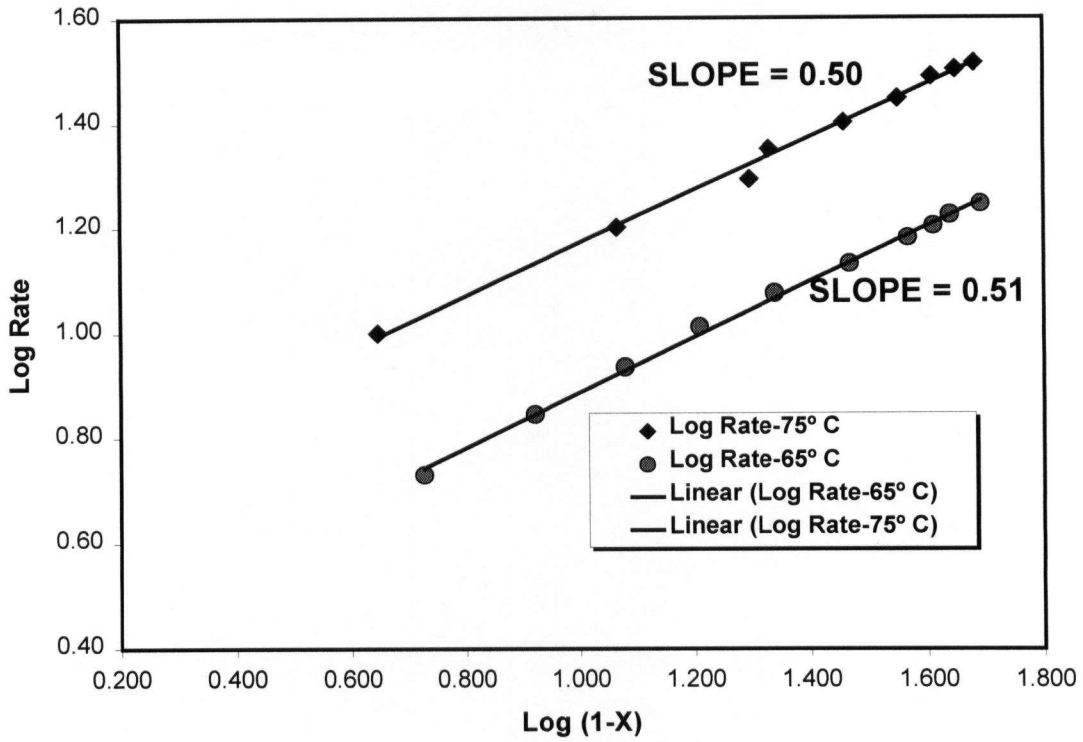


Figure 5-6. Log rate vs. extraction for the second stage leaching of $-250+212 \mu\text{m}$ particles at 65°C and 75°C , 0.116 mol/L ferric and 0.0202 mol/L ferrous.

Hence, the anodic surface area can be represented as follows;

$$A_a = \phi A_o [1 - \alpha_2]^{0.5} \quad (5-21)$$

Where ϕ is a geometric factor and A_o is the original surface area of the second stage covellite. Substituting equation (5-21) in equation (5-20) gives:

$$\frac{d\alpha_2}{dt} = \frac{1}{2(\alpha_b - \alpha_a)n_o} \phi A_o [1 - \alpha_2]^{0.5} \bar{k}_a \left[\frac{\bar{k}_c}{\bar{k}_e} \right]^{0.42} \left[\frac{[Fe^{3+}]}{[Fe^{2+}]} \right]^{0.42} \quad (5-22)$$

In we introduce an Arrhenius function for temperature, then equation (5-22) becomes;

$$\frac{d\alpha_2}{dt} = k e^{-E/RT} [1 - \alpha_2]^{0.5} \quad (5-23)$$

$$\text{Where } k = \frac{1}{2(\alpha_b - \alpha_a)n_o} \phi A_o \bar{k}_a \left[\frac{\bar{k}_c}{\bar{k}_c} \right]^{0.42} \left[\frac{[Fe^{3+}]}{[Fe^{2+}]} \right]^{0.42} \quad (5-24)$$

$$k = k_1 \left[\frac{[Fe^{3+}]}{[Fe^{2+}]} \right]^{0.42}$$

$$\text{Then, } \frac{d\alpha_2}{dt} = k_1 e^{-E/RT} [1 - \alpha_2]^{0.5} \left[\frac{[Fe^{3+}]}{[Fe^{2+}]} \right]^{0.42} \quad (5-25)$$

$$\text{Also, } c = k e^{-E/RT} = k e^{-97000/RT} \quad (5-26)$$

By using the experimental activation energy which is 97000 J/mole;

$$\text{At } 75^\circ\text{C, } c = 2.7532 \times 10^{-15} k \quad (5-27)$$

$$\text{Then, } \frac{d\alpha_2}{dt} = c [1 - \alpha_2]^{0.5} \quad (5-28)$$

By integration, the following relationship was obtained from equation (5-28);

$$\alpha_2 = 1 - \left(\frac{2 - ct}{2} \right)^2 \quad (5-29)$$

At 75°C and different ferric/ferrous ratio, attempts were made to fit the model with the experimental data in Figure 5-6.

At 75°C, 0.116 mol/L ferric and 0.0202 mol/L ferrous with ferric / ferrous ratio of 5.8.

$$c = 0.7943$$

$$k = 2.885 \times 10^{14}$$

$$k_1 = 1.3788 \times 10^{14}$$

At 75°C, 0.082 mol/L ferric and 0.054 mol/L ferrous with ferric / ferrous ratio of 1.52.

$$c = 0.4526$$

$$k = 1.6439 \times 10^{14}$$

$$k_1 = 1.3788 \times 10^{14}$$

The comparison of the predicted and actual data is presented in Figure 5-7.

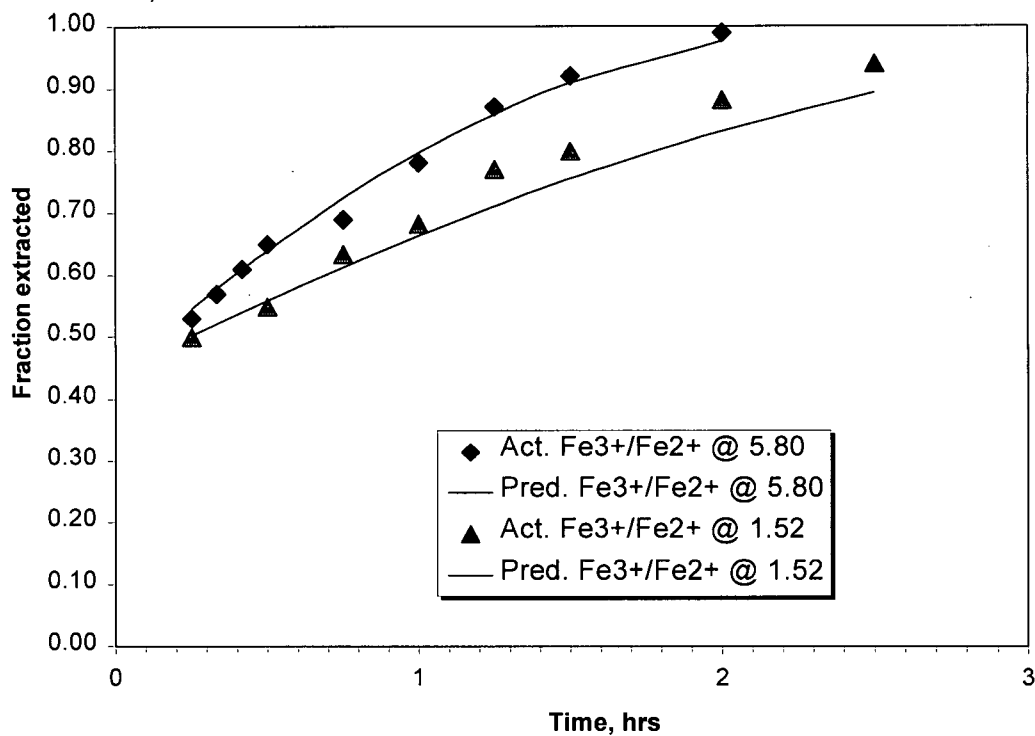


Figure 5-7. Predicted vs. actual extraction for the second stage leaching of $-250+212 \mu\text{m}$ particles at 75°C and different ferric / ferrous ratio.

In Figure 5-8, the logarithm of the instantaneous rate of extraction (of copper available for leaching in the second stage) is plotted against the fraction unreacted ($1-\alpha_2$) at 55°C . The best power law fit obtained in this work leads (approximately) to a chemical controlled mechanism with shrinking cylinder geometry.

At 55°C and by using equation 5-26, $c = 3.5657 \times 10^{-16} k$ (5-30)

Also equation 5-28 can be used to predict the extraction as shown in Figure 5-9.

At 55°C , 0.116 mol/L ferric and 0.0202 mol/L ferrous.

$$c = 0.1029$$

$$k = 2.8849 \times 10^{14}$$

$$k_1 = 1.3788 \times 10^{14}$$

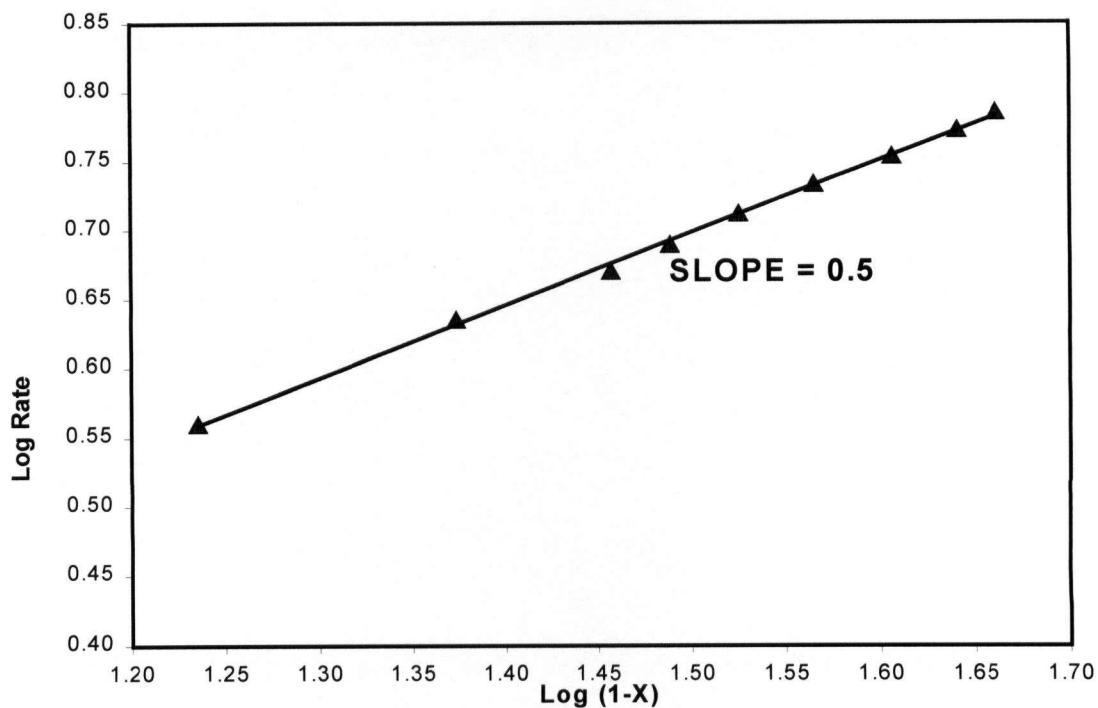


Figure 5-8. Log rate vs. log of extraction for the second stage leaching of $-250+212\ \mu\text{m}$ particles at 55°C , 0.116 mol/L ferric and 0.0202 mol/L ferrous.

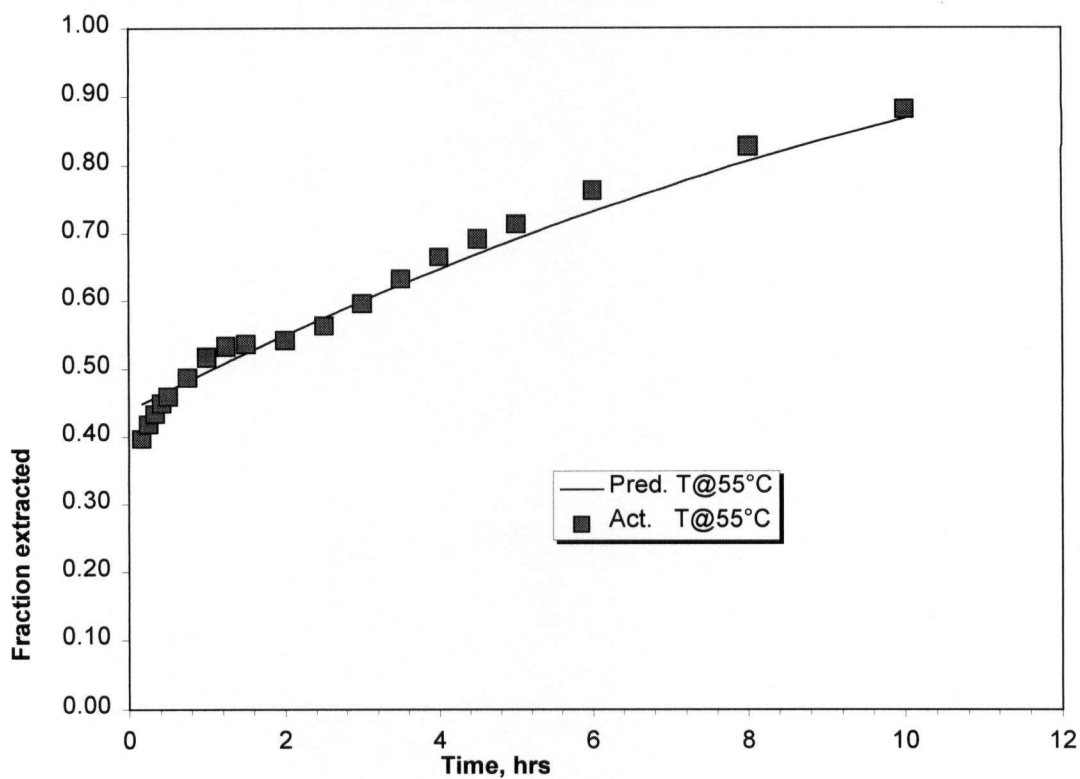


Figure 5-9. Predicted vs. actual extraction for the second stage leaching of $-250+212\ \mu\text{m}$ particles at 55°C , 0.116 mol/L ferric and 0.0202 mol/L ferrous.

At 35°C and by using equation 5-26, $c = 3.5394 \times 10^{-17} k$ (5-31)

Also equation 5-28 can be used to predict the extraction at 35°C and at different concentration of ferrous as shown in Figure 5-10.

At 35°C, 0.116 mol/L ferric and 0.020 mol/L ferrous.

$$c = 0.0102$$

$$k = 2.8849 \times 10^{14}$$

$$k_1 = 1.3788 \times 10^{14}$$

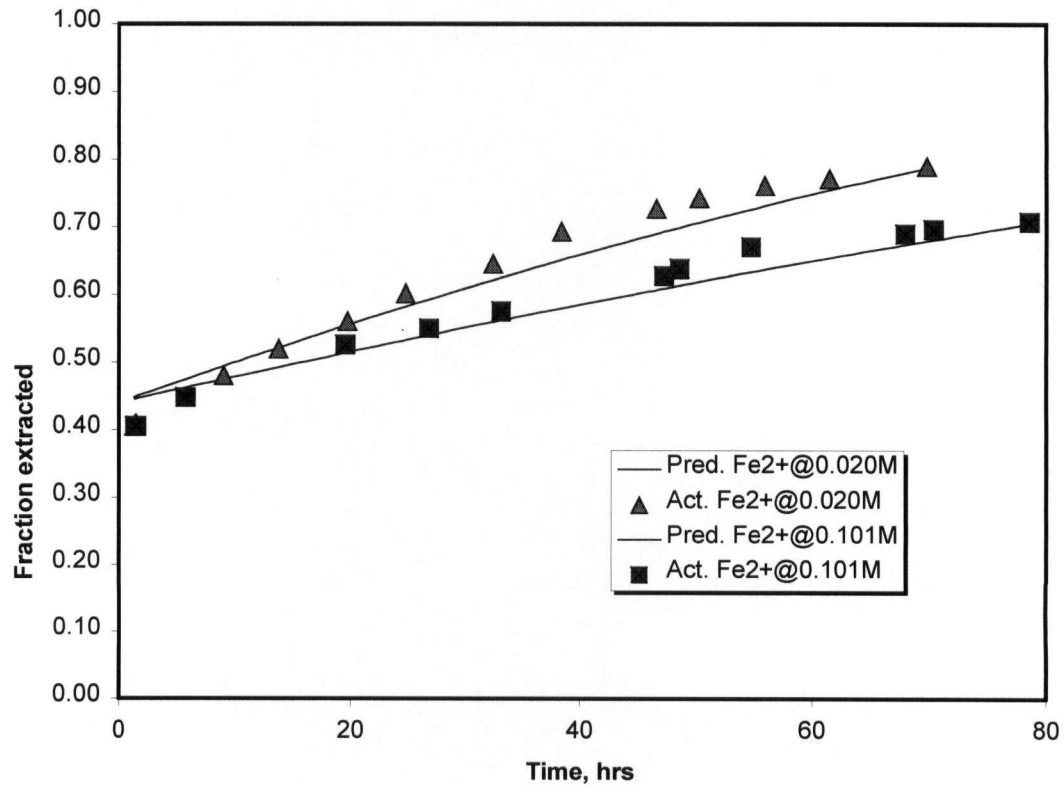


Figure 5-10. Predicted vs. actual extraction for the second stage leaching of $-250+212 \mu\text{m}$ particles at 35°C, 0.116 mol/L ferric and different levels of ferrous.

In order to test the robustness of this model, the initial experimental conditions of Marcantonio [2] were tested as shown in Figure 5-11. It is important to recall that in the work of Marcantonio, the initial ferric / ferrous ratio was allowed to deviate from time zero, before the commencement of the second stage leaching but in Figure 5-11, the

initial conditions were used to predict extraction. This may be responsible for the disparity between his data and that of the model in the present work.

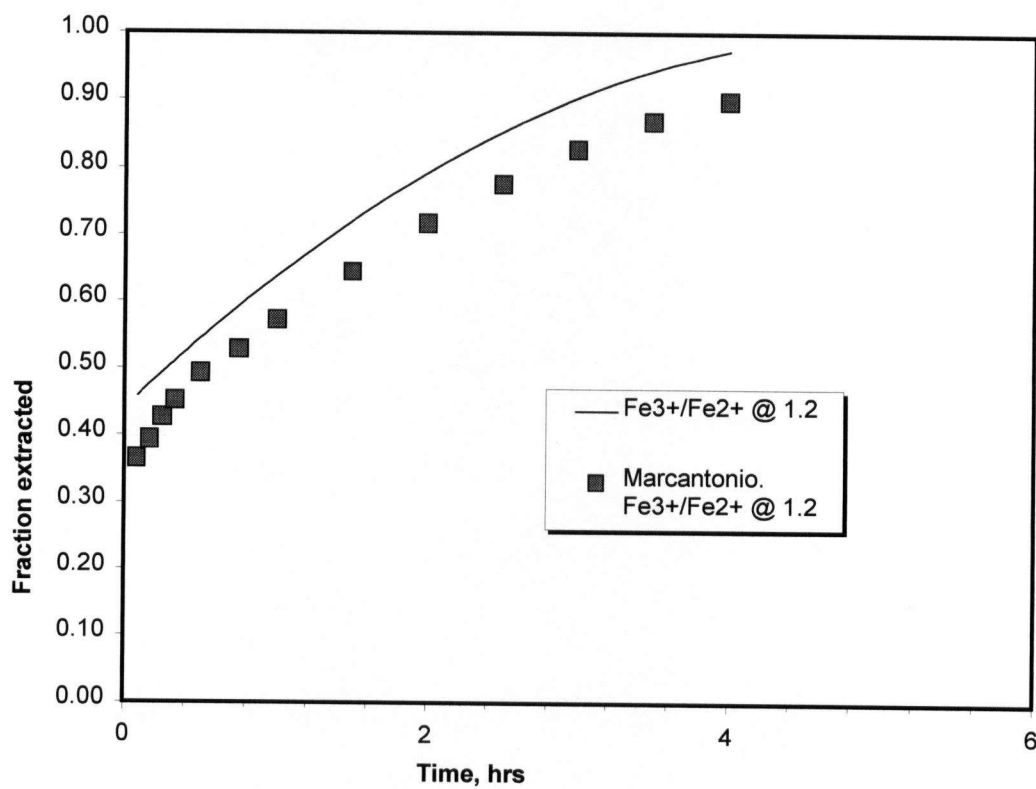


Figure 5-11. Predicted vs. actual extraction (Marcantonio's data [2]) for the second stage leaching of chalcocite particles at 75°C, 0.24 ferric and 0.2 mol/L ferrous.

CHAPTER 6

CONCLUSIONS

The following are the major conclusions reached from this study of the leaching kinetics of chalcocite and second stage covellite.

1. The first stage leaching is very fast and second stage leaching is slow at low temperatures. Non-stoichiometric copper sulfides are formed before the formation of second stage covellite and the rate of reaction of all these phases are fast enough such that none of them affects the rate of second stage leaching. Hence, even though the rate decreases rapidly at about 40% copper extraction, blue-like covellite ($\text{Cu}_{1.2}\text{S}$) is not formed and second stage leaching does not involve this compound.
2. The first stage leaching is controlled simultaneously by the diffusion of ferric ions and the chemical reaction. The particles break before the end of the first stage, thus rendering the surface more reactive, but this does not enhance the rate because of the low concentration of mobile cuprous ions (within the crystal lattice) at this stage. At low ferric concentrations, the rate of reaction is rapid and controlled by mass transfer of the ferric ions to the reaction surface. The rate dependence on ferric concentration decreases with increasing ferric concentration during the first stage leaching. The leaching mechanism changed at high ferric concentration to an electrochemical mechanism in which the rate is controlled by charge transfer in the anodic reaction.
3. The second stage leaching is controlled by chemical reaction and particle breakage during the first stage enhances the dissolution of the second stage covellite by providing fresh and large surfaces for chemical reaction. The half-order dependence of rate on ferric concentration and the fractional order dependence on the ferric / ferrous ratio during second stage leaching suggests an electrochemical mechanism in which the rate is controlled by charge transfer in the anodic reaction. This mechanism operates at both low and high temperatures. Although an increase in temperature

enhances the rate of reaction, it does not alter significantly the (electrochemical) mechanism of anodic dissolution.

4. The rate of second stage leaching is governed by the redox potential. There is also a fractional order inverse dependence of rate on the ferrous concentration. This indicates that the reversible reaction which involves the ferrous ions of the ferric/ferrous couple is significant in the electrochemical mechanism. Hence, there is a need to have low concentration of ferrous during the tank and heap leaching, and this is the primary role of the bacteria. An active bacterial condition, in which the oxidation of ferrous ions takes place faster than the reduction of ferric ions by the second stage covellite is necessary for process efficiency at low temperature.
5. The reaction products of the second stage are sulfur and sulfate at low temperatures, substantial part of the elemental sulfur is formed first and its accumulation at about 70% copper extraction reduces the leaching rate at low temperatures. The sulfur oxidation by bacteria is desirable for achieving a high rate of reaction during low temperatures leaching of the mineral. The sulfate is formed substantially during the latter part of the reaction at low temperature. At high temperatures, the principal product is elemental sulfur, which is porous and does not inhibit leaching. Another possible intermediate product is copper disulfide (CuS_2) which decomposes rapidly at high temperatures to copper and sulfur.
6. The electrochemical leaching model developed to predict second stage leaching has been validated with experimental data from this work and previous work. It predicts the rate response to temperature, ferric and ferrous concentrations which are the important parameters during the second stage leaching.

CHAPTER 7

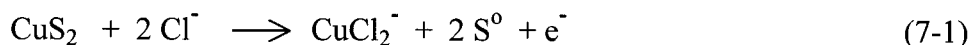
RECOMMENDATIONS FOR FURTHER WORK

These studies have shed light on the conditions which favor the leaching of chalcocite in acidic ferric sulfate solution. The mineralogical studies have identified the formation of intermediate copper sulfides and their probable roles during leaching have been discussed. Further mineralogical characterization of the copper disulfide phase is desirable in order to define this phase more accurately and to establish the conditions affecting its formation and stability. This may involve complete probing by EPMA, all the remaining grains after the leaching reaction rate rather than random selection of the grains. The nature of the elemental sulfur formed at different temperatures needs to be studied further in order to establish its properties (physical and chemical) which may affect the second stage leaching.

The focus of this thesis was to carry out a fundamental investigation of the effects of various leaching conditions on the kinetics of chalcocite oxidation. As a result, the fruitful combination of leaching parameters to be employed so as to improve the operations of heap and tank leaching operations may be inferred and the mathematical models for the leaching of chalcocite are presented. However, the following suggestion is offered as a promising additional approach to pursue in the future.

Use of Chloride

The addition of chloride ions to sulfate media in copper heap leaching is being considered as one way to enhance copper dissolution. The dissolution reaction in chloride has been reported to be faster than that of sulfate media. Also, it can be speculated that the chloride ion will accelerate the decomposition of the copper disulfide through the following reaction:



There will be need to establish the appropriate concentration of total-chloride so as to prevent precipitation of the CuCl_2^- .

REFERENCES

1. Sullivan, J.D., Chemistry of Leaching Covellite, U.S. Bureau of Mines, *Tech. Paper* 487, 1930.
2. Marcantonio, P., Kinetics of Dissolution of Chalcocite in Ferric Sulfate Solutions *Ph.D. Thesis*, Dept. of Mining, Metallurgical and Fuels Engineering, University of Utah, Lake Utah, U.S.A, 1975.
3. Mulak, W., Kinetics of Dissolving Polydispersed Covellite in Acid Solutions of Ferric Sulfate, *Roczn.Chem.*, 45, pp. 1417-1424, 1971.
4. Lowe, D.F., The Kinetics of the Dissolution Reaction of Copper & Copper-Iron Sulfide Minerals Using Ferric Sulfate Solutions, *Unpublished Ph.D. Thesis*, University of Arizona, USA, 1970.
5. Tkachenko, O.B. and Tseft, A.L., Kinetics of the Dissolution of Chalcocite in Ferric Chloride, *Trudy Inst. Metall. Obogashch., Alma Ata*, 30, pp. 1387-1394, 1969.
6. Mulak, W., Kinetics of Cuprous Sulfide Dissolution in Acidic Solutions of Ferric Sulfate, *Roczn. Chem.*, 43, pp. 1387-1394, 1969.
7. Kopylov, G.A. and Orlov, A.I., Rates of Bornite and Chalcocite Dissolution in Ferric Sulfate, *Jr. Irkutsh. Politckh. Inst.*, 46, pp. 127-132, 1969.
8. King, J.A., Solid State Changes in the Leaching of Copper Sulfides, *Unpublished Ph.D. Thesis*, University of London, U.K, 1966.
9. Thomas, G. and Ingraham, T.R., Kinetics of Dissolution of Synthetic Digenite & Chalcocite in Aqueous Acidic Ferric Sulfate Solutions, *Canadian Metallurgical Quarterly*, 6(3), pp. 281 - 292, 1967.
10. Colombo, A.F. and Frommer, D.W., Leaching Michigan Copper Ore & Mill Tailings with Acidified Ferric Sulfate, U.S Bureau of Mines, *Tech. RI-5924*, 1962.
11. Sullivan, J.D., Chemistry of Leaching Covellite, U.S. Bureau of Mines, *Tech. Paper* 87, 1930.
12. Thomas, G. and Ingraham, T.R., Kinetics of Dissolution of Synthetic Covellite in Aqueous Acidic Ferric Sulfate Solutions, *Canadian Metallurgical Quarterly*, 6(2), pp.153 - 165, 1967.

13. Dutrizac, J.E. and Mac Donald, R.J.C, The Kinetics of Dissolution of Covellite in Acidified Ferric Sulfate Solutions, *Canadian Metallurgical Quarterly*, 13(3), pp. 423 -433, 1974.
14. Brennet, P., Jafferli, S., Vanseveren, J., and Winand, R. Study of the Mechanism of Anodic Dissolution of Cu_2S , *Metallurgical Transaction*, 5, pp. 127 -134 1974.
15. Venkatachalam, S. and Mallikarjunan, R., Electrode Potentials and Anodic Polarization of Sulphides, *Transaction of the Institute of Mining and Metallurgy*, 79, pp. C181-188, 1970.
16. Sato, M., Half- Cell Potentials of Semiconductive Simple Binary Sulfides in Aqueous Solution, *Electrochimica Acta*, 11, pp. 361-373, 1966.
17. Mao, M.H. and Peters, E., Direct Electrefining of Cuprous Sulfide-based Particulate Anodes, *Canadian Metallurgical Quarterly*, 22(4), pp. 437-466, 1983.
18. Imai, K. Sakaguchi, H., Sugio, T. and Tano, T., On the mechanism of Chalcocite Oxidation by *Thiobacillus ferrooxidans*, *Journal of Fermentation Technology*, 51(12), pp. 865-870, 1973.
19. Donati, E., Curutchet, G., Pogliani, C. and Tedesco, P., Bioleaching of covellite by individual or combined cultures of *Thiobacillus ferrooxidans* and *Thiobacillus thiooxidans*, *Biohydrometallurgical Processing*, T.Vegas, C.A. Jerez, J.V.Wiertz and H. Toledo, Eds., University of Chile, pp. 91-99, 1995.
20. Sand, W., Gerke, T., Hallmann, R. and Schippers, A., Sulfur chemistry, Biofilm, and the (in)direct attack mechanism - A critical evaluation of bacterial leaching, *Applied Microbiology and Biotechnology*, 43, pp. 961-966, 1995.
21. Curutchet, G., Tedesco, P. and Donati, E., Indirect Bioleaching of Covellite by *Thiobacillus Thiooxidans* with an Oxidant Agent, *Biotechnology Letters*, 17 (11), pp. 251-1256, 1995.
22. Donati, E.R., Curutchet, G., Pogliani, C., and Tedesco, P.H., *Process Biochemistry*, 31, pp. 129-134, 1996.
23. Johnson, A.M., Carlson, D.G., Bagley, S.T. and Johnson, D.L., In-situ Bioleaching Investigations of Michigan Chalcocite Ores, *In: Proceedings of the SME Annual Meeting, Arizona, U.S.A, January 25-28, 1988.*
24. Weston, J. M., Dreisinger, D. B. and Hackl, R. P., Continuous Biological Leaching of Copper from a Chalcocite ore and Concentrate in a saline environment, *Proceedings of COPPER 95-COBRE 95 International Conference* Vol. 3, W. C. Cooper, D.B.

Dreisinger, J.E Dutrizac, H. Hein and G.Ugarte, Eds., Chilean Institute of Mining Engineers, The Metallurgical Society of CIM, and The Minerals, Metals Society of the AIME, Santiago, Chile, pp. 757-772, 1995.

25. Nielsen, A.M. and Beck, J.V., Chalcocite Oxidation and Coupled Carbondioxide Fixation by *Thiobacillus ferrooxidans*, *Science*, 175, pp. 1124-1126, 1972.
26. Sakaguchi, H., Silver, M. and Torma, A.E., Microbiological Oxidation of Synthetic Chalcocite and Covellite by *Thiobacillus ferrooxidans*, *Applied and Environmental Microbiology*, 31(1), pp. 7-10, 1976.
27. Melliish, J.M., Groat, L.A., Dreisinger, D.B., Branion, R., Leong, B.J.Y. and Crombie, D.R., Mineralogical Characterization of Residues from a Microbiologically Leached Copper Sulfide Ore, In: *Biohydrometallurgical Technologies*, A.E. Torma, J.E. Wey and Lakshmanan, Eds., The Minerals, Metals & Materials Society, pp. 127-136, 1993.
28. Wiertz, J.V., Godoy, R. I. and Escobar, M.B., Dissolved Iron Equilibrium in Bacteria Leaching System, In: *Hydrometallurgy '94, Institution of Mining and Metallurgy (IMM) and Society of Chem. Industry (SIC)*, Chapman & Hall, London, U.K., pp. 385-393, 1994.
29. Beck, J.V., Chalcocite Oxidation by Concentrated Cell Suspensions of *Thiobacillus ferrooxidans*, In: *Conference Bacteria Leaching 1977*, Schwartz, W. Ed, Verlag Chemie, New York, U.S.A., pp. 119, 1977.
30. Trudinger, P.A., The metabolism of Inorganic Sulfur Compounds by *Thiobacilli*, *Rev. Pure Appl. Chem.*, 17, pp. 1-24, 1967.
31. Jyotyi, N., Sudha, K.N., Brahmaprakash, G.P., Natarajan, K.A., and Ramananda, R.G., Electrochemical Aspects of Bioleaching of Mixed Sulfides, In: *Biotechnology in Minerals and Metal Processing*, B.J. Scheiner, F.M. Doyle and S.K. Kawatra Eds., Society of Mining Engineers, Inc., Cushing-Malloy, Inc., Ann Arbor, MI, USA, pp. 9-16, 1989.
32. Goodman, A.E., Babij, T. and Ritchie, A.I.M., Leaching of a Sulfide Ore by *Thiobacillus ferrooxidans* under Anaerobic Conditions, In: *Progress in Biohydrometallurgy*, G. Rossi, A.E. Torma, Eds., Associazione Mineraria Sarda, Iglesias, pp. 361-376, 1983.
33. Donati, E., Pogliani, C., and Bioardi, J.L., Anaerobic Leaching of Covellite by *Thiobacillus ferrooxidans*, *Applied Microbiology and Biotechnology*, 47, pp. 636-639, 1997.

34. Curutchet, G., Tedesco, P. and Donati, E., Combined Degradation of Covellite by *Thiobacillus Thiooxidans* and *Thiobacillus Ferrooxidans*, *Biotechnology Letters*, 18 (12), pp. 1471-1476, 1996.
35. Pronk, J.T., Bryn, J.B.P., Kuenen, J.G., Anaerobic Growth of *Thiobacillus ferrooxidans*, *Applied and Environmental Microbiology*, 58, pp. 2227-2230, 1992.
36. Dutrizac J.E., MacDonald R.J.C., Ferric Ion as a Leaching medium, *Minerals Science Engineering*, 6 (2), pp. 59-100, 1974.
37. Evans , H. T, The Crystal Structure of Low Chalcocite and Djurlite, *Nature. Physical Science*, 232, pp. 69 - 70, 1971.
38. Shuey, R.T, *Semi conducting ore Minerals*, Elsevier Scientific Publishing Co., Amsterdam.
39. Evans Jr , H. T, Copper Coordination In Low Chalcocite and Djurleite and Other Copper - rich Sulfides. *American Mineralogist*, 66, pp. 807 - 811, 1981.
40. Evans Jr , H. T, and Konnert , J Crystal Structure of refinement of Covellite, *American Mineralogist*, 61, pp. 996 - 1000, 1976.
41. Lima - de- Faria J. *Structural Mineralogy, An Introduction*, Kluwer Academic Publishers, London, 7, pp. 304, 1994.
42. Nakai, I. Sugitani , Y and Nagashima, K, X - ray photoelectron Spectroscopic Study of Copper minerals, *J.Inorganic. Nucl.Chem.* 40, pp. 789-791, 1978.
43. Folmer, J.C.W and Jellinek, F., The valence of Copper in Sulfides and Selenides: an X- ray Photoelectron Spectroscopy study, *J. Less Common Metals* , 76, pp153-162, 1980.
44. Jellinek, F. *MTP International Review of Science, Inorganic Chemistry Series, Butterworths, London , Series 1, vol 5*, pp. 339, 1972.
45. Vaughan, J.D, Electronic Structures of Sulfides and Leaching Behavior: In *Hydrometallurgical Process Fundamentals*, 10, pp. 23-40, 1982.
46. Vaughan, J.D and Tossell J.A, The Chemical bond and The Properties of Sulfide Minerals. *Canadian Mineralogist*, 18, pp. 157-163, 1980.
47. Hackl, R. P., *The Thermodynamics of leaching: Eh- pH Diagram for Cu-S-H₂O Systems*, Hydrometallurgy I class-notes, University of B.C. Vancouver, B.C., Canada, 1998.

48. Dixon, D. G., *The Eh- pH Diagram at Elevated Temperatures*, Hydrometallurgy II class-notes, University of B.C. Vancouver, B.C., Canada, 1998.
49. Rao, Y.R., *Stoichiometry and Thermodynamics of Metallurgical Process*, Cambridge University Press, New York, NY, USA, 1985.
50. Criss, C.M. and Cobble, J.W., The Thermodynamic Properties of High Temperature Aqueous Solution. VI. Entropies of the Ions up to 200 °C and Correspondence Principle, *Journal of America Chemical Society*, 86, pp. 5385, 1964.
51. Criss, C.M. and Cobble, J.W., The Thermodynamic Properties of High Temperature Aqueous Solution. VI. Applications of Entropy Correspondence to Thermodynamics and Kinetics, *Journal of America Chemical Society*, 86, pp. 5394, 1964.
52. Bard, A.J., Parsons, R., and Jordan, J., *Standard Potentials in Aqueous Solution*, Marcel Dekker Inc., New York, NY, and Basel, 1985.
53. Peters, E., Hydrometallurgical Process Innovation, *Hydrometallurgy*, 29, pp. 431-459, 1992.
54. Cavallotti, P. and Salvago, G. Electrode Behavior of Copper Sulfides in Aqueous Solutions, *Electrochimica Metallorum*, 4 (3), pp. 181 - 210, 1969.
55. Moh, G.H, Blue Remaining Covellite & Its Relations to Phases in the Sulfur Rich Portion of the Copper-Sulfur System at Low Temperatures, *Mineral. Soc. Japan, Spec. Paper 1*, (Proc. IMA- IAGOD Meetings '70, Ima Vol.), pp.180-188, 1971.
56. Whiteside, L. S. and Goble, R.J., Structural and Compositional Changes in Copper Sulfides During Leaching and Dissolution, *Canadian Mineralogist*, 24, pp. 247-258, 1986.
57. Munson, R. A., The Synthesis of Copper disulfide, *Inorganic Chemistry*, 5, pp. 1296-1297, 1966.
58. Taylor, L.A. and Kullerud, G., Phase equilibria associated with the Stability of Copper disulfide, *Neus Jahrbuch Mineral Montash.*, pp. 458-464, 1972.
59. Moh, G., The pyrite-type Cu-rich disulfides in the Providencia mine, Leon, *Neus Jahrbuch Mineral Montash.*, pp. 1-69, 1989.
60. Wright, J.K., The feasibility of electrolytic treatment of sulphide concentrates, *Process and Chemical Engineering*, June, pp. 9-14, 1973.

61. Nicol, M. J., Needes, C.R.S and Finkelstein, N.P., Electrochemical Model for the leaching of Uranium Dioxide: 1. Acid Media, *Leaching and Reduction in Hydrometallurgy*, A.R. Burkin, Ed., Institution of Mining and Metallurgy (IMM), Camelot Press, London, pp. 1-19, 1975.
62. Wadsworth, M. E., Heterogeneous Rate Processes in the Leaching of Base Metal Sulfides, *Hydrometallurgical Process Fundamentals*, R.G. Bautista, Ed., Plenum Press, New York, USA, pp. 41-76, 1984.
63. Dixon, D. G., *The Electrochemical Leaching Reactions*, Hydrometallurgy II class-notes, University of B.C. Vancouver, B.C., Canada, 1999.
64. Vetter, K. J., *Electrochemical Kinetics, Theoretical and Experimental Aspects*, Academic Press, New York, NY, USA, 1967.
65. Li, J., Zhong, T. K. and Wadsworth, M.E., Application of Mixed-Potential Theory in Hydrometallurgy, *Hydrometallurgy*, 29, pp. 47-60, 1992.
66. Wadsworth, M. E. and Zhong, T. K., Coupled Rate Control in the dissolution of electron Conducting Minerals, *Hydrometallurgical Process Fundamentals*, R.G. Bautista, Ed., Plenum Press, New York, USA, pp. 171-193, 1984.
67. Etienne, A., Electrochemical Aspects of the Aqueous Oxidation of Copper Sulfides, Ph.D Thesis, University of British Columbia, Dept. of Metallurgical Engineering, November, pp. 86-97, 1970.
68. Jost, W. *Diffusion*, Academic Press. New York, pp. 87 and pp.168, 1952.
69. Price, D. C., Application of Chrono-potentiometric Analysis to the Anodic Treatment of Copper Sulfides, *Metallurgical Transactions*, 12B, pp. 231-239, 1981.
70. Sato, M., Oxidation of Sulfide Ore Bodies, II; Oxidation Mechanisms of Sulfide Minerals at 25°C, *Economic Geology*, 55, pp. 1202-1231, 1960.
71. Peters, E. and Mao, M.H., Acid Pressure Leaching of Chalcocite, *Hydrometallurgy, Research, Development and Plant Practice, Proceedings of the 3rd International Symposium on Hydrometallurgy*, K. Osseo-Asare and J. D. Miller, Eds., Atlanta, U.S.A, pp. 243-260, 1983.
72. Fisher, W. W., Flores, F.A., and Henderson, J.A., Comparison of Chalcocite Dissolution in the Oxygenated, Aqueous Sulfate and Chloride Systems, *Minerals Engineering*, 5 (7), pp. 817-834, 1992.

73. Fisher, W. W., Comparison of Chalcocite Dissolution in the Sulfate, Perchlorate, Nitrate, Chloride, Ammonia and Cyanide Systems, *Minerals Engineering*, 7 (1), pp. 99-103, 1994.
74. Turney, T.A., *Oxidation Mechanisms*, Butterworth & Co (Publishers) Ltd., London, pp. 56; 90 and 111, 1965.
75. Tompkins, F.C., The Kinetics of the Reaction between Manganous and Permanganate ions, *Transaction of the faraday Society*, 38, pp. 131, 1942.
76. Jeffery, G. H., Bassett, J., Mendham, J., and Denney, R. C., *Vogel's Textbook of Quantitative Chemistry Analysis*, Longman and John Wiley, Newyork, NY, USA.
77. Silverman, M. P. and Lundgren, D. G., Studies on the Chemoautotropic Iron Bacterium *Ferrobacillus Ferrooxidans* I. An Improved Medium and a Harvesting Procedure for Securing High Cell yields, *Journal of Bacteriology*, 77, pp. 642-647, 1959.
78. Burkin, A.R., Composition and Phase Changes during Oxidative acid Leaching Reactions, *Hydrometallurgical Process Fundamentals*, R.G. Bautista, Ed., Plenum Press, New York, USA, pp. 171-193, 1984.
79. Fogler, S. H., *Elements of Chemical Reaction Engineering, Second Edition, Chapter 10, External Diffusion Effects on Heterogeneous Reactions*, Prentice Hall International Series in the Physical and Chemical Engineering Sciences, Prentice Hall Upper Saddle River, NJ. USA, pp. 543-606, 1992.
80. Levenspiel, O., *Chemical Reaction Engineering, Second Edition, Chapter 12, Fluid-particle Reactions*, John Wiley & Sons, New York, NY, USA, pp. 357-408, 1972.

APPENDIX 1

Eh-pH DIAGRAM AT HIGH TEMPERATURE

In order to determine the ΔG_T^o , the following are considered;

$$\Delta G_{298}^o = \Delta H_{298}^o - 298 \cdot \Delta S_{298}^o \quad (\text{A1-1})$$

$$\Delta G_T^o = \Delta H_T^o - T \cdot \Delta S_T^o \quad (\text{A1-2})$$

and subtracting equation A1-1 from equation A1-2, gives the following;

$$\Delta G_T^o = \Delta G_{298}^o + (\Delta H_T^o - \Delta H_{298}^o) - T \cdot \Delta S_T^o + 298 \cdot \Delta S_{298}^o \quad (\text{A1-3})$$

Recognising that,

$$\Delta H_T^o - \Delta H_{298}^o = \int_{298}^T \Delta C_p^o dT \quad (\text{A1-4})$$

$$= \Delta \bar{C}_p^o \int_{298}^T (T - 298) \quad (\text{A1-5})$$

In order to predict the heat capacity ($\Delta \bar{C}_p^o \int_{298}^T$), the following are considered;

$$\text{Since } C_p = \left(\frac{dH}{dT} \right)_p = T \left(\frac{dS}{dT} \right)_p \quad (\text{A1-6})$$

At constant pressure;

$$\Delta S = S_T^o - S_{298}^o = \int_{298}^T \frac{\Delta C_p^o}{T} dT \quad (\text{A1-7})$$

$$= \int_{\ln 298}^{\ln T} \Delta C_p^o d \ln T \quad (\text{A1-8})$$

$$\cong \Delta \bar{C}_p^o \int_{298}^T \ln \left(\frac{T}{298} \right) \quad (\text{A1-9})$$

$$\text{Then, } \Delta S_T^o \cong \Delta S_T^o + \Delta \bar{C}_p^o \int_{298}^T \ln \left(\frac{T}{298} \right) \quad (\text{A1-10})$$

By substituting equation (A1-5) and (A1-10) into equation (A1-3), then we obtain the following equation;

$$\Delta G_T^o = \Delta G_{298}^o + \Delta \bar{C}_P^o \int_{298}^T \left(T - 298 - T \ln \left(\frac{T}{298} \right) \right) - (T - 298) \Delta S_{298}^o \quad (\text{A-11})$$

Where $\theta = \left(T - 298 - T \ln \left(\frac{T}{298} \right) \right)$ (A-12)

Then, $\Delta G_T^o = \Delta G_{298}^o + \Delta \bar{C}_P^o \int_{298}^T \theta - (T - 298) \Delta S_{298}^o$ (A-13)

For the non-ionic species, $C_P \int_{298}^T = \frac{\int_{298}^T C_P(T) dT}{\int_{298}^T dT}$ (A-14)

Therefore, $C_P \int_{298}^T = \frac{\int_{298}^T (a + bT + cT^{-2}) dT}{(T - 298)}$ (A-15)

$$= \frac{a(T - 298) + \frac{b}{2}(T^2 - 298^2) - c \left(\frac{1}{T} - \frac{1}{298} \right)}{T - 298} \quad (\text{A-16})$$

$$= a + \frac{b(T + 298)}{2} + \frac{c}{298.T} \quad (\text{A-17})$$

The following are the free energies used to construct the Eh-pH diagram for the Cu-S-H₂O at 298 and 348 K;

Table A1-1. Free energies (kJ/mol) of the species used in the construction of the Eh-pH diagrams.

Specie	298 K	348 K
Cu ⁰	0.000	-1.211
Cu ²⁺	65.700	69.665
Cu ⁺	50.300	47.633
HSO ₄ ⁻	-756.010	-761.680
SO ₄ ²⁻	-744.600	-744.780
HS ⁻	12.050	9.780
S ²⁻	86.310	87.930
Cu ₂ S	-87.600	-93.864
CuS	-53.200	-56.739
CuO	-134.000	-136.320
Cu ₂ O	-148.100	-153.000
H ₂ S (g)	-33.560	-43.982
S ⁰	0.000	-1.526

The following are the Heat capacity function used to construct the Eh-pH at 348 K;

Table A1-2. Heat capacity function of the species (in J/mol-k) used in the construction of the Eh-pH diagram.

Specie	A	b x 10 ³	C
Cu ⁰	22.635	6.276	0
Cu ₂ S	81.588	0	0
CuS	44.350	11.046	0
CuO	38.786	20.083	0
Cu ₂ O	62.342	23.849	0
H ₂ S (g)	32.677	12.385	-1.925
S ⁰	14.811	24.058	0.728

APPENDIX 2

EXPERIMENTAL DATA

Experimental Conditions:

Variable	Temperature (chalcocite leaching)
Particle Size	-250+212 μm
Initial leach-volume	1000 ml
Acid concentration	0.095 mol/L H_2SO_4
Ferric concentration	0.116 mol/L
Ferrous concentration	0.020 mol/L
Initial mole of Cu in the	
Solid mineral	0.0555 mol.

Table A2-1. Percentage of copper extracted at different temperatures.

Time (min)	35°C	55°C	65°C	75°C
0	0.00	0.00	0.00	0.00
1	9.10	14.69	20.81	34.01
3	20.23	25.47	31.79	40.21
4	N/A	29.00	35.00	41.52
5	28.00	32.25	36.82	42.53
6	N/A	35.08	38.85	43.75
8	N/A	37.77	40.95	44.15
10	34.70	39.68	42.04	46.46
15	37.77	41.88	44.09	48.23

Experimental Conditions:

Variable	Ferric concentration (chalcocite leaching)
Temperature	35°C
Particle Size	-250+212 μm
Initial leach-volume	1000 ml
Acid concentration	0.095 mol/L H_2SO_4
Ferrous concentration	0.010 mol/L
Initial mole of Cu in the	
Solid mineral	0.0555 mol.

Table A2-2. Percentage of copper extracted at different concentrations of ferric.

Time (min)	0.007 M	0.015 M	0.029 M	0.058 M	0.116 M	0.174 M	0.232 M
0	0.00	0.00	0.00	0.00	0.00	0.00	0.00
1	1.42	2.84	4.54	7.20	11.25	13.50	15.99
2	2.28	3.81	7.46	12.25	16.96	19.03	21.60
3	3.36	5.15	9.69	15.76	21.73	23.83	25.97
4	4.20	6.40	12.02	19.22	25.11	26.60	28.97
5	5.62	7.96	13.90	22.25	27.76	29.26	31.67
6	6.68	9.78	16.10	25.27	30.66	31.96	33.04
8	7.84	12.38	19.44	28.85	33.58	34.29	35.52
10	9.39	14.33	22.81	31.88	35.13	35.84	37.13
15	12.46	19.07	28.47	35.60	37.50	38.54	39.36
20	15.98	23.29	32.65	37.42	38.92	39.72	40.63
25	20.53	27.77	34.99	39.07	39.63	40.12	41.29
30	23.83	31.21	36.56	39.67	40.17	41.08	41.50

Experimental Conditions:

Variable	Temperature (secondary-covellite leaching)
Particle Size	-250+212 μm
Initial leach-volume	1000 ml
Acid concentration	0.095 mol/L H_2SO_4
Ferric concentration	0.116 mol/L
Ferrous concentration	0.0202 mol/L
Initial mole of Cu in the	
Solid mineral	0.0555 mol.

Table A2-3. Percentage of copper extracted at different temperatures.

Time (hrs)	35°C	55°C	65°C	75°C
0.25	37.77	41.88	44.09	48.23
0.33	38.17	43.38	44.49	51.99
0.42	38.54	44.99	45.98	55.46
0.50	38.87	45.99	46.73	59.46
0.75	39.24	48.76	50.75	64.49
1.00	39.61	51.76	56.45	71.30
1.25	40.57	53.27	59.20	78.67
1.50	40.90	53.58	63.07	80.27
2.00	N/A	54.17	70.64	88.36
2.50	N/A	56.27	78.19	95.57
3.00	N/A	59.59	83.82	99.84
3.50	N/A	63.25	87.99	N/A
4.00	N/A	66.49	91.66	N/A
4.50	N/A	69.18	94.67	N/A
5.00	N/A	71.34	97.64	N/A
6.00	N/A	76.37	99.25	N/A
8.00	N/A	82.80	N/A	N/A

Experimental Conditions:

Variable	Ferric (second stage leaching)
Particle Size	-250+212 μm
Initial leach-volume	1000 ml
Acid concentration	0.095 mol/L H_2SO_4
Temperature	75°C
Ferrous concentration	0.0101mol/L
Initial mole of Cu in the	
Solid mineral	0.0555 mol.

Table A2-4. Percentage of copper extracted at different ferric levels.

Time (hrs)	0.058 M	0.116 M	0.232 M	0.348 M
0.05	29.43	36.97	38.07	38.77
0.08	37.76	39.55	40.53	41.85
0.13	39.95	43.48	44.82	45.39
0.25	46.30	48.75	50.09	51.37
0.33	49.86	51.62	53.44	55.94
0.42	51.62	54.19	56.80	58.51
0.50	54.11	57.86	60.04	61.61
0.75	61.24	64.17	67.89	69.39
1.00	67.71	71.69	74.24	75.94
1.25	74.71	78.79	81.30	83.06
1.50	80.65	84.84	87.98	89.25
2.00	86.71	91.70	94.75	96.23
2.50	90.56	N/A	N/A	N/A
3.00	93.61	N/A	N/A	N/A

Experimental Conditions:

Variable	Ferrous (second stage leaching)
Particle Size	-250+212 μm
Initial leach-volume	1000 ml
Acid concentration	0.095 mol/L H_2SO_4
Temperature	75°C
Ferric concentration	0.116 mol/L
Initial mole of Cu in the	
Solid mineral	0.0555 mol.

Table A2-5. Percentage of copper extracted at different ferrous levels.

Time (hrs)	0.001 M	0.010 M	0.054 M	0.101 M
0.25	51.85	53.63	49.96	40.55
0.33	55.36	56.78	N/A	N/A
0.42	59.74	59.61	N/A	N/A
0.50	61.48	62.49	58.90	55.42
0.75	69.62	69.30	66.36	N/A
1.00	77.47	77.42	N/A	68.55
1.25	82.35	83.51	78.56	N/A
1.50	89.17	89.93	83.57	79.89
2.00	98.82	99.03	93.68	89.30
2.25	N/A	N/A	98.32	N/A
2.50	N/A	N/A	N/A	98.12

Experimental Conditions:

Variable	Ferric / ferrous ratio
Particle Size	-250+212 μm
Initial leach-volume	1000 ml
Total iron concentration	0.136 mol/L
Temperature	75°C
Total sulfate concentration	0.287 mol/L
Initial mole of Cu in the	
Solid mineral	0.0555 mol.

Table A2-6. Percentage of copper extracted at different ferric / ferrous ratios.

Time (hrs)	ferric	ferrous	Ferric	ferrous	ferric	Ferrous
	0.116 M	0.020 M	0.100 M	0.036 M	0.082 M	0.054 M
0.25	53.05		47.04		49.90	
0.33	57.19		N/A		N/A	
0.42	61.01		N/A		N/A	
0.50	65.41		57.81		54.85	
0.75	69.46		64.76		63.38	
1.00	78.43		76.26		68.29	
1.25	86.54		82.16		76.95	
1.50	92.09		88.74		79.80	
2.00	99.53		97.58		90.33	
2.50	N/A		99.39		93.98	

APPENDIX 3

POTASSIUM PERMANGANATE ADDITION

The comparison between the extraction and the cumulative concentration of potassium permanganate are illustrated in Figure A3-1 to Figure A3-3.

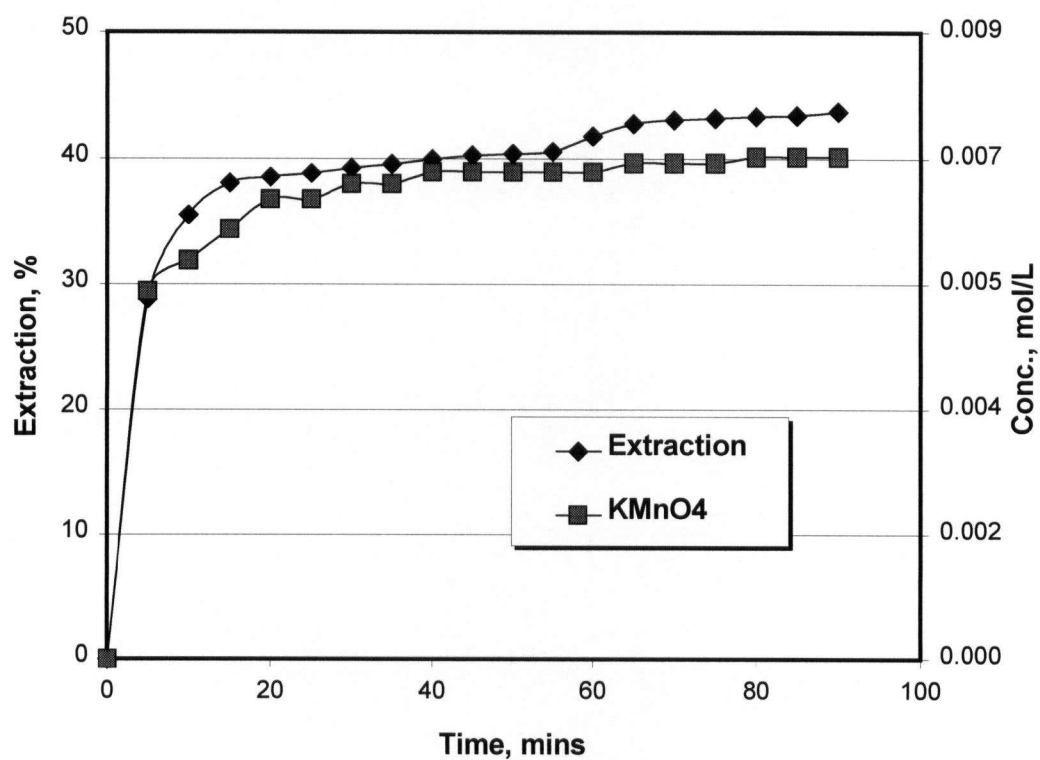


Figure A3-1. Plots of copper extraction and KMnO_4 concentration for the first stage leaching of $-250+212\ \mu\text{m}$ particles of chalcocite at 35°C , $0.116\ \text{mol/L}$ ferric ion and $0.001\ \text{mol/L}$ ferrous ion.

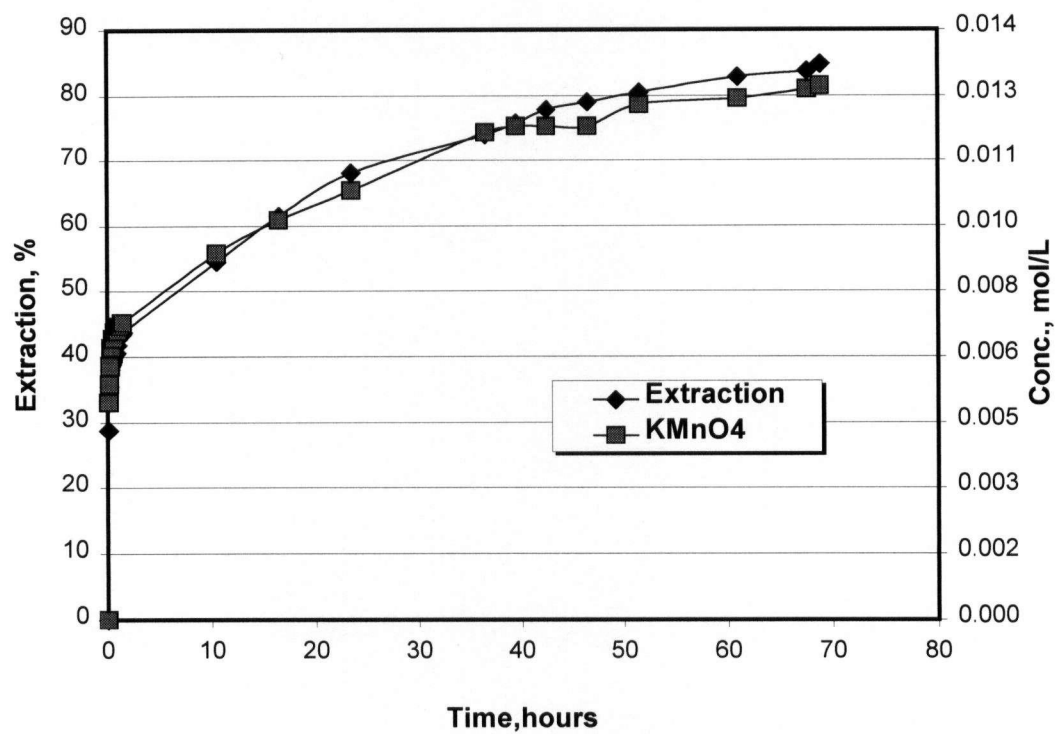


Figure A3-2. Plots of copper extraction and KMnO₄ concentration for the second stage leaching of -250+212 μm particles of chalcocite at 35°C, 0.116 mol/L ferric ion and 0.001mol/L ferrous ion.

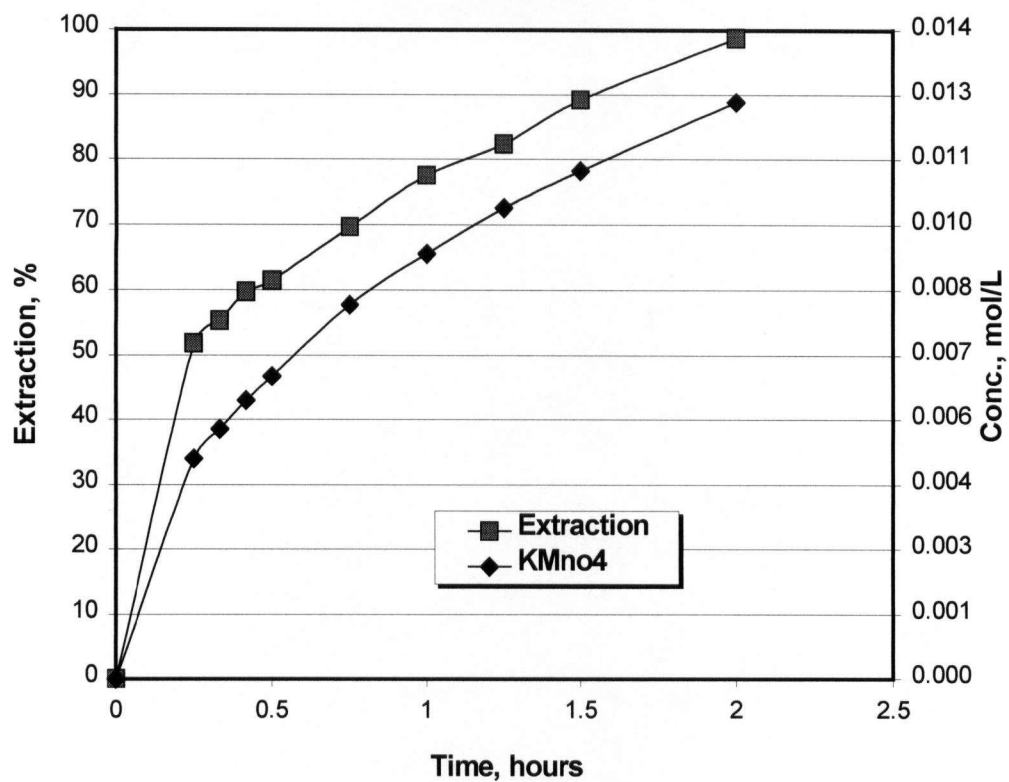


Figure A3-3. Plots of copper extraction and KMnO_4 concentration for the second stage leaching of -250+212 μm particles of chalcocite at 75°C , 0.116 mol/L ferric ion and 0.001 mol/L ferrous ion.

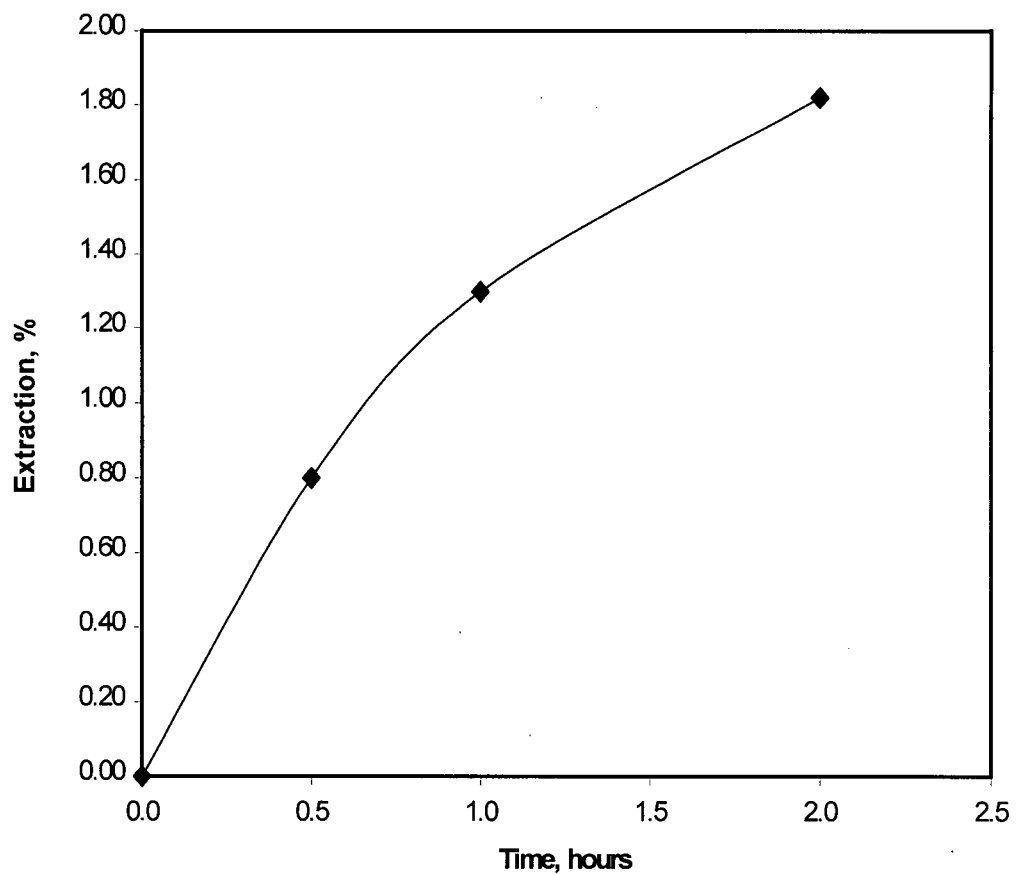


Figure A3-4. Effect of KMnO_4 on the leaching of -250+212 μm particles of chalcocite at 75°C, 0.000 mol/L ferric, 0.095 mol/L sulfuric acid and 0.015 mol/L potassium permanganate.

APPENDIX 4

TOPOCHEMICAL MECHANISM OF LEACHING AND CALCULATION OF INSTANTANEOUS RATE OF LEACHING

The change to the surface area as leaching progresses is related to the instantaneous rate of reaction and this is illustrated by plotting the rate against the percentage of copper extracted as follows;

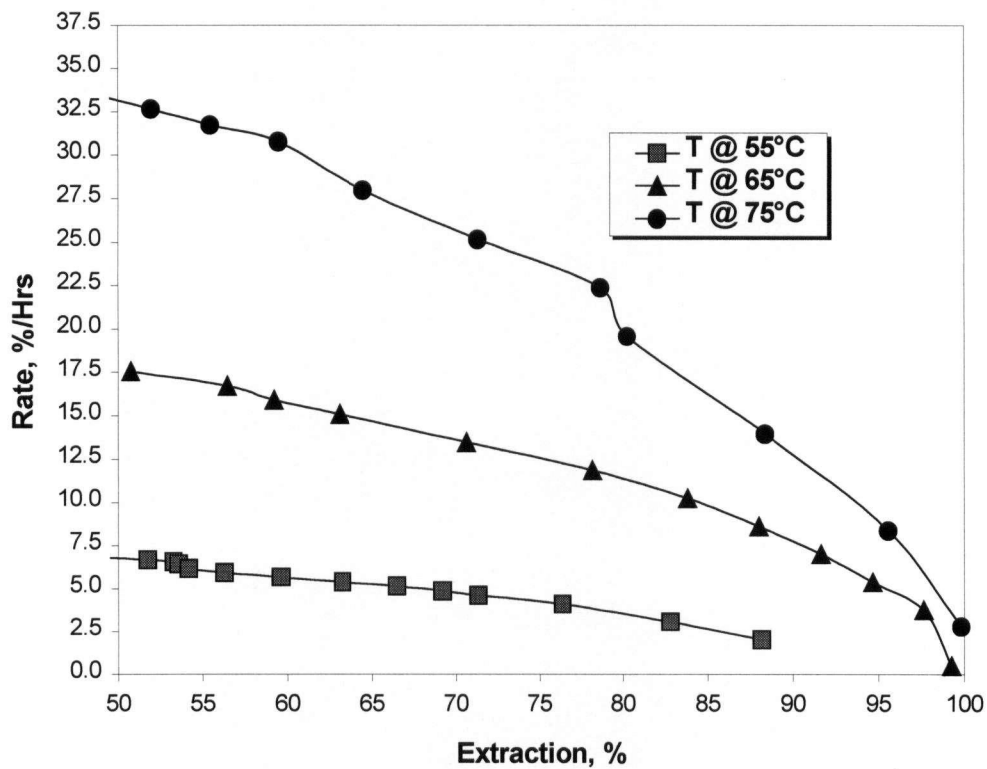


Figure A4-1. Plots of copper leach rate at different temperature vs. extraction for the second stage leaching of -250+212 μm particles of chalcocite at 75°C, 0.116 mol/L ferric ion and 0.0202 mol/L ferrous ion.

In order to determine the instantaneous leach rates, the copper extraction curves (in Figure 4-31 were fitted to a polynomial function by using Microsoft Excel application. The polynomial function is of the following general form;

$$y = A_1x^2 + A_2x + A_3 \quad (A4-1)$$

where,

y = percent Cu extraction, x = leach residence time in hours and A_1, A_2, A_3 are constants.

The equation (A4-1) was differentiated to obtain the following rate equation;

$$\frac{dy}{dx} = 2A_1x + A_2 \quad (A4-2)$$

where,

dy / dx is the instantaneous copper leach rate at any x , in units of % Cu / hour .

Table A4-1 lists the values of the coefficients obtained at different temperature.

Table A4-1. Coefficient values obtained for function fitted copper extraction data.

Temperature (°C)	A_1	A_2	A_3
55	-0.2590	7.2177	41.774
65	-1.5807	19.7800	37.874
75	-5.7185	36.6990	39.967